Contrôle transcriptionnel de la spécification cellulaire dans le cerveau postérieur des Vertébrés

Yassine Bouchoucha

Thèse de Doctorat de l'Université Pierre et Marie Curie – Paris VI

École Doctorale Complexité du Vivant CDV (ED 515)

Présentée par

Yassine Bouchoucha

Pour obtenir le grade de Docteur de l'Université Pierre et Marie Curie

---

Contrôle transcriptionnel de la spécification cellulaire dans le cerveau postérieur des Vertébrés

---

Soutenue le 12 Juillet 2012
Devant le jury composé de :

Dr Sylvie Schneider-Maunoury	Présidente
Dr Corinne Houart	Rapporteur
Dr Serge Plaza	Rapporteur
Dr Nathalie Dostatni	Examinateur
Pr Reiner Veitia	Examinateur
Dr Pascale Gilardi-Hebenstreit	Directrice de thèse
Dr Patrick Charnay	Membre invité

Résumé

Au cours du développement embryonnaire, des processus de spécification cellulaire allouent un destin à chaque cellule de sorte qu'elle accomplisse une tâche précise, à un endroit précis dans l'organisme. Le destin d'une cellule est spécifié par l'expression d'un gène ou d'une combinatoire de gènes dits de lignage. Le contrôle de l'expression de ces gènes est donc essentiel à la cohérence du développement embryonnaire. Pour savoir comment s'effectue ce contrôle, nous avons choisi un modèle de spécification dans le cerveau postérieur des vertébrés, le rhombencéphale. Cet organe est un système de choix parce qu'on y distingue sept compartiments cellulaires homogènes, appelés rhombomères (r) et notés de r1 à r7, qui subissent des processus de spécification distincts. La voie de spécification de r3 et r5 est la mieux connue car elle est contrôlée par un facteur de lignage unique, le facteur à doigt à zinc Krox20. En l'absence de ce facteur, les cellules de r3 et r5 ne sont pas correctement spécifiées et suivent un destin neuronal modifié.

Dans ce travail de thèse, nous étudions les mécanismes qui permettent de contrôler le nombre de cellules exprimant le gène *Krox20*, donc la taille de r3 et r5, et par conséquent l'organisation des neurones dérivés. Ces mécanismes déterminent la dynamique de transcription de *Krox20*, en régulant l'activité de ses éléments régulateurs. Deux éléments, B et C, sont responsables de l'initiation de l'expression de *Krox20*; un troisième, noté A, l'amplifie et la prolonge grâce à une activité autorégulatrice.

Nous montrons que la voie de signalisation Fgf contrôle d'une part le niveau d'initiation de *Krox20*, d'autre part le nombre de cellules *Krox20*$^{+}$. Nous établissons le lien entre ces deux phénotypes en montrant que (i) les cellules ne sont *Krox20*$^{+}$ que si elles activent l'élément A, (ii) l'activation de l'élément A suit un mode tout-ou-rien, déterminé par le niveau d'initiation de *Krox20*. Ces conclusions sont tirées de l'analyse d'un modèle mathématique, contraint par des données expérimentales obtenues chez le poisson-zèbre, et suffisamment résolutif pour décrire l'activation de A à l'échelle moléculaire.

La taille de r3/r5 dépend par ailleurs de la position des frontières d'expression de *Krox20*. Nous proposons que le profil régionalisé du domaine d'activité de C et le niveau d'activité de C définissent la position des frontières r2/r3 et r3/r4.

Notre étude fournit ainsi une illustration détaillée du lien causal entre la régulation transcriptionnelle, la specification cellulaire et le développement d'un organe.

Avant-propos

Les travaux relatés dans ce mémoire ont été réalisés dans le laboratoire de Patrick Charnay, sous la direction de Pascale Gilardi-Hebenstreit, à l'Institut de Biologie de l'École Normale Supérieure de Paris.

Deux brèves remarques sur la forme tout d'abord. Je prie les lecteurs de bien vouloir m'excuser pour le mélange indigeste des langues qui figurent dans ce manuscrit. L'introduction et la discussion sont rédigées en français alors que tous les résultats sont en anglais. Ni voyez là aucune malice ni snobisme. Il s'agit simplement d'anticiper la soumission de la plupart des résultats à des comités de lecture anglophones. Seconde remarque, la notation des gènes et protéines pourra paraître un peu confuse. Je rappelle ici les règles que j'ai utilisées, en prenant l'exemple de Krox20 :
Krox20 : protéine chez la souris et le poisson-zèbre (première lettre majuscule, police romaine)
Krox20 : gène ou ARNm chez la souris (première lettre majuscule, police italique)
krox20 : gène ou ARNm chez la poisson-zèbre (première lettre minuscule, police italique)

Le lecteur attentif aura noté mon nom, inscrit fièrement sur la page de garde de ce mémoire. Il est vrai que je suis, dans une certaine mesure, fier du travail mené. Pas tant vis-àvis du résultat final car j'ai conscience des maladresses, des erreurs que j'ai pu commettre, du temps que j'ai perdu en ignorance, en immaturité. Je suis fier de ce travail parce que je mesure le chemin parcouru, je me rends compte de l'aventure qu'ont été ces quatre années et de la dette que j'ai envers tant de personnes. C'est de cette dette dont je suis le plus fier, ou plutôt de mes créanciers.

Ces créanciers qui m'ont formé au métier de la recherche, en me transmettant le sens des manips bien faites, en m'aidant à les réaliser, en forgeant mes capacités de raisonnement, de critique et peut-être avant tout d'autocritique. Pascale est certainement celle qui se retrouve le plus sur la paille, tant j'ai exploité sa disponibilité, son dévouement, sa rigueur. Pascale, toujours au charbon, m'a tout appris à la paillasse, a soutenu, peaufiné mes réflexions, en a suscité la majorité. Une directrice de thèse au poil en somme, dont le rôle a été très complémentaire de celui de Patrick. Lui, intervient toujours avec brio lorsqu'il s'agit de couper court aux divagations fantasques du thésard désinhibé. D'une incroyable disponibilité, toujours enthousiaste à l'idée de discuter des projets en cours, il est très agréable de pousser la porte de son bureau. Avec ce « duo dirigeant », je pense sincèrement que ma thèse ne pouvait pas mieux se passer sur le terrain des idées, de la réflexion, et aussi de la liberté. Le projet hypophyse (chapitre 5) en est l'illustration la plus flagrante. Alors que nous avions vite compris que ce projet ne serait pas d'une grande utilité pour le laboratoire, Pascale et Patrick m'ont soutenu de bout en bout, m'ont aidé à trouver une porte de sortie honorable, sans reléguer un seul instant ce projet au second plan.

Trois autres personnes ont très directement contribué à ce travail. Charlotte, d'abord, dont le nom figure sur presque toutes les études mentionnées dans cette thèse. Pendant quatre ans, nos projets respectifs ont évolué de manière parallèle et interconnectée, si bien que chacun a pu se nourrir des réflexions de l'autre. Charlotte a deux qualités immenses : elle est optimiste et tenace. Un moteur quoi !...suffisamment puissant pour m'entraîner, me guider dans le tourbillon de la recherche. Michel (Wassef) a aussi eu un rôle prépondérant. Son nom se fait malheureusement plus discret sur mes chapitres de thèse, mais c'est qu'il est parti trop tôt. Michel était un éminent thésard, bien établi au laboratoire au moment où j'ai débarqué. De manière inconsciente, il a dû se dire qu'il ferait bien de moi de la chair à pâté. Il s'est alors mis en tête de me montrer un peu ce que signifiait la recherche. J'en retiens une maxime éternelle : il vaut mieux réfléchir sept fois dans sa tête que de maniper vainement. Malheureusement, je n'ai appliqué ce

principe qu'en troisième année. Michel m'a donc servi d'exemple, de pousse-à-la-réflexion, de contradicteur majeur, de joyeux luron. Un collègue et ami exquis. Enfin, Jürgen a eu un rôle très important. Il a certes écrit le code du modèle présenté dans le chapitre 2, mais il s'est surtout rendu très disponible pour discuter des moindres petits détails du modèle, des interprétations possibles et pour apporter des modifications au code dans des délais très courts. Le point de vue de physicien qu'a eu Jürgen sur notre travail a modifié nos réflexions, comme il se doit dans une vraie collaboration transdisciplinaire. Jürgen a été un interlocuteur de choix pour cette collaboration.

Je me suis permis de singulariser trois personnes, mais je suis redevable de tant d'autres, soit qu'elles ont contribué de près ou de loin à mon travail de thèse, soit qu'elles ont su créer un environnement amical, chaleureux, et subversif ! Je cite ces personnes ci-dessous, un peu rapidement, bien trop rapidement compte tenu de ma gratitude.
- Le personnel de l'animalerie souris : Déborah, Christophe, Abder, Dolorès, Guillaume, Gérard, Jean-Paul, Amandine, Séverine. Je ne pensais pas pouvoir autant m'amuser dans une animalerie !
- Tous les membres de l'équipe Charnay : Carole (grande prêtresse de la transgénèse), Graziella, Aurélie, Virginie, Sophie (co-box n°1, la pauvre), Gaspard (co-box n°2, quelle souffrance), Patricia (co-box n°3, le charme de l'étranger), Fanny, Alexandre, Renata, Laurence, Piotr.
- Un petit spécial dédicace à Johan et Elodie : le premier est mon cher *alter ego* thésard, toujours de bon poil, la seconde est l'héritière inconsciente d'une partie de mes projets. Inconsciente, mais dévouée et efficace, au point de me soulager de certaines manips du chapitre 2.
- Les fiers occupants du premier étage de l'IBENS : Nicolas, Julien, Marika, Aline, Ana-Lila, FX, Raquel, Guillaume L, Florence, Guillaume G, Riadh, Solange, Sylvain, Brigitte, Marina, Barbara, Aurélie, Yessra. Je suis tellement désolé de ne les citer que sous cette forme insipide. A eux tous, ils ont su créer l'atmosphère idéale pour travailler, conseiller, décompresser, s'invectiver, conspuer, s'amuser et rire.
- La plateforme génomique, pour sa machine PCR et ses gâteaux : Sophie, Laurent, Stéphane, Corinne, et bien sûr, Thomas superstar.
- Un grand merci à Frédéric pour son animalerie poissons et ses macarons, et à Firas pour l'entretien des poissons.
- Je n'oublie pas les joyeux représentants des 7ème et 8ème étages (ceux qui sont proches du soleil), toujours prêts à renseigner ou donner des réactifs sans râler, voire en accompagnant leur geste d'une petite boutade : Ludmilla, Marion, Hugo, Cristina, Saïd, Franck, Maryama, Caroline, Béatrice, Paola, Rosette, Mehdi, Samuel.
- J'ai une pensée particulière pour Marie dont la sympathie n'a d'égal que la capacité à râler, pour Sonia qui n'a jamais le temps mais le prend toujours (dumoins lorsqu'il s'agit de papoter) et Eva dont le charme à l'italienne pourrait revigorer des régiments de thésards désespérés.

Vous l'aurez compris, la thèse constitue un effort collectif. Tellement collectif que je n'ai pas pu m'empêcher d'en faire profiter ma famille, mes amis, et ma compagne Alya, à leur dépens. Je les remercie de leur soutien, de leur patience, de leur compréhension.

Je profite enfin de cette page pour remercier le plus chaleureusement possible les membres de mon jury, qui ont tous accepté d'en faire partie avec enthousiasme. J'espère que les quelques pages qui suivent sauront préserver cet enthousiasme.

Sommaire

INTRODUCTION

Les Métazoaires sont par définition des animaux pluricellulaires capables de réaliser au moins une fonction complexe, la locomotion. Ceci impose trois caractéristiques aux cellules des Métazoaires : la spécialisation, l'organisation spatiale et la coordination temporelle. Les cellules doivent en effet être subdivisées en sous-groupes auxquels sont assignés une tâche et un agencement dans l'espace. De la sorte, le mouvement est le résultat de la somme de ces tâches réalisées au bon moment et au bon endroit.

Quels sont les mécanismes qui gouvernent la spécialisation des cellules (en termes consacrés, la spécification et la différenciation), leur position dans l'espace (la régionalisation), leur coordination fonctionnelle ?

Pour répondre à ces questions, il faut avant tout pouvoir définir un groupe de cellules sur un critère solide. Dans le travail que j'expose ici, nous verrons l'exemple précis d'un groupe de cellules qui apparaît au cours de l'embryogenèse des Vertébrés, Métazoaires dits supérieurs. Il s'agit de cellules neurales caractérisées par l'expression du marqueur *Krox20*, et qui se situent dans une partie bien définie du cerveau postérieur précoce, le rhombencéphale. Nous explorerons les mécanismes moléculaires qui contrôlent l'expression du gène *Krox20*, le nombre des cellules *Krox20*$^+$ et leur position dans le rhombencéphale. Ce travail allie donc des questions relatives à la spécification des cellules *Krox20*$^+$ et leur régionalisation dans le cerveau postérieur.

Pour placer ce projet dans son contexte scientifique, nous détaillerons dans cette introduction les principes connus de la spécification cellulaire et de la régionalisation dans le tissu neural des Vertébrés, en insistant sur leur contrôle génétique. Puis, sur un plan plus technique, nous aborderons la façon dont des approches computationnelles peuvent aider à traiter ces questions de spécification et de régionalisation.

1. Développement du système nerveux, par « spécification régionalisée convergente »

1.1. L'induction neurale

L'embryogenèse des Vertébrés peut se résumer schématiquement en quatre étapes :

- la fécondation et la définition des axes dorso-ventral et antéro-postérieur de l'œuf ;
- la phase de clivage pendant laquelle se forme une masse cellulaire, la morula ;
- la gastrulation, caractérisée par des mouvements cellulaires aboutissant à la formation de trois feuillets embryonnaires : l'endoderme, le mésoderme et l'ectoderme. Ces trois feuillets représentent la première étape de spécialisation cellulaire chez les Métazoaires dits triblastiques ;

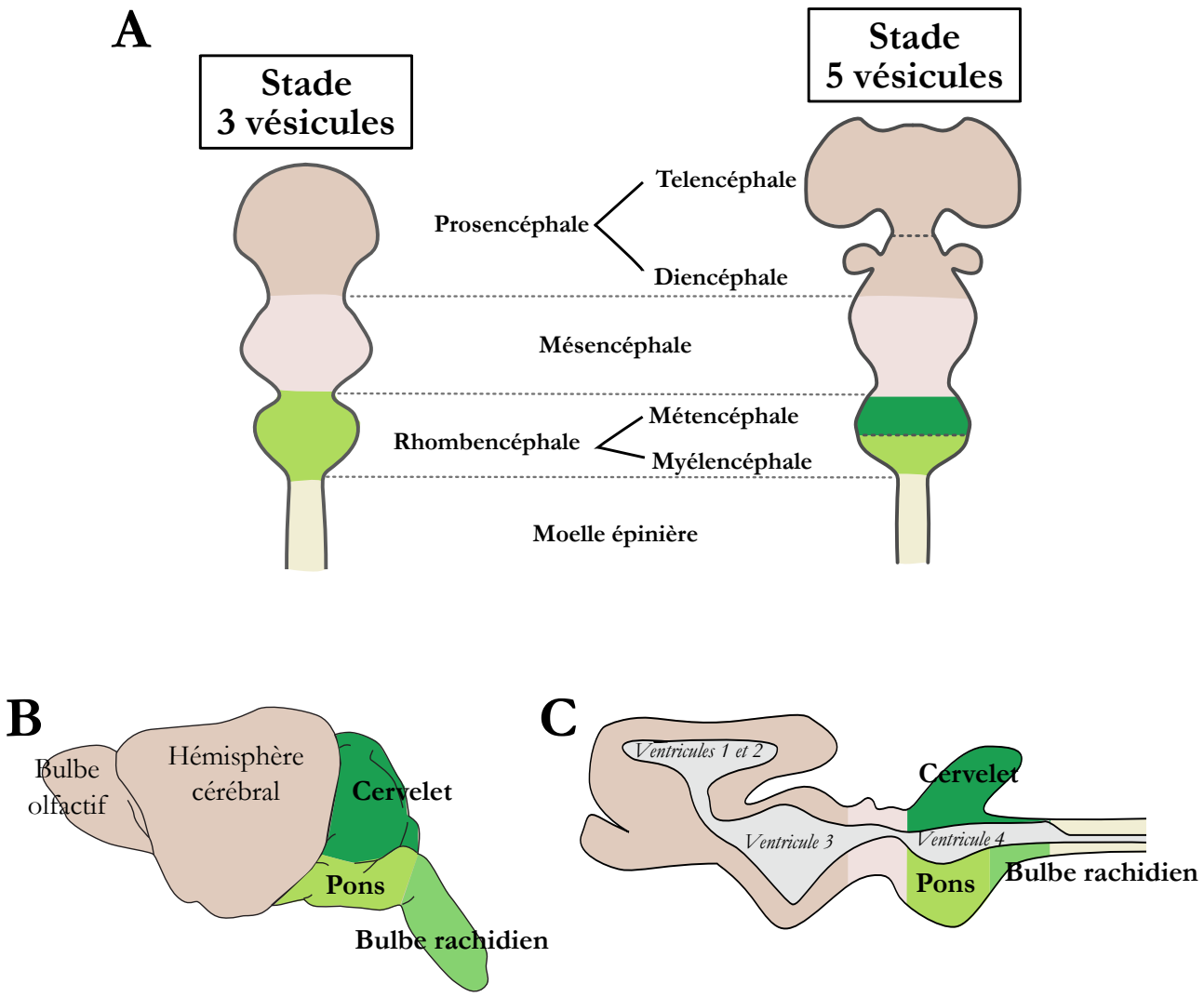

Figure 1 - Les grandes étapes de la régionalisation du cerveau de souris

(A) Le tube neural antérieur est régionalisé selon l'axe antéro-postérieur à travers la formation de trois puis cinq vésicules. Chaque vésicule correspond morphologiquement à une sous-partie du cerveau : d'abord le prosencéphale, le mésencéphale et le rhombencéphale ; puis le prosencéphale donne naissance au télencéphale et diencéphale tandis que le rhombencéphale dérive en métencéphale et myélencéphale. **(B)** Schéma d'une vue latérale d'un cerveau de souris adulte où sont indiquées les trois structures définitives dérivées du rhombencéphale : le cervelet, le pons et le bulbe rachidien (ou medulla). **(C)** Schéma d'une coupe saggitale de cerveau adulte de souris, faisant apparaître les ventricules céphaliques.

- l'organogenèse, c'est-à-dire la formation successive des différents organes.

L'induction neurale a lieu pendant la gastrulation. Un groupe de cellules du mésoderme « induit » la partie dorsale de l'ectoderme sus-jacent à se différencier en neurectoderme. Ce groupe de cellules mésodermiques, appelé « organisateur de Spemann » (Spemann and Mangold, 2001), sécrètent des antagonistes de *Bone Morphogenetic Proteins* (BMP). Il en résulte une levée de l'inhibition qu'exercent les BMP sur le destin neural de l'ectoderme (Stern, 2005). Il a été montré chez le Xénope que cette levée d'inhibition rend possible le rôle instructeur de la voie FGF pour induire l'expression des facteurs de transcription Zic1 et Zic3 (Marchal et al., 2009), qui eux-même induisent Sox2, facteur de transcription spécifique du destin neural (Figure 2A). Une fois spécifié, le neurectoderme s'épaissit pour former la plaque neurale.

1.2. La neurulation

Chez les Mammifères et les Oiseaux, la plaque neurale se replie sur elle-même, forme une gouttière délimitée par des bourrelets neuraux. La fusion des bourrelets neuraux aboutit à la formation du tube neural, distinct désormais de l'épiderme présomptif sus-jacent. Peu après, les cellules les plus dorsales du tube « délaminent », i.e. quittent le toit du tube neural et donnent ainsi naissance aux cellules de la crête neurale, à l'origine du système nerveux périphérique, des mélanocytes, des os et tissus conjonctifs de la face. Chez les poissons, la plaque neurale prend la forme d'un cylindre et subit un processus de cavitation secondaire.

1.3. La régionalisation antéro-postérieure de la plaque neurale

Morphologiquement, la régionalisation antéro-postérieure du tube neural débute par le gonflement de sa partie antérieure, en trois vésicules, le prosencéphale (antérieur), le mésencéphale (moyen), le rhombencéphale (postérieur). Prosencéphale et rhombencéphale donnent ensuite naissance aux télencéphale, diencéphale et métencéphale, myélencéphale respectivement. Le système nerveux antérieur comprend alors cinq vésicules (Figure 1A).

Quelques détails sur les organes dérivés du rhombencéphale, notre objet d'étude : le métencéphale dérive en cervelet et pons ; le myélencéphale donne le bulbe rachidien ou *medulla oblongata* (« moelle longue ») ; la crête neurale du rhombencéphale fournit les cellules des ganglions crâniens (une majorité de neurones sensoriels, les cellules satellites et de Schwann) et des arcs branchiaux qui eux-mêmes dérivent en os, muscles et cartilages de la face (Figure 1B, C).

Les mécanismes contrôlant cette régionalisation comprennent des étapes successives dont chacune aboutit à un degré de régionalisation, d'où l'expression de « régionalisation convergente » : la plaque neurale converge vers un état régionalisé par étapes successives.

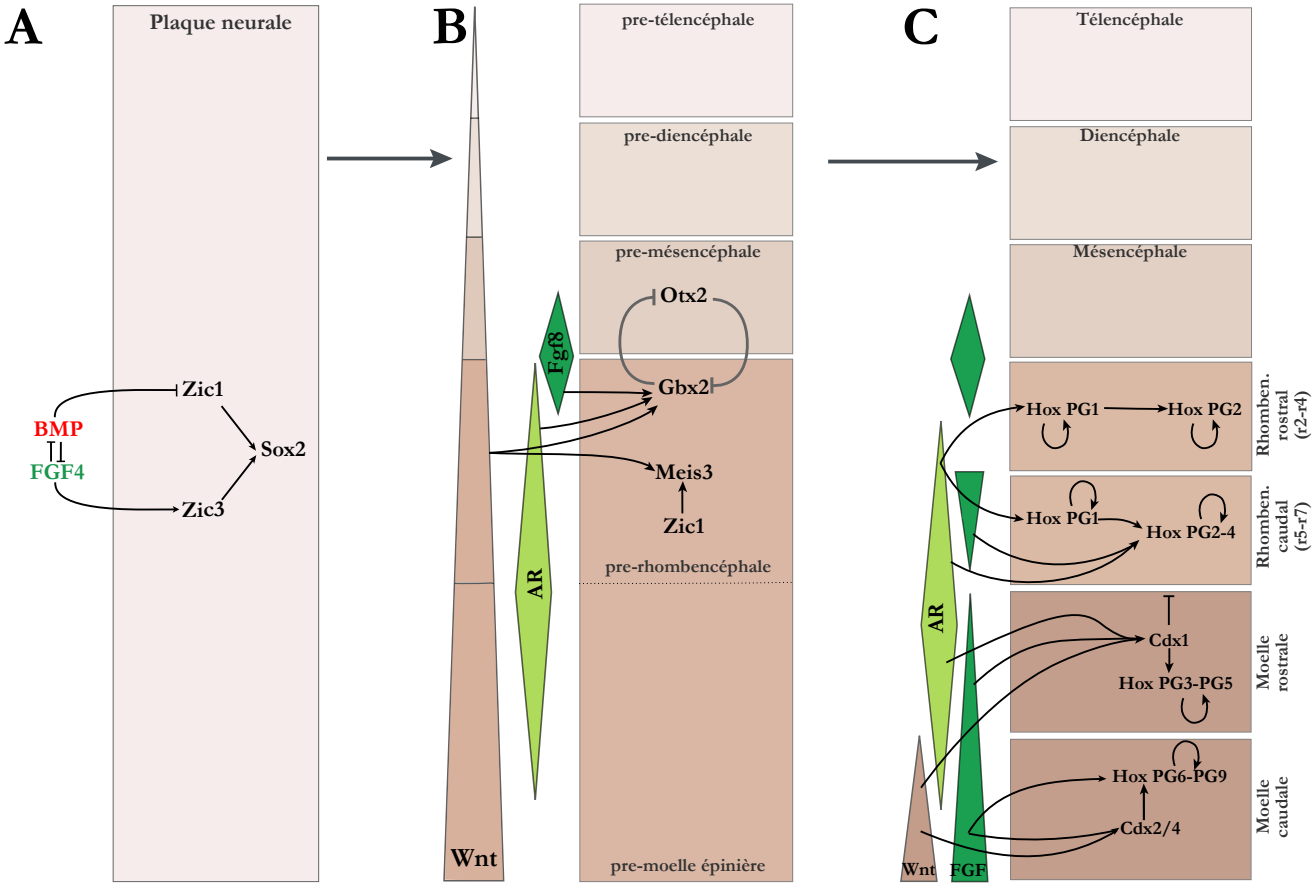

Figure 2 - Les principaux acteurs de la régionalisation de la plaque neurale

(A) L'induction neurale permet aux cellules ectodermiques de prendre un destin neural grâce à la levée de l'inhibition par les BMP et le rôle instructeur des FGF. Cette étape aboutit à la formation de la plaque neurale. **(B)** La régionalisation antéro-postérieure débute lorsque la plaque neurale devient le tube neural. Un signal activateur définit le destin postérieur, depuis le diencéphale présomptif jusqu'à la moelle. Les Wnt transforment ensuite ce territoire postérieur de façon graduée. La définition et le maintien du territoire rhombencéphale requièrent de plus l'action concertée des FGF et de l'AR. **(C)** Enfin, Wnt, FGF et AR affinent la régionalisation du rhombencéphale et de la moelle en activant les gènes *Cdx* et *Hox*.

1.3.1. L'activation-transformation de Niewkoop : Peter Niewkoop propose en 1952 un modèle en deux phases pour expliquer la façon dont la plaque neurale est régionalisée (Stern, 2001) :

1) un signal d' « activation » assigne à tout le neurectoderme une identité prosencéphalique ;

2) un signal de « transformation » agit ensuite de façon graduée le long de l'axe antéro-postérieur : plus la dose (c'est-à-dire l'intégration de la quantité par le temps d'exposition) de ce signal est importante, plus l'identité du neurectoderme est caudale. Sont ainsi spécifiés la moelle épinière, le rhombencéphale, le mésencéphale, le diencéphale.

La régionalisation du neurectoderme est contrôlée par des molécules extrinsèques, sécrétées à partir du mésoderme paraxial, agissant en gradient : les *Wnts*. Il a été montré dans l'embryon de poulet que l'induction de marqueurs neuraux caudaux est abolie en l'absence de mésoderme paraxial ou en présence d'inhibiteurs de la voie Wnt. Réciproquement, des expériences de gain-de-fonction sur des explants de neurectoderme ont mis en évidence l'effet dose-dépendant de Wnt3A dans l'activation des marqueurs caudaux (Nordström et al., 2002; 2006). Ces expériences identifient les Wnt comme facteurs instructeurs du destin caudal. Notamment, Wnt3A active Meis3, un des marqueurs les plus précoces du rhombencéphale (Elkouby et al., 2010) (Figure 2B). Cette transformation par les Wnts n'est possible qu'en présence d'une autre famille de molécules sécrétées, les *Fibroblast Growth Factors* (FGF), dont le rôle est permissif.

1.3.2. L'identité postérieure est « protégée » par Gbx2 : une fois le territoire « rhombencéphale + moelle » défini par le gradient Wnt, il est maintenu grâce à la répression mutuelle entre deux facteurs à homéodomaine, Otx2 et Gbx2. *Otx2* est exprimé dans la partie antérieure du neurectoderme, jusqu'à la frontière entre le mésencéphale et le rhombencéphale (l'isthme), tandis que *Gbx2* est exprimé caudalement à cette même frontière. Dans le mutant murin $Gbx2^{-/-}$, le domaine mésencéphalique, $Otx2^{+}$, s'étend caudalement aux dépens du rhombencéphale antérieur. L'expression de *Gbx2* est contrôlée par l'action combinée des Wnt, de Fgf8 sécrété par l'isthme et d'une autre molécule diffusible émanant du mésoderme paraxial et des somites antérieurs : l'acide rétinoïque (AR) (Figure 2B) (Liu et al., 1999; Li et al., 2009).

1.3.3. L'acide rétinoïque et les FGFs affinent la régionalisation du rhombencéphale et de la moelle et mettent en place le « code Hox » : des gradients d'AR et de FGF (issu du rhombencéphale ou de la ligne primitive) agissent de concert pour définir quatre compartiments : le rhombencéphale rostral, le rhombencpéhale caudal, la moelle rostrale et la moelle caudale. Ces compartiments sont définis par les profils d'expression des facteurs de transcription à

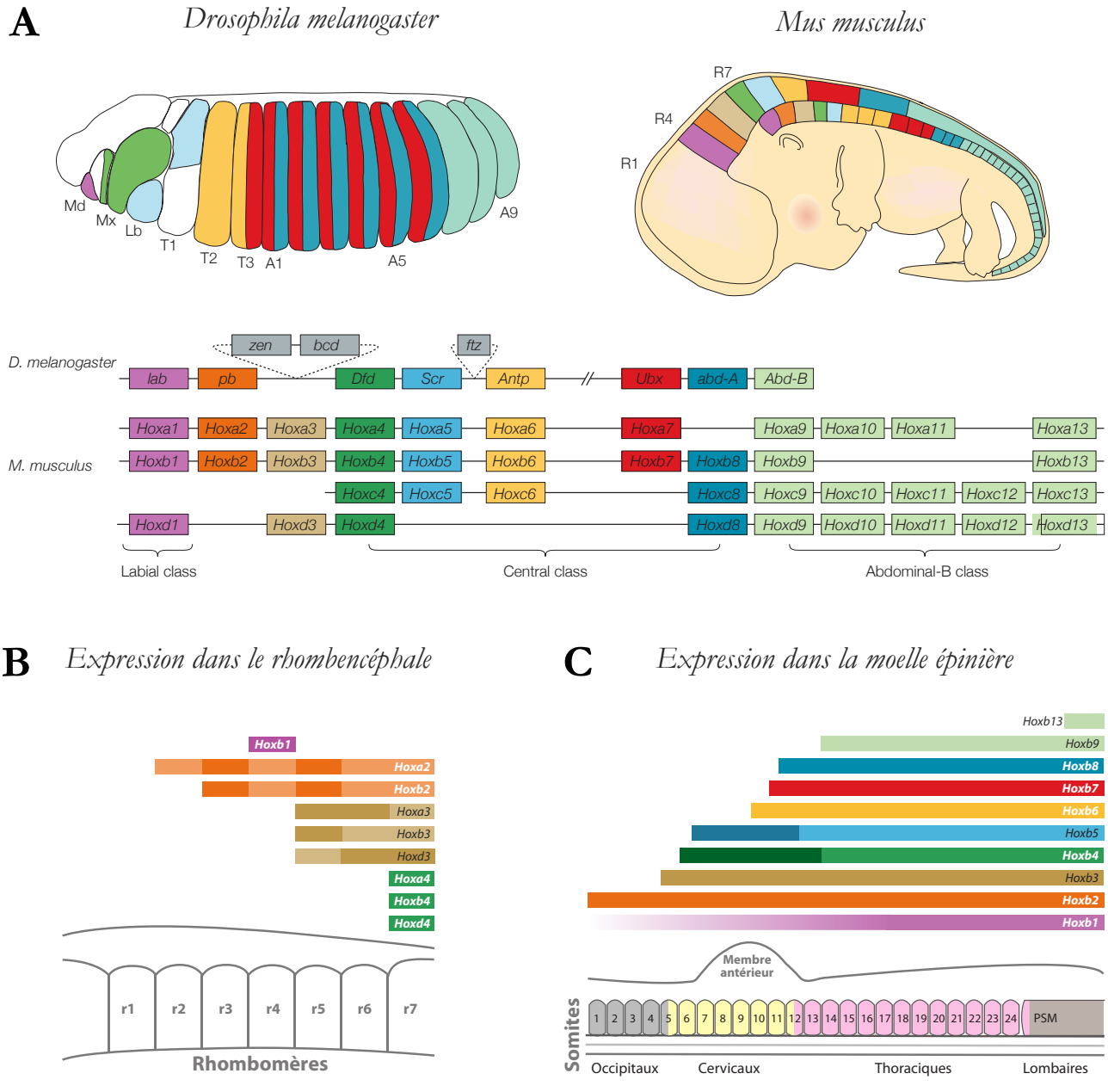

Figure 3 - Organisation génomique et profils d'expression des gènes *Hox* chez la Drosophile et la souris

(A) Organisation des "clusters" *Hox* dans les génomes de Drosophile et de souris. L'expression métamérique de chaque Hox est représentée sur les schémas d'embryons correspondant. Ceci fait apparaître la colinéraité spatiale d'expression des *Hox*, sachant que les clusters sont représentés dans le sens 3'-5'. **(B,C)** Profils d'expression plus précis dans la moelle épinière (B) et dans le rhombencéphale (C). Les *Hox* ont un profil d'expression chevauchant. Chaque métamère se caractérise donc par l'expression d'une combinaison de *Hox* et/ou par des niveaux d'expression différents.
D'après Pearson *et al.*, 2005 (A) et Alexander *et al.*, 2009 (Bet C).

homéodomaine Hox, exprimés depuis le rhombencéphale rostral jusqu'à l'extrémité caudale de la moelle. Dans la moelle, l'activation des gènes Hox requiert la présence d'autres facteurs à homéodomaines, les gènes Cdx, exprimés furtivement dans le rhombencéphale rostral et de façon plus pérenne dans la moelle (Bel-Vialar et al., 2002) (Tabariès et al., 2005; Nordström et al., 2006; Sturgeon et al., 2011). *In fine*, les gènes *Hox* définissent l'identité des différentes populations de neurones le long de l'axe antéro-postérieur, en initiant leurs programmes de différenciation (Figure 2C).

1.4. Le code Hox

La spécification de l'identité antéro-postérieure du rhombencéphale et de la moelle épinière résulte en dernier lieu de la combinatoire d'expression de gènes *Hox*. Dans les années 1970-80, Ed Lewis et Antonio Garcia-Bellido identifient ces gènes chez la Drosophile en caractérisant les phénotypes mutants associés, notamment ceux du complexe Bithorax (Capdevila and Garcia-Bellido, 1974; Garcia-Bellido and Lewis, 1976). Ces études aboutissent à la notion de gène « sélecteurs homéotiques », c'est-à-dire des gènes dont les protéines sélectionnent un destin cellulaire, en activant ou inhibant des programmes de différenciation, selon des informations de position définies par les axes de polarité de l'embryon. De ce fait, les gènes sélecteurs contrôlent la mise en place du plan d'organisation (McGinnis and Krumlauf, 1992).

Chez la Drosophile, ces gènes sont organisés en deux complexes chromosomiques, Antennapædia et Bithorax. Des orthologues aux gènes homéotiques de la Drosophile ont été identifiés chez les Vertébrés grâce aux travaux de Walter Gehring (Gehring, 1987). Ils sont répartis en quatre complexes, issus de duplications successives d'un complexe ancestral (Hox-A, Hox-B, Hox-C, Hox-D) sauf chez les Téléostéens où il existe sept complexes. Chaque complexe comprend 13 gènes paralogues, notés Hox1 à Hox13. Les gènes *Hox* sont donc identifiés chez les Vertébrés par leur complexe et leur groupe de paralogie, d'où une notation de type Hoxa1 ou Hoxc12. Par ailleurs, l'ordre dans lequel sont placés les gènes au sein d'un même complexe est inversement corrélé à la position et le moment de leur expression : les gènes situés en 5' de complexe s'expriment caudalement et tardivement. Cette caractéristique est connue sous le nom de colinéarité spatiale et temporelle (figure 3A) (Duboule, 1998).

Il en résulte une expression chevauchante des gènes *Hox* le long de l'axe rostro-caudal, aussi bien dans le tube neural que dans les somites (Figure 3B, C). Chaque combinatoire d'expression conduit à la différenciation de types neuronaux ou vertébraux différents. Par exemple, les motoneurones (MN) du rhombencéphale et de la moelle épinière se différencient à des positions différentes le long de l'axe antéro-postérieur selon que leurs axones utilisent un point de sortie

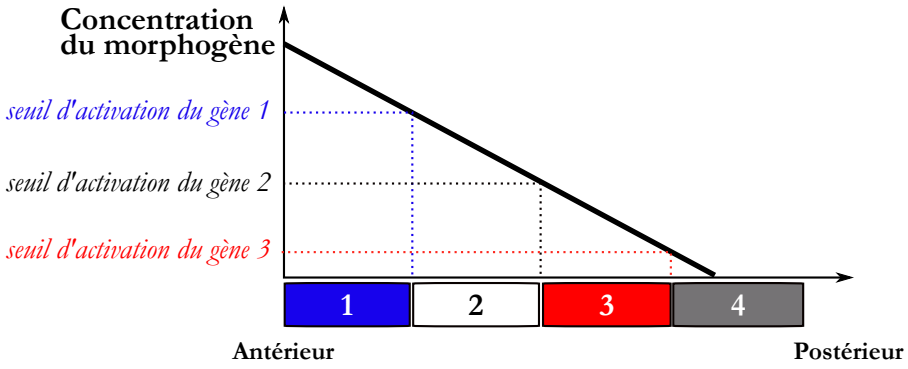

Figure 4 - Information positionelle fournie par un morphogène : modèle du "Drapeau Français"

Lewis Wolpert propose en 1969 que la position des frontières d'expression des gènes peut être le fait d'activateurs, dits morphogènes, dont l'expression est graduée. Cette hypothèse trouvera son illustration la plus élégante quelques années plus tard après la découverte du gène *Bicoid* et du phénotype mutant associé. Le modèle, tel qu'il est représenté ici, prévoit que les gènes 1, 2, 3 et 4 ne se chevauche pas. Ceci requiert des mécanismes d'inhibitions croisées, en plus de l'information de position.

dorsal (dMN) ou ventral (vMN). La combinatoire *Hoxb4+Hoxb8+Hoxc9* définit l'identité vMN dans la moelle caudale, alors que seuls *Hoxb4+Hoxb8* contrôlent les vMN dans la moelle rostrale. Le destin dMN quant à lui est défini par l'expression de Hoxb4 dans le rhombencéphale caudal (Nordström et al., 2006).

Les profils d'expression des gènes *Hox* constituent la manifestation finale du processus de spécification antéro-postérieure.

1.5. Les grands principes de la spécification cellulaire régionalisée

L'exemple du développement précoce du système nerveux détaillé ci-avant est suffisamment emblématique pour que l'on puisse en tirer quelques règles générales. La notion maîtresse de tout processus de régionalisation est la notion de « territoire », indissociable de celle d' « identité ». L'identité d'un territoire est définie par sa morphologie et/ou par le répertoire des gènes qu'il exprime (*Cdx*, *Hox*). L'identité génétique d'un territoire assure l'unité entre les cellules et contrôle leurs destins. Elle est le fait de *gènes de développement*, c'est-à-dire des gènes impliqués dans un processus de spécification cellulaire et/ou de *morphogenèse* (création d'une forme au cours de l'embryogenèse). Pour ce faire, l'expression des gènes de développement est régulée de façon spatio-temporelle. On peut donc définir un *patron d'expression* pour chacun d'entre eux, et les patrons d'expression de plusieurs gènes définissent les territoires. Ce cas est particulièrement bien illustré par le code Hox. Dès lors, la clé de la définition des territoires est le contrôle du patron d'expression des gènes. La manière dont les gènes de développement sont exprimés et façonnent les plans d'organisation répond au terme anglo-saxon consacré de *patterning*, un terme que je me permettrai d'utiliser par la suite car la traduction française n'est pas toujours satisfaisante. Comment est régulée l'expression des gènes de développement ? L'exemple de la morphogenèse de la plaque neurale apporte un élément de réponse à travers les molécules diffusibles Wnt, FGF et AR. Ces molécules fournissent une information spatio-temporelle du fait qu'elles sont exprimées sous forme de gradients spatial et temporel. La première validation expérimentale du rôle de molécules diffusibles comme source d'information positionnelle est apportée par l'étude du gène *Bicoid* chez la Drosophile.

La protéine Bicoid, un facteur de transcription, diffuse dans l'embryon syncitial précoce depuis le pôle antérieur. Sa concentration définit ainsi des coordonnées spatiales le long de l'axe, d'où le terme de gradient *morphogène*. Ces coordonnées sont « lues » ensuite par d'autres facteurs de transcription, les Gap, selon le modèle dit du « drapeau français », théorisé dès la fin des années 60 par Lewis Wolpert (Wolpert, 1969)(Figure 4). La position des territoires d'expression *gap* est déterminée par la concentration de Bicoid, avec une précision estimée à 10% (Gregor et al.,

A Rhombencéphale de souris à 8,5 jpc

B Rhombencéphale de poulet à HH12

C

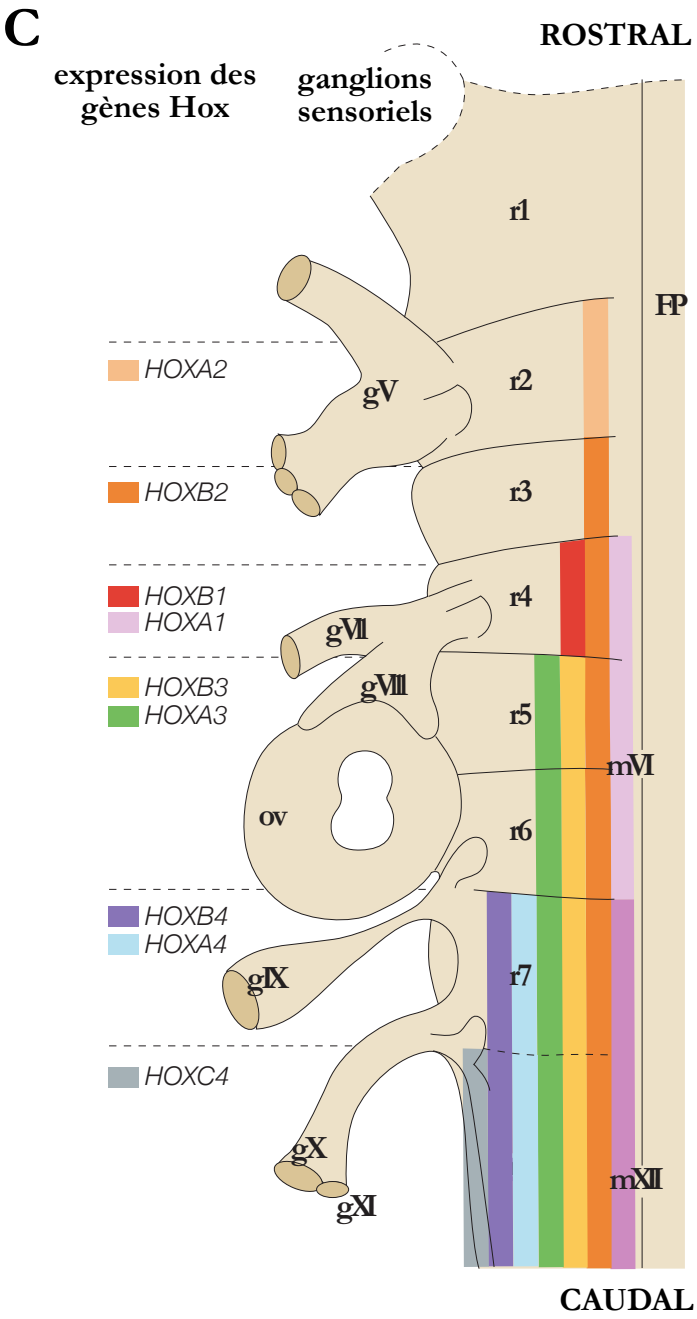

Figure 5 - Segmentation morphologique et moléculaire du rhombencéphale

(A,B) Clichés de microscopie électronique de tubes neuraux en vues dorsales, chez la souris (A, Hunt & Krumlauf, 1991) et chez le poulet (B, Lumsden & Keynes, 1989) **(C)** Schéma d'un rhombencéphale segmenté sur lequel sont représentés le profil des gènes *Hox*, la position des sorties de nerfs (r2, r4, r6 et r7) et celles des ganglions sensoriels. r: rhombomère m: noyau moteur ; g: ganglion ; ov: vésicule otique. D'après Kiecker *et al.*, 2005.

2007a; 2007b). Il a été montré par la suite que l'information apportée par le gradient morphogénétique Bicoid ne suffit pas à définir les territoires. Des boucles d'autorégulation et de répression mutuelle parmi les *gap* sont nécessaires pour affiner et maintenir les domaines. Les gènes *gap* activent ensuite des gènes *pair-rule* qui eux-même activent des gènes *segment-polarity*. À chaque étape de cette « cascade de segmentation », les territoires formés sont plus restreints, pour aboutir à l'unité fonctionnelle du plan d'organisation des Bilatériens : le métamère. Le métamère est caractérisé par une combinatoire de gènes Hox. La cascade de segmentation chez la Drosophile fait écho à l'expression « spécification cellulaire régionalisée » que je me permets d'utiliser ici, bien que non-homologuée.

Le parallèle entre les Wnt, les FGF, l'AR et Bicoid est osé d'une part parce que la plaque neurale est un système cellulaire alors que l'embryon précoce de Drosophile est un syncitium, d'autre part parce que la définition d'un morphogène appelle deux démonstrations: (i) l'existence de molécules diffusibles présentes en gradient, (ii) l'existence de gènes cibles à ce gradient dont on peut montrer que leur domaine d'expression varie en fonction de la forme du gradient (selon le modèle du drapeau français). Si le premier pré-requis est vraisemblablement vérifié en ce qui concerne les Wnt, les FGF et l'AR, le second est affaibli par l'absence de données *in vivo*.

En résumé, les études menées chez la Drosophile notamment par Ed Lewis, Chritiane Nusslein-Volhard et Eric Wieschaus, ont conduit à la notion de patron d'expression des gènes de développement, sous contrôle de signaux exprimés en gradient, eux-mêmes à l'origine d'une information positionnelle et/ou temporelle. Les patrons d'expression définissent des territoires morphogénétiques. L'organisation en cascade de ces gènes affine les territoires jusqu'au plus restreint d'entre eux : le métamère. Ce travail des Drosophilistes a initié une nouvelle discipline, la génétique moléculaire du développement. Dès lors, deux défis majeurs sont apparus évidents dès les années 1990 : le premier consiste à identifier les acteurs de la morphogenèse antéro-postérieure dans les systèmes cellulaires, et non plus syncitiaux, des Vertébrés. Le second défi vise à définir les processus transcriptionnels qui contrôlent l'expression des gènes. Comment les informations temporelles ou positionnelles sont-elles intégrées au niveau génétique et définissent le patron d'expression des gènes ? Cette dernière question ouvre deux champs de recherche, toujours très actifs aujourd'hui : l'identification des éléments régulateurs de l'expression des gènes et des mécanismes régissant leur fonctionnement ; la description des processus épigénétiques, chromatiniens, qui régulent l'activité de ces éléments. Le travail détaillé plus bas se situe dans le premier champ, dans le cadre d'un système emblématique de spécification cellulaire le long de l'axe rostro-caudal : la segmentation du rhombencéphale.

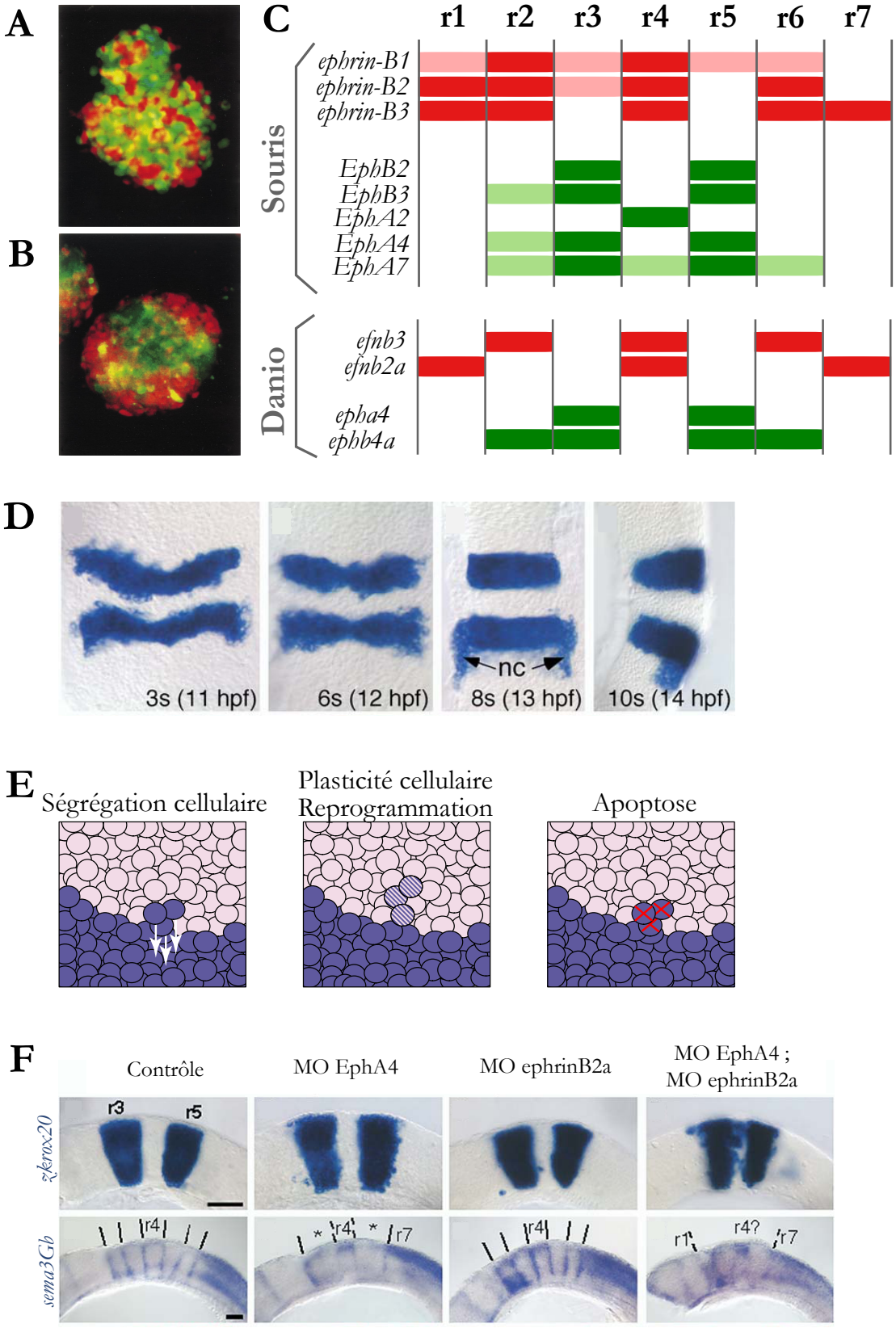

Figure 6 - Le système Eph/ephrine dans la segmentation du rhombencéphale

(A) Aggrégation homotypique de cellules de poulet issues de r4 dont une partie à été marquée par un marqueur fluorescent rouge, l'autre par par un marqueur vert. **(B)** Même expérience réalisée entre des cellules de r4 (vert) et de r5 (rouge). La ségrégation des deux types de cellules est ici mise en évidence (Wizenmann & Lumsden, 1997). **(C)** Profils d'expression des récepteurs Eph et des ligands ephrine dans le rhombencéphale, chez la souris et le poisson-zèbre (d'après Xu *et al.*, 2000). **(D)** Profil d'expression de Krox20 au cours du temps dans l'embryon de poisson-zèbre, faisant apparaître le phénomène d'affinement des frontières. (E) Trois mécanismes peuvent être avancés pour expliquer cet affinement : la ségrégation cellulaire grâce au système Eph/ephrine, la reprogrammation des cellules et l'apoptose (Cooke & Moens, 2002). **(F)** Phénotypes induits par la perte de fonction *EphA4* et/ou *ephrineB2a* chez le poisson-zèbre : les cellules *Krox20*$^{+}$ colonisent les rhombomères pairs ; les marqueurs de frontières inter-rhombomériques disparaissent (ici sema3Gb) (Cooke *et al.*, 2005)

2. Un exemple de spécification cellulaire régionalisée : la segmentation du rhombencéphale

Au moment de la fermeture du tube neural, le rhombencéphale se subdivise en sept unités le long de l'axe antéro-postérieur, appelées segments ou rhombomères (r). On définit ainsi les rhombomères de type pair (r2, r4, r6) et ceux de type impair (r3, r5). Cette nomenclature exclut r1 et r7 car ils ont un mode de développement singulier qui ne répond pas aux mêmes règles de segmentation que le « rhombencéphale central » (r2-r6).

Les rhombomères sont visibles morphologiquement ; ils correspondent à des renflements du tube délimités par des constrictions, les frontières inter-rhombomériques (Figure 5A, B). Les limites d'expression des gènes Hox coïncident avec ces frontières (Figure 5C). Ce processus de segmentation transitoire du rhombencéphale est emblématique, voire caricatural, parmi les systèmes de spécification cellulaire car chaque segment, véritable métamère, est une unité homogène sur les plans cellulaire et moléculaire, dont l'identité dépend de la position rostro-caudale. La segmentation du rhombencéphale est un processus conservé chez les Vertébrés. Des signes de segmentation ont même été décrits chez les urochordés et les céphalochordés, mais sans preuve d'identité homogène au sein des compartiments, ni de frontières nettes (Jackman, 2000; Knight et al., 2000).

2.1. Identité cellulaire des rhombomères

Des études de lignage réalisées chez le poulet démontrent l'absence de migration cellulaire entre les rhombomères (Fraser et al., 1990). Quels mécanismes assurent cette restriction de lignage ? Les frontières inter-rhombomériques ne sont pas directement impliquées puisqu'elles n'apparaissent que secondairement, après contact entre cellules des rhombomères pairs et cellules des rhombomères impairs (Guthrie and Lumsden, 1991). En outre, l'ablation des cellules frontières ne modifie pas la restriction de lignage (Nittenberg et al., 1997). Les frontières sont en fait constituées de cellules spécialisées impliquées dans la différenciation neuronale à des stades ultérieurs (Amoyel et al., 2005). Par agrégation de cellules de poulet issues soit de segment pairs, soit de segments impairs, Andrea Wizenmann et Andrew Lumsden ont pu montrer que les cellules paires et impaires ségrègent (Figure 6B), alors que des cellules issues de deux rhombomères pairs différents ne ségrègent pas, ou très peu (Figure 6A) (Wizenmann and Lumsden, 1997). Ces expériences réalisées *ex vivo* suggèrent que les rhombomères disposent de propriétés intrinsèques qui imposent une ségrégation entre les cellules de types pair et impair, à l'origine de la compartimentation du rhombencéphale.

2.2. Identité moléculaire des rhombomères

L'identité cellulaire des rhombomères est sous-tendue par une identité moléculaire. Cette assertion est basée sur la découverte de mutants –dont nous détaillerons les études plus loin– caractérisés par l'absence d'un ou plusieurs rhombomères. Ainsi, l'identité moléculaire des rhombomères est définie en premier lieu par des « gènes de segmentation », c'est-à-dire des gènes dont le patron d'expression préfigure la position des segments et des frontières. À ce jour, les gènes de segmentation connus chez la souris sont le gène *Krox20* exprimé dans r3 et r5, *MafB* (*valentino* chez le poisson-zèbre) dans r5-r6, *Hoxb1* dans r4. Ces gènes définissent l'identité cellulaire des rhombomères dans lequels ils sont exprimés en couplant l'activation des systèmes de ségrégation cellulaire et l'activation des gènes *Hox* (Sham et al., 1993) (Nonchev et al., 1996) (Vesque et al., 1996) (Seitanidou et al., 1997) (Manzanares et al., 1997) (Manzanares et al., 1999) (Manzanares et al., 2001).

2.2.1. Effecteurs de la ségrégation cellulaire : la ségrégation cellulaire entre les cellules des rhombomères pairs et impairs s'exprime de deux manières. La première, tel que décrit ci-dessus, correspond à l'immiscibilité des cellules révélée par transplantation ou agrégation ; la seconde est le tri cellulaire, en partie responsable de l'affinement des frontières d'expression des gènes d'expression, comme montré pour *Krox20* en figure 6D (les autres processus responsables de cet affinement sont la reprogrammation et l'apoptose, Figure 6E). Ces deux phénomènes ont la même base moléculaire : le système de récepteurs-ligands à activité tyrosine kinase Eph/ephrines, responsables d'interactions répulsives ou adhésives entre les cellules. Chez la souris, les cellules impaires expriment les récepteurs transmembranaires EphA4, B2, B3, tandis que les cellules paires expriment les ligands transmembranaires ephrinB1, B2, B3 (Xu et al., 2000). Chez le poisson-zèbre, la situation est sensiblement plus complexe puisque deux systèmes semblent imbriqués : un système comparable à la souris où l'expression de *epha4* (r3, r5) est complémentaire de celle de *ephrinb3* (r2,r4,r6) ; un second système faisant intervenir *ephb4a* dans r2-r3 et r5-r6 de façon complémentaire à *ephrinb2a* dans r1, r4 et r7 (Cooke and Moens, 2002) (Figure 6 C). La redondance entre les différents récepteurs Eph et ligands ephrine n'a pas permis d'étudier leur fonction chez la souris. En revanche, l'utilisation d'embryons de poisson mosaïques a permis de mettre en évidence les interactions répulsives entre cellules exprimant un Eph et des cellules exprimant une ephrine, ainsi que les interactions adhésives entre cellules exprimant des Eph ou cellules exprimant des ephrines. Par ailleurs, des expériences de perte de fonction par surexpression d'un dominant-négatif ont montré que la compartimentation du rhombencéphale est abolie en absence de système Eph/ephrine, que les cellules frontières sont absentes, et que

l'organisation des dérivés neuronaux est fortement perturbée (Xu et al., 1999; Cooke et al., 2005) (Figure 6F).

Peu de données sont disponibles concernant le contrôle génétique des effecteurs de la ségrégation cellulaire par les gènes de segmentation. La découverte des éléments régulateurs de *EphA4* chez la souris a permis d'établir l'activation directe de *EphA4* par Krox20 (Theil et al., 1998). Chez le poisson mutant *valentino* (*MafB*), r5 et r6 disparaissent au profit d'un domaine transitoire mal spécifié (rX) ; les cellules de rX n'expriment pas *EphB4a*, donc *valentino* est requis pour l'activation de *EphB4a* (Cooke et al., 2001). Au delà de ces deux exemples, la dépendance des récepteurs Eph ou des ligands ephrines vis-à-vis des gènes de segmentation n'est pas établie. Ce type d'étude s'avère en effet difficile à mener car la mutation des gènes de segmentation provoque généralement la perte des cellules des rhombomères correspondants (voir plus bas).

2.2.2. Activation des gènes Hox : L'expression des gènes de segmentation est transitoire ; elle s'achève entre 20 et 25 somites. La segmentation est ensuite définie par une combinaison de gènes *Hox*, qui suit la règle de colinéarité (excepté pour *Hoxa1* et *Hoxb1*) (Figure 5C). Les gènes *Hox* du rhombencéphale sont activés par les gènes de segmentation. À ce jour, un lien transcriptionnel direct a été établi entre *Krox20* et *Hoxa2* (dans r3, r5) (Nonchev et al., 1996), *Hoxb2* (dans r3, r5) (Sham et al., 1993), *Hoxb3* (dans r5) (Seitanidou et al., 1997), et entre *MafB* et *Hoxa3*, *Hoxb3* (dans r5, r6) (Manzanares et al., 1997; 1999). Ces études ont toutes été rendues possible par la caractérisation des éléments régulateurs des différents gènes *Hox* du rhombencéphale.

2.3. Principaux acteurs contrôlant le développement de la région r2-r6 (Moens and Prince, 2002; Alexander et al., 2009)

La segmentation du rhombencéphale est un modèle de spécification cellulaire *a priori* idéal car les lignages cellulaires sont séparés physiquement et il existe un gène maître, dit de segmentation, pour chacun d'entre eux. Ci-dessus, nous avons détaillé la façon dont les gènes de segmentation contrôle le destin des différents segments en assurant la ségrégation des cellules et la mise en place du code Hox (voir schéma synthétique, Figure 7A). Dès lors, comment l'expression des gènes de segmentation est-elle contrôlée ? Comment les signaux diffusibles présentés plus haut (Wnt, FGF, AR) interviennent pour définir les rhombomères ? Cette partie vise à présenter le réseau de gènes aboutissant à la formation des rhombomères, tel qu'il est compris aujourd'hui. Ce réseau intervient peu de temps avant la somitogenèse sur un territoire présomptif dont l'identité par défaut est r1 (Waskiewicz et al., 2002).

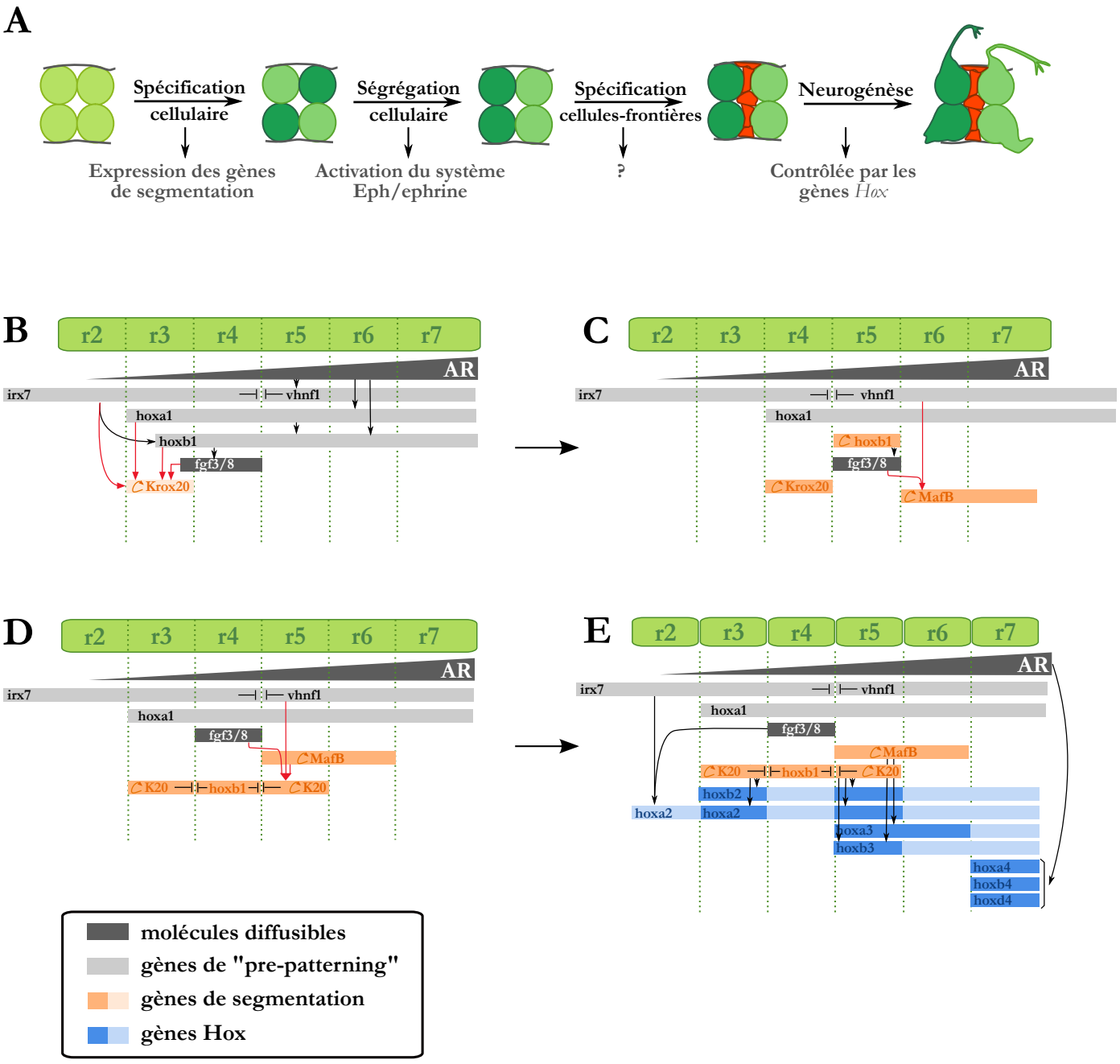

Figure 7 - Réseau de gènes contrôlant la segmentation du rhombencéphale

(A) Les grandes étapes de la segmentation du rhombencéphale. **(B-E)** Les principaux facteurs responsables de la segmentation du rhombencéphale et leur interdépendance. Les flèches peuvent indiquer des interactions directes ou indirectes. L'expression et l'activation des Eph et des ephrines ne sont pas indiquées sur ce schéma, par souci de concision.

L'acide rétinoïque (AR) est sécrété à partir des cellules qui expriment la rétinaldehyde déshydrogénase (Raldh2) situées dans le mésoderme paraxial et les somites antérieurs. Antérieurement à r3, l'AR est dégradé dans les cellules exprimant l'enzyme Cyp26. Ce système « *source-sink* » créé un gradient d'AR dans le rhombencéphale, avec de fortes concentrations dans r7 et faible vers r3 (Sirbu et al., 2005). L'AR contrôle l'expression d'un certain nombre de gènes en liant les récepteurs hormonaux nucléaires RAR et RXR qui, sous forme de dimères, se lient à l'ADN via des séquences RARE (*Retinoic Acid Response Element*).

Chez l'embryon de poisson-zèbre, le DEAB, un inhibiteur de Raldh2, provoque la disparition des rhombomères postérieurs (r5-r7) au profit de r3 et r4 (Maves and Kimmel, 2005). Ceci suggère l'implication de l'AR dans la régionalisation du rhombencéphale postérieur. De fait, l'AR induit l'expression des *Hox* du groupe paralogue 1 (*HoxPG1* : *Hoxa1*, *Hoxb1*), de façon directe comme le suggère la présence de RARE dans les séquences régulatrices de *Hoxa1* et *Hoxb1*(Marshall et al., 1992). L'AR active aussi le gène postérieur *vHnf1* (Figure 7B) (Pouilhe et al., 2007). Dans la partie antérieure du rhombencéphale, le rôle de l'AR n'est pas établi. Les *HoxPG1* sont bien exprimés dans les territoires présomptifs r3 et r4 mais leur activation dépend vraisemblablement d'une voie parallèle à l'AR, inconnue à ce jour.

De manière concomitante à la mise en place des *HoxPG1*, les cellules de pre-r4 et, de manière non-pérenne celles de pre-r3, activent l'expression de ligands FGF : Fgf3/8 chez le poisson-zèbre (Maves et al., 2002; Walshe et al., 2002; Wiellette and Sive, 2004), Fgf3 chez le poulet (Weisinger et al., 2008). Cette expression créent un gradient de ligands FGF dont l'inhibition affecte la segmentation de la région r3-r5 (Marín and Charnay, 2000; Walshe et al., 2002; Weisinger et al., 2010).

La mise en place de deux sources de molécules diffusibles, des domaines d'expression des *HoxPG1* et de *vHnf1* constitue la première étape de la segmentation du rhombencéphale. La deuxième étape consistera en la définition des rhombomères par la mise en place des gènes de segmentation. Enfin, l'identité de chaque segment sera assurée par l'activation des gènes *Hox*.

Les *HoxPG1* agissent de concert avec les cofacteurs *irx1b/7*, *Meis2* et *Pbx2/4* pour activer *Krox20* dans r3 (Wassef et al., 2008; Stedman et al., 2009). Cette activation requiert aussi l'activation de la voie FGF dans les cellules de pre-r3 (Figure 7B) (Marín and Charnay, 2000; Walshe et al., 2002). Krox20 exerce ensuite un retro-contrôle négatif sur *Hoxb1* en séquestrant un coactivateur essentiel à son expression, PiASxß (Giudicelli et al., 2001; Garcia-Dominguez et al., 2006). Ceci contribue à l'établissement de la frontière antérieure de *Hoxb1*. De manière symétrique,

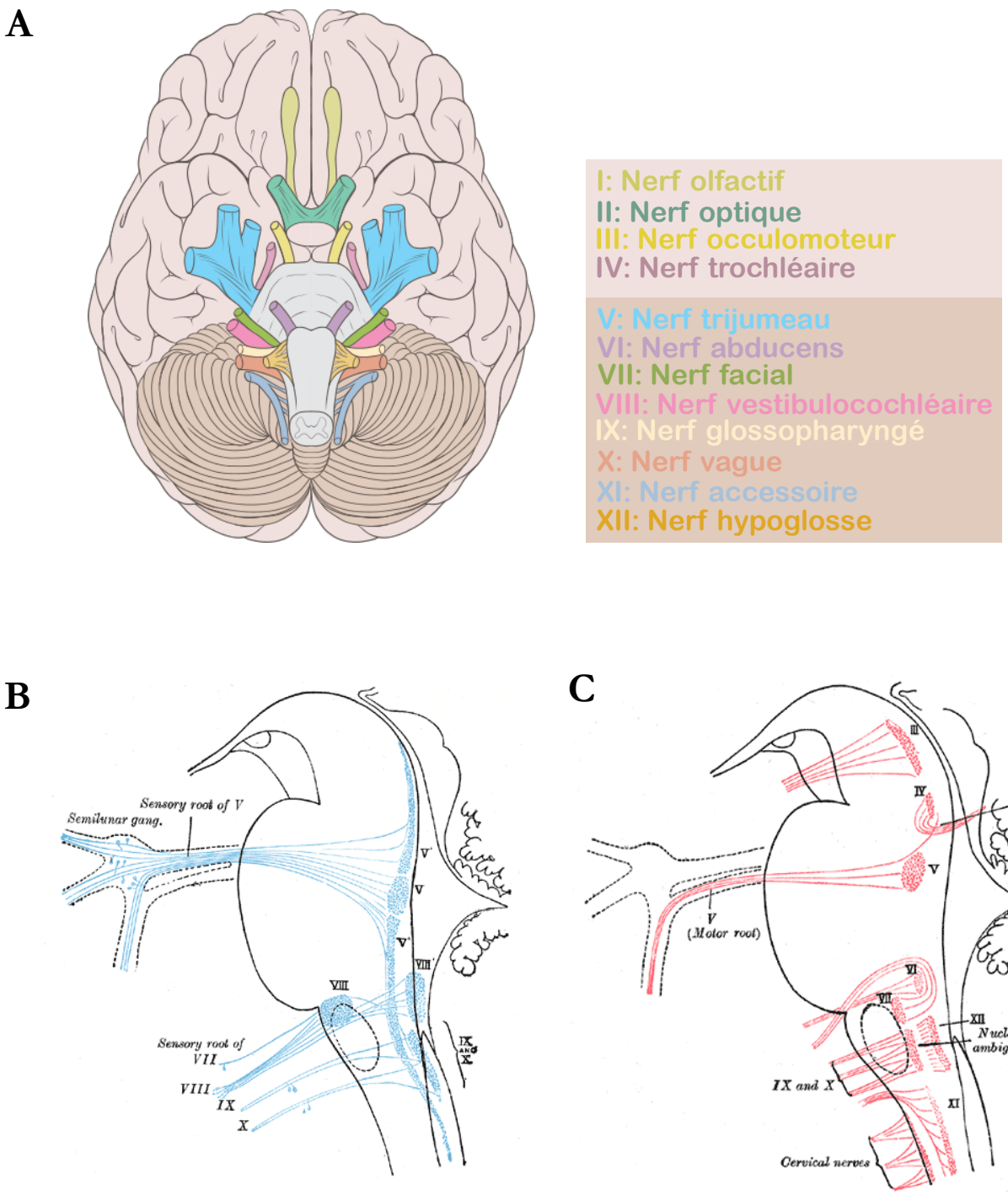

Figure 8 - Organisation des neurones sensoriels et moteurs du pons et de la medulla

(A) Schéma d'une vue ventrale d'un cerveau adulte humain, montrant l'organisation des nerfs crâniens. **(B,C)** Schémas des noyaux neuronaux et des projections sensoriels (B) et moteurs (C). Seul le volumineux ganglion trijumeau est représenté. Le chiffre en lettre romaine indique le nerf dans lequel chaque noyau neuronal projette. Ce même chiffre est utilisé dans les tableaux de la figure 9.

l'extension postérieure de *Krox20* est limitée par l'activité inhibitrice combinée de *Hoxb1* et *Hoxa1* (Capecchi, 1999). Le mécanisme de cette inhibition est en cours d'analyse par Charlotte Labalette au laboratoire.

La frontière postérieure du domaine *Hoxb1*$^{+}$, donc de r4, est définie par l'inhibition de l'identité r5. Cette inhibition est assurée par *irx7* sur *vHnf1* (Lecaudey et al., 2004). Le niveau d'*Hoxb1* est ensuite renforcé par autorégulation (Figure 7C).

Dans r5 et r6, *vHnf1* inhibe l'identité r4 en réprimant *Hoxb1* et *irx1b/7* (Hernandez et al., 2004; Lecaudey et al., 2004). En outre, *vHnf1* synergise avec la voie de signalisation FGF pour activer directement *MafB/val* (Figure 7C)(Kim et al., 2005). vHnf1, MafB et les FGFs coopèrent ensuite pour activer *Krox20* dans r5 (McKay et al., 1994; Moens et al., 1996), et ce de manière directe (Figure 7D) (Chomette et al., 2006; Labalette et al., 2011). Le mécanisme qui empêche *Krox20* d'être exprimé dans r6 reste inconnu à ce jour.

Les gènes de segmentation mis en place dans la région r3-r6 activent ensuite les *Hox* : comme vu plus haut, *Hoxa2/b2* sont sous contrôle de Krox20, *Hoxa3* sous contrôle de MafB et l'activation de *Hoxb3* requiert à la fois Krox20 et MafB. Dans r4, *Hoxb1* active l'expression des *Hoxa2/b2* à faible niveau (Maconochie et al., 1997; Ferretti et al., 2005; Tümpel et al., 2007)..

Enfin, l'identité r2 est définie par l'expression de *Hoxa2* à l'exception de tout autre *Hox*. *Hoxa2* est activé par les FGF, *irx1b/7* et *Sox1/2/3* (Walshe et al., 2002; Tümpel et al., 2008; Stedman et al., 2009). L'identité r7 quant à elle est définie par la coexpression de *Hoxb4* et *Hoxa4*, sous contrôle de l'AR (Figure 7E) (Packer et al., 1998; Serpente et al., 2005).

De ces interactions génétiques émerge un organe composé de sept segments qui sont autant d'unités homogènes de lignage cellulaire. Quelles sont les manifestations de cette segmentation à des stades plus tardifs, au moment où les cellules se sont différenciées en neurones ?

2.4. Dérivés neuronaux du rhombencéphale

Le rhombomère 1 dérive au stade adulte en cervelet, tandis que la région r2-r7 donne naissance au pons et à la *medulla oblongata*. Nous centrerons le propos sur ces deux dernières structures. Le pons et la medulla sont peuplées de neurones, organisés en noyaux, aux fonctions aussi diverses que les mouvements du cou, de la face, la mastication, la déglutition, le contrôle du rythme respiratoire, de la pression artérielle, de la température corporelle. Au stade adulte, l'anatomie de cette région est dominée par l'organisation segmentée de huit des douze nerfs crâniens (du V au XII) et des ganglions associés (Figure 8A, B, C). Des expériences de traçage ont été réalisées pour savoir s'il existe un lien entre la segmentation du rhombencéphale et l'architecture des nerfs

A

Noyau	Type	Projection dans nerf...	Spécifié		Situation finale	Cibles	Remarques
			dans...	par...			
Trijumeau moteur	Branchimoteur → BA1	Trijumeau (V)	r2-r3 (s,p)	*Hoxa2* + *Hoxb2* (r3)	Pons	Muscles de la mastication, digastriques, *tensor tympani.*	Absent chez *Krox20*$^{-/-}$
Abducens	Somatomoteur	Abducens (VI)	r5 (s), r5-r6 (p)	*Hoxa3/b3*	Pons	Muscle droit lateral (rotation de l'oeil)	Absent chez *Krox20*$^{-/-}$ et *MafB*$^{-/-}$
Facial moteur	Branchimoteur → BA2	Facial (VII)	r4 (s), r4-r5 (p)	*Hoxa1/b1*	Pons	Muscles de la face, digastriques	
Salivatoire supérieur	Visceromoteur	Facial (VII)	r5 (s)		Pons	Ganglions submandibulaires, pterygo/ sphenopalatin	Absent chez *Krox20*$^{-/-}$ et *MafB*$^{-/-}$
Ambiguus	Branchimoteur → BA3	Glossopharyngé (IX)	r6 (s), r7 (p)		Medulla	Muscle stylopharyngé	Nerf IX fusionné avec le nerf X chez le mutant *Krox20*$^{-/-}$
Salivatoire inférieur	Visceromoteur	Glossopharyngé (IX)	r6 (s)		Pons	Ganglion otique	
Ambiguus (bis)	Branchimoteur → BA3	Vague (X)	r7 (s,p)		Medulla	Muscles du pharynx, du larynx	
Dorsal moteur	Visceromoteur	Vague (X)	r7-r8 (s,p)		Medulla	Muscles lisses des viscères throraciques et abdominaux	
Ambiguus (ter)	Branchimoteur → BA4	Accessoire (XI)	r7-r8 (s,p)		Medulla	Muscles du pharynx et du larynx	
Hypoglosse	Somatomoteur	Hypoglosse (XII)	r8 (s,p)	*Hoxa3/b3*	Medulla	Muscles de la langue	

B

Noyau	Type	Afférences du nerf...	Spécifié dans...	Situation finale	Organes sensoriels
Trijumeau spinal/descendant	Sensoriel	Trijumeau (V)	r2-r6 (p)	Medulla	Toucher, douleur, température
Trijumeau principal	Sensoriel	Trijumeau (V)	r1 (p)	Pons	Toucher, propriocéption de la mâchoire
Cochléaire	Sensoriel	Vestibulo-cochléaire (VIII)		Pons	Cochlée / Son
nucleus magnocellularis			r6-r7 (p)		
nucleus angularis			r3-r6 (p)		
nucleus laminaris			r5-r6 (p)		
noyau de l'olive supérieure			r5 (p)		
noyau lemniscal latéral			r1-r3 (p)		
Vestibulaire	Sensoriel	Vestibulocochléaire (VIII)		Medulla/Pons	Canaux semi-circulaires de l'oreille interne
nucleus quadrangularis			r1-r3 (p)		
noyau supérieur			r1-r3 (p)		
noyau A de Wold			r1-r3 (p)		
noyau de Deiters ventral			r4 (p)		
noyau vestibulaire supérieur			r4 (p)		
nucleus tangentialis			r4-r5 (p)		
noyau vestibulaire médian			r6-r7 (p)		
noyau de Deiters dorsal			r3-r5 (p)		
Solitaire principal	Sensoriel	Facial (VII), Glossopharyngé (IX), Vague (X)	r7-r8 (p)	Medulla	Barorécepteurs artériels, carotide, corps aortiques
Pontin/pontique	Réticulaire		r1-r7 (p-	Pons	Relais cervelet -cortex moteur
Olive inférieure	Réticulaire		r6 (p)	Medulla	Relais cervelet-moelle

Figure 9 - Nomenclature et caractéristiques des neurones spécifiés dans le rhombencéphale

(A) Tableau des noyaux moteurs. **(B)** Tableau des noyaux sensoriels dont les neurones sont spécifiés dans le rhombencéphale (par opposition aux neurones sensoriels dérivant des placodes ectodermiques et des crêtes neurales). p: poulet ; s: souris.
D'après Marin & Puelles 1995 et Guthrie 2007.

crâniens (voir par exemple (Marín and Puelles, 1995; Dymecki et al., 2010)). La réponse est variable selon le type de neurones : certains sont spécifiés dans le rhombencéphale et migrent très peu, donc conservent leur organisation en segments ; d'autres sont spécifiés dans le rhombencéphale mais migrent en dehors ; d'autres enfin viennent peupler le pons et la medulla alors qu'il n'ont pas été spécifiés dans le rhombencéphale. Ainsi, la segmentation des nerfs crâniens ne fait pas vraiment écho à la spécification segmentée des neurones, mais plutôt à la position des points de sortie de nerfs, disposés très tôt au cours du développement, au niveau de r2, r4, r6 et r7 (Figure 5C). Dans cette partie, les grands types de neurones sont décrits puis leurs caractéristiques essentielles, notamment leur origine embryonnaire, sont consignées deux tableaux récapitulatifs (Figure 9A, B).

Les trois grands types de neurones sont spécifiés dans le rhombencéphale, à savoir les motoneurones, les neurones sensoriels et les « interneurones » (au sens large, c'est-à-dire des neurones multipolaires établissant des connexions avec d'autres neurones).

Les mieux connus sont les motoneurones. Il en existe de trois types : les branchiomotoneurones innervent les arcs branchiaux, à l'origine des muscles et tissus conjonctifs de la face, de la mâchoire, du pharynx et du larynx ; les somatomotoneurones innervent les muscles striés de l'œil, de la langue ; les visceromotoneurones innervent les ganglions sympathiques et parasympathiques, et prolongent leurs terminaisons vers les glandes salivaires, lacrymales, les muscles lisses des viscères (Lumsden and Keynes, 1989; Lumsden and Krumlauf, 1996). Tous ces motoneurones sont spécifiés dans le rhombencéphale, et projettent dans les nerfs crâniens.

En ce qui concerne les neurones sensoriels, certains sont spécifiés dans le rhombencéphale mais la majorité dérive des placodes ectodermiques et des crêtes neurales. Ces neurones ont leurs corps cellulaires dans les ganglions crâniens.

Enfin, les interneurones constituent la famille la plus disparate et la plus mal connue (en ce qui concerne l'origine embryonnaire). La majorité d'entre eux constitue la formation réticulée. Il s'agit d'environ cent petits réseaux neuronaux dont les fonctions sont variées : relais des informations sensorielles (œil, toucher, ouïe) vers le cervelet pour assurer la coordination motrice, production de signaux rythmiques (respiration et réflexe d'avalement), contrôle de la vasodilatation, contrôle de l'endormissement, de l'état de conscience (via des projections vers le thalamus et le cortex cérébral). Une bonne partie de ces neurones est spécifiée dans le rhombencéphale mais les données de traçage sont lacunaires, eu égard à la complexité de l'anatomie réticulaire. Voici quelques exemples de noyaux réticulés connus :

- les noyaux du raphé, sérotoninergiques, spécifiés dans tout le rhombencéphale sauf r4 ;

- le noyau rétrotrapezoïde, responsable de la sensibilité au CO_2/pH dans le sang, et donc du rythme respiratoire. Ces neurones sont spécifiés dans r5 (Dubreuil et al., 2009).
- le noyau sensoriel principal : relais entre les vibrisses (*whisker-pad*) et le cortex en tonneaux (*barrel cortex*). Ce noyau est spécifié dans r3 par *Hoxa2* et conserve la même topographie « barreloïde » que le *whisker-pad*, le relais thalamique et le *barrel cortex*. La segmentation du rhombencéphale joue ici un rôle dans la somatotopie du système vibrisse-cortex en tonneaux (Oury, 2006).

Un réseau génétique permet la formation de segments dont chacun dérivera en un certain nombre de neurones. Ainsi, la structure des rhombomères, leur taille, leur forme, leur position peut avoir un impact direct sur l'architecture neuronale du cerveau postérieur. Comment le nombre de cellules contenues dans chaque rhombomère est-il déterminé ? Cela peut être en partie lié à la position des frontières le long de l'axe rostro-caudal. Comment le positionnement des frontières s'opère-t-il ? Les gradients d'AR ou FGF jouent-ils un rôle dans ce processus ? Ont-il alors un rôle de morphogène ? Ces questions requièrent une meilleure compréhension des mécanismes qui déterminent le patron d'expression des gènes, puisque finalement la morphologie des rhombomères est directement liée à ces patrons. Pour comprendre comment un gène s'exprime à un endroit précis, à un moment donné, il convient d'étudier la façon dont les facteurs situés en amont régulent l'activité de leur cible au niveau transcriptionnel.

3. Contrôle transcriptionnel de la « spécification cellulaire régionalisée »

3.1. Fonctionnement canonique des promoteurs et séquences régulatrices

De manière générale, la régulation de l'expression génétique opère à différents niveaux : le niveau transcriptionnel en régulant les étapes de démarrage et/ou d'élongation de la transcription ; le niveau post-transcriptionnel, à travers la maturation, le transport, la dégradation des ARNm ; le niveau traductionnel, avec la régulation de l'initiation et la terminaison de la traduction ; et le niveau post-traductionnel, par la modification des structures secondaire, tertiaire ou quaternaire des protéines et surtout la régulation de leur demi-vie. Dans cette partie, seuls les mécanismes de régulation transcriptionnelle seront abordés qui, eux-mêmes, peuvent être répartis en deux catégories : la régulation de l'activité des promoteurs transcriptionnels par l'action de séquences *cis*-régulatrices ou par la modulation de leur état chromatinien. Nous verrons que ces deux niveaux de régulation sont en fait intimement liés.

La transcription de gènes codant pour des protéines est assurée par un enzyme, l'ARN polymérase II (PolII). La régulation de la transcription peut s'effectuer à quatre niveaux : le

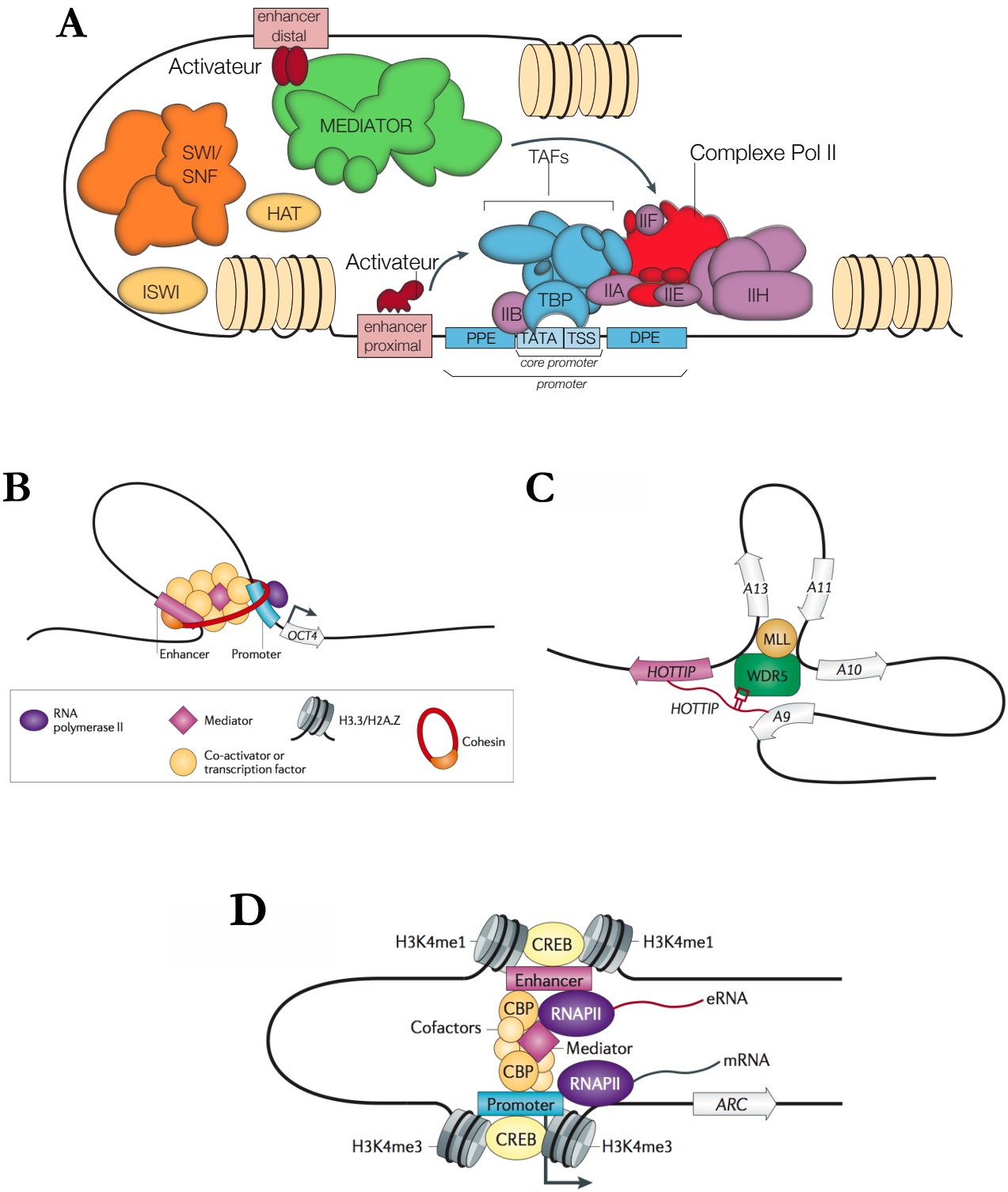

Figure 10 - Fonctionnement et régulation de la machinerie transcriptionnelle

(A) Les principaux acteurs en présence au niveau du promoteur d'un gène, au moment de son activation. La formation d'une boucle d'ADN assure l'interaction entre le promoteur, les enhancers et leurs protéines associées. **(B)** Le maintien des boucles d'ADN est notamment assuré par les cohésines. Contrairement à ce qui est représenté ici, les cohésines coopèrent dans certains types cellulaires avec le FT CTCF et le complexe Mediator. **(C)** Rôle du lincRNA HOTAIR dans l'activation du cluster HoxA chez l'homme : maintien de la boucle et recrutement d'un complexe de remodelage chromatinien. **(D)** L'ARN PolII recrutée au niveau du complexe enhancer-promoteur peut transcrire le gène cible et l'enhancer lui-même. La quantité de eRNA ainsi produit est positivement corrélée au niveau d'activation du gène, mais le mécanisme moléculaire sous-jacent reste inconnu. D'après Taatjes et al., 2004 (A) et Ong & Corces, 2011 (B,C,D).

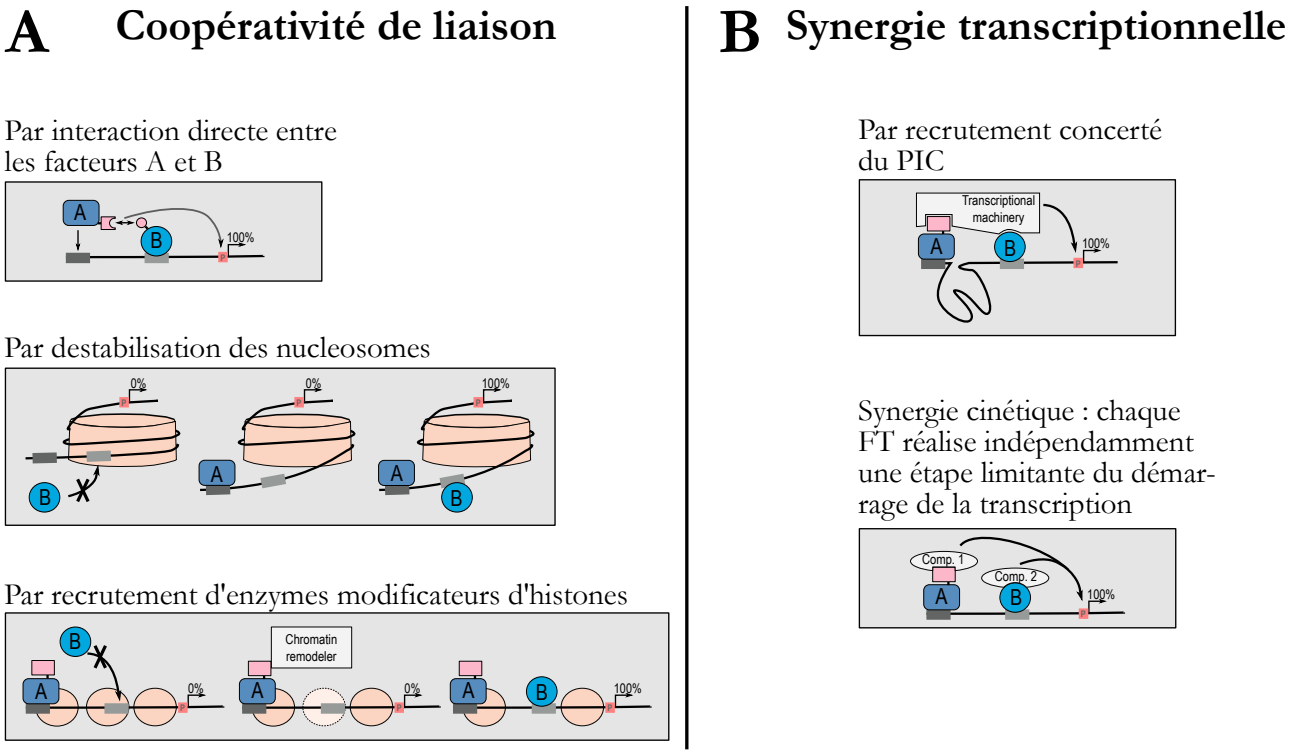

Figure 11 - Différentes stratégies de coopération entre facteurs de transcription liés à une même séquence

La concentration de sites de liaison rencontrée sur les éléments régulateurs augmente la spécificité de liaison des FT. Plusieurs mécanismes peuvent être envisagés, selon que les FT coopèrent pour lier l'ADN (A) ou pour activer la machinerie transcriptionnelle (B).
D'après Vashee *et al.*, 1998

recrutement de la machinerie transcriptionnelle impliquant la PolII sur le site de démarrage de la transcription (TSS, *transcription start site*), le démarrage de la transcription, l'élongation, la terminaison. Le premier niveau de contrôle est semble-t-il le plus utilisé. Il est le fait de protéines capables de lier l'ADN, les facteurs de transcription (FT). Les FT généraux (*basal transcription factors*) lient le promoteur du gène, c'est-à-dire une séquence de 100 pb environ, située juste en amont du gène, comprenant la boîte TATA, le TSS, des éléments promoteurs proximaux (PPE) et des éléments promoteurs d'aval (DPE) (Taatjes et al., 2004). Ces facteurs s'assemblent et forment le complexe de pré-démarrage (PIC, *pre-initiation complex*). La formation du PIC est généralement conditionnée par la présence de FT spécifiques, véritables instructeurs de la transcription, liant des séquences d'ADN plus distantes, en amont ou en aval du promoteur. Ces séquences régulatrices agissent en *cis,* i.e. sur un promoteur situé sur le même chromosome. Elles sont des « amplificateurs transcriptionnels » (*enhancer*) lorsque les FT (agissant en *trans*) qui s'y lient favorisent la formation du PIC, ou des « répresseurs transcriptionnels » (*silencer*) lorsque les FT sont des répresseurs. Une fois le PIC formé, le démarrage de la transcription est rendu possible par une modification de l'état chromatinien de la région promotrice grâce au recrutement des complexes Mediator et SWI/SNF (Figure 10A).

Sur le plan de leur structure, la définition des séquences régulatrices n'est pas triviale. En première approche, elles correspondent à des zones restreintes du génome dont la taille varie de quelques dizaines à quelques milliers de nucléotides. Elles peuvent se situer en amont, en aval ou dans la séquence codante du gène. Elles sont caractérisées par la présence de sites de liaison pour des FT spécifiques. La plupart des séquences régulatrices comprennent plusieurs sites, pour plusieurs types de FT, formant ainsi des « îlots de régulation ». Ceci n'exclut pas que des sites isolés dans le génome contribuent à modifier l'activité des promoteurs. Ces sites isolés sont aussi des séquences régulatrices. Ceci dit, le fonctionnement en îlots de régulation est le plus fréquent. Il permet à plusieurs FT de coopérer soit pour lier l'ADN (coopérativité de liaison), soit pour recruter le PIC (synergie transcriptionnelle), et ainsi d'assurer une spécificité de reconnaissance entre FT et séquence (Vashee et al., 1998a; 1998b; Georges et al., 2010) (Figure 11). L'idée d'un code de coopération entre FT partenaires a fait émerger le concept d'*enhanceosome* (Panne, 2008).

L'expression d'un gène dans une population donnée de cellules, à un moment précis du développement et à un certain niveau dépend donc du type et du nombre de FT spécifiques qui le régulent. Ces informations sont contenues dans les séquences *cis*-régulatrices d'où l'importance de les identifier et de les analyser. Par ailleurs, le contrôle de l'expression génétique par les séquences régulatrices constitue un avantage évolutif. L'expression de certains gènes est complexe, soit par leur dynamique, soit par le nombre de sites d'expression. L'utilisation de

plusieurs séquences régulatrices permet de découpler le contrôle transcriptionnel des différentes phases de l'expression dans le temps, ou des différents sites d'expression. Ceci offre une grande souplesse évolutive car chaque élément peut évoluer indépendamment, d'où l'idée que l'évolution des séquences régulatrices – et non seulement de la séquence codante – sous-tend un grand nombre de changements évolutifs (Carroll, 2005; Prud'homme et al., 2007).

3.2. Statut chromatinien du promoteur et des séquences régulatrices

La vision des éléments régulateurs décrite ci-dessus est dans le prolongement de celle du promoteur : il s'agit de séquences liant des FT spécifiques qui interagissent avec les FT généraux pour recruter l'ARN PolII. Le développement récent d'outils d'étude des séquences cis-régulatrices à l'échelle du génome, par ChIP-seq notamment, a permis de sensiblement modifier cette vision. Grâce à ces techniques, il a été possible de caractériser les séquences régulatrices sur des critères chromatiniens, à savoir la présence/absence de nucléosome, le type de variants d'histones composant ces nucléosomes, le type de modifications post-traductionnelles que portent ces histones. Ces critères sont rassemblés sous le terme d' « épigénétique » qui, dans ce contexte, appelle tout processus héritable aboutissant à la modification de l'expression d'un gène sans altération de la séquence nucléotidique (Heintzman et al., 2007). Ainsi, les frontières des séquences cis-régulatrices sont marquées par un fort taux de remplacement d'histones, en faveur des variants H3.3 et H2A.Z (Mito et al., 2005; 2007). Ces variants promeuvent la plasticité des nucléosomes et par la même accommodent la liaison aux FT spécifiques. Par ailleurs, les enhancers en particulier sont marqués par la liaison à deux acétyltransférases, CBP et p300 (Bedford et al., 2010) et des modifications post-traductionnelles de type H3K4me1/me2 (méthylation unique ou double de la lysine 4 de l'histone 3), H3K27ac (acétylation de la lysine 27 de l'histone 3). Le rôle de l'information épigénétique portée par les séquences régulatrices et les promoteurs est apparu prépondérant dans la décision d'activer tel ou tel gène ou bien encore dans l'interaction entre les éléments régulateurs et les promoteurs.

3.2.1. Signatures chromatiniennes associées à l'activation d'un gène : un locus peut se trouver dans trois états, caractérisés par des états chromatiniens différents (Creyghton et al., 2010; Rada-Iglesias et al., 2011) (Heintzman et al., 2009):

- réprimé : l'ARN PolII est absente du promoteur

- prêt (*poised*) : l'ARN PolII est sur le promoteur mais l'élongation n'a pas démarré ; les enhancers sont riches en variants H3.3, H2A.Z et les histones présentent les modifications H3K4me1/me2 , H3K27me3.

- actif : l'élongation de la transcription démarre. La marque H3K27me3 des enhancers est modifiée en H3K27ac.

Dans l'état « prêt », les marques d'histones assurent le recrutement de FT dits « pionniers » qui par la suite recrutent d'autres enzymes modificateurs d'histones pour acétyler la lysine 27 de l'histone 3 et les FT spécifiques nécessaires à l'activation (Lupien et al., 2008; Zaret et al., 2008).

Un tel état « prêt » des enhancers a pu être mise en cause dans la spécification de certains lignages cellulaires. Ceci implique que la population de cellules donnant naissance à deux lignages n'est pas strictement homogène. Il existe, avant même l'activation des deux programmes de développement, une marque épigénétique qui définit le destin cellulaire. Ce déterminisme précoce des lignages cellulaires vient affaiblir les modèles d'activation stochastique des différents programmes de développement (Laslo et al., 2006; Krysinska et al., 2007).

3.2.2. Modulation de l'interaction promoteur-enhancer : comment des séquences régulatrices situées à plusieurs dizaines de kilobases du promoteur – jusqu'à 1 Mb dans le cas du gène *Sonic-Hedgehog* (Sagai et al., 2005) – peuvent contrôler le recrutement de la machinerie transcriptionnelle ? Il existe en fait une interaction physique entre les éléments régulateurs et le promoteur de chaque gène, comme le suggèrent des expériences récentes de « Capture de Conformation Chromosomique » (3C). Cette interaction a lieu dans des zones spécifiques du noyau, riches en PolII et ses cofacteurs (les « usines à transcription », *transcription factories*). Ainsi, des boucles d'ADN sont formées par l'interaction entre les FT spécifiques et la machinerie transcriptionnelle, mais aussi par l'association d'enzymes modificateurs d'histones positionnés aux enhancers et au promoteur. Ces enzymes forment des complexes de remodelage chromatinien responsables *in fine* de la décompaction de l'ADN avant l'activation du gène. Enfin, le maintien de ces boucles est assuré par la cohésine, protéine recyclée en mitose pour assurer la cohésion des chromatides sœurs (Figure 10B) (Hadjur et al., 2009; Nativio et al., 2009; Hou et al., 2010; Kagey et al., 2010).

Quels mécanismes restreignent l'activité des éléments régulateurs envers leur promoteur cible alors qu'ils en sont si éloignés ? Un premier mécanisme consiste à rendre spécifique l'interaction enhancer-promoteur. Des séquences propres au promoteur, la DPE ou des motifs TATA, peuvent être impliqués dans cette spécificité (Butler and Kadonaga, 2001). Un autre mécanisme consiste à définir des domaines de régulation au sein du chromosome. Ces domaines sont isolés les uns des autres par des frontières, de sorte que l'action d'un élément ne puisse pas affecter l'activité d'un promoteur au-delà de cette frontière. Sur le plan moléculaire, ces frontières sont appelées des insulateurs, eu égard à leurs propriétés d'isolement. Les insulateurs peuvent

fonctionner de deux manières : il s'agit soit d'*enhancer-blockers* qui bloquent les interactions enhancer-promoteur, soit d'insulateurs-barrières qui protègent contre la propagation de l'hétérochromatine (Gaszner and Felsenfeld, 2006; Raab and Kamakaka, 2010).

3.2.3. Rôle des ARN non-codants : deux types d'ARN non-codants ont un rôle régulateur dans l'activation de la transcription :

- les ARN-enhancer (eRNA) sont transcrits à partir de la séquence des enhancers. Leur abondance est positivement corrélée au degré d'activation des gènes alentours ; leur transcription requiert la présence d'un promoteur. Les eRNA sont transcrits par l'ARN PolII, au sein des complexes enhancer-promoteurs. Leur rôle est encore mal compris : ils pourraient faciliter l'activation de la transcription et/ou assurer la cohésion des complexes (Figure 10D) (Lei and Corces, 2006; Yao et al., 2010).

- les longs ARN intergéniques (lincRNA), dont l'exemple le plus emblématique est l'ARN HOTAIR qui, chez l'humain, participe à l'activation du cluster HoxA et la répression de HoxD (Tsai et al., 2010). HOTAIR est responsable de l'assemblage d'une protéine adaptatrice WDR5 et d'un complexe de méthyltransférases d'histones MLL. MLL triméthyle ensuite le locus HoxA d'où l'activation de la transcription (Figure 10C).

Dans la suite de ce travail, nous nous intéresserons aux mécanismes transcriptionnels contrôlant la mise en place du patron d'expression de *Krox20* dans le rhombencéphale. Le rôle des marques épigénétiques ne sera pas abordé dans la partie « Résultats », mais sera discuté ensuite.

4. Spécification des rhombomères r3 et r5 : *Krox20* en chef d'orchestre

4.1. La petite histoire du gène *Krox20* dans la grande histoire de la biologie du développement

Le grand public a découvert le gène *Krox20* en 1988, à l'occasion d'une publication du jeune groupe de Patrick Charnay à l'EMBL (Chavrier et al., 1988). L'article présente *Krox20* comme un gène impliqué dans la réponse précoce au sérum et donc dans la transition G0/G1 en culture cellulaire. Il faudra attendre 1989 pour voir *Krox20* impliqué dans la segmentation du rhombencéphale, grâce à une hybridation *in situ* radioactive sur embryons de souris réalisée par David Wilkinson (Wilkinson et al., 1989). Comment le gène *Krox20* a-t-il été découvert ? Comment l'idée d'une hybridation *in situ* sur embryon est-elle venue ? Pour répondre à ces questions, il faut se replacer dans le contexte de l'époque.

La fin des années 1980 fait suite à deux décennies d'études poussées sur l'embryon de Drosophile. La célèbre cascade de segmentation responsable du *patterning* de l'axe antéro-postérieur chez la Drosophile vient d'être décrite. Avec elle le rôle des gènes homéotiques dans l'assignation d'une identité à chaque métamère séduit la communauté scientifique tant ce concept paraît « naturel ». Dès lors, de nombreuses équipes se mettent à rechercher des homologues des gènes de segmentation et des gènes homéotiques chez les Vertébrés. En 1984, les premiers homologues des gènes Hox sont clonés chez la souris (McGinnis et al., 1984). Patrick Charnay décide de rechercher des homologues du gène gap *Krüppel*. Chez la Drosophile, Krüppel possède un domaine de liaison à l'ADN composé de trois unités quasi-identiques d'une trentaine d'acides aminés, contenant deux histidines et deux cystéines en positions invariantes, et capables de se replier autour d'un ion Zn^{2+}(Preiss et al., 1985). Ces unités forment trois doigts à zinc de type C_2-H_2 (Klug and Rhodes, 1987; Redemann et al., 1988; Klug, 2010). Le parallèle avec l'homéodomaine des protéines Hox laisse supposer que les protéines à doigts à zinc forment une famille conservée entre la Drosophile et les Vertébrés. Philippe Chavrier utilise les doigts à zinc de Krüppel pour réaliser un crible à faible stringence contre une banque d'ADN génomique murin – 23 clones identifiés – et contre une banque d'ADNc originaires de fibroblastes murins 3T3 induits aux FGF : 1 clone identifié est commun à ces deux cribles. Il s'agit de *Krox-20*. Le fait que ce gène soit induit par des facteurs de croissance le rendait à l'époque singulièrement intéressant, d'où la publication de 1988 montrant que *Krox20* est activé lors de la transition G0/G1 après induction par le sérum. Cette caractéristique placera *Krox20* quelques années plus tard dans la famille des Egr (*Early Growth Response factors*) sous le sobriquet *egr2*. Des gènes induits par des facteurs de croissance, donc des signaux extra-cellulaires, sont de bons candidats de gènes de développement. David Wilkinson, le pape de l'hybridation *in situ* dont le succès, à l'époque, était une véritable prouesse, est alors mandaté pour réaliser l'expérience sur embryons de souris à des stades précoces de développement, i.e. au moment où les *Hox* sont exprimés dans le système nerveux : *Krox20* est exprimé à 8,5 jpc en deux bandes dans le cerveau postérieur (Figure 12A). Un tel profil, dans un organe destiné à être morphologiquement segmenté, ne pouvait pas mieux rappeler les gènes de segmentation de la Drosophile. Bien des études par la suite corroboreront ou affaibliront ce parallèle (Schneider-Maunoury et al., 1998). Aujourd'hui les circuits génétiques responsables de la segmentation chez la Drosophile ou dans le rhombencéphale présentent plus de différences que d'homologies. Deux raisons, les plus évidentes, peuvent être avancées : la segmentation du rhombencéphale a lieu dans un système cellulaire et non syncitial. Les processus de diffusion, à l'origine de la grande efficacité et rapidité des premières étapes de la segmentation de la Drosophile ne s'appliquent donc pas au rhombencéphale. En outre, les gènes maternels

A Première hybridation *in situ* anti-*mKrox20*
Wilkinson *et al.*, 1988

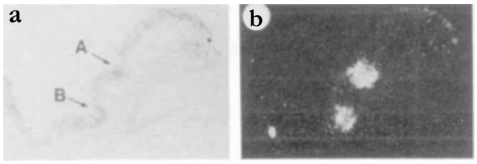

B Structure de la protéine Krox20 de souris
Desmazières *et al.*, 2009

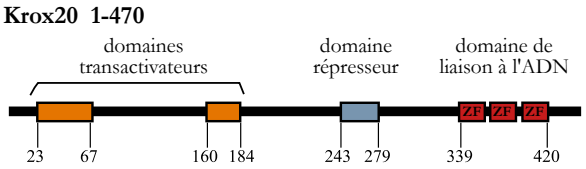

C Marquage lacZ sur embryons de souris sauvages et mutantes pour le gène *Krox20*
Schneider-Maunoury *et al.*, 1993

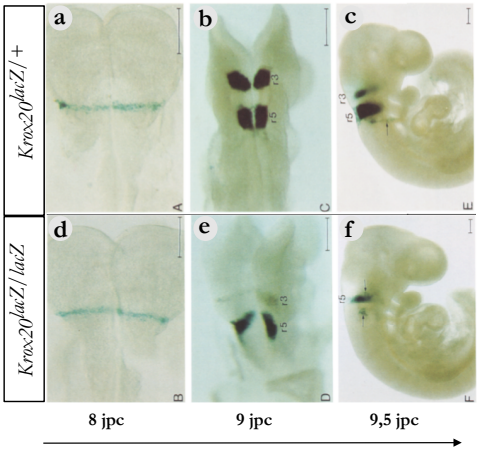

D Expérieces de gain de fonction Krox20 réalisées par électroporation dans le tube neural de poulet
Giudicelli *et al.*, 2001

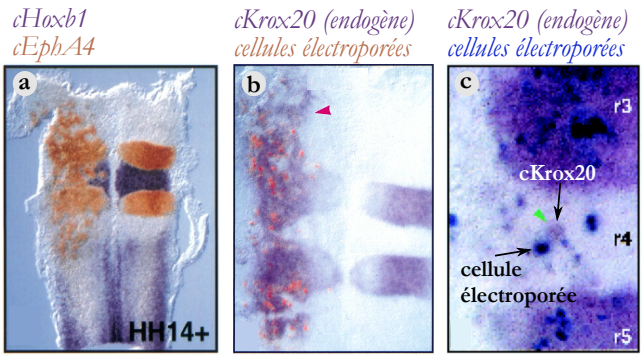

E Modèle de développement des rhombomères 3 et 5 proposé en 2001. Ici, seul le cas de r3 est illustré
Giudicelli *et al.*, 2001

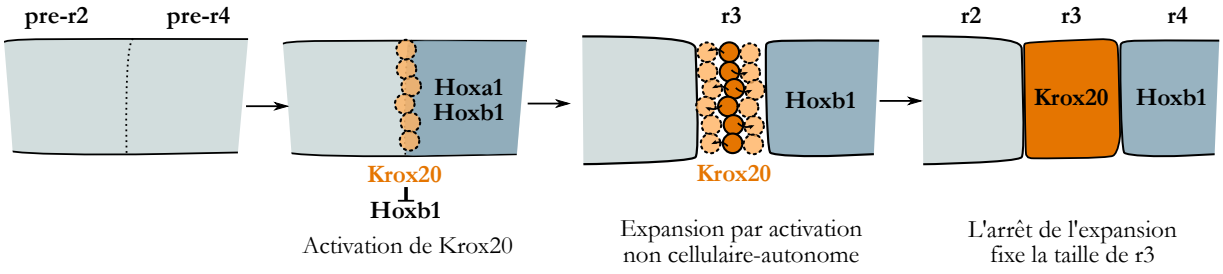

Figure 12 - Les grandes étapes de la recherche sur le gène *Krox20* (1)

(A).Première hybridation *in situ* radioactive ciblant *Krox20* réalisée sur embryon de souris à 8,5 jpc. **(B)** Schéma de la structure de la protéine Krox20. **(C)** Marquages ßGal réalisés sur des embryons sauvages (a-c) ou mutants (d-f) pour *Krox20*. La ßGal a été insérée à la place de la séquence codante de *Krox20*. Ceci révèle (i) que le maintien de l'expression du gène n'est pas assuré chez le mutant alors que le démarrage est intact, (ii) que l'expression de *Krox20* dans r3 requiert une phase d'expansion, elle aussi absente chez le mutant. (D) Marquages sur tubes neuraux de poulet réalisés par hybridation in situ après l'électroporation par un vecteur d'expression de *mKrox20*. La protéine mKrox20 ectopique active *EphA4*, réprime *Hoxb1* (a), active le gène endogène *cKrox20* (b) et ce de façon cellulaire-autonom et non cellulaire-autonome (c). **(E)** Modèle de développement de r3 en deux temps : initiation de *Krox20* dans une fine bande de cellules, puis expansion du territoire *Krox20*$^{+}$ par activation non cellulaire-autonome.

Bicoïd et *Caudal*, dont l'expression en gradient fournit une information de position chez la Drosophile, ne trouvent pas d'analogues évidents chez les Vertébrés.

4.2. Krox20 : structure, fonction, formation de r3 et r5

L'équipe de Patrick Charnay a logiquement décidé de se concentrer sur le rôle de *Krox20* dans le rhombencéphale. L'étude des propriétés de la protéine a permis d'identifier Krox20 comme un facteur de transcription activateur comprenant trois doigts à zinc de type C_2-H_2 (Chavrier et al., 1989; 1990) et définir les bases moléculaires de la spécificité de reconnaissance entre Krox20 et l'ADN (Nardelli et al., 1991; 1992). Par la suite, deux domaines de la protéine impliqués dans l'activation transcriptionnelle (domaines transactivateurs) et un domaine répresseur liant les protéines Nab1/2 ont été identifiés (Figure 12B) (Vesque and Charnay, 1992; Russo et al., 1995). Dès lors, l'étude de *Krox20* au cours du développement embryonnaire s'est articulée autour de trois axes :

- L'identification de certaines cibles transcriptionnelles directes, dont les premières recherchées ont été parmi les *Hox* (*Hoxb2* (Sham et al., 1993), *Hoxa2* (Nonchev et al., 1996) et *Hoxb3* (Seitanidou et al., 1997)), puis dans la famille des récepteurs à tyrosine kinase (*EphA4* (Theil et al., 1998)). *EphA4* avait en effet été identifié comme un bon candidat pour expliquer la ségrégation des cellules paires et impaires, car exprimé spécifiquement dans r3 et r5 (Gilardi-Hebenstreit et al., 1992; Nieto et al., 1992). L'identification de ces cibles a nécessité la description des éléments régulateurs de chaque gène, la démonstration d'une liaison directe de Krox20 par expériences de retard sur gel (*electromobility shift assay*) et la mise en évidence d'une transactivation Krox20-dépendante par transgénèse murine.

- L'analyse du phénotype mutant *Krox20*, après remplacement du gène par la séquence codante de la ß-galactosidase (Schneider-Maunoury et al., 1993). La majorité des mutants meure très peu de temps après la naissance ; certains néanmoins survivent jusqu'à deux ou trois semaines. Chez des embryons mutants aux stades 9,5-11,5 jpc, une désorganisation profonde des nerfs crâniens a pu être mise en évidence (Schneider-Maunoury et al., 1997). Les causes de ces deux phases de mortalité n'ont pas été formellement identifiées. La phase précoce peut être liée à des défauts respiratoires et/ou de mastication, en lien avec les anomalies détectées dans le rhombencéphale, décrites ci-dessous. *Krox20* est aussi exprimé dans les valves cardiaques. Un dysfonctionnement du cœur ne peut donc pas être exclu. La phase tardive de mortalité est vraisemblablement liée à l'affection sévère du système nerveux périphérique provoquée par l'absence de cellules de Schwann myélinisantes. Des mutants conditionnels, spécifiques de chaque lieu d'expression du gène, sont requis pour trancher ces questions.

Le marquage ß-gal sur embryons mutants à E8,0-E8,5 (0 somite) a révélé que le démarrage de l'expression de *Krox20* dans r3 a lieu correctement chez le mutant, dans une fine bande de cellules (Figure 12Ca,d). En revanche, ce marquage précoce disparaît rapidement, vers 8 somites, comme révélé par hybridation *in situ* (et non par marquage *lacZ*, compte tenu de la longue demi-vie de la ß-gal) (Figure 12Cb,e).

Dans r5, la situation est sensiblement différente : l'expression de *Krox20* démarre dans un large domaine dont la taille est proche de la taille finale de r5 (Figure 12Cb,e) ; l'expression est ensuite maintenue jusqu'aux stades 13-15 somites puis disparaît prématurément, la fin d'expression de *Krox20* ayant lieu à 25 somites dans un embryon sauvage. Ces profils indiquent que l'expression de *Krox20* est biphasique, comprenant une phase de démarrage, puis une phase de maintien absente chez le mutant. Ceci suggère que le maintien de l'expression dépend de la protéine Krox20 elle-même, d'où la première mise en évidence d'une autorégulation, directe ou indirecte. En outre, dans r3, le territoire ß-gal$^+$ est toujours plus fin que la taille définitive du rhombomère dans un embryon sauvage, d'où l'hypothèse d'une phase d'expansion du territoire *Krox20*$^+$ consécutive à la phase de démarrage. À nouveau, l'expansion étant absente chez le mutant, elle est sous contrôle de la protéine Krox20.

Enfin, de manière générale, l'étude du mutant a révélé l'absence de rhombomères r3 et r5, suggérant soit que les cellules de ces deux rhombomères meurent, soit qu'elles sont reprogrammées en cellules paires. Des expériences de traçage, réalisées au moyen d'un *knock-in* de la recombinase Cre au locus *Krox20* (allèle Krox20^{Cre}), montrent que les deux phénomènes ont lieu : dans un premier temps, les cellules de r3 sont reprogrammées en cellules de r2 et r4 alors que celles de r5 sont reprogrammées en cellules de r6. Dans un second temps, la taille du rhombencéphale diminue à travers un réajustement de la taille des rhombomères pairs par apoptose, de sorte que les rhombomères pairs subsistant dans le rhombencéphale mutant ont une taille comparable aux rhombomères sauvages (Voiculescu et al., 2001).

- La fonction de *Krox20* a ensuite été étudiée par expériences de gain-de-fonction. Des essais ont été réalisés par transgénèse chez la souris, mais se sont soldés par des échecs douloureux, sans que les raisons soient clairement identifiées. La surexpression de *Krox20* a donc été réalisée par électroporation dans le tube neural de poulet. L'expression ectopique de *Krox20* dans les rhombomères pairs est suffisante pour changer leur identité : les cellules de r2, r4 acquièrent une identité r3 (activation de *EphA4*, suractivation de *Hoxb2*, répression de *Hoxb1* dans r4) et les cellules de r6 prennent une identité r5 (activation de *EphA4* et suractivation de *Hoxb3*) (Figure 12Da). Ces expériences ont aussi confirmé l'autorégulation de *Krox20* : des cellules électroporées avec un vecteur contenant une version murine de *Krox20* activent le gène

endogène de poulet, et ce de manière cellule-autonome et non cellule-autonome (Figure 12Db,c). Les cellules voisines de celles électroporées expriment aussi le gène endogène. Il a été alors proposé que cette surprenante activation non cellulaire-autonome de *Krox20* sous-tend l'expansion du territoire *Krox20*$^{+}$ dans r3 (Figure 12E) (Giudicelli et al., 2001).

En résumé, *Krox20* est nécessaire et suffisant à l'acquisition par les rhombomères d'une identité impaire. Il œuvre en couplant la spécification de l'identité cellulaire (par l'activation de certains gènes *Hox*) et le contrôle de la ségrégation cellulaire (par l'activation de *EphA4*). L'expression de *krox20/egr2* est conservée chez les Vertébrés. Une analyse succincte du mutant *egr2b* chez le poisson zèbre, obtenu en 2007 dans le laboratoire de Cecilia Moens (Monk and Talbot, 2009), suggère que sa fonction est aussi conservée, du moins entre la souris et le poisson-zèbre. Lorsque *Krox20* est utilisé comme marqueur de la formation de r3 et r5, expériences par perte et gain de fonction ont révélée une dynamique en quatre phases : (i) le démarrage de l'expression, (ii) l'extension du domaine d'expression (surtout visible pour r3), (iii) l'affinement des frontières par activation du système Eph/ephrine, (iv) la fin de l'expression, progressive, impliquant d'abord r3 puis r5. Comment ces phases d'expression de *Krox20* sont-elles contrôlées au niveau transcriptionnel ?

4.3. Régulation transcriptionnelle de *Krox20* dans le rhombencéphale

La recherche des séquences cis-régulatrices contrôlant l'expression de *Krox20* dans le rhombencéphale s'est révélée bien plus laborieuse que celle des gènes *Hox*, principalement à cause de la distance qui les sépare du promoteur. Le projet a débuté par l'utilisation de plasmides puis de cosmides contenant la séquence codante murine de *Krox20* et les fragments génomiques alentour. Le test de ces cosmides par transgénèse chez la souris s'est révélé négatif. Le laboratoire s'est alors tourné vers des BACs de poulet, dont le génome est trois fois plus compact. Un BAC de 150 kb –contenant la séquence codante *cKrox20*, 100kb de séquence amont et 50kb de séquence aval– a donné un fort signal dans r3, r4 et r5, révélé par hybridation *in situ* contre *cKrox20* (Figure 13D). Un travail minutieux de découpage du BAC suivi de tests systématiques soit en transgénèse murine (Figure 13A,B), soit en électroporation chez le poulet (Figure 13C), a permis d'aboutir à 3 séquences régulatrices minimales (Chomette et al., 2006) :

- l'élément A, situé à 235 kb en amont du TSS de *Krox20* chez la souris, est actif dans r3 et r5 (Figure 13Ea,d). L'activité de cet élément est nulle chez le mutant *Krox20*, suggérant une fonction d'autorégulation. Six sites de liaison à la protéine Krox20 ont été identifiés dans sa

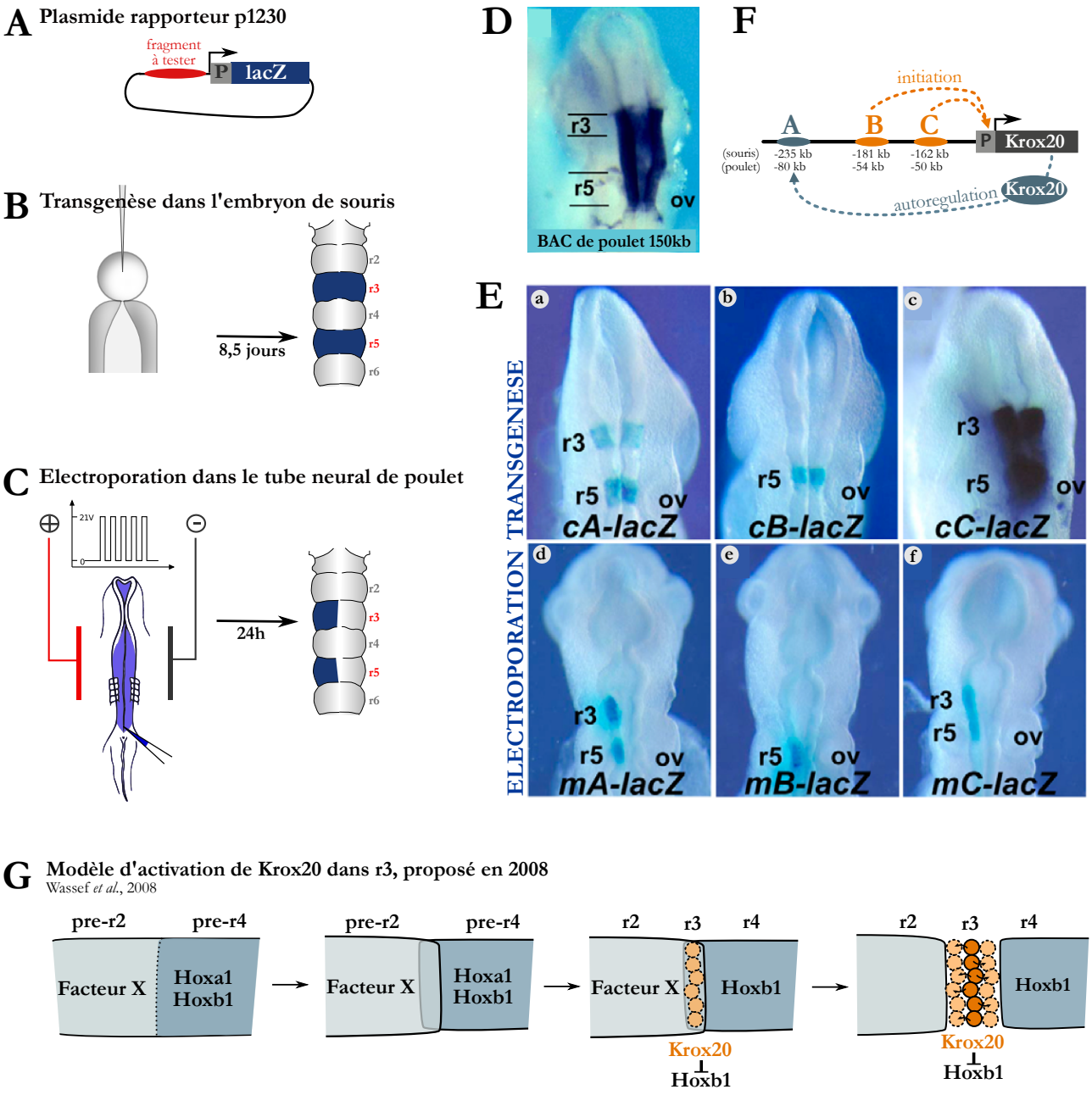

Figure 13 - Les grandes étapes de la recherche sur le gène *Krox20* (2)

(A-C) L'utilisation de plasmides rapporteurs en transgenèse murine ou en électroporation chez le poulet permet d'étudier l'activité d'élément régulateur à travers l'expression du gène *lacZ*. **(D)** Hybridation *in situ* anti-*cKrox20* réalisée sur embryons de souris après transgenèse d'un BAC de poulet contenant le gène *cKrox20* (i.e. le gène de poulet) et 150kb d'ADN génomique avoisinant (Chomette *et al.*, 2006). **(E)** Tests de trois sous-fragments de ce BAC, placés dans un plamside rapporteur lacZ, par transgenèse murine (a,b,c) et électroporation chez le poulet (d,e,f). Ces trois fragments correspondent à aux éléments A (a,d), B (b,e) et C (c,f) (Chomette *et al.*, 2006). **(F)** Schéma représentant le contrôle transcriptionnel des deux phases d'expression de *Krox20* : l'initiation et l'autorégulation. **(G)** Modèle d'activation de *Krox20* dans r3, par co-expression transitoire des HoxPG1 et d'un facteur inconnu (d'après Wassef *et al.*, 2008).

séquence, et la mutation de ces sites abolit son activité. L'élément A est donc le siège d'une autorégulation directe (Chomette et al., 2006).

- l'élément B, situé à -181 kb, est actif dans r5 et n'est pas affecté par la mutation de *Krox20* (Figure 13Eb,e). Il s'agit donc d'un élément « initiateur », spécifique à r5. Son activité requiert la liaison directe à vHnf1 (Chomette et al., 2006) et à MafB (Labalette et al., 2011).

- l'élément C, à -162 kb, est actif dans r3, faiblement dans r4 et dans r5 (Figure 13Ec,f). De même que pour B, C est un élément initiateur. Son activité dans r3 dépend de la coopération entre les facteurs Hoxa1/b1, Pbx1 et Meis1/2. Il a été proposé que l'allumage de C commence dans une fine bande de cellules (r3), suite à la co-expression furtive de Hoxa1/b1 et d'un autre facteur, inconnu à ce jour (Figure 13G) (Wassef et al., 2008). L'activité de C dans r5 semble être consécutive au démarrage de l'expression de *Krox20*, contrôlée principalement par B. Ceci suggère que C est impliqué dans une boucle d'autorégulation indirecte : Krox20 active l'expression des *HoxPG2* qui en retour lient et activent l'élément C. Cette boucle peut *a priori* tout aussi bien fonctionner dans r3. La démonstration de cette boucle d'autorégulation indirecte est menée actuellement par Charlotte Labalette et Carole Desmarquet au laboratoire. Enfin, l'activité de C dans r4 demeure une énigme car le gène *Krox20* n'est pas activé dans les cellules de r4, même précocement.

Deux réserves peuvent être émises concernant l'identification des éléments régulateurs de *Krox20*. Tout d'abord, la méthode employée ne permet d'identifier que des éléments activateurs et non des *silencers*. L'existence d'un site répresseur contrôlant l'activité de C mais absent dans la séquence isolée pourrait expliquer par exemple l'activité de l'élément dans r4. Par ailleurs, la liste des trois enhancers citée plus haut n'est pas exhaustive. D'autres éléments peuvent exister en dehors du BAC utilisé initialement. Ceci dit, les trois éléments identifiés sont suffisants pour expliquer la mise en place du patron d'expression de *Krox20* : C initie l'expression dans r3 puis A (et C) est responsable de l'expansion et du maintien ; B initie l'expression dans r5 puis A (et C) en assure le maintien (Figure 13F).

Ainsi, en attendant la démonstration formelle, ces trois éléments peuvent expliquer le *patterning* de r3 et r5. Mais cela n'est pas suffisant. Notamment, comment la position de la fine bande de cellules *Krox20*$^{+}$ est-elle fixée le long de l'axe rostro-caudal ? De plus, si B est activé par MafB, pourquoi n'est-il pas actif dans r6 ? Pour ces deux questions liées à la position des profils d'activité des enhancers de *Krox20*, deux hypothèses s'opposent : soit l'information de position est donnée directement par des facteurs exprimés en gradient ; soit il existe des facteurs précédant *Krox20* qui préfigurent la segmentation du rhombencéphale, par exemple un répresseur

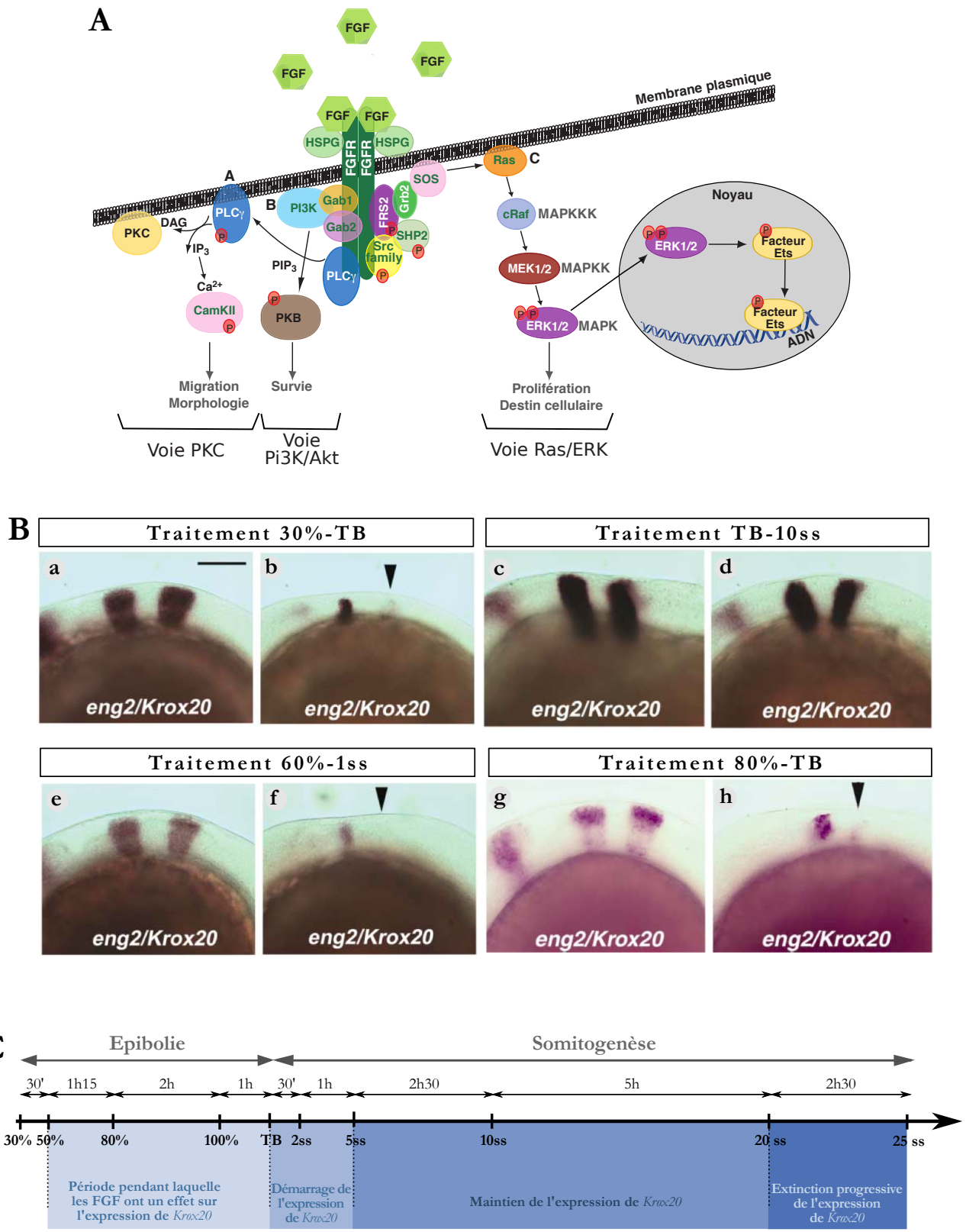

Figure 14 - Effets de la voie de signalisation FGF sur le patron d'expression de *Krox20*

(A) La signalisation FGF et ses trois voies de transduction canoniques. **(B)** Traitements d'embryons de poisson-zèbre par un inhibiteur de FGFR (SU5402, 60µM). Une hybridation *in situ Krox20* révèle la réduction du nombre de cellules *Krox20*$^{+}$. L'effet s'aggrave avec la durée d'exposition au SU5402 (comparer a,b/e,f/g,h). La drogue n'a en revanche plus d'effet lorsqu'elle est appliquée après le stade tailbud (Walshe *et al.*, 2002). **(C)** Schéma récapitulant les étapes de développement de l'embryon de poisson-zèbre, au moment de l'expression de *Krox20*.
D'après Dorey & Amaya, 2010 (A).

spécifiquement exprimé dans r6. Ces facteurs seraient des facteurs de *pre-patterning*. Les profils d'expression précoce de *Hoxa1* et *Hoxb1*, exprimés jusqu'à la future frontière r2/r3 en font déjà des facteurs de *pre-patterning*, car leurs profils ne sont pas segmentés mais ils définissent au moins une frontière. Mon travail de thèse prend racine dans ces questions générales de régionalisation. Comment, au moyen de ces trois éléments *cis*-régulateurs et quelques *trans*-facteurs, sont définis les rhombomères, leur position, leur taille, leur forme ? La variable du nombre de cellules *Krox20*$^+$ sera placée au centre de ce travail. Je propose alors d'aborder cette question sous deux angles. D'abord, l'étude d'un phénotype caractérisé par une modification du nombre de cellules *Krox20*$^+$, obtenu par perte ou gain-de-fonction FGF. Ensuite, l'étude de la relation fonctionnelle entre les éléments initiateurs et l'autorégulateur de *Krox20*, impliquée dans le contrôle du nombre de cellules *Krox20*$^+$. Pour cette partie, nous avons combiné une approche expérimentale et une approche computationnelle.

Avant de traiter ces points en détail, voici un bref compte-rendu des connaissances concernant les FGF dans le rhombencéphale, suivi d'un mémo sur ce que nous entendons par « approche computationnelle ».

5. La signalisation FGF dans le rhombencéphale

5.1. Activité pléiotropique de la voie de signalisation FGF

Initialement, les *Fibroblast Growth Factors* ont été identifiés comme des facteurs mitogéniques de fibroblastes en culture (Gospodarowicz and Moran, 1974). Depuis, ils ont été impliqués dans des processus aussi divers que la survie, la migration, la différenciation cellulaire, et toujours la prolifération. Pendant l'embryogenèse, on relève un rôle déterminant des facteurs FGF dans :

- l'induction et le maintien du mésoderme et du neurectoderme (Hongo et al., 1999; Draper et al., 2003);

- le contrôle des mouvements morphogénétiques pendant la gastrulation (Amaya et al., 1991; Yamaguchi et al., 1994; Meyers et al., 1998) ;

- le contrôle de la somitogenèse (Reifers et al., 1998; Dubrulle et al., 2001)

- le développement de plusieurs organes, dont le foie et les poumons (Serls et al., 2005) ;

- le *patterning* de l'axe dorso-ventral (Kumano and Smith, 2002) ;

- le contrôle de la symétrie gauche/droite (Meyers and Martin, 1999) ;

- le *patterning* de l'axe antéro-postérieur, de deux façons différentes au moins : le contrôle des migrations cellulaires responsables de l'élongation de l'axe (Dubrulle and Pourquié, 2004; Bénazéraf et al., 2010) et l'activation de gènes de spécification cellulaire. Ce dernier point est l'objet de notre préoccupation principale dans la suite de cet exposé.

5.2. Fonctionnement canonique de la voie de signalisation

Les FGF représentent une famille de ligands composée de 22 membres dont la plupart est sécrétée. Les ligands lient des récepteurs transmembranaires à activité tyrosine kinase. Il existe quatre gènes chez les Vertébrés codant pour ces récepteurs, FGFR1-4, mais chaque récepteur existe sous plusieurs isoformes générées par épissage alternatif. Un co-récepteur est nécessaire à l'activation des FGFR ; il s'agit de l'héparane sulphate (HS). La liaison de deux ligands FGF permet la formation d'un complexe FGF-FGFR-HS dont la stœchiométrie est 2:2:2 (Figure 14A). Ainsi, la dimérisation des récepteurs FGF produit la transphosphorylation des tyrosines intracellulaires et l'activation de voies de transduction cytoplasmiques. Trois voies canoniques existent : la voie Ras/ERK (ou MAP Kinase, plutôt impliquée dans la prolifération et la différenciation), la voie PI3Kinase/Akt (survie cellulaire) et la voie Protéine Kinase C (migrations et morphologie cellulaires). Notre intérêt portera sur la voie Ras/ERK car il a été montré chez le poulet qu'elle est celle régulant la formation de r3 et r5 (voir plus bas) (Aragon and Pujades, 2009; Weisinger et al., 2010). Il s'agit d'une cascade de phosphorylations impliquant un module très conservé de trois kinases successives : une MAPKKK ou MAPKinase-kinase-kinase (Raf), une MAPKK (MEK) et une MAPK (ERK). La cascade aboutit à la double-phosphorylation de ERK (noté ppERK) qui peut alors être transloqué dans le noyau et activer des facteurs de transcription. Les plus connus sont les facteurs de la famille des Ets (Wasylyk et al., 1993).

Dans le rhombencéphale, les ligands exprimés sont *fgf3* et *fgf8* chez le poisson-zèbre, d'abord dans les territoires r3 et r4 présomptifs (pre-r3 et pre-r4), puis ils se restreignent à r4 au stade 2-3 somites (Maves et al., 2002). Chez le poulet, Fgf3 semble exprimé dans pre-r4 et pre-r5 (Aragon and Pujades, 2009; Weisinger et al., 2010). En ce qui concerne les récepteurs, les quatre semblent être présents dans le rhombencéphale avec des profils d'expression dynamiques, de sorte qu'il soit difficile d'associer un récepteur au développement d'une sous-partie des rhombomères (Blak et al., 2005; Weisinger et al., 2010). Enfin, chez le poulet, la voie Ras/ERK aboutit à l'activation du facteur Ets Pea3 (Weisinger et al., 2010).

5.3. Rôle des FGF dans la régionalisation de l'axe antéro-postérieur

Le rôle des FGF dans la régionalisation de la plaque neurale a été évoqué plus haut. Il s'agissait de la promotion du destin postérieur dans le neurectoderme, à travers la régulation des facteurs Cdx puis Hox. Cette activité précoce est sous contrôle des ligands Fgf4 et Fgf8 chez tous les

Vertébrés. Les FGF interviennent aussi à des stades plus tardifs de la régionalisation du système nerveux central :

5.3.1. Effet morphogénétique dans le cerveau antérieur : l'*Anterior Neural Ridge* (ANR) constitue la partie la plus rostrale du télencéphale ; elle comprend des cellules sécrétrices de Fgf8. Il a été montré chez la souris que la protéine Fgf8 s'établit en gradient, traduit par la suite en gradient de ppERK. Par ailleurs, des expériences de perte et gain de fonction réalisées par électroporation chez la souris permettent d'identifier des cibles (*Sprouty4* et deux facteurs Ets, *Etv4* et *Etv5*) dont le comportement se conforme au « modèle du drapeau français » de Lewis Wolpert (Toyoda et al., 2010). Ces résultats identifient Fgf8 comme morphogène responsable de la régionalisation du néocortex.

5.3.2. Effet dose-dépendant dans le patterning du cervelet : Fgf8 est aussi sécrété à partir des cellules de l'isthme, à la frontière du rhombencéphale et du mésencéphale. La signalisation FGF participe à l'induction des structures dites tecto-isthmo-cerebellaires, à savoir le tectum (colliculi inférieur et supérieur, dans le mésencéphale), l'isthme lui-même et le cervelet (Wurst and Bally-Cuif, 2001). Des expériences d'invalidation conditionnelle de Fgf8 chez la souris ont permis d'établir un mécanisme d'induction dépendant de la durée d'exposition à Fgf8 : lorsque l'invalidation a lieu tôt, l'exposition au Fgf8 est courte et les structures les plus proches de l'isthme sont affectées (à savoir l'isthme lui-même, le cervelet antéro-médian, le colliculus inférieur) ; à l'inverse, les structures les plus éloignées requièrent une durée d'exposition plus courte pour leur développement (colliculus supérieur, cervelet latéral) (Sato and Joyner, 2009). Cet effet durée-dépendant peut être étendu à un effet dose-dépendant, c'est-à-dire l'intégration de la quantité au cours du temps. L'effet dose-dépendant des FGF avait d'ailleurs déjà été révélé dans un tout autre système : la régionalisation du tube digestif ventral, aboutissant à la spécification du foie et des poumons. L'effet de la quantité et de la durée d'exposition aux Fgf1 et 2 a été évalué *ex vivo* sur des explants murins. Une faible dose induit des cellules de foie tandis qu'une forte dose induit des cellules de poumons (Serls et al., 2005).

5.3.3. Rôle des FGF dans la segmentation du rhombencéphale : ce sujet a été en partie défloré dans un paragraphe précédent. Des détails importants pour la suite sont exposés ici. Le rôle de la signalisaton FGF a été établi pour le maintien des cellules *Krox20*$^{+}$ chez le poulet (Marín and Charnay, 2000; Aragon and Pujades, 2009; Weisinger et al., 2010) et chez le poisson-zèbre (Maves et al., 2002; Walshe et al., 2002; Wiellette and Sive, 2003; 2004). Plusieurs techniques ont été employées pour réduire le niveau de la signalisation : l'utilisation d'un

inhibiteur de FGFR (SU5402), de morpholinos ciblant *fgf3*, *fgf8* (chez le poisson) ou *Fgf3* (chez le poulet), de dominants négatifs dnFGFR1. À chaque fois, le nombre de cellules *Krox20*$^{+}$ est réduit, avec un phénotype toujours plus marqué dans r5 que dans r3. Par ailleurs, la taille des r3 et r5 résiduels dépend du niveau de l'inhibition (Figure 14B,C). Les mécanismes moléculaires de cette perte d'expression dose-dépendante sont examinés et discutés dans la partie « Résultats » de ce travail.

Il convient de préciser ici que la voie FGF affecte le rhombencéphale en deux temps : lorsqu'un dominant-négatif dNFGFR est injecté dans un embryon de poisson au stade 1 cellule, tous les marqueurs du rhombencéphale, y compris les *HoxPG1* sont affectés. En revanche, lorsque des morpholinos anti-*fgf3/8* sont injectés, le rhombencéphale est correctement spécifié (présence des *HoxPG1*) mais sa segmentation est perturbée (Roy and Sagerström, 2004). Ceci suggère que les FGF agissent précocement pour spécifier le territoire rhombencéphale, puis à travers les ligands Fgf3/8 pour le segmenter. Le traitement d'embryons de poissons au SU5402 a permis de fixer la limite entre ces deux phases au stade 50% epibolie. C'est sur la seconde phase de signalisation FGF que notre attention se portera.

6. Contribution des modèles mathématiques à l'étude des systèmes dynamiques

6.1. Les systèmes dynamiques, les modèles et la biologie

Par définition, un système dynamique représente un ensemble d'objets liés par une même loi, fixe, déterministe qui régit l'évolution de ces objets au cours du temps. Ainsi, à partir d'une condition initiale, un système dynamique est défini par la série de ses états au cours du temps. L'évolution d'un système dynamique étant déterministe, à une condition initiale ne peut correspondre qu'un unique état à la date *t*. La loi d'évolution du système est donnée par une ou plusieurs équations, dites différentielles, de la forme $\frac{dx}{dt}$, x étant un des objets du système. Pour connaître tous les états futurs du système, il faut le résoudre, c'est-à-dire résoudre ses équations maîtresses en les intégrant au cours du temps. Un système résolu et une condition initiale permettent de définir une *trajectoire* du système, à savoir l'expression de tous les points futurs. Les trajectoires d'un système peuvent être obtenues analytiquement, en résolvant le système d'équations par la mathématique, ou bien numériquement en demandant à un ordinateur de tracer la courbe sans obtenir au préalable d'expression algébrique de la trajectoire. Le tracé numérique d'une trajectoire répond au terme de *simulation*.

Un système dynamique est donc un objet mathématique qui aspire par essence à s'évertuer dans les domaines de la physique ou de la biologie. Ceci implique quelques aménagements :

- en biologie, le système d'étude n'est toujours connu que partiellement. Des paramètres, ou même certains termes des équations peuvent manquer. Dès lors, les équations ne décrivent plus un système mais un *modèle* du système, et les trajectoires ne sont pas nécessairement équivalentes à celles du système. Pour amenuiser cet effet d'approximation, un nouveau domaine de la *biologie des systèmes* à été développé à la fin du siècle dernier : la biologie « synthétique ». Le principe de la biologie synthétique consiste à modifier des systèmes biologiques existants (le système d'activation tetOff, le système de l'opéron lactose ou celui du cycle lyse/lysogénie du bactériophage λ) en les simplifiant puis de les adapter à des cellules en culture ou des organismes généralement unicellulaires (*E. coli* ou *S. cerevisiae*). L'objectif est d'obtenir des données quantitatives fiables pour répondre à des questions simples : quelles sont les conditions minimales pour créer un système d'interrupteur transcriptionnel, ou bien un système oscillateur, quelle est l'influence de petites fluctuations stochastiques sur ces systèmes, etc. (Becskei and Serrano, 2000; Elowitz and Leibler, 2000; Becskei et al., 2001; Elowitz et al., 2002; Guet et al., 2002; Atkinson et al., 2003; Rosenfeld et al., 2005; Robert et al., 2011). En fait de biologie synthétique, il s'agit plutôt d'ingénierie biologique. La contribution de tels systèmes artificiels a été déterminante ces dix dernières années pour la mise en place d'un cadre théorique indispensable à l'interprétation des données quantitatives obtenues à partir de systèmes biologiques complexes.

- parfois, la trajectoire elle-même importe moins que la façon dont elle est modifiée par l'altération d'un paramètre. Pour certaines valeurs de paramètres, le système peut changer son comportement qualitatif, passer par exemple d'une trajectoire périodique à une trajectoire chaotique. Ces points singuliers de l'espace des paramètres sont des *points de bifurcation*. L'identification de ces points, par une « analyse de bifurcation », est souvent déterminante pour la compréhension d'un système biologique car ils définissent les valeurs-limites de paramètres avant la transition d'un état stable vers un autre état stable.

- la trajectoire des systèmes biologiques comporte souvent une part d'aléatoire (cette assertion sera justifiée plus bas). Lorsque les variations sont importantes, il peut s'avérer difficile de détecter une tendance de fond. Il faut alors réduire les trajectoires à l'expression de leur moyenne (calculée à partir d'un grand nombre de trajectoires simulées). La trajectoire résultante devient l'expression d'une probabilité : son tracé est le plus probable, étant donnée la variation intrinsèque au système. Les modèles de systèmes dynamiques prenant en compte la variabilité des trajectoires sont dits stochastiques ou probabilistes. Les équations différentielles qui les gouvernent sont de type $\frac{dp(x)}{dt}$, p(x) étant la probabilité de trouver l'objet x dans un état donné.

À l'inverse, les modèles déterministes sont décrits par des équations différentielles dites ordinaires, de type $\frac{dx}{dt}$: l'évolution de x au cours du temps est connue de façon exacte.

En résumé, l'utilisation de modèles mathématiques en biologie permet d'approximer un système dont on ne connaît qu'une sous-partie, pour en tracer les trajectoires lorsqu'elles ne sont pas triviales, ou bien pour décrire le comportement du système en fonction de certains paramètres d'intérêt. Selon le système à modéliser, deux voies sont possibles : les modèles déterministes ou les modèles stochastiques.

6.2. L'expression génétique, un système dynamique stochastique à l'échelle cellulaire

L'expression d'un gène aboutit à la production d'un certain nombre de molécules d'ARNm puis de protéines. Ce nombre varie au cours du temps. Le déterminisme de cette évolution est en partie connu ; comme précisé plus haut, il fait intervenir un promoteur, des éléments régulateurs, des facteurs de transcription et des enzymes modificateurs de la chromatine. En ce sens, l'expression d'un gène est un système dynamique.

Ce système a ceci de particulier qu'il est intrinsèquement stochastique. Soit X(*t*) la variable représentant le nombre de molécules d'ARNm. À chaque instant *t*, on ne peut pas assigner à X une valeur donnée, mais une certaine probabilité de prendre cette valeur. Prenons le cas d'une expression constante. À *t*, la probabilité que X=10 est de 0,90. À *t*+*dt*, cette probabilité s'établit à 0,88. Autrement dit, la probabilité que X=9 ou X=11 est sensiblement supérieure à *t*+*dt* qu'à *t*. Ce petit écart de probabilité entre *t* et *t*+*dt* traduit les fluctuations de la variable X, même si en moyenne l'expression est constante. Ces variations sont qualifiées de stochastiques, à l'origine du *bruit* intrinsèque de l'expression génétique.

Ce bruit intrinsèque provient de la stochasticité des événements moléculaires qui sous-tendent l'expression génétique : la formation du PIC, le démarrage de l'élongation, le remodelage de l'ADN, la fixation des FT aux séquences régulatrices, sans compter la stochasticité inhérente à la traduction.

Le bruit intrinsèque intervient pour tous les gènes dans tous les types cellulaires. Il s'oppose à la stochasticité extrinsèque qui concerne des gènes différents et/ou des types cellulaires différents et qui a trait à des fluctuations dans le volume nucléaire, l'environnement ionique, l'accessibilité de l'ADN, etc. (Elowitz et al., 2002).

6.3. Le choix du destin cellulaire : un système dynamique à l'échelle d'une population de cellules

En biologie du développement, la modélisation de l'expression génétique en elle-même n'est qu'un préalable. L'intérêt est souvent porté ensuite sur l'effet de cette expression génétique sur une population de cellules. Notamment, les modèles de spécification cellulaire s'intéressent à la façon dont un groupe de cellules se choisit un destin en exprimant le gène A, par opposition à un autre groupe qui, lui, exprime B. Ce type de système requiert la modélisation de l'expression de A, celle de B et des relations cellulaires-autonomes et non cellulaires-autonomes entre A et B. Le système dynamique étudié n'est alors plus l'expression d'un gène mais le choix du destin cellulaire. Certes, à la base d'un modèle de destin cellulaire réside un modèle d'expression génétique. Mais le résultat est analysé à l'échelle de la population et non plus à celle de la cellule.

Pour prendre en compte les fluctuations intrinsèques de l'expression des gènes, les modèles devraient être de type stochastique. Seulement, il peut s'avérer que les petites variations des gènes n'aient aucun effet sur le processus étudié, à savoir l'allocation d'un destin cellulaire. De nombreux auteurs préfèrent dans ce cas modéliser l'expression des gènes de façon déterministe car les simulations numériques sont beaucoup moins exigeantes en capacités de calcul. Par extension, on peut introduire beaucoup plus de complexité dans des modèles déterministes que dans des modèles stochastiques. Il faut bien noter enfin que si l'expression génétique est intrinsèquement stochastique, cela ne présage en rien de la qualité des systèmes de spécification cellulaire, certains étant déterministes d'autres stochastiques. Des exemples représentatifs sont illustrés plus bas.

6.4. Modèles de *switch* bistable

Reprenons le modèle binaire de spécification cellulaire abordé plus haut, entre les cellules exprimant A et celles exprimant B. La situation initiale est une population homogène de cellules. Puis, l'allocation du destin A ou B est consécutive au basculement d'une partie de la population vers l'expression de A, de l'autre partie vers B. Ce phénomène de basculement est connu sous le terme d' « effet interrupteur » ou *switch* car certaines cellules allument A, d'autres l'éteignent et inversement pour B. La spécification cellulaire par *switch* représente un nombre important des modèles de spécification décrits à ce jour. Le phénomène a été identifié en premier lieu chez *Escherichia coli* où l'expression de l'opéron lactose passe brutalement d'un état bas à un état haut lorsque la concentration en glucose du milieu diminue. Cet effet tout-ou-rien requiert l'activation d'une boucle de rétrocontôle positif impliquant la perméase lacY (Novick and Weiner, 1957). Un second exemple historique fait intervenir un autre mécanisme : l'alternance entre les cycles lytique

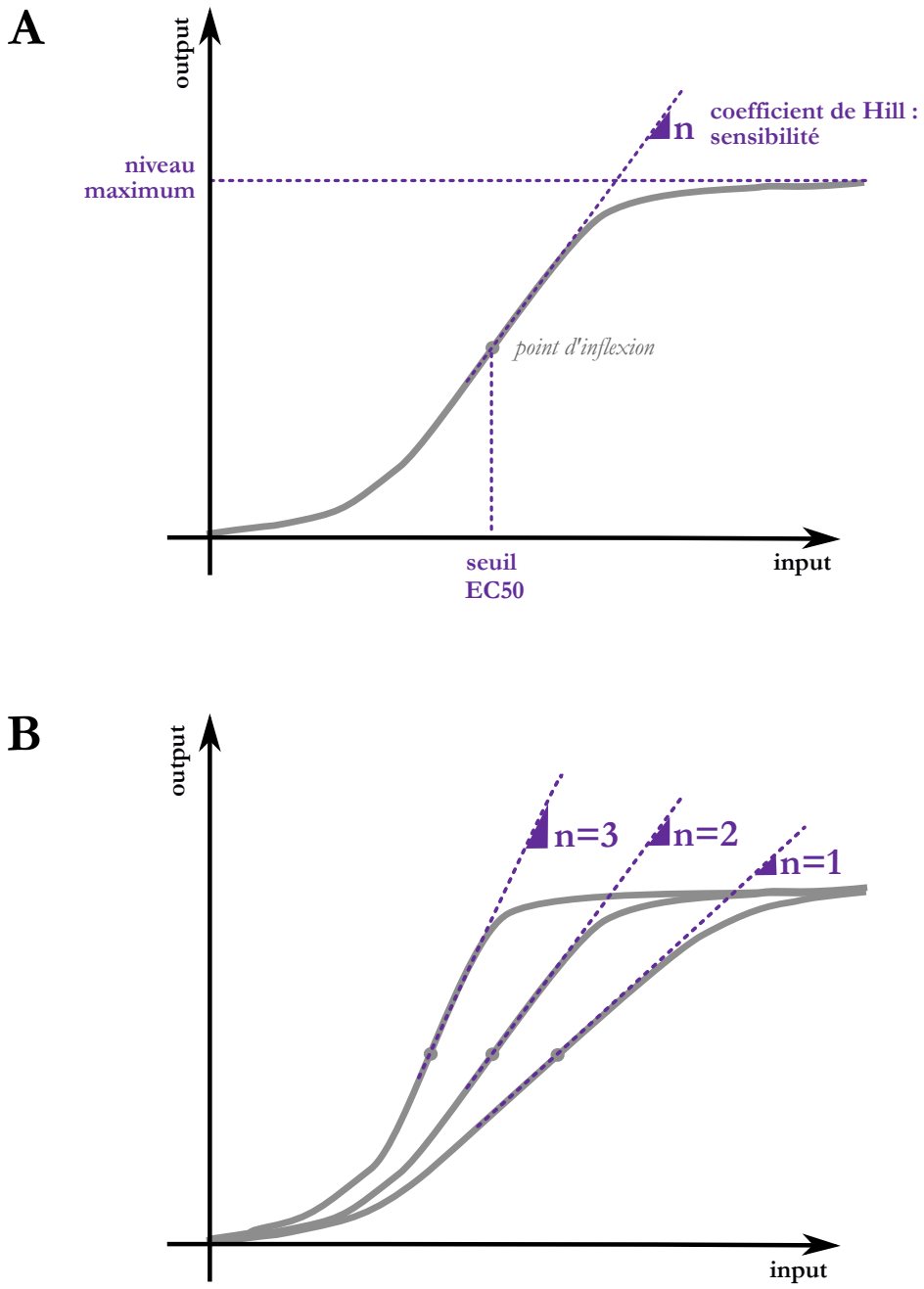

Figure 15 - Caractéristiques de la fonction de Hill

La fonction de Hill est largement utilisée pour modéliser les courbes input/ouput des séquences régulatrices de gènes car elle prend en compte leur caractère sigmoïde. **(A)** Allure théorique d'une fonction de Hill, caractérisée par trois paramètres majeurs : le niveau maximal d'activation, le seuil d'activation (ou EC50, pour *half-maximal Effective Concentration*) et la sensibilité ou coefficient de Hill **(B)** Plus le coefficient de Hill est grand, plus la pente du *switch* est importante, plus le switch est "brutal". Sur le plan mécanistique, de forts coefficients de Hill sont classiquement obtenus lorsque les séquences régulatrices sont activées de manière coopérative, soit par coopérativité de liaison, soit par synergie transcriptionnelle.

et lysogénique du bactériophage λ est contrôlée par la répression mutuelle entre les gènes CI et Cro. CI réprime l'expression de Cro et des gènes de la phase lytique d'où la promotion de la phase lysogénique. Inversement pour Cro (JACOB et al., 1962; Ptashne, 1986).

Rétrocontrôles positifs et/ou inhibitions croisées sont des motifs à l'origine de la grande majorité des *switches* décrits à ce jour. La version la plus commune de rétrocontrôle positif est l'autorégulation qui ne concerne, par définition, qu'un seul gène, A par exemple ; elle permet donc de faire évoluer un système d'un état stable par défaut où A n'est pas exprimé vers un autre état stable où A est exprimé. Des modèles synthétiques ont même montré qu'une simple boucle d'autorégulation directe peut suffire à établir un effet *switch* (Becskei et al., 2001; Kramer et al., 2004; Kramer and Fussenegger, 2005). L'inhibition croisée, entre A et B, permet en revanche de créer deux états stables, l'un caractérisé par l'expression de A, l'autre par l'expression de B ; dans ce cas, la situation initiale est un état stable où A et B sont absents ou co-exprimés. Des systèmes enfin sont construits autour d'inhibitions croisées dont les deux gènes antagonistes s'autorégulent. Ce schéma assure une grande robustesse dans l'allocation du destin cellulaire.

Les effets *switch* conduisent un système à la coexistence de deux états stables au moins. Il sont qualifiés pour cela de *switch bistable*. À vrai dire, la notion de bistabilité n'est pas qualitative ; elle requiert une démonstration mathématique, d'où l'importance de la modélisation. Je vous propose, dans la partie qui suit, d'appréhender la notion de bistabilité par une analyse graphique.

6.5. Analyse graphique de la bistabilité

Un *switch* génétique est par essence une réponse non-linéaire apportée soit par rétrocontrôle positif soit par inhibition croisée (Cinquin and Demongeot, 2002). Cette non-linéarité est mise en évidence expérimentalement par la courbe dose-réponse (courbe i/o pour *input/output*) d'un gène, c'est-à-dire le niveau de transcription du gène (*output*) en fonction de la concentration de son activateur principal (*input*). Ce genre de courbe, dite GRF pour *Gene Regulation Function*, prend systématiquement une forme sigmoïde, modélisable dès lors par une équation de Hill de la forme : $output = \frac{input^n}{EC50^n + input^n}$, *EC50* étant une constante définie comme le seuil d'activation du gène et *n* le coefficient de Hill représentant la sensibilité de l'activation (Figure 15A) (Veitia, 2003). L'effet *switch* est défini pour n>1. Plus *n* est grand, plus le *switch* est marqué. On parle alors d'ultrasensibilité de l'activation du gène (Figure 15B). Peut-on déduire les états stables du système à partir de cette courbe i/o ?

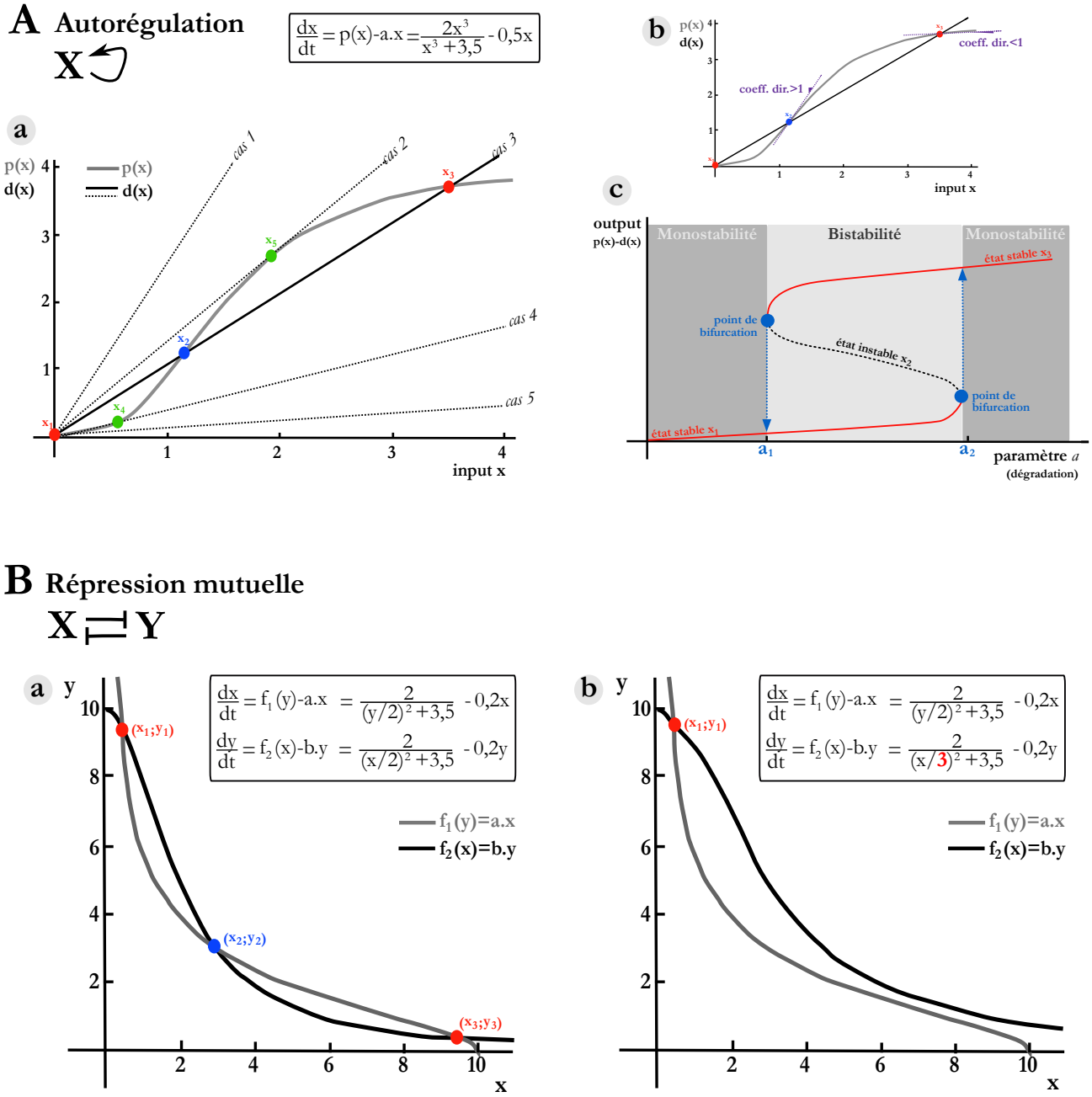

Figure 16 - Analyse graphique de modèles de *switch* bistables

(A) Modèle d'autorégulation - (a) Un exemple d'équation différentielle est donné dans l'encadré. Les états stationnaires sont définis par une évolution dx/dt nulle, soit lorsque les deux termes de l'équation sont égaux. Selon, la valeur du taux de dégradation *a*, le système comprend 1, 2 ou 3 états stationnaires. (b) La stabilité des états stationnaires peut être déduite à partir du coefficient directeur de la tangente à la courbe p(x) : s'il est supérieur à 1, comme en x_2, l'état est instable ; s'il est inférieur à 1, l'état est stable. (c) Diagramme de bifurcation schématique représentant l'évolution du système en fonction des valeurs de *a*, faisant apparaître les deux bifurcations du système, en a_1 et a_2, et par la même le phénomène d'hystérèse. **(B)** Modèle de répression mutuelle - (a) La même analyse graphique permet d'identifier trois états stationnaires dont deux stables. (b) Deux de ces états stationnaires disparaissent après modification d'un paramètre dans les équations (en rouge dans l'encadré).
Daprès Graham *et al.*, 2010.

Prenons un premier exemple : le gène *X* est autorégulé ; la concentration de l'ARNm, notée *x*, dépend de son niveau de production *p* et de dégradation *d*. La fonction $p(x) - d(x)$ est la fonction i/o du gène ; elle représente donc la variation de *x* au cours du temps, d'où $\frac{dx}{dt} = p(x) - d(x)$. Vu que le gène est autorégulé, la production *p(x)* prend la forme non-linéaire de Hill suivante : $p(x) = \frac{x^n}{EC50^n + x^n}$. Quant à la dégradation, prenons ici le cas simple où elle est liée à *x* par une relation de premier ordre. On obtient ainsi $\frac{dx}{dt} = \frac{x^n}{EC50^n + x^n} - a.x$.

Les états stationnaires du système sont definis par l'équilibre entre production et dégradation : $\frac{dx}{dt} = 0 \Leftrightarrow p(x) = d(x) \Leftrightarrow \frac{x^n}{EC50^n + x^n} = a.x$. Graphiquement, les états stationnaires sont donc les points d'intersection des courbes p(x) et d(x). Selon la valeur du paramètre de dégradation *a* choisie, le système peut ne comprendre qu'un état stationnaire (cas 1 et 5), deux états stationnaires (cas 2 et 4) ou 3 états stationnaires (cas 3) (Figure 16Aa) :

- au point x_3, le gène est fortement exprimé. Cet état est stable car le coefficient directeur de la tangente à la courbe *p(x)* en ce point est inférieur à 1 (Figure 16Ab). Autrement dit, lorsqu'on s'éloigne de ce point en augmentant *x*, le taux de dégradation dépasse celui de production, dont *p(x)* diminue pour retrouver sa valeur à l'état stationnaire x_3. Inversement lorsque l'on s'éloigne de x_3 en diminuant *x*.

- au point x_2, le niveau d'expression du gène est intermédiaire. Cet état est instable car il ne résiste pas aux petites variations de *x* : lorsque l'on s'éloigne de x_2 en augmentant *x* par exemple, la production l'emporte sur la dégradation et *p(x)* dérive jusqu'à x_3. La tangente à la courbe en x_2 a un coefficient directeur supérieur à 1 (Figure 16Ab).

- enfin, dans l'état x_1, le gène n'est pas exprimé. Par le même raisonnement graphique que pour x_1 et x_2, on conclut que l'état stationnaire x_1 est stable.

Les états x_4 et x_5 sont des cas limites où la stabilité est asymétrique : une augmentation de *x* ramène le système vers x_4 ou x_5, alors qu'une légère diminution le fait dériver vers x_1.

Dans les cas 1 et 5, l'unique état stationnaire est stable ; le système est en configuration monostable. Dans le cas 3, deux états stationnaires parmi les trois sont stables ; on parle de système bistable. Les propriétés de mono/bistabilité dependent donc des valeurs de paramètres, ici le taux de dégradation *a*. Pour mieux visualiser l'effet des paramètres sur la stabilité d'un système, il est opportun de tracer l'*output* en fonction des valeurs du paramètre d'intérêt. Pour cela, il faut déterminer par le calcul une expression analytique de l'*output* en fonction des paramètres du système. Le diagramme ainsi obtenu est appelé diagramme de bifurcation car il fait

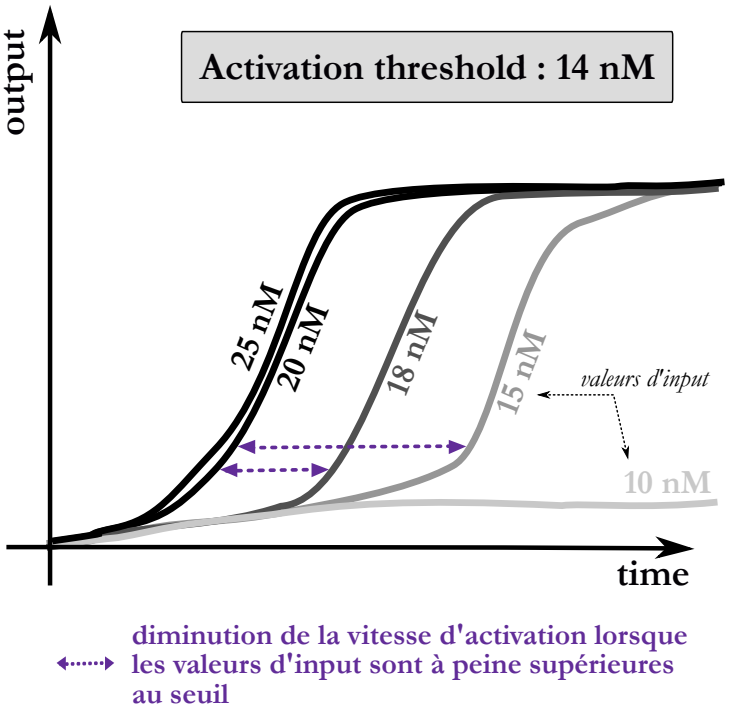

Figure 17 - Effet de "ralentissement critique", caractéristique des systèmes dynamiques bistables

Exemple théorique de *switch* dont le seuil se situerait à une valeur de 14 nM d'*input*. Lorsque ce système est étudié au cours du temps, on s'aperçoit que pour des valeurs d'*input* légèrement supérieures au seuil, le *switch* n'intervient qu'après un certain retard, sont la durée est inversement corrélée à l'*input*.

apparaître les valeurs de *a* pour lesquelles le système bascule d'un état stable vers l'autre état stable (Figure 16Ac). On s'aperçoit alors que la transition de x_1 vers x_3 n'est pas la symétrique de x_3 vers x_1 : la première intervient à une valeur a_2, la seconde à une valeur a_1, de sorte que $a_1<a_2$. Ce phénomène est connu sous le nom d'hystérèse : le système tend à rester dans l'état x_3 lorsque $a<a_2$, alors que cette condition le contraignait jadis à demeurer dans l'état x_1. Cela peut s'interpréter comme un effet « mémoire », car le système demeure dans un état alors que la cause qui lui a permis d'atteindre cet état a cessé d'exister.

Appliquons maintenant les mêmes méthodes pour analyser un système basé sur l'inhibition mutuelle de deux gènes X et Y. De la même façon que précédemment, les évolutions de *x* et *y* au cours du temps sont données par les équations déterministes suivantes : $\frac{dx}{dt} = f_1(y) - a.x$ et $\frac{dy}{dt} = f_2(x) - b.y$, où f_1 est une fonction décroissante dépendante de *y* vu que X est inhibé par Y. Réciproquement pour f_2. Les états stationnaires de ce système sont donnés par la résolution du système d'équations $\begin{cases} f_1(y) = a.x \\ f_2(x) = b.y \end{cases}$. Graphiquement, il s'agit des points d'intersection des courbes $f_1(y) - a.x$ et $f_2(x) - a.y$. Un exemple est présenté en figure 16Ba. Comme dans le cas du seul gène autorégulé, le nombre d'états stationnaires et *a fortiori* d'états stables dépend des paramètres du système (comparer les figures 16Ba et 16Bb), d'où l'importance de la modélisation pour identifier les valeurs clés à l'origine des transitions/bifurcations.

En résumé, un système bistable est caractérisé graphiquement par son ultrasensibilité (coefficient de Hill supérieur à 1), son seuil d'activation, son niveau maximum d'activation et la propriété d'hystérèse. Une autre propriété, non triviale et dissimulée dans les graphiques présentés ci-avant, définit les systèmes bistables : l'« effet de ralentissement critique» (*critical slowing-down effect*). Pour mettre en évidence cet effet, il faut s'intéresser à l'évolution du système non plus à l'équilibre mais au cours du temps. On s'aperçoit alors que des valeurs d'*input* sensiblement supérieures au seuil d'activation provoquent le *switch* mais avec un certain retard dont la durée est inversement proportionnelle à la concentration de l'*input* (Figure 17) (Sha et al., 2003; Wang et al., 2009).

6.6. Exemples de modèles de spécification cellulaire par *switch* bistable

Sont présentés ci-dessous des exemples emblématiques de spécification cellulaire dont le mécanisme sous-jacent –établi ou proposé– est un *switch* bistable.

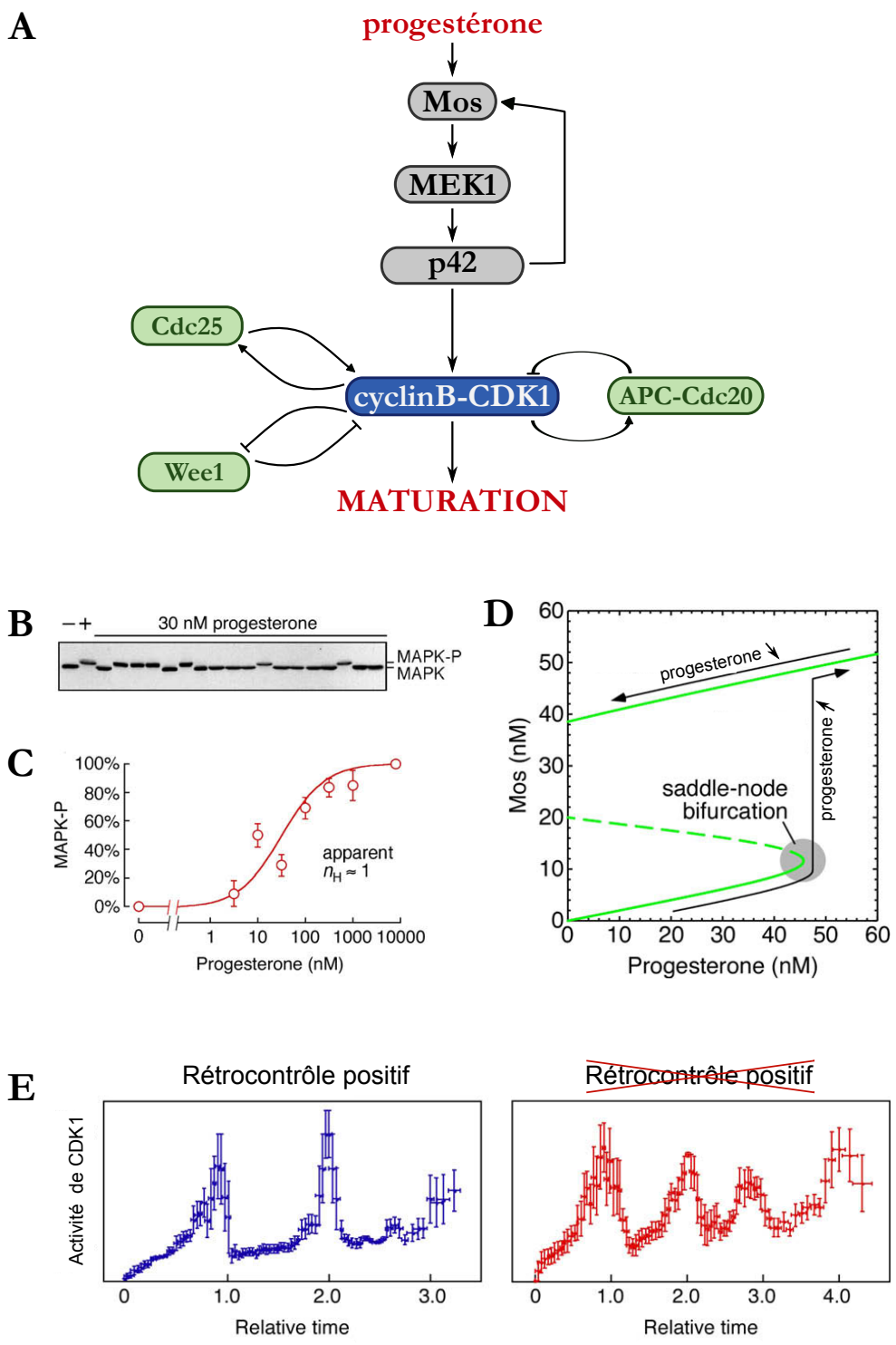

Figure 18 - La maturation des ovocytes de Xénope, un modèle historique de bistabilité

(A) Les deux circuits génétiques contrôlant la maturation des ovocytes de Xénope : (i) la voie MAPK, directement en aval de la progestérone et aboutissant à l'activation de p42, (ii) l'activation oscillante du complexe CyclineB-CDK1, ou MPF. Une fois le MPF actif, l'ovocyte entre en mitose I. **(B)** Western-blot réalisé contre les formes phosphorylées et non phosphorylées de p42. Dans chaque puit, sont chargés les extraits totaux d'**un** ovocyte traité préalablement avec 30nM de progestérone. La réponse des ovocytes à la prgestérone est de type tout-ou-rien. **(C)** A l'inverse, le taux de phosphorylation d'extraits collectés à partir de plusieurs ovocytes répond à la,prgestérone de façon graduée. L'effet *switch* ne peut être caractérisé qu'à l'échelle cellulaire. **(D)** Diagramme de bifurcation établi à partir d'un modèle d'activaion de p42 à l'échelle cellualaire. Le système ne comprend qu'une bifurcation, d'où l'irréversibilité de la phosphorylation. **(E)** Diagramme expérimental montrant les oscillations d'activité de CDK1, et donc du MPF (courbe bleue). Lorsque les rétrocontrôles positifs impliquant Wee1 et Cdc25 sont abolis, les oscillations deviennent moins explosives.
D'après Ferrell *et al.*, 2009.

6.6.1. Maturation des ovocytes de Xénope (Ferrell et al., 2009)*:* la maturation est le processus qui conduit les ovocytes de Xénope d'un premier blocage en prophase I de méiose (long de plusieurs mois et conduisant à une forte augmentation du volume) au second, en métaphase II. La transition entre ces deux états de blocage intervient sous l'effet de signaux extracellulaires de la famille des gonadotropines, principalement la progestérone. Le mécanisme de cette transition brutale comprend deux étapes dont chacune est un *switch* bistable (Figure 18A) :

- une cascade MAPKinase dont l'activation aboutit à la double phosphorylation de p42 suivant un mode tout-ou-rien au niveau cellulaire (Figure 18B). La réponse empirique de p42 à des doses croissantes de progestérone peut être modélisée par une fonction de Hill de coefficient 5. En revanche, lorsque la phosphorylation de p42 est étudiée sur des extraits d'une population d'ovocytes, l'effet switch devient invisible : le coefficient de Hill devient dès lors proche de 1 (figure 18C). Enfin, la modélisation d'un tel système permet d'obtenir un diagramme de bifurcation où n'apparaît qu'une seule transition (Figure 18D). La bifurcation basse n'existe pas dans ce système. Il s'agit là d'un cas d'hystérèse extrême, l'irréversibilité.

- dans un second temps l'activation du *Maturation-Promoting Factor* MPF (complexe cyclineB-CDK1) par p42 suit aussi un mode tout-ou-rien qui, de plus est, oscille. L'oscillation est procurée par le rétrocontrôle négatif qu'exerce le complexe APC-Cdc20 sur le MPF. L'ultrasensibilité des réponses est quant à elle le fait d'une boucle de régulation positive et d'une inhibition croisée impliquant Cdc25 et Wee1 respectivement (Figure 18A). En absence de ces rétrocontrôles positifs, les oscillations apparaissent moins nettes (Figure 18E).

Cet exemple historique étudié en détail illustre élégamment la façon dont un signal gradué extérieur, la progestérone, peut être intégré sous la forme d'un *switch* puis d'un oscillateur. Seulement, dans ce cas, un seul destin s'offre aux cellules et toutes le suivent de façon déterministe. Qu'en est-il lorsqu'un choix entre deux lignages est possible ?

6.6.2. Spécification des lignages neutrophiles vs macrophages (Laslo et al., 2006; Huang et al., 2007)*:* les macrophages et les neutrophiles dérivent d'un progéniteur myéloïde commun (PMC). L'allocation des destins macrophage ou neutrophile est contrôlée par l'expression des déterminants primaires PU.1 et C/EBPα respectivement. Ces facteurs primaires activent chacun des déterminants secondaires, Egr1/2 et Gfi-1, coexprimés à faible niveau dans les PMC puis renforcés dans l'un ou l'autre des lignages. Le mécanisme dépend principalement de l'inhibition croisée entre Krox20 et Gfi-1 (Figure 19A). La modélisation de ce système a permis de mettre en évidence les deux états stables neutrophile *vs* macrophage et a confirmé l'existence d'un état dit

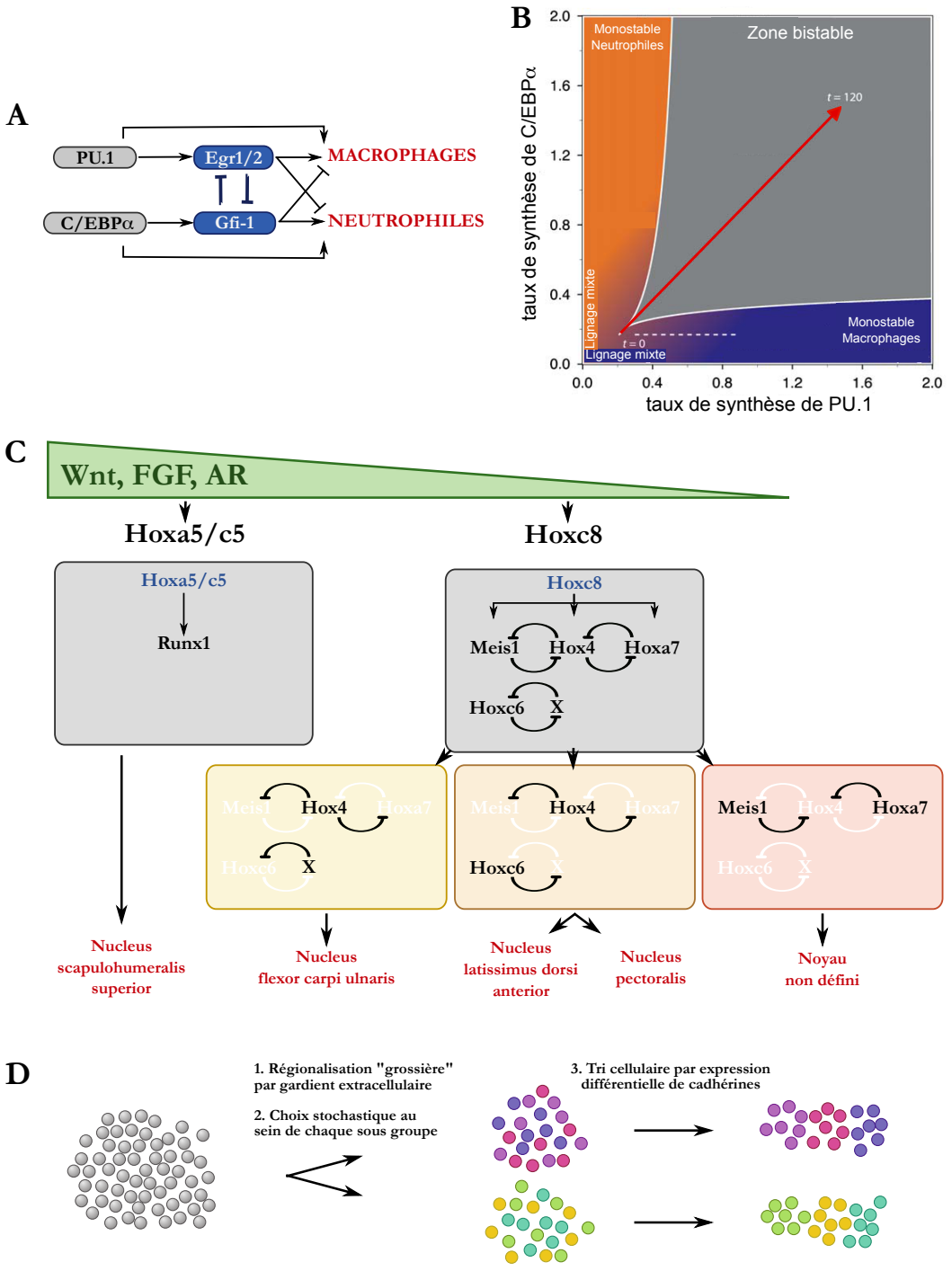

Figure 19 - Modèles de spécification de lignages non régionalisé et régionalisé

(A) Circuit génétique utilisé pour modéliser la spécification non-régionalisée des neutrophiles et des macrophages dans le système immunitaire. **(B)** Le diagramme de bifurcation obtenu met en évidence quatre zones : deux zones de monostabilité en faveur des neutrophiles ou des macrophages, une zone de bistabilité et une zone "mixte", caractérisée par de faibles taux de synthèse de PU.1 et C/EBPα. Si une cellule suit la trajectoire rouge, c'est-à-dire des niveaux comparables de PU.1 et de C/EBPα, elle s'éloigne de la zone mixte au cours du temps, entre dans la zone bistable le long de la diagonale ; son destin est alors fixé de façon purement stochastique. **(C)** Circuit génétique à l'origine de la spécification des noyaux neuronaux de la colonne motrice latérale dans la moelle épinière. Cinq noyaux en particulier sont montrés en exemple. L'allocation du destin cellulaire comprend deux phases : (i) la définition d'un territoire rostral et d'un territoire caudal grâce à des signaux extracellulaires exprimés en gradient, (ii) un choix stochastique réalisé au sein de chaque territoire par des boucles d'inhibition d'inhibitions croisées. **(D)** A terme, la régionalisation des noyaux neuronaux est contrôlée par l'expression différentielle de cadhérines à l'origine d'un tri cellulaire.
D'après Laslo *et al.*, 2006 (A, B) et Johnston & Desplan, 2010 (C, D).

métastable de coexpression à bas niveau (Figure 19B). Les PMC se trouvant dans cet état métastable basculent dans l'un ou l'autre des lignages de façon *a priori* stochastique, puisqu'à ce jour, aucun biais n'a pu être identifié.

Ce système neutrophiles *vs* macrophages est caractéristique des modèles binaires d'allocation de destin cellulaire : l'inhibition croisée entre deux facteurs de lignage, renforcée parfois par l'autorégulation de ces mêmes facteurs, et l'existence d'un court état métastable où les facteurs sont coexprimés à faible niveau. Dans un contexte non-régionalisé comme l'est le système immunitaire, il se peut que la transition entre l'état métastable et un des états stables soit parfaitement stochastique ; en système régionalisé, il peut exister soit un biais qui impose aux cellules de se déterminer en fonction de leur localisation, soit un mécanisme de tri cellulaire *a posteriori*. C'est le cas dans l'exemple des motoneurones de la colonne motrice latérale (CML) dans la moelle épinière.

6.6.3. Spécification des types neuronaux de la colonne motrice latérale (Dasen and Jessell, 2009; Johnston and Desplan, 2010) *:*

les motoneurones de la moelle épinière sont organisés en colonnes innervant les muscles le long de l'axe rostro-caudal. Ces colonnes sont spécifiées à des stades précoces par les gradients de Wnt, FGF et AR abordés au début de cette introduction. Une de ces colonnes, la CML, contient 50 noyaux neuronaux dont chacun est caractérisé par l'expression de facteurs de lignage spécifiques, appartenant à la famille des Hox. Les circuits génétiques à l'origine de cinq de ces noyaux sont présentés en figure 19C : les gradients extracellulaires cités plus haut définissent deux territoires disjoints de même taille, exprimant Hoxa5/c5 et Hoxc8. Les cellules Hoxa5/c5$^+$ forment à terme les 25 noyaux les plus rostraux dont le mieux connu, le *nucleus scapulohumeralis posterior*. Dans les cellules Hoxc8$^+$ se met en place un système complexe d'inhibitions croisées entre Meis1, Hox4, Hoxa7 et entre Hoxc6 et un facteur X inconnu. Ce double système aboutit à l'activation stochastique de Hox4 ou Hox4 et Hoxc6 ou Meis1 et Hoxa7. L'activation de ces sous-réseaux de gènes donnera notamment naissance aux 4 noyaux indiqués en figure 19C. Le destin de ces cellules étant alloué de façon stochastique, comment la robustesse du *patterning* de la CML est-elle assurée ? Price *et al.* ont montré qu'à l'organisation mosaïque des types cellulaires succède une organisation spatiale reproductible grâce à des mécanismes de tri cellulaire contrôlés par l'expression différentielle de cadhérines (Price et al., 2002).

Cet exemple illustre la façon dont la robustesse des mécanismes de *patterning* s'accommode de la stochasticité des destins cellulaires. Mais le destin est ici déterminé de façon convergente : un groupe de cellules est subdivisé par *switch* successifs jusqu'à aboutir à un groupe homogène, le

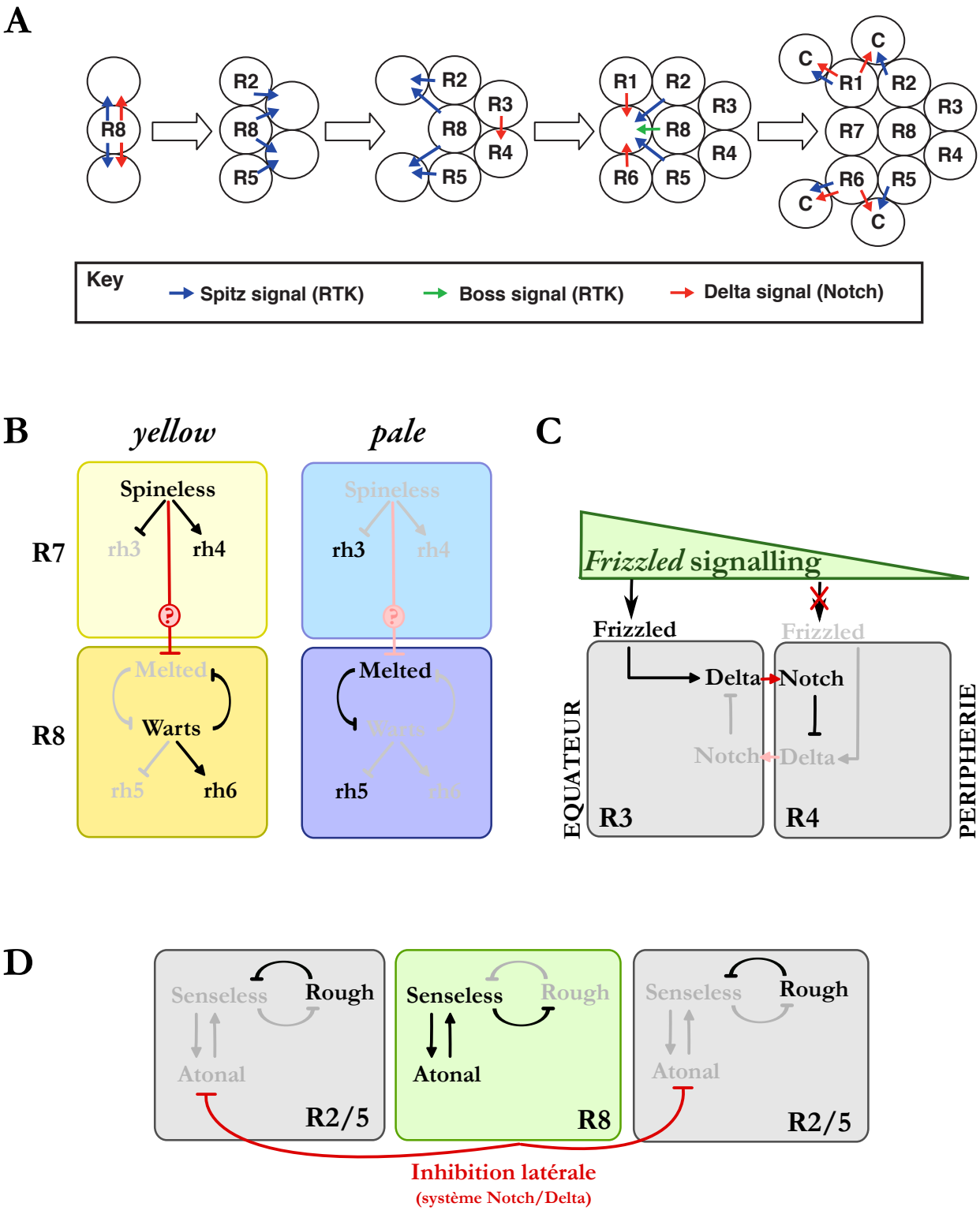

Figure 20 - Spécification des neurones photorécepteurs dans l'oeil de Drosophile

(A) Séquence de spécification des neurones ommatidiens chez la Drosophile. La nature des signaux inducteurs est indiquée dans l'encadré (RTK: récepteur tyrosine kinase). Les circuits génétiques à l'origine de la spécification des destins pale *vs* yellow **(B)**, R3 *vs* R4 **(C)**, R8 *vs* R2/5 **(D)**.
D'après Graham *et al.*, 2010 (A, C, D), Jonhston & Desplan, 2010 (B).

noyau neuronal ; ce mécanisme est par essence cellulaire-autonome. Il existe un autre moyen de coordonner stochasticité et exigence de robustesse à l'échelle du tissus : le contrôle non cellulaire-autonome du destin cellulaire : l'identité d'une cellule dépend de celle de sa voisine.

6.6.4. Spécification des types neuronaux ommatidiens chez la Drosophile (Losick and Desplan, 2008; Graham et al., 2010) *:* l'œil de Drosophile est composé d'environ 800 ommatidies, unités répétées contenant 20 cellules dont 8 neurones photorécepteurs, notés de R1 à R8. Chaque photorécepteur exprime un pigment de la famille des rhodopsines (rh). Les ommatidies se développent à partir d'un disque imaginal de façon séquentielle et principalement non cellulaire-autonome au moyen des signaux inducteurs signalés en figure 20A. Plusieurs de ces inductions font *a priori* intervenir des *switch* bistables :

- le destin des ommatidies *pale vs yellow* est défini au sein des cellules R7 par l'expression stochastique du facteur Spineless (Figure 20B). Lorsque Spineless est présent, rh4 s'exprime et le facteur Melted est réprimé de façon non cellulaire-autonome dans R8. L'expression de rh6 est alors activée par Warts. La présence de rh4 dans R7 et rh6 dans R8 signe les ommatidies *yellow*. A l'inverse dans les ommatidies *pale*, R7 est dépourvu de Spineless, exprime donc rh3 et Melted s'active dans R8, d'où l'expression de rh5. L'inter-inhibition indirecte entre Warts et Melted assure la divergence entre les deux voies dans R8. En revanche, les mécanismes à l'origine de la stochasticité d'expression de *spineless* et de la communication entre R7 et R8 restent mal documentés à ce jour.

- Un autre mécanisme non cellulaire-autonome intervient dans la décision entre R3 et R4. La signalisation extracellulaire Frizzled, présente sous la forme d'un gradient, active le récepteur Fz du côté équatorial du disque imaginal, d'où l'activation du ligand transmembranaire Delta dans la future cellule R3 puis celle du récepteur Notch dans R4 (Figure 20C). La dissymétrie entre R3 et R4 est maintenue par l'inhibition de Delta par Notch. Cette signalisation juxtacrine Notch/Delta qui aboutit à la distinction de deux types cellulaires est connue sous le nom d'« inhibition latérale ». La décision entre les cellules $Delta^+$ et les cellules $Notch^+$ est intrinsèquement stochastique. Dans ce cas précis néanmoins, le biais apporté par la signalisation Frizzled rend obligatoire le destin R3 du côté équatorial.

- le destin R8 s'établit par opposition au destin R2/5. Dans les cellules R8, le système d'activation croisée entre Senseless et Atonal s'auto-entretient tout en réprimant l'expression de Rough. À l'inverse, dans les deux cellules adjacentes, un signal émanant de R8 réprime Atonal d'où l'activation de Rough et l'activation du destin R2/5 (Figure 20D). Ce contrôle non cellulaire-autonome de R2/5 par R8 fait intervenir le système d'inhibition latérale par la voie Notch/Delta.

A travers ces exemples s'illustrent trois façons de coordonner des décisions stochastiques à l'échelle de plusieurs cellules, voire d'un tissu, afin de satisfaire l'exigence de robustesse imposée par la spécification régionalisée des Métazoaires :

- l'introduction d'un biais par une voie de signalisation présente en gradient ;
- le tri cellulaire *a posteriori* ;
- l'allocation non cellulaire-autonome du destin, qui permet en fait de propager un biais princeps dans un « groupe d'équivalence » cellulaire dont les membres sont liés par une signalisation juxtacrine.

Ci-dessous sont présentés et discutés des résultats acquis lors de ma thèse concernant la spécification des cellules *Krox20*$^{+}$ dans le rhombencéphale des Vertébrés. Quels mécanismes transcriptionnels contrôlent cette spécification et quel est son déterminisme ? Pour répondre à ces questions, nous nous concentrerons sur deux phénotypes essentiels à la morphogenèse du rhombencéphale : la taille de r3 et r5 et leur position selon l'axe antéro-postérieur.
Nous montrons dans cette étude que la taille de r3 et r5 dépend de la voie de signalisation FGF (**chapitre I**) et du fonctionnement de la boucle d'autorégulation de *Krox20* (**chapitre II**). En outre, l'interaction entre ces deux mêmes mécanismes intervient dans le positionnement de r3 le long de l'axe antéro-postérieur **(chapitre III)**. Nous discutons enfin d'un processus d'expansion des territoires d'expression de *Krox20* et de son rôle éventuel dans la morphogenèse de r3 et r5 **(chapitre IV, Annexe).**

Un tout autre sujet est abordé dans le **chapitre V (Annexe)** : le rôle de *Krox20* dans le développement de l'hypophyse antérieure.

RESULTATS

– Chapter 1 –

Hindbrain patterning requires fine-tuning of early *krox20* transcription by *Sprouty 4*

C. Labalette[1], Y.X. Bouchoucha[1], M.A. Wassef[1], P.A. Gongal[1], J. Le Men[1], T. Becker[2], P. Gilardi-Hebenstreit[1], P. Charnay[1]

[1]IBENS, Ecole Normale Supérieure, Paris, France – INSERM U1024, CNRS UMR 8197

[2]Brain and Mind Research Institute, Sydney medical School, Camperdown, Australia

Author contributions:

CL, YXB, MAW, PGH and PC conceived the experiments and interpreted the results.

YXB performed SU treatments on wild-type, *krox20* mutant and A:gfp embryos.

CL, MAW, PAG, JLM, PGH performed all other experiments.

CL, PGH and PC wrote the manuscript.

Foreword

First reports on FGF loss-of-function in the zebrafish hindbrain were published a decade ago and reported a marked reduction of r3 and r5 sizes. At that time, the underlying mechanisms remained elusive. The work presented in this chapter provides an explanation. It begun with two parallel studies: (i) the putative involvement of FGF in the extension of r3 territory; (ii) the functional analysis of the FGF signalling inhibitors *sprouty*, after *sprouty4* was identified in an enhancer-trap screen in Tom Becker's lab.

As we hypothesized that element A plays a key role in the extension mechanism (see chapter 4), the first study concentrated on the dependence of element A activity on the FGF pathway. This was further supported by the identification of three conserved Ets-binding sites on element A whose mutations lead to dramatic decrease of the enhancer activity (not shown). This part led to the conclusion that FGF does not affect an active element A, but we could not decide at that time if it influences the initiation of element A activation.

The second study led to the conclusion that FGF signalling is modulated in the zebrafish hindbrain by *sprouty* genes and primarily affects the initiation of *Krox20* expression by acting on element B and C. An excess of FGF signalling for example leads to more potent activation of B and C, hence retarded *Krox20* expression at early stages.

The following chapter presents the results of these two studies, with more emphasis on the second one.

Development 138, 317-326 (2011) doi:10.1242/dev.057299

Hindbrain patterning requires fine-tuning of early *krox20* transcription by Sprouty 4

Charlotte Labalette[1,2,3], Yassine Xavier Bouchoucha[1,2,3], Michel Adam Wassef[1,2,3], Patricia Anne Gongal[1,2,3], Johan Le Men[1,2,3], Thomas Becker[4], Pascale Gilardi-Hebenstreit[1,2,3] and Patrick Charnay[1,2,3,*]

SUMMARY

Vertebrate hindbrain segmentation is an evolutionarily conserved process that involves a complex interplay of transcription factors and signalling pathways. Fibroblast growth factor (FGF) signalling plays a major role, notably by controlling the expression of the transcription factor Krox20 (Egr2), which is required for the formation and specification of two segmental units: rhombomeres (r) 3 and 5. Here, we explore the molecular mechanisms downstream of FGF signalling and the function of Sprouty 4 (Spry4), a negative-feedback regulator of this pathway, in zebrafish. We show that precise modulation of FGF signalling by Spry4 is required to determine the appropriate onset of *krox20* transcription in r3 and r5 and, ultimately, rhombomere size in the r3-r5 region. FGF signalling acts by modulating the activity of *krox20* initiator enhancer elements B and C; in r5, we show that this regulation is mediated by direct binding of the transcription factor MafB to element B. By contrast, FGF signalling does not control the *krox20* autoregulatory element A, which is responsible for amplification and maintenance of *krox20* expression. Therefore, early *krox20* transcription sets the blueprint for r3-r5 patterning. This work illustrates the necessity for fine-tuning in a common and fundamental patterning process, based on a bistable cell-fate choice involving the coupling of an extracellular gradient with a positive-feedback loop. In this mode of patterning, precision and robustness can be achieved by the introduction of a negative-feedback loop, which, in the hindbrain, is mediated by Spry4.

KEY WORDS: FGF, Segmentation, Rhombomere, Feedback loop, Zebrafish

INTRODUCTION

Vertebrate hindbrain morphogenesis has been the focus of intensive study as a model for vertebrate patterning. The establishment of hindbrain anteroposterior (AP) identity involves a transient segmentation, which leads to the formation of seven to eight metameres called rhombomeres (r) (Lumsden, 1990; Lumsden and Krumlauf, 1996). These territories constitute compartments and developmental units for neuronal differentiation, branchiomotor nerve organisation and neural crest specification (Lumsden and Keynes, 1989). The gene regulatory network underlying hindbrain segmentation includes several transcription factor genes that show spatially restricted patterns of expression along the AP axis, with limits corresponding to prospective or established boundaries between adjacent rhombomeres (Lumsden and Krumlauf, 1996). Among them, *Krox20* (also known as *Egr2*) is specifically expressed in r3 and r5 (Wilkinson et al., 1989) and has been shown to be essential for the establishment and specification of these rhombomeres (Schneider-Maunoury et al., 1993; Schneider-Maunoury et al., 1997; Swiatek and Gridley, 1993; Voiculescu et al., 2001). However, how relative rhombomere sizes are controlled, an essential issue related to many patterning and morphogenetic processes, has not been addressed.

Control of hindbrain segmentation involves several cell signalling pathways. Among them, Fibroblast growth factor (FGF) signalling is necessary in particular to promote Krox20-mediated r3 and r5 development (Aragon and Pujades, 2009; Marin and Charnay, 2000; Maves et al., 2002; Walshe et al., 2002; Wiellette and Sive, 2003; Wiellette and Sive, 2004). It has been shown in zebrafish and chick embryos that *Krox20* expression requires prior FGF signalling (Aragon and Pujades, 2009; Walshe et al., 2002). However, the molecular mechanisms of this regulation have not been investigated. Furthermore, despite the importance of FGF signalling in hindbrain patterning, its possible modulation by antagonists has not been analysed. A negative regulator of the FGF pathway, Sprouty (Spry; Sty – FlyBase), has been identified in *Drosophila* (Hacohen et al., 1998). *spry* is induced by FGF signalling and therefore functions as a negative-feedback regulator (Hacohen et al., 1998). Spry acts intracellularly, through inhibition of the Ras/MAPK pathway (Gross et al., 2001; Yusoff et al., 2002). Four vertebrate orthologues of *spry* have been identified. In mice, *Spry1*, *Spry2* and *Spry4* are widely expressed in the embryo, whereas *Spry3* expression is restricted to the adult (Minowada et al., 1999).

In this study, we have investigated the role of Spry genes in zebrafish hindbrain development and show that Spry4 plays a key role in hindbrain patterning, controlling the relative size of odd- and even-numbered rhombomeres in the r3-r5 region. We demonstrate that Spry4 sets the appropriate onset of *krox20* transcription in r3 and r5 by fine-tuning FGF control of *krox20* initiator enhancer elements. By contrast, Spry4 and FGF signalling do not affect the activity of the *krox20* autoregulatory element responsible for the later amplification and maintenance of *krox20* expression. Therefore, the size of mature rhombomeres is determined at the onset of *krox20* expression, and this work

[1]Ecole Normale Supérieure, IBENS, Paris Cedex 75230, France. [2]Inserm, U1024, Paris Cedex 75230, France. [3]CNRS, UMR 8197, Paris Cedex 75230, France. [4]Brain and Mind Research Institute, Sydney Medical School, 100 Malett St, Camperdown NSW 2050, Australia.

*Author for correspondence (charnay@biologie.ens.fr)

Accepted 15 November 2010

presents a mechanism that combines negative and positive autoregulatory loops to achieve precise and robust pattern formation.

MATERIALS AND METHODS

In situ hybridisation

To generate a *spry1* probe, a cDNA was subcloned into the pCRII-TOPO vector, after RT-PCR using primers 5′-GAATTCGTCCTGTCCCTG-GACCAG-3′ and 5′-CTCGAGCTTTAACGCAGCCTTTCG-3′. For the *spry2* and *spry4* probes, the 3′UTR regions (IMAGE 7227962 and IMAGE 3719315, respectively) were subcloned into pBluescript (Stratagene). Other probes used were zebrafish *krox20* (Oxtoby and Jowett, 1993), chicken *Krox20* (Giudicelli et al., 2001), *ntl* (Schulte-Merker et al., 1994), *her5* (Muller et al., 1996), *mafba* (Moens et al., 1998), *fgf8* (Furthauer et al., 1997) and *hoxb1a* (Prince et al., 1998). Single and double whole-mount in situ hybridisations were performed as described (Hauptmann and Gerster, 1994).

Constructs and zebrafish lines

For all constructs, cloning junction and point mutations were verified by sequencing. The pCS2-spry4 vector was obtained by subcloning the zebrafish *spry4* open reading frame into pCS2+ (RZPD). To generate the dominant-negative form of Spry4 (Spry4Y52A), a mutation of TAC (tyrosine) to GCC (alanine) was introduced at codon 52 (Sasaki et al., 2001) using the Transformer Site-Directed Mutagenesis Kit (Clontech). A morpholino-resistant *spry4* RNA was generated by introducing five silent mismatches into the morpholino target sequence: 5′-(C>G)AGATG-GA(G>A)TC(A>T)(A>T)GGGT(T>G)-3′. For electroporation in the chick neural tube, wild-type and dominant-negative *spry4* cDNAs were tagged with a sequence encoding an HA epitope (5′-TACCCATACGACG-TACCAGACTACGCATCG-3′) just before the stop codon and subcloned into the pAdRSV vector (Wassef et al., 2008). Chicken elements A and B were cloned upstream of the *gfp* reporter in a modified pTol2 vector (Stedman et al., 2009). Chicken element C was cloned into pBGZ40 (Yee and Rigby, 1993) upstream of the minimal β-*globin* promoter-*gfp* reporter. The mutations in the MafB binding sites were introduced using the Phusion Site-Directed Mutagenesis Kit (Finnzymes) and/or the QuikChange Multi Site-Directed Mutagenesis Kit (Stratagene). To generate the *zB:gfp* construct, a 720 bp zebrafish element B (PCR amplified using primers 5′-GATATGCATGGTAAAATCTCCCACCATCG-3′ and 5′-GCGCTC-GAGCACCGCCGAAAAACAATAGC-3′) was cloned upstream of the *gfp* reporter in the modified pTol2 vector. Transgenic lines were obtained from embryos injected at the 1-cell stage with the pTol2 constructs together with *tol2 transposase* mRNA.

mRNA and morpholino injections

spry4 capped sense RNAs were obtained using the mMESSAGE mMACHINE Kit (Ambion) and 300 pg were injected at the 1-cell stage. The sequence of the *spry1* morpholino (Spry1mo) is 5′-CGCG-GAGATCCATAAGACACGATCA-3′. Morpholinos for *spry2* and *spry4* (Spry2mo and Spry4mo) have been described previously (Furthauer et al., 2001; Furthauer et al., 2004). A control *spry4* morpholino (Ctrlmo) was designed by introducing five mismatches into Spry4mo (5′-GTAA-CACTTGAATCGATCTGAAGGT-3′). Morpholinos (Gene Tools) were diluted in Danieau buffer and 2 pmoles were injected at the 1- to 4-cell stage.

Proliferation assay, phosphorylation analysis and SU5402 treatment

For proliferation assays, embryos were immunostained using a rabbit polyclonal antibody against phospho-Histone H3 (Upstate) and Alexa 488-coupled goat anti-rabbit IgG (Jackson). This analysis was preceded by fluorescent in situ hybridisation for *krox20* using FastRed substrate (Roche). Confocal optical sections of flat-mounted embryos were obtained with an inverted Leica DMIRE2 microscope. Western blot analysis was performed as described (Pezeron et al., 2008) using monoclonal phosphoERK (Cell Signaling), polyclonal ERK (Cell Signaling) and monoclonal β-actin (Sigma) antibodies. The phosphoERK and total ERK levels on the immunoblots were quantified using ImageJ software (NIH). Polyclonal phosphoERK antibody (Cell Signaling) was used for whole-mount immunostaining. Treatment of embryos with 60 μM SU5402 was performed as described (Walshe et al., 2002).

In ovo electroporation, X-gal staining and whole-mount immunostaining

In ovo electroporation of the chick neural tube, recovery of embryos and immunodetection were performed as previously described (Desmazières et al., 2009). GFP expression was detected using a rabbit polyclonal antibody (Molecular Probes). Fluorescent signals were quantified using ImageJ. X-gal staining was performed as described (Ghislain et al., 2003).

Gel retardation analysis

Band shift assays were performed with MafB protein purified from bacterial extracts as described (Manzanares et al., 2002). The following double-stranded oligonucleotides were used as probes or competitors: wtM1, 5′-GGAAAGTACAGACAGTGCATTTTCCC-3′; mutM1, 5′-GGAAAGGTAAGACAGTGCATTTTCCC-3′; wtM2, 5′-CAAATTTG-CTGATTTTCACCAGTATC-3′; and mutM2, 5′-CAAATTGCAT-GATTTTCACCAGTATC-3′.

RESULTS

Expression of the Sprouty gene family in the developing hindbrain

In the zebrafish embryo, expression of *spry1*, *spry2* and *spry4* has been reported in the midbrain-hindbrain region at mid-somitogenesis stages (Furthauer et al., 2001; Furthauer et al., 2002; Furthauer et al., 2004; Komisarczuk et al., 2008). To further analyse their expression, we performed an in situ hybridisation analysis starting from 80% epiboly. We found that these genes were expressed from 90% epiboly in a large transverse stripe of the neural plate, which is likely to correspond to the prospective hindbrain (data not shown). At 100% epiboly, *spry1* was still expressed in a broad band corresponding approximately to the hindbrain (Fig. 1A), whereas *spry2* and *spry4* showed more restricted AP patterns within the hindbrain (Fig. 1B,C). At the 1-somite stage, to evaluate the limits of the Spry gene expression domains, we performed double in situ hybridisations with *krox20*. At this stage, *krox20* expression is well established in r3, but is only beginning to be initiated in prospective r5. *spry1* was expressed from approximately r1 to r6 (Fig. 1D) and *spry2* from r1/r2 to r4 (Fig. 1E). In contrast to *spry1* and *spry2*, which were uniformly expressed in single domains, *spry4* showed strong expression in r2 and r3 and weaker expression in r4 and r5 (Fig. 1F). At the 4- to 6-somite stages, *spry1* and *spry2* were highly expressed in r1, ventral r2 and r4, and in the midbrain-hindbrain boundary (MHB) (Fig. 1G,H,J,K). By contrast, *spry4* expression became prominent in r3, r5 and the MHB (Fig. 1I,L).

Spry4 controls hindbrain patterning in the r3-r5 region

To investigate the effects of Spry loss-of-function on hindbrain patterning, we performed knockdown experiments with morpholino oligonucleotides. We used morpholinos that had been previously tested: Spry1mo (Marika Kapsimali, personal communication), Spry2mo (Furthauer et al., 2004) and Spry4mo (Furthauer et al., 2001). As a control we used a version of Spry4mo containing five mismatches (Ctrlmo). To evaluate the consequences of morpholino injections, we first performed double in situ hybridisations at the 10-somite stage for *krox20* and *her5*, a marker of the MHB. Spry1mo-injected embryos (n=23) did not show any obvious phenotype (Fig. 2A,B). Spry2mo induced a lateral broadening of the neural plate and a shortening of the AP axis

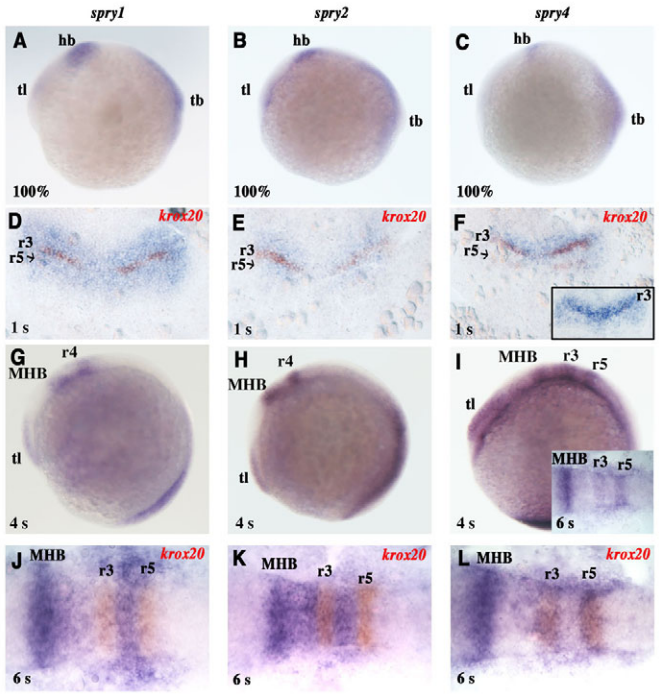

Fig. 1. Spry gene expression in the early zebrafish hindbrain. (**A-L**) In situ hybridisations were performed with *spry1* (A,D,G,J), *spry2* (B,E,H,K) and *spry4* (C,F,I,L) probes (blue) at the indicated somite (s) or epiboly (%) stages, shown as lateral views with anterior to the left (A-C,G-I) and flat-mounts with anterior at the top (D-F) or left (inset in I and J-L). Where indicated (D-F,J-L), double in situ hybridisation was performed with a *krox20* probe (red) to allow precise localisation of r3 and r5. The inset in F shows the *spry4* pattern without *krox20* labelling. hb, hindbrain; tb, tailbud; tl, telencephalon; MHB, midbrain-hindbrain boundary.

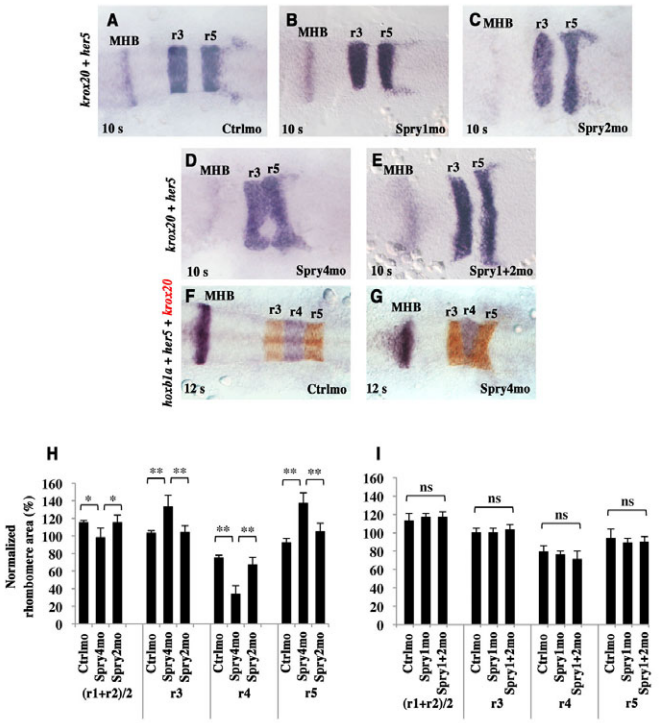

Fig. 2. Spry4 loss-of-function results in hindbrain patterning defects. (**A-G**) Zebrafish embryos injected with either control morpholino (Ctrlmo) (A,F), Spry1mo (B), Spry2mo (C), Spry4mo (D,G) or both Spry1mo and Spry2mo (E) were collected at the 10-somite (A-E) or 12-somite (F,G) stage and subjected to in situ hybridisation for *krox20* and *her5*, a marker of the MHB (A-E, both purple), or for *krox20* (red), *her5* and *hoxb1a* (purple) (F,G). Embryos are flat-mounted with anterior to the left. (**H**,**I**) Quantitative evaluation of rhombomere areas. Normalised areas were obtained by dividing each rhombomere area by one fifth of the area of the neural plate from r1 to r5. ns, not significant ($P>0.05$); *, $P<0.004$; **, $P<0.0001$; Student's *t*-test. Errors bars indicate s.e.m.

(n=22; Fig. 2C). These malformations might result from dorsalisation and/or convergent-extension defects, as previously described (Furthauer et al., 2004). As expected (Furthauer et al., 2001), similar malformations were observed in Spry4mo-injected embryos (Fig. 2D). The severity of these morphological defects was comparable between Spry2 and Spry4 morphants (for quantification, see Fig. S1 in the supplementary material). However, Spry4mo injection resulted in an additional phenotype, with a dramatic reduction of the area of r4, often resulting in a partial fusion of r3 and r5 territories (Fig. 2D). Co-injection of the Spry4mo with a p53 morpholino (Robu et al., 2007) resulted in the same change in hindbrain patterning, excluding an artefact of morpholino-induced cell death (see Fig. S2 in the supplementary material). These modifications did not lead to any overlap between r3/r5 and r4 markers as revealed by double in situ hybridisation with *krox20* and *hoxb1a* probes (Fig. 2F,G).

Quantification of the areas of individual rhombomeres, after normalisation to the area of the r1-r5 territory, revealed a 55% decrease in the area of r4 in Spry4mo-injected embryos (n=18) as compared with controls (n=12; *t*-test, $P<0.0001$; Fig. 2H). By contrast, the r1/r2 territory was only decreased by 15% in Spry4 morphants (*t*-test, $P<0.004$) (Fig. 2H). The specific reduction in the r4 area in Spry4 morphants coincided with increases in the areas of r3 and r5 (by 29% and 48%, respectively; *t*-test, $P<0.0001$; Fig. 2H), suggesting that these rhombomeres had expanded at the expense of r4. No such differences in r3, r4 and r5 areas were observed in Spry1 or Spry2 morphants (Fig. 2H,I). As the Spry1 and Spry2 amino acid sequences are more closely related to each other than to that of Spry4, these proteins might have redundant functions. We therefore evaluated the consequences of combined Spry1 and Spry2 loss-of-function. Although co-injected embryos appeared highly laterally broadened, no significant change in the relative area of the rhombomeres was observed (n=25; Fig. 2E,I). Altogether, these data demonstrate that Spry4 loss-of-function specifically results in an expansion of r3 and r5, presumably at the expense of r4, and that it is unlikely that these effects are related to the morphological broadening phenotype.

We then investigated whether this mispatterning of the hindbrain persisted at later stages. At the 20-somite stage, rhombomere boundaries are well established and the formation of the neural rod is complete. In Spry4mo-injected embryos (n=18), the r4 area was reduced by 53%, as compared with control embryos (n=12; *t*-test, $P<0.0001$; see Fig. S3 in the supplementary material). Conversely, r3 and r5 areas were increased by 28% and 37%, respectively, as

compared with controls (*t*-test, $P<0.0001$; see Fig. S3 in the supplementary material). The specificity of the phenotype was confirmed by RNA rescue experiments. For this purpose, Spry4mo was co-injected with a full-length *spry4* mRNA that contained silent mutations in the morpholino target sequence. In Spry4 morphants co-injected with this mRNA (n=18), the reduction of the r4 area (by 11%) and the extensions of r3 and r5 (by 10% and 11%, respectively) were much milder than without co-injection (see Fig. S3 in the supplementary material), indicating that the phenotype associated with the Spry4mo was largely rescued by *spry4* mRNA and is therefore specific. Altogether, these data establish that Spry4 loss-of-function results in a permanent expansion of the r3 and r5 territories and in a commensurate reduction of r4.

Spry4 does not regulate cell proliferation

The differential expansion of r3/r5 and r4 in embryos associated with Spry4 loss-of-function might have resulted from abnormalities in the rates of cell proliferation. We investigated whether Spry4 loss-of-function differentially affected cell proliferation during early somitogenesis. We identified cells in mitosis by immunostaining with an antibody directed against phospho-Histone H3 in control (n=17) and Spry4mo-injected (n=23) embryos at the 5-somite stage. The immunostaining was combined with *krox20* mRNA detection by fluorescent in situ hybridisation to localise r3 and r5. No significant changes in the distribution of mitotic cells were observed in r3, r4 or r5 upon Spry4 knockdown (see Fig. S4 in the supplementary material). Thus, the relative expansion of r3 and r5 with respect to r4 cannot be explained by differential cell proliferation.

Spry4 modulates the onset of *krox20* expression

The expansion of r3 and r5 and the corresponding reduction of r4 in Spry4 morphants might occur during the growth of the rhombomeres or result from very early cell-fate decisions. To address this, we investigated whether Spry4 loss-of-function affected the early expression of *krox20*. To precisely stage embryos, we performed double in situ hybridisations for *krox20* and *no tail* (*ntl*). *ntl* is expressed in the germ ring and can be used to precisely evaluate the extent of tailbud closure (Fig. 3A-C, insets). In control embryos at the 100% epiboly stage, expression of *krox20* was observed in 46% of the embryos in r3, but never at the level of prospective r5 (n=24; Fig. 3A,D). By contrast, all Spry4mo-injected embryos expressed *krox20* in r3 and in a larger territory than in the controls (n=27; Fig. 3B,D). Furthermore, 22% of Spry4 morphants also expressed *krox20* in r5. This phenotype was specific to Spry4 as it did not occur in Spry2mo-injected embryos (20% expressed *krox20* in r3 and none expressed *krox20* at the level of r5; n=20; Fig. 3C,D). Similarly, Spry1 or double Spry1;Spry2 morphants did not show any detectable change in *krox20* expression compared with controls (data not shown). The specificity of this phenotype in Spry4 morphants was confirmed by rescue experiments. As shown in Fig. 3E, the phenotype was strongly reduced by co-injection of *spry4* mRNA. Thus, Spry4 loss-of-function leads to both premature *krox20* expression and larger early expression domains.

To further investigate the timing of this premature *krox20* expression, we examined earlier stages. At the 95% epiboly stage, all Spry4 morphants expressed *krox20* in r3 and 4% already showed expression at the level of prospective r5 (n=28; Fig. 3D). By contrast, *krox20* expression was detected at the level of r3 in only 27% of control and 10% of Spry2mo-injected embryos (n=26 and n=42, respectively; Fig. 3D). At the 90% epiboly stage, neither control (n=28) nor Spry2mo-injected (n=40) embryos displayed *krox20* expression (Fig. 3D). By contrast, 40% of the Spry4mo-injected embryos already expressed *krox20* at the level of prospective r3 (n=40; Fig. 3D).

To confirm these data, *krox20* expression was investigated following injection of an mRNA encoding a dominant-negative form of Spry4 (Spry4Y52A) (Sasaki et al., 2001), which is another approach to obtain loss-of-function. At the 95% epiboly stage, 70% of *spry4Y52A* mRNA-injected embryos showed *krox20* expression in r3 (n=36), in contrast to only 20% of *gfp* mRNA-injected control embryos (n=50; Fig. 3F). Therefore, consistent with the morpholino experiments, injection of the dominant-negative RNA results in premature and expanded *krox20* expression in r3.

Finally, we investigated whether we could obtain phenotypes converse to those of the loss-of-function experiments by Spry4 gain-of-function. For this purpose, we injected embryos with *spry4* mRNA. As shown in Fig. 3E, at 100% epiboly only 13% of the *spry4* mRNA-injected embryos (n=23) showed expression of *krox20* in r3, as compared with 43% of the *gfp* mRNA-injected controls (n=21; χ^2-test, $P<0.05$). *krox20* expression in r5 was also affected by the misexpression of *spry4*. At 10.25 hours post-fertilisation (hpf) 73% of the *gfp* mRNA-injected embryos expressed *krox20* in r5 (n=26) as compared with only 37% of the *spry4* mRNA-injected embryos (n=27; χ^2-test, $P<0.05$; Fig. 3G). These data indicate that *spry4* overexpression delays the onset of *krox20* expression, an effect opposite to that of Spry4 loss-of-function.

In conclusion, our results indicate that Spry4 modulates the onset and early expansion of *krox20* expression. This early phenotype correlates with the expansion of r3 and r5 territories at later stages, suggesting that early *krox20* expression is a critical determinant of the patterning of the r3-r5 region.

The onset of *krox20* expression is determined by FGF signalling

Our data indirectly implicated FGF signalling in the onset of *krox20* expression. To confirm that modulations of Spry4 activity resulted in modifications at the level of FGF signalling, we analysed activation of the ERK pathway, which is known to require FGF signalling (Aragon and Pujades, 2009; Roy and Sagerstrom, 2004). Control and Spry4mo-injected embryos were collected at 100% epiboly and western blot analysis was performed on whole embryo protein extracts, using an antibody against phosphorylated (p) ERK1/2 (Mapk3/1 – Zebrafish Information Network), a read-out of ERK pathway activation. The pERK1/2 level, normalised to total ERK1/2, was increased in Spry4 morphants (see Fig. S5 in the supplementary material). To reveal FGF signalling in situ, we performed whole-mount immunostaining against pERK1/2 and in situ hybridisation for a target of the pathway, *pea3*. pERK1/2 and *pea3* were detected in the hindbrain, and, in Spry4 morphants, their expression levels were higher (see Fig. S5 in the supplementary material). Together, these data indicate that Spry4 loss-of-function leads to enhanced FGF signalling, consistent with Spry4 acting as an antagonist of this pathway.

Previous studies have revealed that *krox20* expression at mid- and late somitogenesis stages is dependent on prior FGF signalling (Marin and Charnay, 2000; Maves et al., 2002; Walshe et al., 2002; Wiellette and Sive, 2003). However, the role of the pathway has not been examined at early stages of *krox20* expression. To directly investigate this, we treated embryos with SU5402, an inhibitor of FGF receptor activity, from 50% epiboly. We first checked that this treatment prevented expression of *spry4* at the 100% epiboly stage

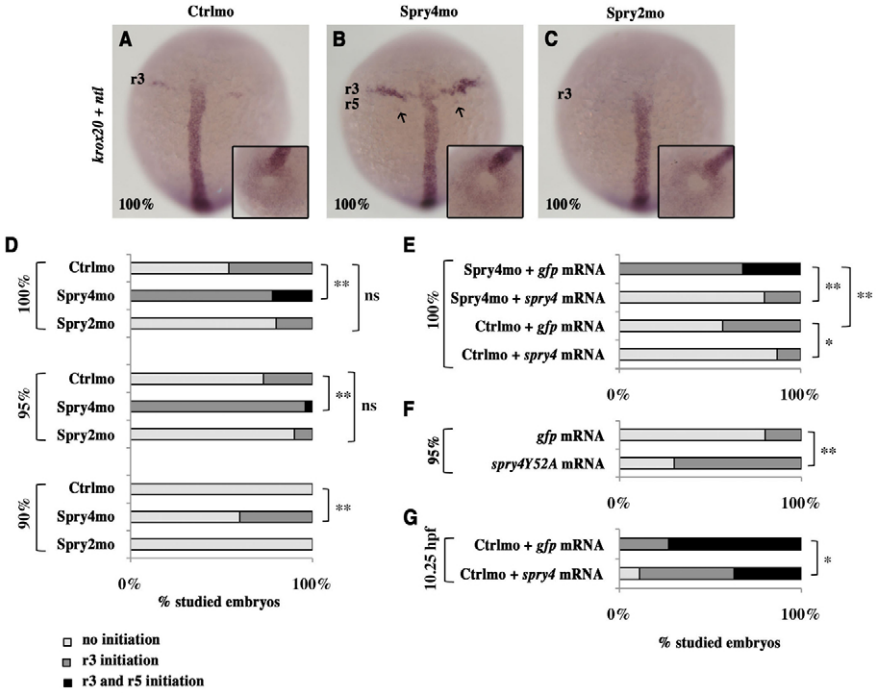

Fig. 3. Spry4 controls the onset of *krox20* expression. (**A-C**) Zebrafish embryos injected with either control morpholino (Ctrlmo) (A), Spry4mo (B) or Spry2mo (C) were collected at 100% epiboly and subjected to in situ hybridisation with *krox20* and *ntl* probes (purple). Arrows in B indicate *krox20* expression in a few r5 cells. The insets show tailbud views of the embryos, allowing determination of the developmental stage by evaluation of the closure of the tailbud, as revealed by *ntl* expression. (**D-G**) Distribution of embryos showing either no *krox20* expression, limited expression in r3 or expression in both r3 and r5 at 90, 95 or 100% epiboly or at 10.25 hours post-fertilisation (hpf). ns, not significant; *, $P<0.05$; **, $P<0.0001$; χ^2-test.

in the hindbrain (see Fig. S6 in the supplementary material), establishing that Spry4 is indeed part of a negative-feedback loop. At 10.25 hpf, only 63% of the SU5402-treated embryos ($n=19$) expressed *krox20* in r3, as compared with 95% of the control embryos ($n=22$; χ^2-test, $P<0.0001$; Fig. 4A,B,E), which in addition showed larger *krox20* expression domains. Furthermore, none of the embryos treated with SU5402 expressed *krox20* in r5, as compared with 50% of the control embryos at this stage. A defect at the level of r5 was still observed at 10.5 hpf (1-somite stage), with no *krox20* expression in SU5402-treated embryos ($n=28$; χ^2-test, $P<0.0001$; Fig. 4C,D,E).

These data were confirmed by an alternative approach. A stable transgenic line that expresses a heat shock-inducible dominant-negative form of Fgfr1 (Lee et al., 2005) was used to downregulate FGF signalling. Expression of the dominant-negative receptor was induced at the 80% epiboly stage and embryos were collected at 10.25 hpf. At this stage, *krox20* was expressed at the level of r3 in 94% of the non-transgenic embryos ($n=72$), in contrast to only 64% of *hsp70l:dnfgfr1-gfp* transgenic embryos ($n=74$; χ^2-test, $P<0.0001$; data not shown). Overall, these results establish that FGF signalling is essential for the normal onset of *krox20* expression in r3 and r5.

FGF signalling controls initiator but not maintenance *krox20* enhancers

Krox20 transcription in r3 and r5 is subject to two regulatory phases controlled by distinct cis-acting regulatory elements (Chomette et al., 2006; Wassef et al., 2008). Transcription is first induced in a cell under the control of initiator enhancers (element C in r3 and elements B and C in r5) leading to the early accumulation of Krox20 protein (the onset phase); this protein can then activate a positive autoregulatory loop by binding to a third enhancer, element A (the amplification and maintenance phase). Our observations of the consequences of the modulation of FGF signalling on early *krox20* expression suggest that this pathway might be required during the onset phase. To test this, we performed the SU5402 treatment on embryos carrying a point mutation in the *krox20* coding sequence that inactivates the protein and therefore prevents the establishment of the autoregulatory loop [$krox20^{fh227/fh227}$ (Monk et al., 2009)]. We found that at the 4-somite stage, the *krox20*-positive territories (corresponding only to the onset phase in the homozygous mutants) were dramatically reduced in SU5402-treated, as compared with DMSO carrier-treated, mutant embryos, as was the case for wild-type embryos (Fig. 4F-I). This definitively demonstrates that FGF signalling affects the onset phase of *krox20* expression.

To investigate whether FGF signalling was acting on *Krox20* at the transcriptional level, we analysed the dependence of the different cis-acting regulatory elements on FGF signalling. We first made use of a chick hindbrain electroporation system that we have shown previously to largely reflect the in vivo activities of the enhancers (Chomette et al., 2006). Constructs in which a GFP reporter is driven by each of the *Krox20* chick enhancers were co-electroporated with expression vectors for wild-type or dominant-negative (Spry4Y52A) HA-tagged forms of Spry4 to modulate FGF signalling. The level of endogenous *Krox20* expression was not affected after electroporation of wild-type ($n=14$; Fig. 5A,B, compare left and right) or Y52A ($n=17$; Fig. 5C,D) Spry4 at the 7- to 8-somite stage [Hamburger-Hamilton (HH) stage 9]. This suggests that endogenous *Krox20* expression is no longer sensitive to FGF signalling at this stage, consistent with previous observations (Aragon and Pujades, 2009). By contrast, co-electroporation with the enhancer constructs revealed that the activities of both the B and C enhancers were significantly reduced when co-electroporated with the wild-type Spry4 construct as compared with the dominant-negative form (59% and 63% reduction, respectively; $n=17$; Fig. 5I-P,R,S). It should be noted that we used a version of element C that contains additional sequences compared with the previously published enhancer (Chomette et al., 2006). This results in a higher specificity of the enhancer for r3 (data not shown). In contrast to its effect on the initiator elements, alteration of FGF signalling had no effect on enhancer A activity (Fig. 5E-H,Q). In conclusion, these data indicate that elements B and C, which are responsible for the onset of *krox20* transcription, are controlled by FGF signalling, whereas element A, which is in charge of the amplification and maintenance phase, is not.

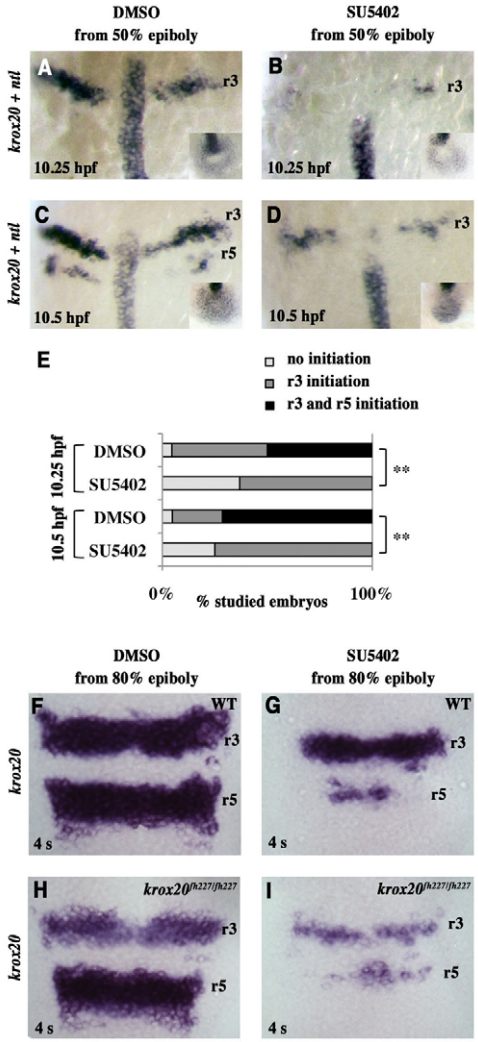

Fig. 4. FGF signalling is required for the appropriate onset of *krox20* expression. (**A-D**,**F-I**) Zebrafish embryos were incubated in either DMSO carrier or SU5402 from 50% epiboly to 10.25 hpf (A,B) or from 50% epiboly to the 1-somite stage (10.5 hpf) (C,D) or from 80% epiboly to the 4-somite stage (F-I) and analysed by in situ hybridisation for *krox20* and *ntl* (A-D) or for *krox20* alone (F-I). The insets in A-D show tailbud views of the corresponding embryos (see Fig. 3). Wild-type (WT) and *krox20*$^{fh227/fh227}$ mutant embryos are compared in F-I. (**E**) Distribution of the embryos according to *krox20* expression in r3 and r5 (see Fig. 3). **, $P<0.0001$; χ^2-test.

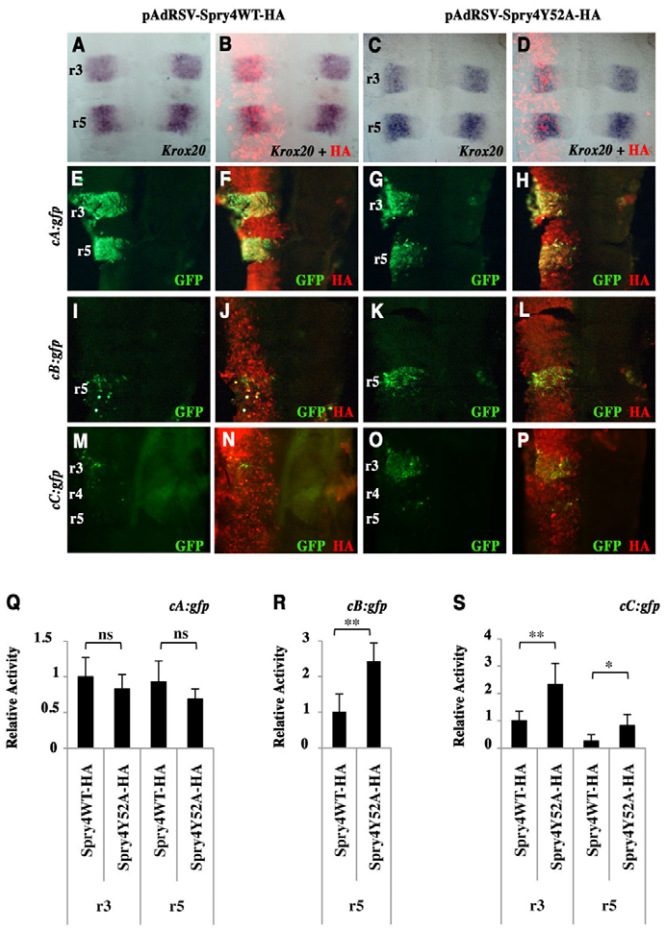

Fig. 5. Spry4 regulates *Krox20* initiator enhancers in the chick embryo. (**A-D**) Chick embryo neural tubes were electroporated on the left side with HA-tagged wild-type or Y52A dominant-negative zebrafish *spry4*-expressing vectors (pAdRSV-Spry4WT-HA and pAdRSV-Spry4Y52A-HA), and flat-mounted after in situ hybridisation with a *Krox20* probe. No difference was detected between the left (experimental) and right (control) sides. The efficiency of electroporation and *spry4* expression were monitored by immunolabelling against the HA tag (B,D). (**E-P**) Chick embryo neural tubes were co-electroporated with HA-tagged wild-type or Y52A dominant-negative *spry4*-expressing vectors and constructs carrying chicken *Krox20* enhancer elements cA, cB or cC driving the *gfp* reporter, and subjected to HA (red) and GFP (green) immunostaining (merge in yellow). (**Q-S**) Quantitative evaluation of relative reporter activity obtained by dividing the GFP signal intensity by the HA signal intensity, both quantified using ImageJ. ns, not significant; *, $P<0.0005$; **, $P<0.0001$; Student's *t*-test. Errors bars indicate s.e.m.

To test whether these finding are also applicable to zebrafish, we generated stable transgenic lines carrying a *gfp* reporter under the control of chick element A (cA; zebrafish element A has not yet been identified) or zebrafish element B (zB). Transgenic embryos were exposed to SU5402 or DMSO carrier from the 1- to 8-somite stages, then fixed and analysed by double in situ hybridisation for *gfp* and *krox20*. In *cA:gfp* transgenic embryos, *gfp* expression always precisely overlapped with *krox20* expression in both r3 and r5, even after SU5402 treatment, which led to a reduction in the size of the r5 territory (n=16 and n=19, respectively; Fig. 6A,B). This suggests that the activity of element A is not affected by FGF signalling (the reduction in the r5 domain of A activity is likely to reflect the consequences of a lack of initiation of *krox20* expression). In *zB:gfp* transgenic embryos, *gfp* expression was restricted to r5 as expected in DMSO-treated control embryos (n=14), and was almost entirely absent from the remaining r5 territory after SU5402 treatment (n=15; Fig. 6C,D), indicating that element B absolutely requires FGF signalling for its activity.

Together, these chick and zebrafish experiments establish that FGF signalling controls *Krox20* transcription by regulating its onset phase through elements B and C. By contrast, the amplification and maintenance phase, controlled by element A, is not dependent on FGFs. This latter point explains why endogenous *Krox20*

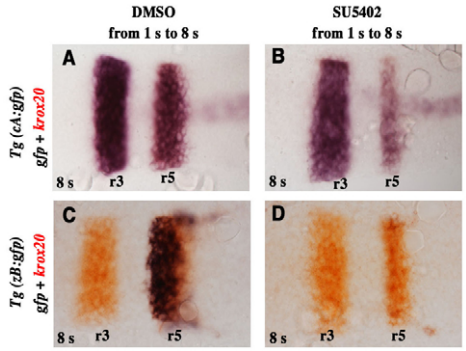

Fig. 6. FGF signalling is required for *krox20* enhancer B activity in the zebrafish embryo. (**A-D**) Transgenic embryos carrying the *gfp* gene under the control of the chicken *Krox20* A enhancer [*Tg(cA:gfp)*] (A,B) or the zebrafish *krox20* B enhancer [*Tg(zB:gfp)*] (C,D) were incubated in DMSO carrier (A,C) or SU5402 (B,D) from the 1-somite stage, collected at the 8-somite stage and subjected to double in situ hybridisation for *gfp* (blue) and *krox20* (orange); overlap is purple (A-C). Embryos were flat-mounted with anterior to the left.

expression is not sensitive (chick) or only partially sensitive (zebrafish) to a block in FGF signalling when the autoregulatory loop has become engaged.

MafB mediates FGF signalling by direct binding to element B

Since the effect of FGF signalling on *Krox20* expression in r5 is at least in part mediated by element B, we searched for the trans-acting factors involved. The transcription factor MafB, which is encoded in zebrafish by *mafba*, is necessary for *Krox20* expression in r5 (Cordes and Barsh, 1994; Moens et al., 1996; Wiellette and Sive, 2003). MafB expression requires FGF signalling (Aragon and Pujades, 2009; Maves et al., 2002; Walshe et al., 2002; Wiellette and Sive, 2003; Wiellette and Sive, 2004). We investigated the dynamics of *mafba* expression and found that Spry4 loss-of-function led to the premature onset of *mafba* in r5/r6: at 95% epiboly, all Spry4 morphants expressed *mafba* (n=28), versus only 12% of control embryos (n=33; χ^2-test, P<0.0001; see Fig. S7 in the supplementary material). These data raise the possibility that the premature onset of *krox20* expression in r5 is due to precocious activation of *mafba*.

To investigate whether MafB directly controls element B, we searched for potential MafB binding sites within enhancer B sequences conserved in vertebrate species. We found two motifs similar to the consensus MafB recognition element (MARE), termed MafB-1 and MafB-2 (Fig. 7A,B). The MafB-1 sequence is conserved between zebrafish, *Xenopus*, chick and mouse (Fig. 7A) and is followed by a sequence of lower similarity to MARE in reverse orientation (Fig. 7A). MafB-2 is well conserved between *Xenopus*, chicken and mouse enhancers, but was not found in the zebrafish enhancer at this position (Fig. 7A), although an identical sequence is present in zebrafish at a more 5′ position. Interestingly, MafB-2 is located close to a vHnf1 (Hnf1ba – Zebrafish Information Network) binding site (Fig. 7A) that we have previously shown to be required for element B activity in r5 (Chomette et al., 2006). We investigated whether MafB interacts with the two putative binding sites by gel retardation. Incubation of oligonucleotides carrying each sequence (Fig. 7A) with bacterially expressed mouse MafB led to the formation of specific retarded bands (Fig. 7C). To establish that the binding sites corresponded to the sequences identified in silico, we introduced mutations into the putative MafB sites (Fig. 7B). Band shift analysis demonstrated that the affinity of MafB was strongly reduced for the mutated MafB-1 oligonucleotide and abolished for the mutated MafB-2 oligonucleotide (Fig. 7C). In the former case, residual binding might be due to the presence of the related sequence in reverse orientation, which was also present in the oligonucleotide.

To investigate the functional significance of these binding sites in the enhancer, we compared the activities of wild-type and mutant versions of chick element B driving the *lacZ* reporter in the chick electroporation system. Wild-type enhancer activity was restricted to r5 as expected (Fig. 7D). Mutation of the MafB-1 or MafB-2 site strongly reduced the activity of element B (Fig. 7E,F) and the double mutation abolished it (Fig. 7G). This demonstrated that both sites are important for enhancer activity. To investigate the ability of MafB to activate the enhancer via these sites and to cooperate with vHnf1, we performed co-electroporation experiments. Co-electroporation of the wild-type enhancer with MafB or vHnf1 expression vectors led to slight expansions of the domain of enhancer activity (Fig. 7H,I). However, co-electroporation with both expression vectors led to generalised and high-level activation of the enhancer throughout the neural tube (Fig. 7J). By contrast, almost all activity was abolished when the enhancer carried mutations in both MafB sites (Fig. 7K) or in the vHnf1 binding site (data not shown). Finally, we analysed endogenous chick *Krox20* expression upon ectopic expression of *MafB*, *vHnf1* or both, and it responded in a manner similar to element B, although the ectopic activation was more limited (see Fig. S8 in the supplementary material).

In conclusion, this analysis establishes that in r5, MafB activates element B and therefore *Krox20* expression by direct binding to the MafB-1 and MafB-2 sites, and that it synergistically cooperates with vHnf1 bound to its nearby cognate site. Since MafB is itself under FGF (Wiellette and Sive, 2003) and Spry4 (this study) control, this demonstrates that in r5, *Krox20* regulation by the FGF pathway and fine-tuning by Spry4 involve direct transcriptional control by MafB.

DISCUSSION

In this study, we have investigated FGF-dependent mechanisms that control the size of rhombomeres during zebrafish hindbrain development. We have established the role of a negative-feedback regulatory loop governed by Spry4, which fine-tunes FGF signalling to control early *krox20* transcription and the subsequent expansion of r3, r4 and r5. The tight correlation between these two processes suggests a direct causative link between them. We propose that fine-tuning, negative-feedback regulation and positive autoregulation can combine at the molecular level to ensure robust and precise patterning.

FGF signalling controls early *krox20* transcription

Previous studies have shown that FGF signalling plays an essential role in the control of *Krox20* expression in r3 and r5 (Aragon and Pujades, 2009; Marin and Charnay, 2000; Maves et al., 2002; Walshe et al., 2002; Wiellette and Sive, 2003; Wiellette and Sive, 2004). Here we investigated the timing, the level of action and the mechanisms of FGF control. We had previously shown that *krox20* is initially transcribed under the control of two initiator cis-acting regulatory elements: C in r3 and r5 and

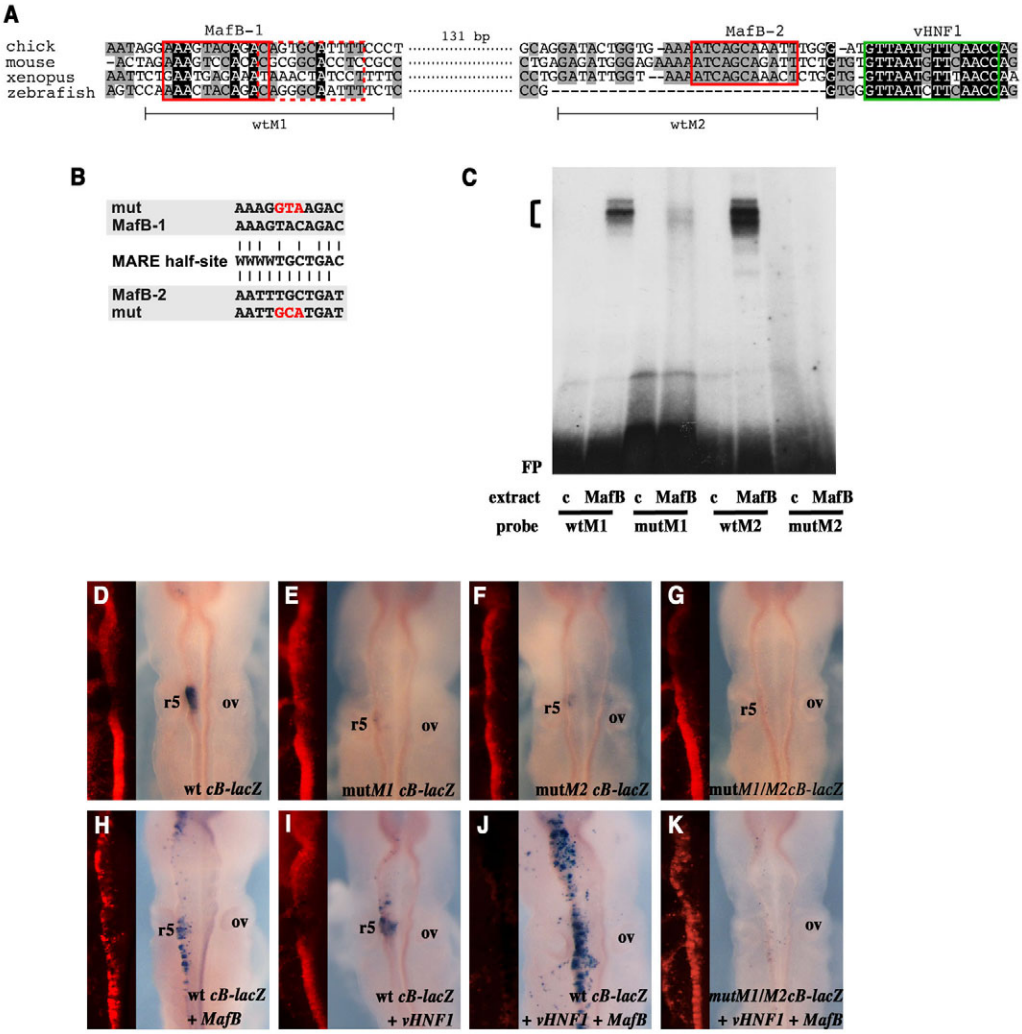

Fig. 7. Identification of functional MafB binding sites in *Krox20* enhancer B. (**A**) Alignment of zebrafish, *Xenopus*, chick and mouse *Krox20* element B nucleotide sequences showing the two conserved putative MafB sites MafB-1 and MafB-2 (red boxes). A sequence of lower similarity to the MafB consensus binding site, adjacent to MafB-1 and in the reverse orientation, is also indicated (dashed red box). A vHnf1 binding site is indicated by the green box. The oligonucleotides used for gel retardation (wtM1 and wtM2) are indicated beneath. (**B**) Alignment of MafB-1 and MafB-2 with the consensus MafB recognition element (MARE) half-site (W=A or T). The mutations introduced into the MafB-1 and MafB-2 sites are indicated in red. (**C**) Gel retardation analyses were performed with the indicated bacterial protein extracts (c, control without MafB protein) and oligonucleotides carrying the chick versions of the MafB-1 and MafB-2 sites, either wild-type (wtM1, wtM2) or mutated (mutM1, mutM2). FP, free probe. The bracket indicates MafB-probe shift complexes, which are abolished or largely abolished by mutation of the MafB-2 and MafB-1 sites, respectively. (**D-K**) Chick embryos were analysed by X-gal staining after electroporation with constructs containing wild-type (D,H-J) or mutant (E-G,K) versions of chick element B driving a β-*globin* promoter-*lacZ* reporter. Embryos were co-electroporated with *MafB* alone (H), *vHnf1* alone (I), or both (J,K). In all cases, a *Cherry*-expressing vector was co-electroporated to monitor electroporation efficiency; Cherry visualisation (red) was carried out following X-gal staining and is shown to the left of each image. Note that strong X-gal staining quenches Cherry fluorescence. ov, otic vesicle.

B in r5 (Chomette et al., 2006; Wassef et al., 2008). Later on, *krox20* expression is amplified and maintained under the control of the autoregulatory enhancer A (Chomette et al., 2006). In this study, using different methods to perturb FGF signalling, we have established that early levels of FGF signalling modulate the onset of *krox20* expression in r3 and r5, i.e. its timing and the expansion of its early domains, whereas *krox20* expression is only marginally dependent on FGF signalling after the 1-somite stage (Fig. 6). Consistently, FGF signalling controls both of the *krox20* initiator enhancers, whereas it has no effect on the autoregulatory element (Figs 5 and 6) and does not require the autoregulatory loop (Fig. 4F-I). Therefore, although we cannot exclude the possibility that FGF signalling also affects *krox20* expression at another level (e.g. translational), all available data converge toward the idea that its major site of action is the onset of transcription.

In the case of r5, we went on to investigate the detailed molecular mechanisms of the pathway. We have shown that the early expression of *krox20* is mediated by direct binding of MafB to enhancer B (Fig. 7). This activation involves vHnf1, which also binds to enhancer B and cooperates synergistically with MafB (Fig. 7). Since the onset of *mafba* expression is itself controlled by FGF signalling (see Fig. S7 in the supplementary material), our data provide a detailed chain of events for the regulation of enhancer B by FGF signalling and ultimately for the control of early *krox20* expression in r5.

Early *krox20* expression sets the blueprint for r3-r5 patterning

The modifications in the onset of *krox20* expression following modulation of FGF signalling correlated with drastic variations in the sizes of mature r3, r4 and r5 at mid-somitogenesis. To explain these correlations, we propose that the number of Krox20-positive cells at early stages actually determines the later size of these territories. This idea is consistent with our current representation of the development of the r3-r5 region. It has been established that the specification of r3 and r5 absolutely requires Krox20 (Schneider-Maunoury et al., 1993; Seitanidou et al., 1997; Swiatek and Gridley, 1993; Voiculescu et al., 2001). As discussed above, *krox20* expression in r3 and r5 is initiated under the control of elements B and C. We propose that once Krox20 levels have reached a certain threshold in a cell, the autoregulatory loop based on element A is switched on. Therefore, the duration of activity of elements B and C required for permanent *krox20* expression in a cell may be very short. In addition, whereas the autoregulatory loop specifies the level of *krox20* expression during the stationary phase, it cannot modulate the number of stably expressing cells, which is determined by the level of *krox20* expression reached under the control of elements B or C and the affinity of the Krox20 binding sites present in element A. Cell proliferation will then contribute to the absolute size of the rhombomeres. However, since the rate of cell proliferation appears to be similar in the different rhombomeres (see Fig. S4 in the supplementary material), it does not affect their relative size.

In conclusion, these results fully support the idea that the mature sizes of r3 and r5 are primarily determined by the number of cells in which *krox20* is initially activated. This link explains why perturbations in FGF signalling, a pathway that precisely modulates the efficiency of initial *krox20* activation, have such dramatic effects on the relative size of the mature rhombomeres. Finally, the development of r4 inversely mirrors the number of cells stably expressing *krox20*, as *krox20* gain-of-function in a cell results in loss of r4 identity, and *krox20* loss-of-function causes a gain of r4 identity (Giudicelli et al., 2001; Voiculescu et al., 2001).

Fine-tuning of early *krox20* expression requires negative-feedback regulation of FGF signalling

As discussed above, we propose that segment formation in the r3-r5 region is based on a bistable cell-fate choice that is dependent on the activation (or not) of the Krox20 positive autoregulatory loop. Such switch-like mechanisms play central roles in the patterning of multicellular organisms (Graham et al., 2010; Kitano, 2004). Here, the binary choice is coupled with the translation of the local FGF concentration into the initial activation of *krox20*. However, because of fluctuations in the environment and in ligand concentration, transcriptional noise and the occurrence of mutations, this type of network organisation is expected to lack precision and robustness (Jaeger et al., 2008). More specifically, if the number of cells that initially activate *krox20* in r3 and r5 is of such importance for hindbrain patterning, a very precise regulation of this aspect of *krox20* expression is likely to be required. A way to buffer fluctuations and to improve precision is to introduce a cell-autonomous negative-feedback loop in the target cells (Freeman, 2000). We think that this is precisely the role of Spry4 in this system. *spry4* is positively regulated by FGF and acts intracellularly to negatively regulate FGF signalling through inhibition of the Ras/MAPK pathway (see Figs S5 and S6 in the supplementary material) (Furthauer et al., 2001; Ozaki et al., 2005; Sasaki et al., 2001). We have shown by loss- and gain-of-function experiments that Spry4 negatively modulates early *krox20* expression (Fig. 3). If a feedback loop is already established when target gene activation occurs, the outcome can be a reduction in fluctuations in expression of the target gene (Brandman and Meyer, 2008). Our system works under these conditions, as the expression of *spry4* precedes that of *krox20* (Fig. 1; data not shown). In addition, release of the antagonistic action of Spry4 is expected to lead to increased expression of the target genes, resulting in premature activation. This is precisely what is observed for *krox20* activation (Fig. 3). In conclusion, the bistable cell-fate choice required for efficient and non-ambiguous hindbrain patterning is likely to impose fine-tuning of FGF control, which is achieved through the establishment of the Spry4 negative-feedback loop.

Acknowledgements

This work was supported by grants to P.C. from INSERM, MESR and ANR. C.L. was supported by FRM and Neuropole Ile-de-France, Y.X.B. by MESR, M.A.W. by MESR and ARC, P.A.G. by the ENS and Fondation Pierre-Gilles de Gennes and J.L.M. by MESR.

Competing interests statement

The authors declare no competing financial interests.

Supplementary material

Supplementary material for this article is available at
http://dev.biologists.org/lookup/suppl/doi:10.1242/dev.057299/-/DC1

References

Aragon, F. and Pujades, C. (2009). FGF signaling controls caudal hindbrain specification through Ras-ERK1/2 pathway. *BMC Dev. Biol.* **9**, 61.
Brandman, O. and Meyer, T. (2008). Feedback loops shape cellular signals in space and time. *Science* **322**, 390-395.
Chomette, D., Frain, M., Cereghini, S., Charnay, P. and Ghislain, J. (2006). Krox20 hindbrain cis-regulatory landscape: interplay between multiple long-range initiation and autoregulatory elements. *Development* **133**, 1253-1262.
Cordes, S. P. and Barsh, G. S. (1994). The mouse segmentation gene kr encodes a novel basic domain-leucine zipper transcription factor. *Cell* **79**, 1025-1034.
Desmazières, A., Charnay, P. and Gilardi-Hebenstreit, P. (2009). Krox20 controls the transcription of its various targets in the developing hindbrain according to multiple modes. *J. Biol. Chem.* **284**, 10831-10840.
Freeman, M. (2000). Feedback control of intercellular signalling in development. *Nature* **408**, 313-319.
Furthauer, M., Thisse, C. and Thisse, B. (1997). A role for FGF-8 in the dorsoventral patterning of the zebrafish gastrula. *Development* **124**, 4253-4264.
Furthauer, M., Reifers, F., Brand, M., Thisse, B. and Thisse, C. (2001). sprouty4 acts in vivo as a feedback-induced antagonist of FGF signaling in zebrafish. *Development* **128**, 2175-2186.
Furthauer, M., Lin, W., Ang, S. L., Thisse, B. and Thisse, C. (2002). Sef is a feedback-induced antagonist of Ras/MAPK-mediated FGF signalling. *Nat. Cell Biol.* **4**, 170-174.
Furthauer, M., Van Celst, J., Thisse, C. and Thisse, B. (2004). Fgf signalling controls the dorsoventral patterning of the zebrafish embryo. *Development* **131**, 2853-2864.
Ghislain, J., Desmarquet-Trin-Dinh, C., Gilardi-Hebenstreit, P., Charnay, P. and Frain, M. (2003). Neural crest patterning: autoregulatory and crest-specific elements co-operate for Krox20 transcriptional control. *Development* **130**, 941-953.
Giudicelli, F., Taillebourg, E., Charnay, P. and Gilardi-Hebenstreit, P. (2001). Krox-20 patterns the hindbrain through both cell-autonomous and non cell-autonomous mechanisms. *Genes Dev.* **15**, 567-580.
Graham, T. G., Tabei, S. M., Dinner, A. R. and Rebay, I. (2010). Modeling bistable cell-fate choices in the Drosophila eye: qualitative and quantitative perspectives. *Development* **137**, 2265-2278.
Gross, I., Bassit, B., Benezra, M. and Licht, J. D. (2001). Mammalian sprouty proteins inhibit cell growth and differentiation by preventing ras activation. *J. Biol. Chem.* **276**, 46460-46468.
Hacohen, N., Kramer, S., Sutherland, D., Hiromi, Y. and Krasnow, M. A. (1998). sprouty encodes a novel antagonist of FGF signaling that patterns apical branching of the Drosophila airways. *Cell* **92**, 253-263.
Hauptmann, G. and Gerster, T. (1994). Two-color whole-mount in situ hybridization to vertebrate and Drosophila embryos. *Trends Genet.* **10**, 266.
Jaeger, J., Irons, D. and Monk, N. (2008). Regulative feedback in pattern formation: towards a general relativistic theory of positional information. *Development* **135**, 3175-3183.

Kitano, H. (2004). Biological robustness. *Nat. Rev. Genet.* **5**, 826-837.
Komisarczuk, A. Z., Topp, S., Stigloher, C., Kapsimali, M., Bally-Cuif, L. and Becker, T. S. (2008). Enhancer detection and developmental expression of zebrafish sprouty1, a member of the fgf8 synexpression group. *Dev. Dyn.* **237**, 2594-2603.
Lee, Y., Grill, S., Sanchez, A., Murphy-Ryan, M. and Poss, K. D. (2005). Fgf signaling instructs position-dependent growth rate during zebrafish fin regeneration. *Development* **132**, 5173-5183.
Lumsden, A. (1990). The cellular basis of segmentation in the developing hindbrain. *Trends Neurosci.* **13**, 329-335.
Lumsden, A. and Keynes, R. (1989). Segmental patterns of neuronal development in the chick hindbrain. *Nature* **337**, 424-428.
Lumsden, A. and Krumlauf, R. (1996). Patterning the vertebrate neuraxis. *Science* **274**, 1109-1115.
Manzanares, M., Nardelli, J., Gilardi-Hebenstreit, P., Marshall, H., Giudicelli, F., Martinez-Pastor, M. T., Krumlauf, R. and Charnay, P. (2002). Krox20 and kreisler co-operate in the transcriptional control of segmental expression of Hoxb3 in the developing hindbrain. *EMBO J.* **21**, 365-376.
Marin, F. and Charnay, P. (2000). Hindbrain patterning: FGFs regulate Krox20 and mafB/kr expression in the otic/preotic region. *Development* **127**, 4925-4935.
Maves, L., Jackman, W. and Kimmel, C. B. (2002). FGF3 and FGF8 mediate a rhombomere 4 signaling activity in the zebrafish hindbrain. *Development* **129**, 3825-3837.
Minowada, G., Jarvis, L. A., Chi, C. L., Neubuser, A., Sun, X., Hacohen, N., Krasnow, M. A. and Martin, G. R. (1999). Vertebrate Sprouty genes are induced by FGF signaling and can cause chondrodysplasia when overexpressed. *Development* **126**, 4465-4475.
Moens, C. B., Yan, Y. L., Appel, B., Force, A. G. and Kimmel, C. B. (1996). valentino: a zebrafish gene required for normal hindbrain segmentation. *Development* **122**, 3981-3990.
Moens, C. B., Cordes, S. P., Giorgianni, M. W., Barsh, G. S. and Kimmel, C. B. (1998). Equivalence in the genetic control of hindbrain segmentation in fish and mouse. *Development* **125**, 381-391.
Monk, K. R., Naylor, S. G., Glenn, T. D., Mercurio, S., Perlin, J. R., Dominguez, C., Moens, C. B. and Talbot, W. S. (2009). A G protein-coupled receptor is essential for Schwann cells to initiate myelination. *Science* **325**, 1402-1405.
Muller, M. V., Weizsacker, E. and Campos-Ortega, J. A. (1996). Expression domains of a zebrafish homologue of the Drosophila pair-rule gene hairy correspond to primordia of alternating somites. *Development* **122**, 2071-2078.
Oxtoby, E. and Jowett, T. (1993). Cloning of the zebrafish krox-20 gene (krx-20) and its expression during hindbrain development. *Nucleic Acids Res.* **21**, 1087-1095.
Ozaki, K., Miyazaki, S., Tanimura, S. and Kohno, M. (2005). Efficient suppression of FGF-2-induced ERK activation by the cooperative interaction among mammalian Sprouty isoforms. *J. Cell Sci.* **118**, 5861-5871.
Pezeron, G., Lambert, G., Dickmeis, T., Strahle, U., Rosa, F. M. and Mourrain, P. (2008). Rasl11b knock down in zebrafish suppresses one-eyed-pinhead mutant phenotype. *PLoS ONE* **3**, e1434.
Prince, V. E., Moens, C. B., Kimmel, C. B. and Ho, R. K. (1998). Zebrafish hox genes: expression in the hindbrain region of wild-type and mutants of the segmentation gene, valentino. *Development* **125**, 393-406.
Robu, M. E., Larson, J. D., Nasevicius, A., Beiraghi, S., Brenner, C., Farber, S. A. and Ekker, S. C. (2007). p53 activation by knockdown technologies. *PLoS Genet.* **3**, e78.
Roy, N. M. and Sagerstrom, C. G. (2004). An early Fgf signal required for gene expression in the zebrafish hindbrain primordium. *Brain Res. Dev. Brain Res.* **148**, 27-42.
Sasaki, A., Taketomi, T., Wakioka, T., Kato, R. and Yoshimura, A. (2001). Identification of a dominant negative mutant of Sprouty that potentiates fibroblast growth factor- but not epidermal growth factor-induced ERK activation. *J. Biol. Chem.* **276**, 36804-36808.
Schneider-Maunoury, S., Topilko, P., Seitandou, T., Levi, G., Cohen-Tannoudji, M., Pournin, S., Babinet, C. and Charnay, P. (1993). Disruption of Krox-20 results in alteration of rhombomeres 3 and 5 in the developing hindbrain. *Cell* **75**, 1199-1214.
Schneider-Maunoury, S., Seitanidou, T., Charnay, P. and Lumsden, A. (1997). Segmental and neuronal architecture of the hindbrain of Krox-20 mouse mutants. *Development* **124**, 1215-1226.
Schulte-Merker, S., Hammerschmidt, M., Beuchle, D., Cho, K. W., De Robertis, E. M. and Nusslein-Volhard, C. (1994). Expression of zebrafish goosecoid and no tail gene products in wild-type and mutant no tail embryos. *Development* **120**, 843-852.
Seitanidou, T., Schneider-Maunoury, S., Desmarquet, C., Wilkinson, D. G. and Charnay, P. (1997). Krox-20 is a key regulator of rhombomere-specific gene expression in the developing hindbrain. *Mech. Dev.* **65**, 31-42.
Stedman, A., Lecaudey, V., Havis, E., Anselme, I., Wassef, M., Gilardi-Hebenstreit, P. and Schneider-Maunoury, S. (2009). A functional interaction between Irx and Meis patterns the anterior hindbrain and activates krox20 expression in rhombomere 3. *Dev. Biol.* **327**, 566-577.
Swiatek, P. J. and Gridley, T. (1993). Perinatal lethality and defects in hindbrain development in mice homozygous for a targeted mutation of the zinc finger gene Krox20. *Genes Dev.* **7**, 2071-2084.
Voiculescu, O., Taillebourg, E., Pujades, C., Kress, C., Buart, S., Charnay, P. and Schneider-Maunoury, S. (2001). Hindbrain patterning: Krox20 couples segmentation and specification of regional identity. *Development* **128**, 4967-4978.
Walshe, J., Maroon, H., McGonnell, I. M., Dickson, C. and Mason, I. (2002). Establishment of hindbrain segmental identity requires signaling by FGF3 and FGF8. *Curr. Biol.* **12**, 1117-1123.
Wassef, M. A., Chomette, D., Pouilhe, M., Stedman, A., Havis, E., Desmarquet-Trin Dinh, C., Schneider-Maunoury, S., Gilardi-Hebenstreit, P., Charnay, P. and Ghislain, J. (2008). Rostral hindbrain patterning involves the direct activation of a Krox20 transcriptional enhancer by Hox/Pbx and Meis factors. *Development* **135**, 3369-3378.
Wiellette, E. L. and Sive, H. (2003). vhnf1 and Fgf signals synergize to specify rhombomere identity in the zebrafish hindbrain. *Development* **130**, 3821-3829.
Wiellette, E. L. and Sive, H. (2004). Early requirement for fgf8 function during hindbrain pattern formation in zebrafish. *Dev. Dyn.* **229**, 393-399.
Wilkinson, D. G., Bhatt, S., Chavrier, P., Bravo, R. and Charnay, P. (1989). Segment-specific expression of a zinc-finger gene in the developing nervous system of the mouse. *Nature* **337**, 461-464.
Yee, S. P. and Rigby, P. W. (1993). The regulation of myogenin gene expression during the embryonic development of the mouse. *Genes Dev.* **7**, 1277-1289.
Yusoff, P., Lao, D. H., Ong, S. H., Wong, E. S., Lim, J., Lo, T. L., Leong, H. F., Fong, C. W. and Guy, G. R. (2002). Sprouty2 inhibits the Ras/MAP kinase pathway by inhibiting the activation of Raf. *J. Biol. Chem.* **277**, 3195-3201.

– Chapter 1 –

Supplementary information

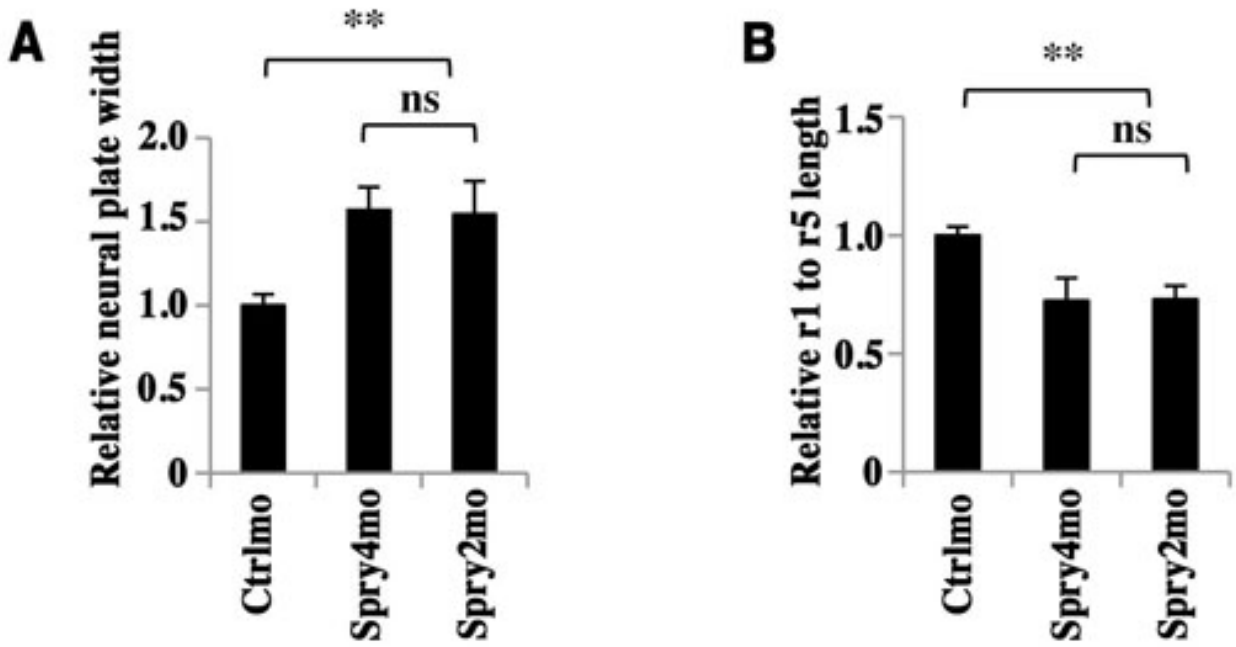

Fig. S1. Quantitative evaluation of the width and length of the neural plate in Spry2 and Spry4 morphants. The width (A) and length (B) of the neural plate between r1 and r5 of embryos injected with the indicated morpholinos were measured and compared with those of control embryos. Values obtained with the control morpholino (Ctrlmo) were set at 1. ns, not significant; **, P<0.0001; t-test. Errors bars indicate s.e.m.

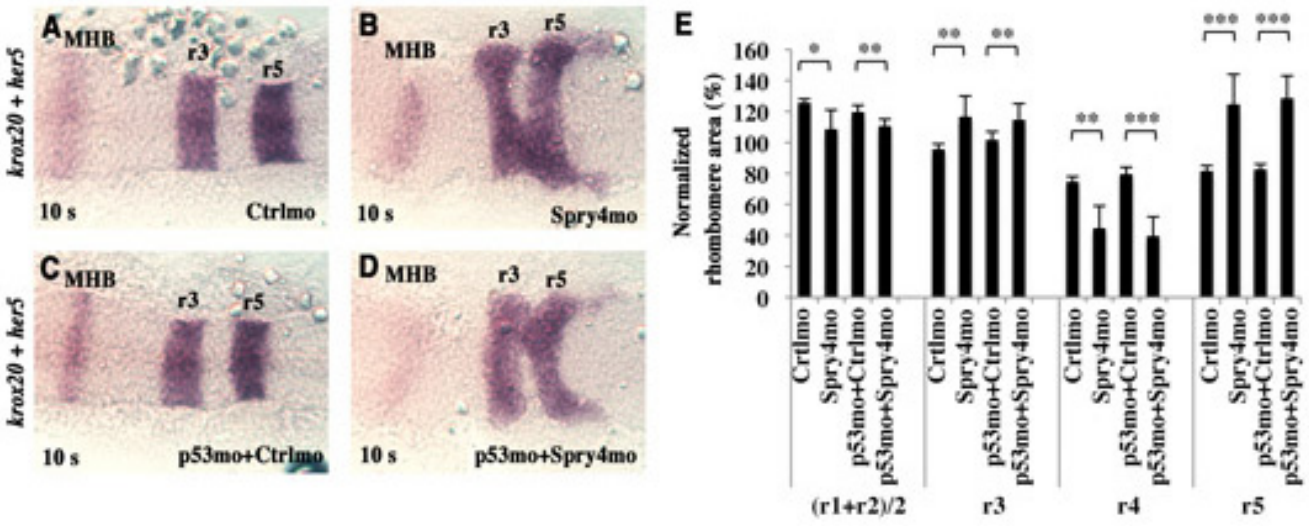

Fig. S2. The hindbrain patterning phenotype is not affected by a p53 morpholino.
(A-D) Embryos injected with either control morpholino (Ctrlmo) (A; n=12) or Spry4mo (B; n=19), and embryos co-injected with p53 morpholino and Ctrlmo (p53mo+Ctrlmo) (C; n=12) or Spry4mo (p53mo+Spry4mo) (D; n=20) were collected at the 10-somite stage and subjected to *in situ* hybridisation for *krox20* and *her5*. Embryos were flat-mounted with anterior to the left. **(E)** Quantitative evaluation of rhombomere areas was carried out as described in Fig. 2. *, not significant after Bonferroni corrections considering eight comparisons, P>0.006; **, P<0.006; ***, P<0.0001; t-test. Errors bars indicate s.e.m.

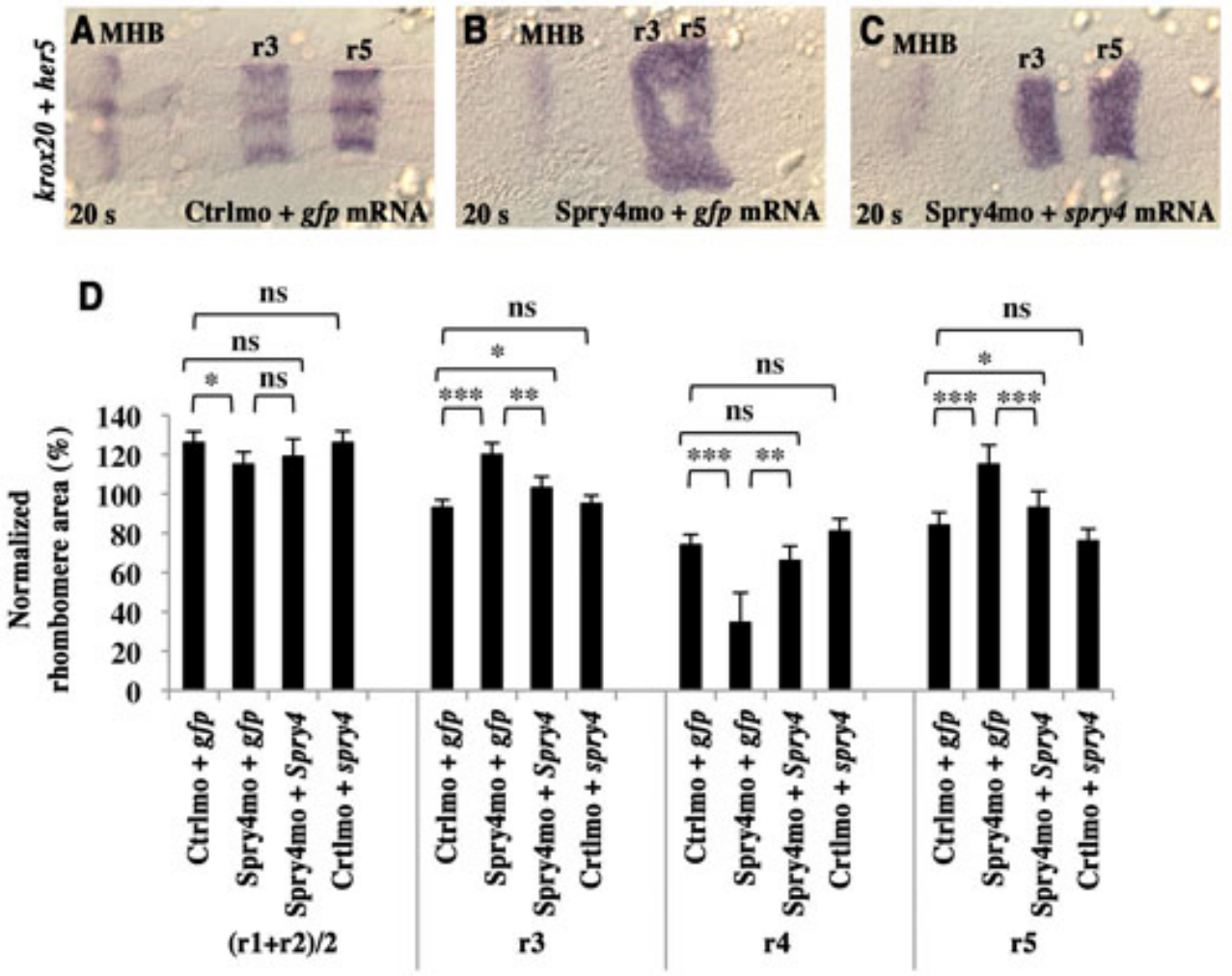

Fig. S3. Hindbrain patterning defects resulting from Spry4mo injection are persistent and can be rescued by injection of *spry4* mRNA.

(A-C) Embryos were injected with either control morpholino (Ctrlmo) and *gfp* mRNA (A), Spry4mo and *gfp* mRNA (B), or Spry4mo and a morpholino-resistant form of *spry4* mRNA (C), collected at the 20-somite stage and subjected to *in situ* hybridisation for *krox20* and *her5*, a marker of the MHB. **(D)** Quantitative evaluation of rhombomere areas, carried out as described in Fig. 2. ns, not significant, P>0.05; *, not significant after Bonferroni corrections considering 12 comparisons, P>0.004; **, P<0.004; ***, P<0.0001; t-test. Errors bars indicate s.e.m.

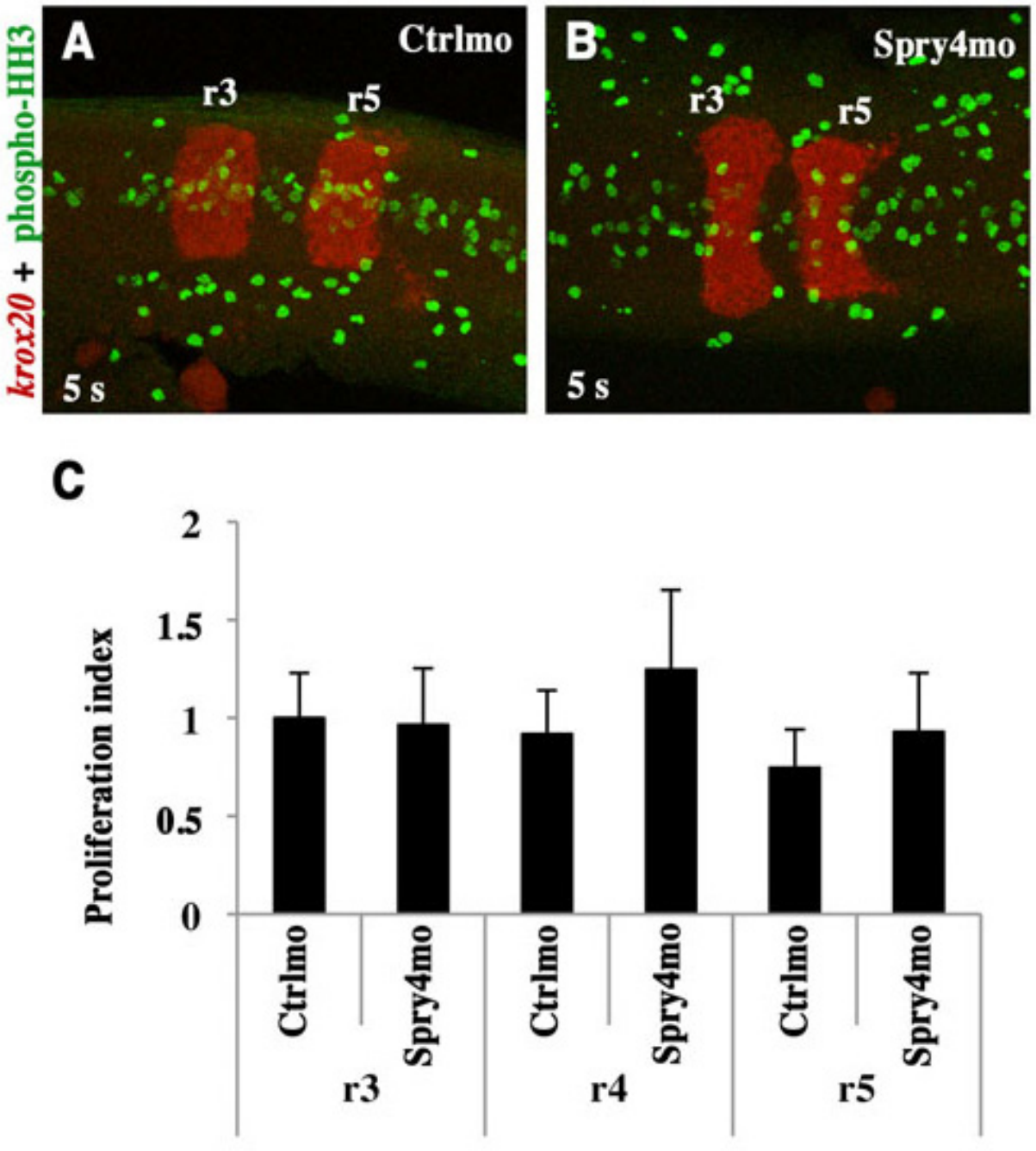

Fig. S4. Cell proliferation in the hindbrain is not affected in Spry4 morphants.
(A,B) Immunostaining against phospho-Histone H3 (phospho-HH3, green) was carried out following fluorescent *in situ* hybridisation using a *krox20* probe (red) in 5-somite stage embryos injected with control morpholino (A) or Spry4mo (B). The images are z-projections of nine confocal sections. **(C)** Normalised proliferation indexes were obtained by dividing the average number of phospho-HH3-positive cells per confocal section in a given rhombomere by the area of the corresponding rhombomere. The ratio obtained in r3 with the control was arbitrarily set at 1, to which the others were then normalised. No significant difference was detected by t-test, P>0.05. Errors bars indicate s.e.m.

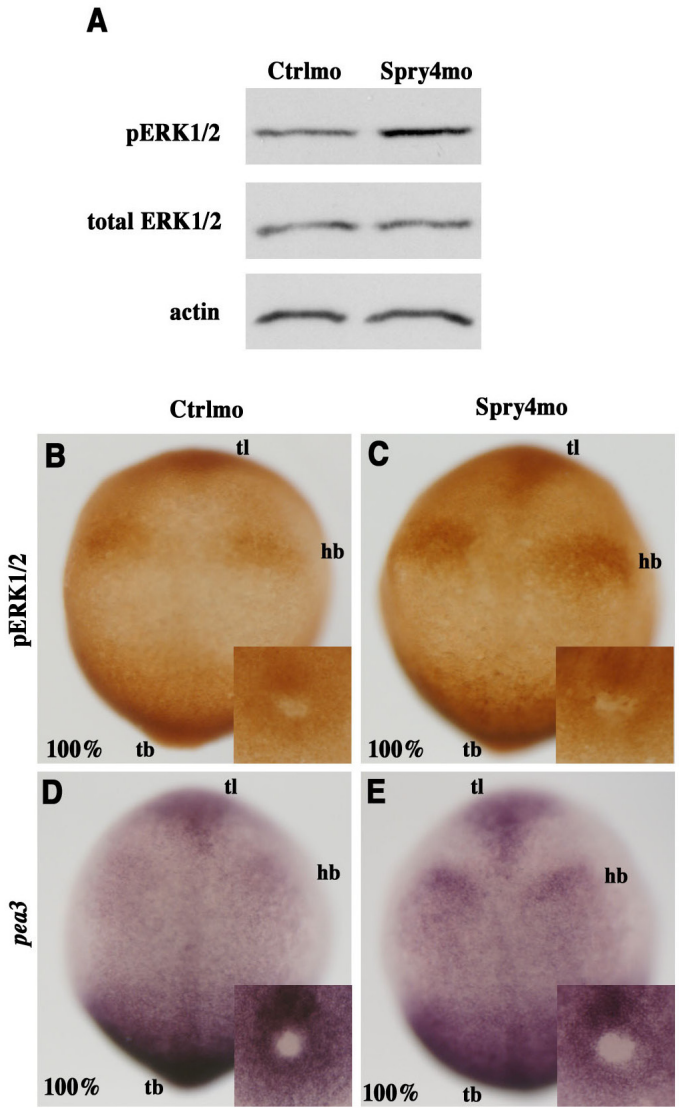

Fig. S5. Enhanced FGF signalling in Spry4 morphants.
(A) Enhanced ERK1/2 phosphorylation in Spry4 morphants. Control and Spry4mo-injected embryos were collected at 100% epiboly and subjected to western blot analysis using antibodies against phosphoERK1/2 (pERK1/2) or total ERK1/2. Actin was used as a loading control. **(B-E)** Immunostaining for pERK1/2 (B,C) and *in situ* hybridisation for *pea3* (D,E) of Ctrlmo- and Spry4mo-injected embryos at 100% epiboly. Embryos are shown as dorsal views with anterior to the top. The insets show tailbud views, allowing determination of the developmental stage by evaluation of the closure of the tailbud. tb, tailbud; hb, hindbrain; tl, telencephalon.

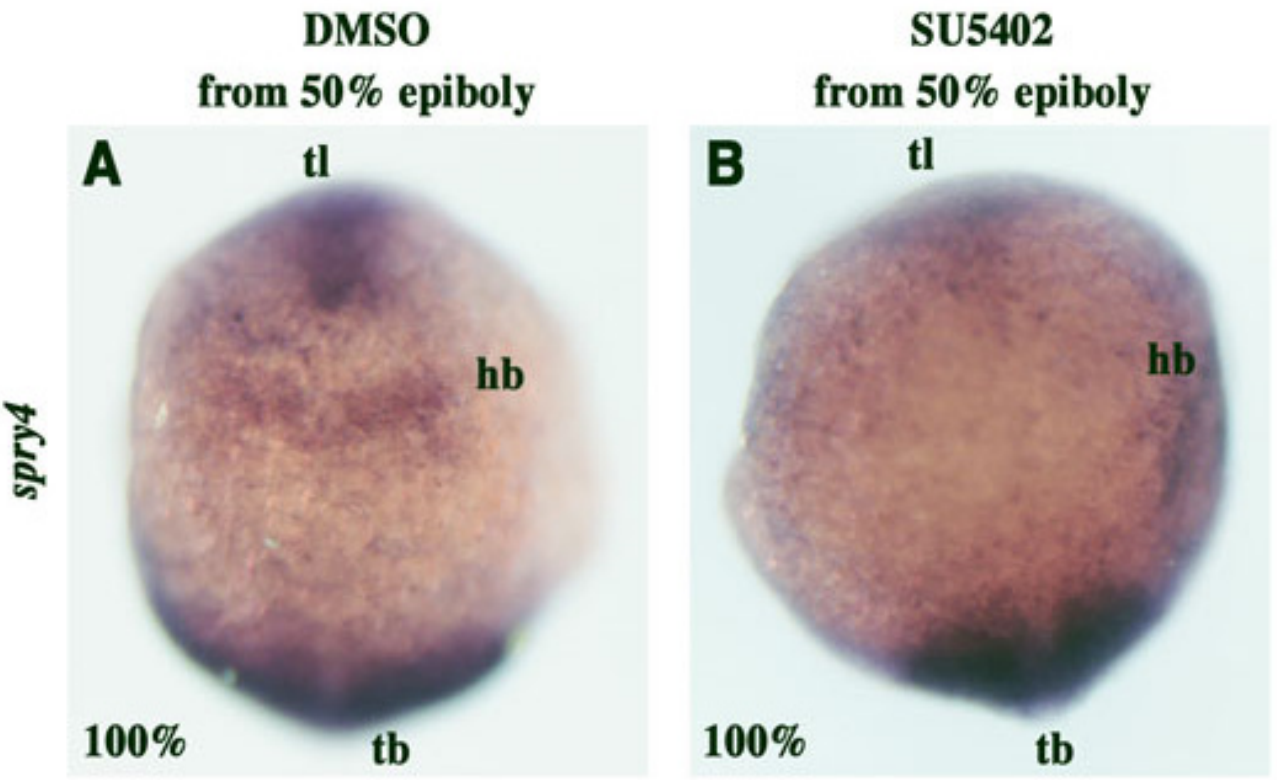

Fig. S6. spry4 expression in the hindbrain is dependent on FGF signalling.
Embryos were incubated in either DMSO carrier (A) or SU5402 (B) from 50% to 100% epiboly and analysed at this latter stage by *in situ* hybridisation for *spry4*. Embryos are shown as dorsal views with anterior to the top. The stripe of *spry4* mRNA at the level of the hindbrain is absent after SU5402 treatment, whereas tailbud expression is unaffected. tb, tailbud; hb, hindbrain; tl, telencephalon.

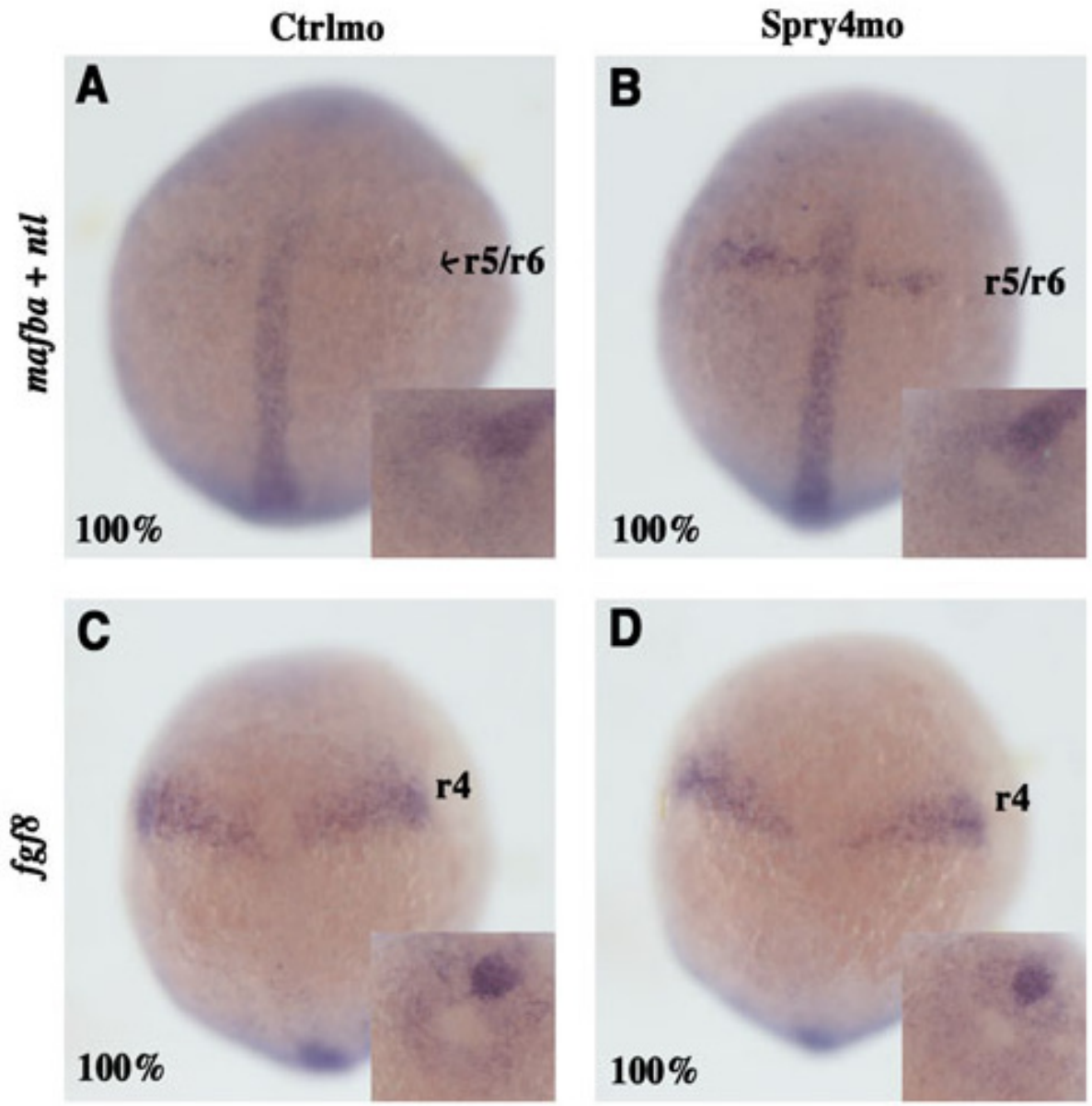

Fig. S7. Spry4 controls the onset of mafba expression.
(A-D) Embryos injected with either control morpholino (Ctrlmo) (A,C) or Spry4mo (B,D) were collected at 100% epiboly and subjected to *in situ* hybridisation with *mafba* and *ntl* probes (A,B) or an *fgf8* probe (C,D). The arrow in A indicates mafba expression in only a few r5/r6 cells. Embryos are shown as dorsal views with anterior to the top. The insets show tailbud views, allowing determination of the developmental stage by evaluation of the closure of the tailbud, as revealed by ntl (A,B) or fgf8 (C,D) expression.

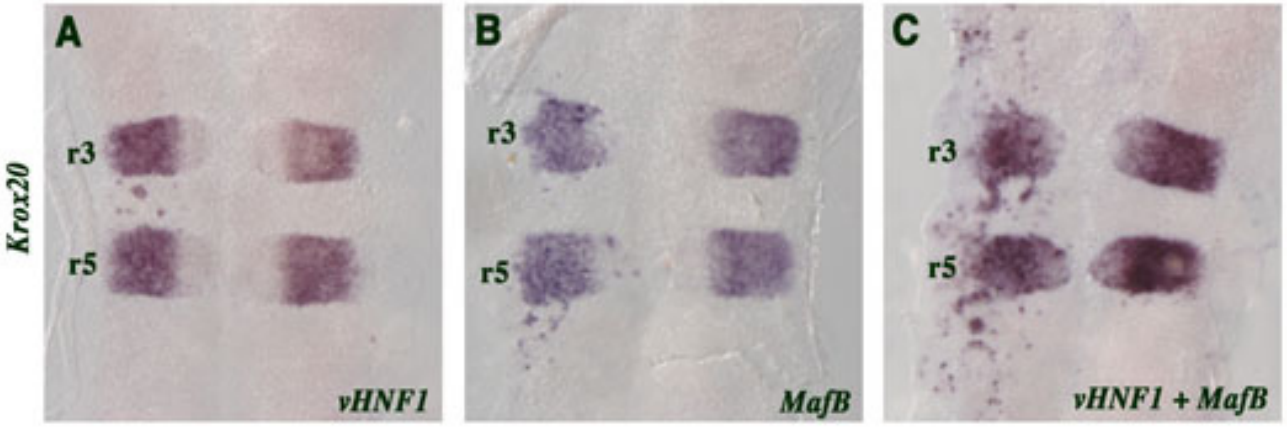

Fig. S8. Synergy between *vHnf1* and *MafB* for the activation of endogenous *Krox20* in chick.
Chick embryos were analysed by *in situ* hybridisation for *Krox20* after electroporation with expression vectors for (A) *vHnf1*, (B) *MafB* or (C) both. Hindbrains were flat-mounted with anterior to the top. With *vHnf1*, limited ectopic *Krox20* expression occurs specifically in r4. With *MafB*, limited ectopic activation of *Krox20* is observed in the posterior hindbrain. With both expression vectors together, ectopic expression occurs more frequently and throughout the entire hindbrain.

– Chapter 2 –

A bistable cell-fate switch controls the patterning of the r3-r5 region in the vertebrate rhombencephalon

Y.X. Bouchoucha*, J. Reingruber*, M.A. Wassef, E. Thierion, D. Holcman, P. Gilardi-Hebenstreit, P. Charnay

IBENS, Ecole Normale Supérieure, Paris, France – INSERM U1024, CNRS UMR 8197

Author contributions:

YXB performed the experiments.

ET participated to the analysis of the mouse knock-out of the element A

JR and DH built the mathematical model.

YXB, MAW, PGH and PC conceived the experiments and interpreted the results

YXB wrote the manuscript

PC, JR and PGH reviewed the manuscript.

* equal contributions

Foreword

In the preceding chapter, we formulate a hypothesis to explain how delayed expression of *Krox20* leads to smaller rhombomeres? To explain the relationship between early transcriptional events and late patterning phenotype, we proposed a model based on the interplay between initiator enhancers and element A (see Figure). The model is based on the assumption that A is necessary to amplify and maintain *Krox20* expression. Thus the discriminative parameter between *Krox20*-positive and *Krox20*-negative cells is the activation of element A. The activation of A requires that Krox20 initial level, provided by the activity of initiator elements, resides above a certain level corresponding to the activation threshold of element A. Hence the second assumption of the model: A functions as a cellular switch. At the population level, low initiation signal results in low proportion of cells activating A. Graded FGF loss-of-function is thus expected to result in the graded rarefaction of *Krox20*$^{+}$ cells. The two assumptions of this model are challenged in the following chapter.

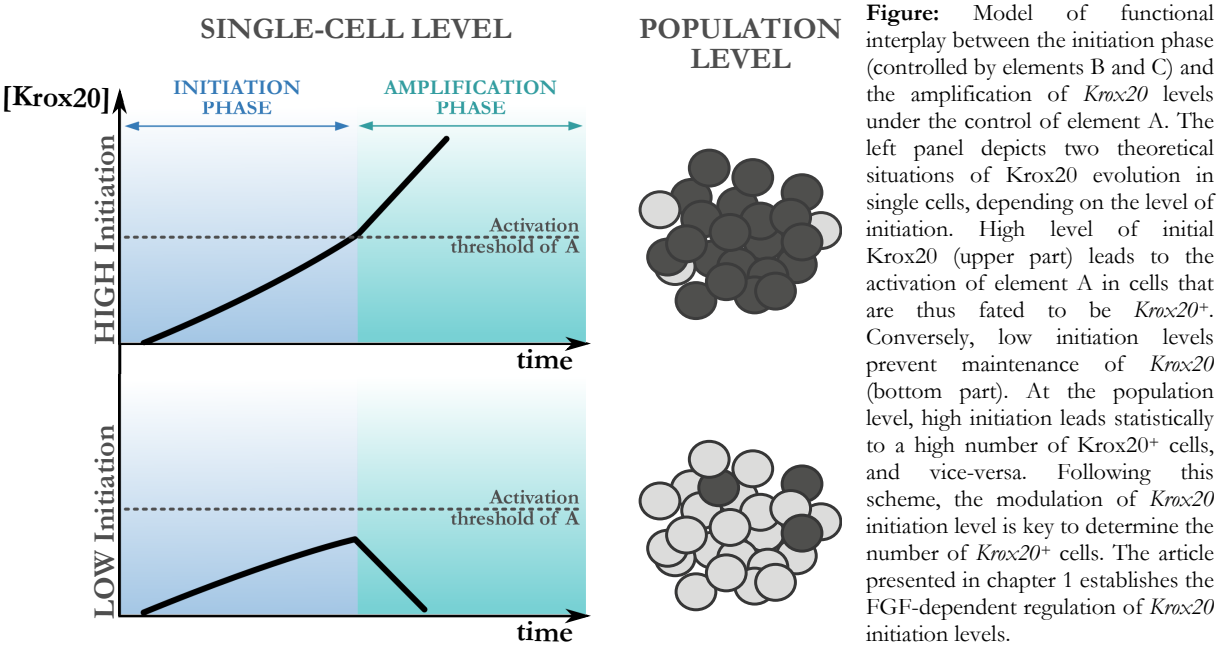

Figure: Model of functional interplay between the initiation phase (controlled by elements B and C) and the amplification of *Krox20* levels under the control of element A. The left panel depicts two theoretical situations of Krox20 evolution in single cells, depending on the level of initiation. High level of initial Krox20 (upper part) leads to the activation of element A in cells that are thus fated to be *Krox20*$^{+}$. Conversely, low initiation levels prevent maintenance of *Krox20* (bottom part). At the population level, high initiation leads statistically to a high number of Krox20^{+} cells, and vice-versa. Following this scheme, the modulation of *Krox20* initiation level is key to determine the number of *Krox20*$^{+}$ cells. The article presented in chapter 1 establishes the FGF-dependent regulation of *Krox20* initiation levels.

A bistable cell-fate switch controls the patterning of the vertebrate hindbrain

INTRODUCTION

Patterning of the hindbrain involves a transient segmentation process that is highly conserved during vertebrate evolution and leads to the formation of a series of cellular territories termed rhombomeres (r). Rhombomere corresponds to units of genetic expression as well as cell lineage restriction. The genetic control of hindbrain segmentation has been the subject of intense studies over the past two decades. An early step involves the expression of segmentation genes such as *Krox20*, *Hoxb1*, *MafB*, respectively in r3/r5, r4 and r5/r6. Segmentation genes define segmental territories and ensure lineage restriction by controlling cell specification and promoting cell segregation. The proper establishment of their expression patterns is key to the segmentation pattern and ultimately to the stereotyped organisation of cranial nerves and neural crest migratory paths. The complex network controlling segmentation gene transcription is still poorly understood. *Krox20* encodes a zinc-finger transcription factor and controls the development of r3 and r5. Our laboratory focuses on its regulation and investigates the molecular mechanisms allowing establishment and maintenance of *Krox20* expression, and cell fate specification in r3/r5.

Using a *lacZ* knock-in into the *Krox20* locus, we have previously shown that *Krox20* loss-of-function results in an aborted establishment of the *Krox20* expression pattern, with reduced levels of expression and shorter expression time, whereas the initial phase of activation is not affected (Schneider-Maunoury et al., 1993). Gain-of-function experiments performed in the chick embryo later demonstrated that *Krox20* can activate its own expression in the developing hindbrain (Giudicelli et al., 2001). Together these data suggest that the establishment of the *Krox20* expression pattern in the hindbrain involves two steps, an initiation process that is *Krox20*-independent and an amplification/maintenance phase that relies on a positive autoregulatory loop. This hypothesis is consistent with the analysis of the cis-acting regulatory elements governing *Krox20* expression in the hindbrain. Three transcriptional enhancers have been identified, termed A, B and C (Chomette et al., 2006). Element A drives reporter expression in r3 and r5 in transgenic mice. It contains several Krox20 binding sites and mutation of these sites or absence of Krox20 abolishes its activity. Furthermore, ectopic expression of *Krox20* in the chick embryo leads to the activation of element A. Element A therefore constitutes a good candidate for contributing to a direct, positive autoregulatory loop responsible for the maintenance/amplification phase of *Krox20* expression. In contrast, elements B and C do not

require Krox20 for enhancer activity. They are active in r5 and r3/r5 respectively and are likely to be responsible for the initiation of *Krox20* expression.

We have also shown previously that *Krox20* expression in the hindbrain is controlled by FGF signalling (Marín and Charnay, 2000) and that this regulation is mediated by the initiator cis-acting elements in r3 and r5 (Labalette et al., 2011). Strikingly, in r3 FGF loss- and gain-of-function do not affect the level of *Krox20* expression, but rather the number of cells that eventually maintain *Krox20* expression, and therefore determine the size of the rhombomeres. We hypothesized that this phenomenon reflects the fact that the activation of the autoregulatory loop occurs only when *Krox20* initiation level lies above a certain threshold. Cells that maintain *Krox20* expression are cells that exhibited high initiation level. This hypothesis implies that *Krox20* autoregulatory loop acts as a switch for a bistable cell-fate choice, deciding whether a cell is *Krox20*-positive or *Krox20*-negative and whether it should belong to an odd- or even-numbered rhombomere.

Autoregulation is a recurrent feature in developmental networks. In the hindbrain, besides *Krox20*, *MafB* and *Hoxb1* genes have been shown to be self-regulated (Pöpperl et al., 1995; Giudicelli et al., 2003). In general, positive feedback loops, made of either direct autoregulation or cross-inhibition motifs, have been proposed to serve multiple purposes: precise regulation of the levels of outputs, amplification and maintenance of expression including memory effects, reduction of genetic noise, increase in robustness, and switching between multiple fates (Becskei and Serrano, 2000; Ferrell, 2002). The latter case is best exemplified in cell-specification systems where positive feedbacks participate in bistable transcriptional modules that enable two-level expression states with a discontinuous switch between OFF and ON states. Collection of quantitative data in developmental systems allowed to build models that illustrate this property. This was done mainly in Drosophila on wing vein patterning, early D/V patterning, regulation of gap gene domains positions (Jaeger et al., 2004; Umulis et al., 2006; Yan et al., 2009). These models usually provide descriptions of the genetic interactions without taking into account the molecular events occurring on the DNA promoters or enhancers. As all cell-fate choices described to date rely on gene expression switches, understanding how gene promoters or enhancers function at the molecular level is crucial. To this end, gene expression levels were modelled according to the promoter/enhancer architecture, in order to capture the binding dynamics. So far, this type of study has been performed mainly in single-celled organisms or *in vitro* cellular systems because experimental procedures are more adapted for the collection of quantitative data. Representative examples are found in E. coli (Robert et al., 2011), yeast (Ellis et al., 2009; Gertz et al., 2009), Xenopus ovocytes (Ferrell et al., 2009) or hematopoietic cells (Laslo

et al., 2006; Huang et al., 2007). Few models were developed in invertebrates, like Drosophila (Lopes et al., 2005), sea urchins (Yuh et al., 1998) or worms (Brown et al., 2007). Mathematical representation of promoter/enhancer functioning in vertebrates is still missing. One recent study describes a model for the *Pax6* enhancer in the mouse eye (Rowan et al., 2010), with a deterministic formulation, such that the involvement of binding site affinity is analysed regarding the gene production at equilibrium, and not the full dynamics. In other words, the discrete molecular events responsible for enhancer activation may not be captured by this type of model.

The aim of the present work was to perform a detailed and quantitative analysis of the *Krox20* autoregulatory loop, to uncover its mechanisms and function. In particular, we have shown that the element A is absolutely required for autoregulation and that the loop underlies a bimodal behaviour of the cells, suggesting that it generates a switch-like mechanism. We have then built a stochastic mathematical model of the loop that was constrained by *in vivo* quantitative measurements obtained in zebrafish embryos. The model provides a full description of the stochastic binding of Krox20 to element A and simulates the dynamics of *Krox20* expression during development in a rhombomere cell population, as well as in single cells. Moreover it explains the bimodal behaviour of the cells, shows that this is based on a bistable molecular switch and reveals the importance of Krox20 cooperative binding to element A. Simulations also allow to predict phenotypes resulting from *Krox20* or element A mutations and the existence of an additional factor responsible for the decline in *Krox20* expression at late stages. Our model therefore fully recapitulates the molecular mechanisms regulating a simple positive feedback loop that controls a binary cell-fate choice in vertebrates.

MATERIALS & METHODS

Mouse lines

Two newly generated mouse lines are used in this study. First, Krox20^{NA*AK}: this line results from the recombination of a targeting vector in the *Krox20* locus of ES cells, as presented in figure 1A. Three types of recombination sites were introduced in the targeting vector: FRT and F3 sites that are both recombined by the Flippase without possible heterologous recombination of type FRT-F3; loxP sites that are recombined by the Cre. The Krox20^{NA*AK} line was obtained at the *Institut Clinique de la Souris* (Illkirch, France). By crossing Krox20^{NA*AK} mice with lines expressing ubiquitously either the Flippase or the Cre, we could obtain the Krox20^{NA} and Krox20^{A*} alleles. Additional Cre-mediated recombination on the latter allele provided the Krox20$^{\Delta A}$ line where the 465-bp sequence of element A is deleted from the genome. The primers used to genotype these alleles are presented in the supplementary table S1.

The second mouse line used in this study carries the transgene *A:Krox20-2ER$_{HA}$*, where the expression of a mutant *Krox20* gene, termed *Krox20-2ER*, is expressed under the control of A. The promoter used in the construct is a heterologous ßglobin minimal promoter. To generate this transgenic line, the *A:Krox20-2ER$_{HA}$* construct was extracted from the corresponding p1230 vector, purified by agarose gel electrophoresis and Elutip-d (Schleicher & Schuell) and suspended in TE (10 mM Tris pH 7.5, 0.1 mM EDTA) for microinjection. Transgenesis was performed as described previously (Sham et al., 1993). Briefly, fertilised eggs from superovulated B6D2F1 females were injected with DNA at a final concentration of 1.5 ng/µL. Injected embryos were reimplanted at the one-cell stage into pseudopregnant B6/CBA mice and allowed to develop to term. Genotyping of the newborns was performed using the primers shown in the supplementary table S1.

Fish stocks and breeding

Zebrafish (*Danio rerio*) were raised and staged as previously described (Kimmel et al., 1995). Embryos were grown in embryo medium (recipe detailed in the Zebrafish Book) at 24°C, 28°C or 33°C to adjust the speed of development to the experimental constraints. The wild-type lines used were TL and TU. The *zkrox20* mutant line was described earlier as *egr2b^{fh227}* (Monk et al., 2009). The *cA::h2bmcherry* and *hsp:mKrox20$_{HA}$* lines were obtained by Tol2-mediated transgenesis. In the former (gift from N. Peyrieras, Gif-sur-Yvette, France), the chick ortholog of element A drives the expression of a nuclear mcherry flurorescent protein. In the latter, a HA-tagged

version of murine *Krox20* was placed under the control of an *hsp70* promoter in a modified pTol2 vector.

In situ hybridizations and immunohistochemistry

Mouse and zebrafish *in situ* hybridizations were performed on whole embryos using digoxigenin-labelled riboprobes and following procedures described in (Giudicelli et al., 2001) and (Hauptmann and Gerster, 1994) respectively. The probes used were *mKrox20* (Wilkinson et al., 1989), *mEphA4* (Gilardi-Hebenstreit et al., 1992) and *zkrox20* (Oxtoby and Jowett, 1993). Digoxygenin was then detected using an alkaline phosphatase-coupled antibody (Roche, 1:2000) followed by NBT/BCIP staining. Embryos were flat-mounted in 87% glycerol and photographed using a DM5500B Leica microscope under brightfield illumination.

For antibody staining in zebrafish and chick embryos, the primary antibodies used were a rabbit anti-DsRed (1:200, Clonetech) and a rat anti-GFP (1:500, Nacalai Tesque). The secondary antibodies were an Alexa594 anti-rabbit and a Dy488 anti-rat (Jackson ImmunoResearch). Nuclei were stained with Hoechst (Sigma).

Bimodality assay

Five-somite *hsp:mKrox20HA* ; *cA:h2bcherry* zebrafish embryos were heat-shocked for 10 minutes at 35 or 37°C, and allowed to develop during 4 hours, up to the 15-somite stage, at 28°C in embryo medium. Anti-cherry immunostaining was then performed as described in the previous section. Flat-mounted embryos were visualized and pictured with a Leica TCS sp5 confocal microscope: optical sectioning allowed to picture the r2-r6 region along the whole D/V axis with a 1-µm z-step. Stacks were made with the 10 centralmost sections, corresponding approximately to the depth of one nuclei. Fluorescence levels were quantified in single nuclei using the Fiji software. A round-shaped area of fixed surface was placed manually on each nucleus. Measurements were collected independently for each rhombomere. 50 to 80 nuclei were typically quantified in each rhombomere.

Protein extracts and gel retardation assays (EMSA)

Bacterial Krox20 protein extracts were prepared as described in (Nardelli et al., 1992). For gel retardation, the DNA probes consisted of the HindIII-XhoI restriction fragment containing the chick ortholog of element A. Once dephosphorylated, the fragment was labelled by incubation with a polynucleotide kinase (PNK, New England Biolabs) in presence of [γ-^{32}P]-labelled nucleotides. The competitors consisted of two annealed complementary oligonucleotides whose

sequences corresponded to Krox20 binding sites (underlined): K2 5'-CTCTGTACGAGTAGGAGGTTA-3', K5 5'-CTCTGTACGTGTGGGCTGTTA-3', and K7 5'-CTCTGTACGTGTGGGAGGTTA-3'. The bacterial extracts were first pre-incubated on ice for 10 min in binding buffer (20mM Tris-HCl pH 7.5, 50mM KCl, 10 mM $MgCl_2$, 1mM EDTA, 1mM DTT) supplemented with 3 μg of polydidC (Sigma) and 8% Ficoll. Labelled DNA fragment and the competitors (if used) were then added and the incubation was pursued for 30 additional minutes in order to reach the equilibrium. The binding reaction was performed in a total of 20 μL. In the competitive experiments shown in figure S5, 2.5 μM of protein extracts were used, 25 nM of labelled DNA probe and two different amounts of unlabelled competitors: 25 nM and 100 nM. In saturation experiments shown in figure S4B, a series of protein extracts, ranging from 65 nM to 1300 μM, was put in presence of 25 nM of labelled DNA fragments. The protein-to-DNA ratio ensured no protein depletion. After the 30-min incubation, the mixture was loaded on a 5% polyacrylamide gel and electrophoresis was performed for 4 hours at 14.5V/cm in 1X TBE buffer. The gels were dried and autoradiographic exposures were performed at room temperature with an intensifying screen. The proportion of DNA fragments retarded due to complex formation was quantified using a FLA3000 PhosphoImager.

mRNA quantitative analysis

zkrox20$^{-/-}$ or *hsp:mKrox20*$_{HA}$ embryos and their control clutch mates were collected at various stages from 100% epiboly to 22 ss. They were individually dissected in embryo medium in order to remove a maximum of yolk material and cut off a small piece of embryonic tissue in prevision of genotyping. Dissected embryos were then placed in 30 μL of the conservative solution *RNA later* (Ambion, Life Applied) at -20°C until processed for analysis. Total RNA was isolated using the Ambion RNAqueous Micro-kit (Life Applied) following the manufacturer's instructions. Primers for *mKrox20*, *zkrox20* and the housekeeping genes *zßactin* and *zeif1a* were designed in single exons to yield amplicons of approximate length 150 bp. Reverse transcription was performed using the Superscript III (Life Invitrogen) and quantitative PCR reactions using SYBR Green Master Mix (Roche Applied Biosystems) in a LightCycler 480 device (Roche Applied Bisosystems). In each experiment, a standard curve was created by measuring the threshold-crossing cycle number (Ct) for a series of known dilutions of purified genomic DNA. This allowed to normalize the measurements with the assay-dependent, primer-dependent amplification efficiency, and therefore compare them among different experiments and different primers. In one single qPCR experiment, the Ct values for all genes were obtained in two duplicate reactions. Error bars shown (y axis in transcriptional induction profiles) are sem values

calculated from the two duplicates of a minimum of 3 independent experiments (6 measurements in total).

Fgf loss-of-function assay in *zkrox20*$^{-/-}$ embryos

zkrox20$^{-/-}$ embryos and their control clutch mates were dechorionated at 30% epiboly after incubation in a 1 mg/mL pronase (Sigma) solution during 7 minutes followed by five baths of rinsing medium. Chorions were gently removed with forceps in Petri dishes with a layer of 1% agarose on their base. Embryos were allowed to develop at 28°C until 50% or 80% epiboly. Upon reaching this stage, they were incubated with SU5402 (Calbiochem) diluted in DMSO at a stock concentration of 3 mM. The 60 µM working concentration was obtained after dilution in embryo medium. Control embryos were incubated in embryo medium containing an equivalent volume of DMSO. At the 1-somite stage, embryos were washed in several changes of embryo medium and then grown up to 5 ss. At this stage, 36 embryos were treated as previously described for quantitative mRNA analysis in order to assess the level of *zkrox20* initiation. The rest of the clutch was allowed to develop up to 12 ss after which it was fixed overnight in 4% paraformaldehyde and processed for *zkrox20 in situ* hybridization, so that the size of r3 and r5 could be measured.

Plasmid constructs and *in ovo* electroporation

The constructs used for chick electroporation were cloned into a modified pTol2 plasmid where different versions of element A control the expression of either GFP or mcherry. Mutant versions of the element A were obtained by PCR-mediated directed mutagenesis using the high-fidelity Pusion Taq (Finnzyme): oligonucleotides carrying the desired mutations were designed in order to amplify the full plasmid; the purified PCR product was then auto-ligated with a T4 DNA ligase (New England Biolabs) and transformed into DH5α competent E. coli cells. To avoid non-specific mutations in the DNA template due to PCR amplification, the PstI-XhoI fragment containing the mutant element A was systematically subcloned into an intact empty pTol2 vector. The sequences of all mutant elements were eventually verified by direct sequencing.

For electroporation, commercial fertilized hen eggs were incubated for 30h, up to HH8-HH10, before injection. Plasmid DNA was resuspended at a concentration of 0.5 µg/µL in 10 mM Tris (pH 8) solution supplemented with 0.025% Fast-Green (Sigma). The DNA solution was injected into the embryo neural tube by use of a pulled glass capillary, directly in the hindbrain, i.e. the region anterior to the third somite. A drop of L15 medium (Life Technologies) was poured onto the egg membrane and electroporation was performed with a BTX280 electroporator (Quantum)

and CUY611 platinum-coated electrodes (Tr Tech) using the following parameters: four pulses of 21 V and 50 ms at a frequency of 1 Hz. 18 hours later, embryos were harvested in phosphate-buffered saline (PBS), fixed in 4% paraformaldehyde for 3 hours and processed for immunostaining as described above.

Computational analysis and modelling

The activation of *Krox20* element A was modelled using a stochastic formulation based on Markov chains, and for the numerical evaluation we used the software MATLAB. Descriptions of the model and the parameterization methods are given in the main text and in the supplementary information #1 respectively.

RESULTS

Element A is required for *Krox20* autoregulation in the mouse

Element A orthologs were identified in the mouse and the chick genomes and located 235 and 80 kb upstream of the *Krox20* coding sequence, respectively. Their autoregulatory activity was established by mouse transgenesis in wild type and *Krox20* mutant backgrounds and chick embryo electroporation (Chomette et al., 2006), but such experiments cannot demonstrate a functional role *in vivo* nor discard the possible existence of additional, redundant, autoregulatory mechanisms. To address these issues, we generated a knock-out of the element A in the mouse. The targeting vector contains two versions of element A, flanked by loxP and F3 recombination sites, and homologous genomic sequences (Fig. 1A): the first one corresponds to the wild-type mouse element A and the second one to a mutant version of the chick ortholog, termed cA* (unpublished, full description in chapter 4). A* has been modified by introduction of specific mutations in the Krox20 binding sites so that it no longer binds the wild type Krox20 protein (as demonstrated by electromobility shift assay, data not shown), but instead a mutant variant of Krox20, Krox20*, carrying a two amino-acid change in the second zinc-finger (Nardelli et al., 1991). The targeting vector was used to transfer the complete version of the modified locus to ES cells and then to the mouse germ line, creating the so-called $Krox20^{NA*A}$ allele. Appropriate crossing of the mutant mouse with lines constitutively expressing the Cre and Flippase recombinases (see Materials & Methods) allows the generation of three additional alleles, termed $Krox20^{NA}$, $Krox20^{A*}$, where element A is replaced by cA*, and $Krox20^{\Delta A}$, where element A is deleted.

Consequences of element A deletion on *Krox20* expression was analyzed by mRNA *in situ* hybridization in embryos homozygous for the $Krox20^{\Delta A}$ mutation (Fig. 1B). In r3, onset of *Krox20* expression normally occurs around the 0-somite stage (0 ss). At this stage, *Krox20* expression was found similar in mutant and control littermates. Later on, the r3 *Krox20* domain of expression extends and the level of the mRNA increases to reach a maximum at around 8 ss (Fig. 1B). In the mutant, this extension and increase occur normally until 6 ss, when the level of *Krox20* mRNA starts decreasing as compared to controls. At 8 ss *Krox20* expression is almost abolished, whereas it persists beyond 12 ss in controls. r5 expression, which shows delayed dynamics as compared to r3, is modified in a similar way in the mutant: although initiation occurs normally at 2-3 ss (data not shown), down-regulation occurs much earlier than in control embryos, around 12 ss, whereas expression persists beyond 16 ss in controls. These results suggest that 465-bp sequence of element A is required for both the early amplification and the

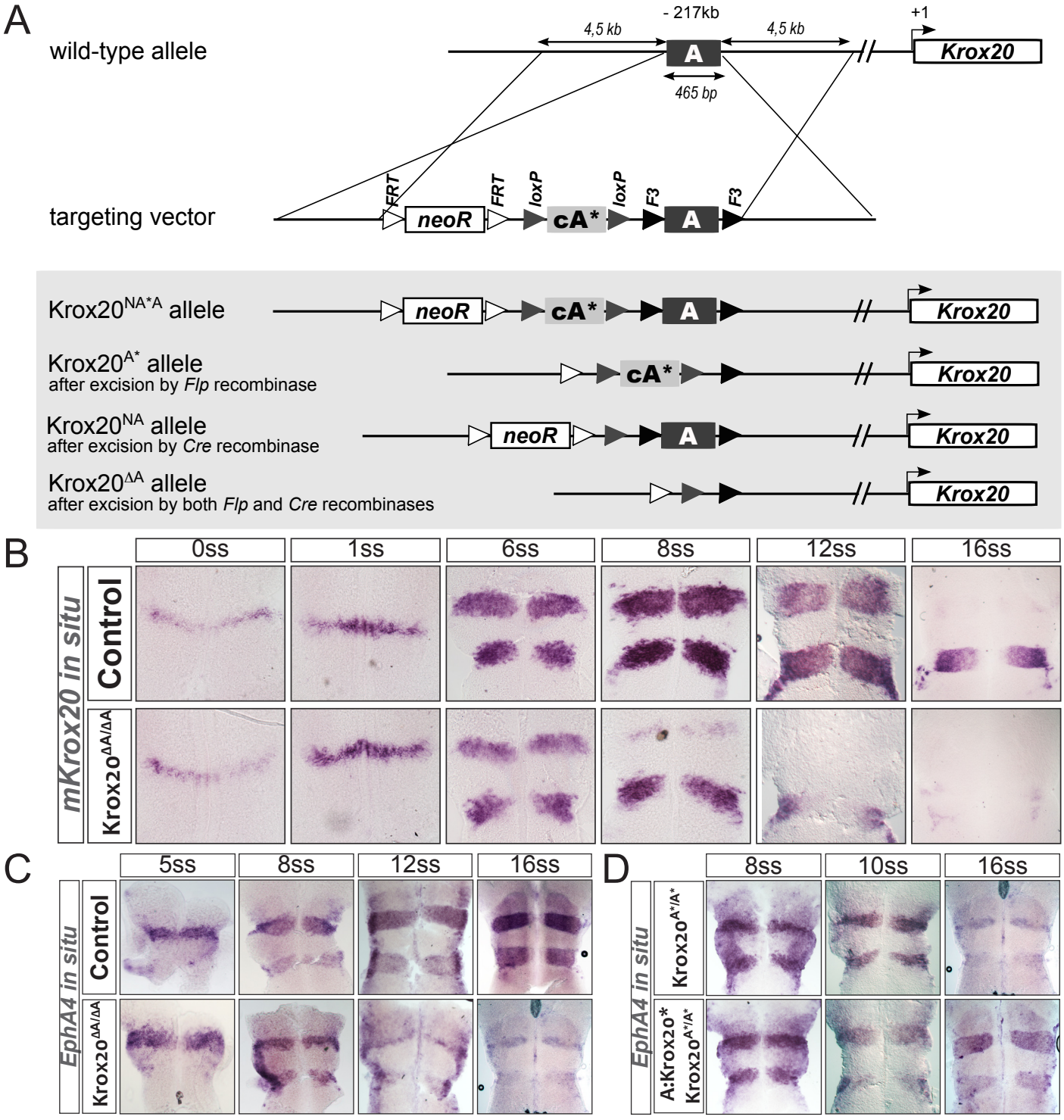

Figure 1: The element A is required for the maintenance of *Krox20* expression in the mouse hindbrain. **(A)** Knock-in strategy targeting the element A in the mouse genome. The strategy was designed to provide the Krox20^{NA*A} allele. 'N' stands for the *neomycin* cassette, 'A*' stands for a mutant form of the element A that can be bound and activated only by an altered version of Krox20 termed Krox20*. Through Cre or Flp-mediated recombination, three alleles can be obtained: (i) Krox20^{A*} expected to be null, (ii) Krox20^{NA} expected to behave as the wild-type allele, (iii) Krox20$^{\Delta A}$ corresponding to the knock-out of element A. **(B)** *Krox20 in situ* hybridization performed on *Krox20*$^{\Delta A/+}$ (control) and *Krox20*$^{\Delta A/\Delta A}$ embryos. **(C)** Similar timecourse experiment performed on *EphA4, a* key target of *Krox20* in the hindbrain **(D)** *EphA4 in situ* hybridization performed on Krox20$^{A*/A*}$ embryos that carry in addition the transgene *A:Krox20**, responsible for the activation of *Krox20** in r3 and r5. In these embryos, the expression of *EphA4* is rescued in comparison with non-transgenic *Krox20*$^{A*/A*}$ embryos.

maintenance of *Krox20* expression. To investigate the consequences of this altered *Krox20* expression on hindbrain patterning, we analyzed the expression of one of the Krox20 targets, the tyrosine kinase receptor *EphA4*, which is involved in the segregation between odd- and even-numbered rhombomeres (Mellitzer et al., 1999; Xu et al., 1999). Both the extent of the domain and the level of *EphA4* expression were markedly reduced from 8 ss onwards (Fig. 1C), suggesting that cells normally fated to belong to r3 and r5 undergo either apoptosis or reprogramming towards an even-numbered fate. However, a reduced domain of *EphA4* expression persists at 16 ss (Fig. 1C), raising the possibility that transient expression of *Krox20* might be sufficient to engage a limited number of cells into the r3/r5 fate.

Defective autoregulation can be rescued by an artificial indirect loop

As we obtained only one targeted mouse line, it was necessary to demonstrate that the defects in *Krox20*$^{\Delta A/\Delta A}$ animals specifically originate from the knock-down of *Krox20* autoregulation. For this purpose we attempted to rescue the phenotype by re-establishing a positive feedback loop, taking advantage of the specific interaction between Krox20* and A* (Supplementary Fig. S1). We first verified that *Krox20*$^{A*/A*}$ embryos display a phenotype similar to *Krox20*$^{\Delta A/\Delta A}$ animals in terms of *Krox20* and *EphA4* expressions (data not shown). We then engineered a transgenic mouse line carrying the *Krox20** coding sequence under the control of the element A (*A:Krox20**) and verified that this results in *Krox20** expression in r3 and r5 (data not shown). The *A:Krox20** transgene was subsequently transferred into a *Krox20*$^{A*/A*}$ background. In *A:Krox20*;Krox20*$^{A*/A*}$ embryos, hindbrain expression of *Krox20* (data not shown) and *EphA4* (Fig. 1D) were largely rescued as compared to *Krox20*$^{A*/A*}$ embryos. Our interpretation of this result is that, in absence of a functional direct autoregulatory loop involving the endogenous element A, we have been able to re-create an indirect loop that involves production of Krox20, binding to the transgenic element A, production of Krox20*, binding to endogenous the A* element and further production of Krox20. These results establish that the defects in *Krox20* autoregulation in *Krox20*$^{\Delta A/\Delta A}$ embryos are exclusively due to the absence of the A element, which appears necessary and sufficient to build a positive autoregulatory loop.

Conservation of *krox20* autoregulation in the zebrafish and quantitative analysis

In order to perform a quantitative analysis of the *Krox20* autoregulatory loop, we decided to move to the zebrafish. It was first necessary to demonstrate that an autoregulatory loop is also involved in the control of *Krox20* hindbrain expression in this species. For this purpose, we used both gain- and loss-of-function approaches. In order to provide exogenous *Krox20*, we

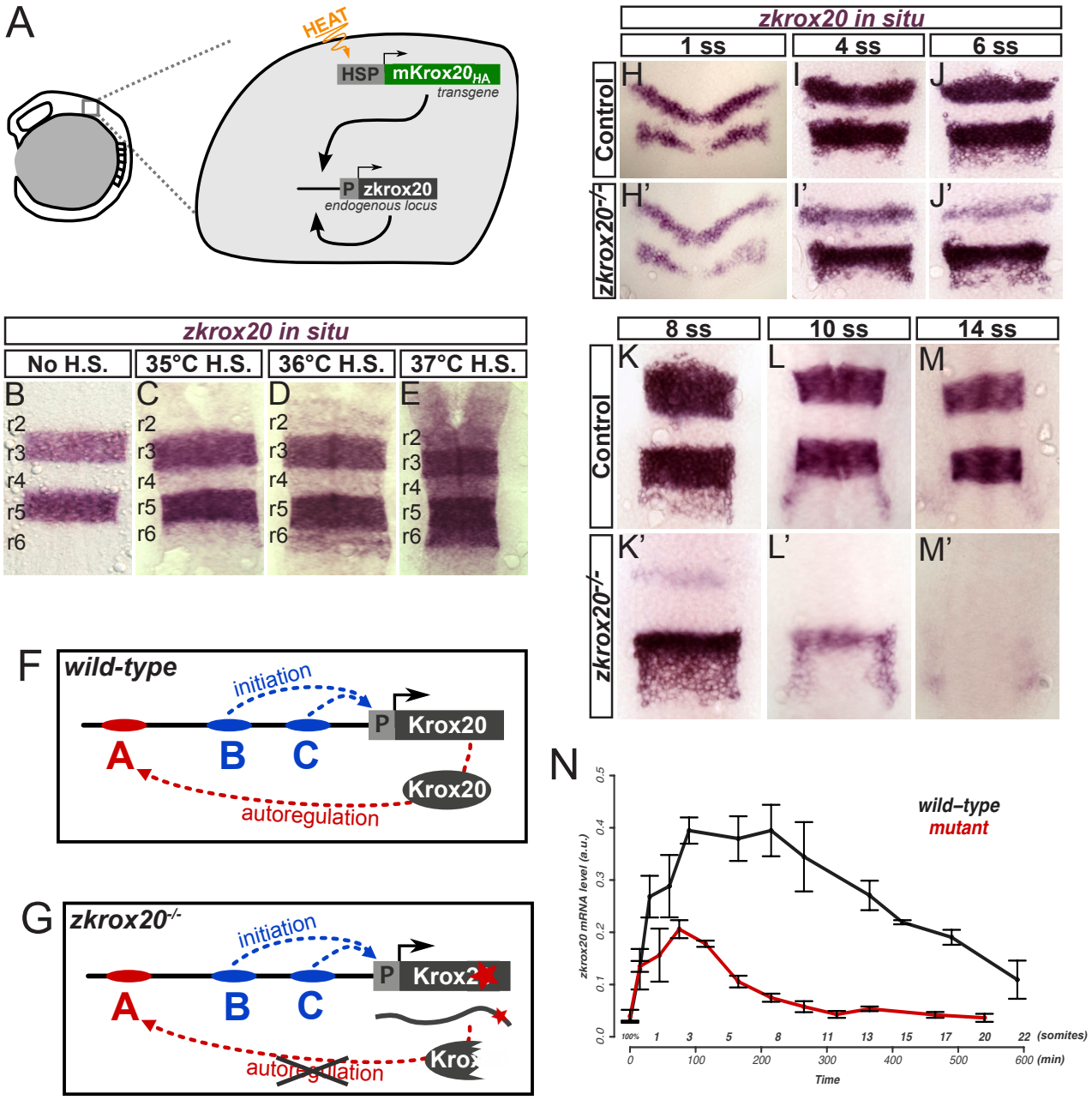

Figure 2. Analysis of krox20 autoregulation in zebrafish embryos.
(A) *hsp:mKrox20*$_{HA}$ fish embryos carry a transgene leading to the expression of murine Krox20 in all cells upon heat-shock. In turn mKrox20 triggers the endogenous *zkrox20* autoregulatory loop and leads to ectopic activation of *zkrox20*, outside r3 and r5. **(B-E)** *zkrox20 in situ* hybridization performed on *hsp:mKrox20*$_{HA}$ embryos after heat-shocks of increasing temperatures. **(F)** In mouse and chick, the cis-regulatory network controlling the activation of *Krox20* in the hindbrain includes an autoregulatory element, A, and two initiator elements, B and C. Although element A has not yet been identified in zebrafish, the same scheme is likely to apply. **(G)** A point mutation in *zkrox20* coding sequence leads to the formation of a truncated, inactive protein and abolishes the autoregulatory loop. **(H,H'-M,M')** *zkrox20 in situ* hybridization in control and *zkrox20*$^{-/-}$ embryos at the indicated stages. **(N)** Control and *zkrox20*$^{-/-}$ mutant embryos were collected at different timepoints and processed for quantification of *zkrox20* mRNA level by RT-qPCR.

engineered a transgenic fish line in which a sequence encoding a murine, HA-tagged version of *Krox20* is placed under the control of a heat-shock promoter, *hsp:mKrox20*$_{HA}$ (Fig. 2A). Using this system, we can modify the temperature or duration of the heat-shock to adjust the amount of *mKrox20* produced in all embryonic cells. As shown in Fig. 2B-E, increasing temperature of heat-shock leads to progressive accumulation of *zkrox20* mRNA in r2, r4 and r6. Therefore expression of exogenous *mKrox20* is able to activate the expression of endogenous *zkrox20* in these rhombomeres that normally do not express the gene, suggesting the existence of an autoregulatory mechanism. Interestingly, the level of expression is not modified in r3 and r5, suggesting that the autoregulatory system is saturating in these rhombomeres. Furthermore efficient activation of the endogenous gene is mainly restricted to the hindbrain, despite expression of the exogenous gene in the entire embryo, suggesting that the autoregulatory system is subject to a specific regulation in the hindbrain. A second approach allowing the investigation of *krox20* autoregulation in the fish was made possible by the recent availability of a fish mutant line carrying a point mutation in the *krox20* coding sequence (Monk et al., 2009). The mutation introduces a premature stop codon in the second zinc-finger and abolishes zKrox20 function (Fig. 2F,G). We compared *zkrox20* expression in mutant and wild-type embryos using *in situ* hybridization (Fig. 2H-M and H'-M'). The *zkrox20* mutation did not prevent activation of its own expression in r3 and r5, but rapidly led to its extinction from 6 ss in r3 and 10 ss in r5, whereas expression in both rhombomeres was maintained beyond 14 ss in wild type embryos. This phenotype is very similar to what was observed with the *lacZ* knock-in into the mouse *Krox20* gene (Schneider-Maunoury et al., 1993), suggesting that *Krox20* is required for maintaining its own expression. In conclusion, gain and loss-of-function studies support the idea that maintenance and amplification of *krox20* expression during zebrafish hindbrain segmentation involves an autoregulatory mechanism. Does the autoregulatory loop involve the same elements as in the mouse and chick, in particular the A enhancer? Despite our efforts, we have not been able to identify an element A fish ortholog by *in silico* analysis. Nevertheless, as indicated below, the chick element A is perfectly functional in the zebrafish hindbrain, suggesting that the molecular elements involved in *Krox20* autoregulation are conserved from fish to mammals.

To obtain quantitative evaluations of the respective contributions of the initiation and autoregulation mechanisms to *krox20* expression, we measured *krox20* mRNA levels in whole wild type (Fig. 2N, black curve) and *krox20* mutant zebrafish embryos (Fig. 2N, red curve) by reverse transcriptase-quantitative polymerase chain reaction (RT-qPCR), between 100% epiboly and 25 ss. During this period, *krox20* expression is restricted to the hindbrain and the measurements therefore reflect the added expression in r3 and r5. Mutant expression levels

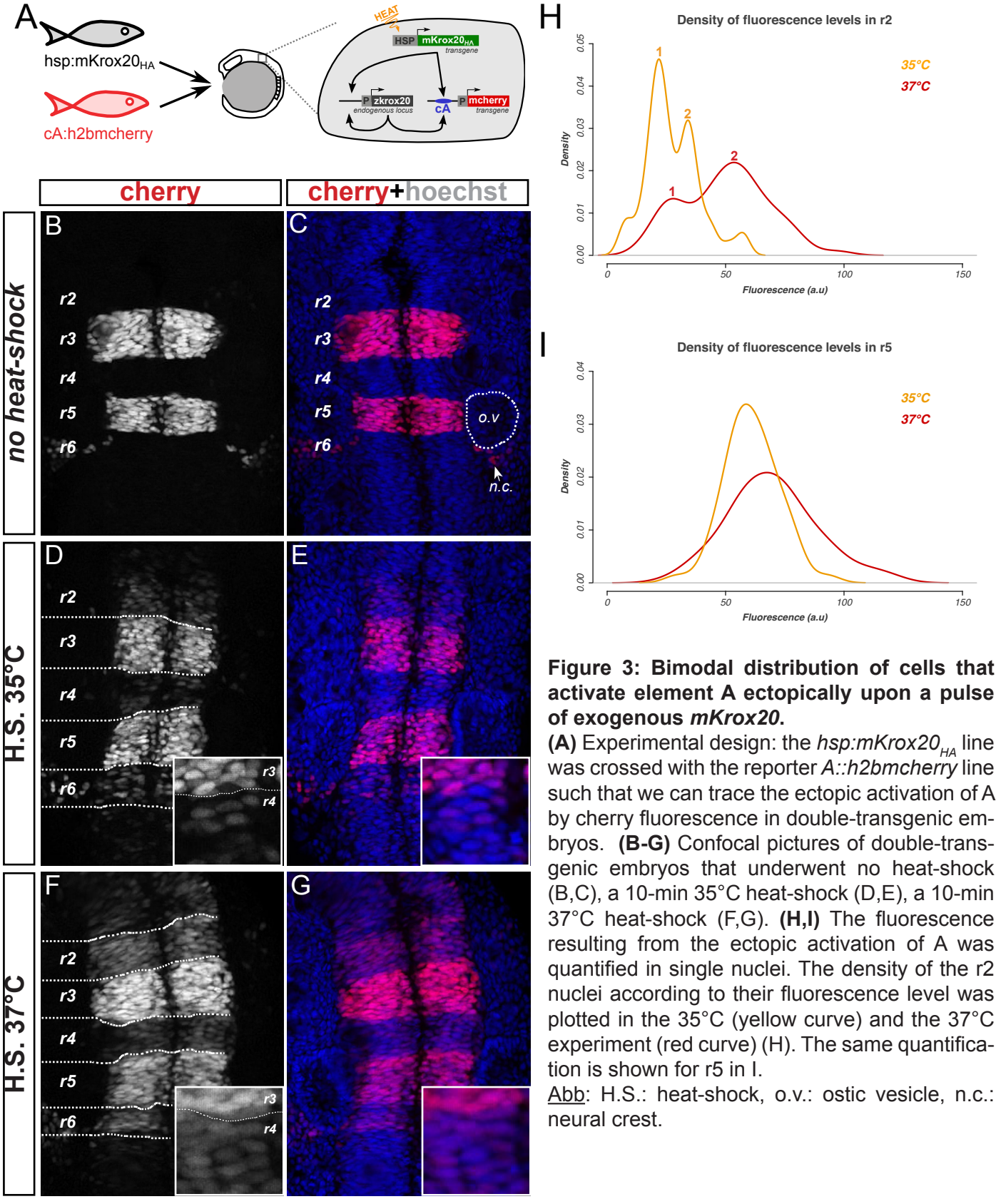

Figure 3: Bimodal distribution of cells that activate element A ectopically upon a pulse of exogenous *mKrox20*.
(A) Experimental design: the *hsp:mKrox20*$_{HA}$ line was crossed with the reporter *A::h2bmcherry* line such that we can trace the ectopic activation of A by cherry fluorescence in double-transgenic embryos. **(B-G)** Confocal pictures of double-transgenic embryos that underwent no heat-shock (B,C), a 10-min 35°C heat-shock (D,E), a 10-min 37°C heat-shock (F,G). **(H,I)** The fluorescence resulting from the ectopic activation of A was quantified in single nuclei. The density of the r2 nuclei according to their fluorescence level was plotted in the 35°C (yellow curve) and the 37°C experiment (red curve) (H). The same quantification is shown for r5 in I.
Abb: H.S.: heat-shock, o.v.: ostic vesicle, n.c.: neural crest.

reflect the initiation process, whereas wild type expression corresponds to the combined output of initiation and autoregulatory mechanisms. mRNA resulting only from initiation mechanisms accumulates rapidly, peaks at around 3 ss and then decays in an exponential-like manner, as expected from mRNA degradation. The addition of the autoregulatory loop leads to a 2-fold increase of the mRNA maximal level and the prolongation of the expression, with a plateau between 3 and 8 ss, followed by a linear-like decline. Therefore, the initiator elements only provide a short pulse of *krox20* expression, necessary for the engagement of the autoregulatory loop. In conclusion, this analysis allowed to obtain quantitative data on the contribution of the autoregulatory loop to *krox20* expression, which we will use below to constrain a mathematical model.

Krox20 transcription in the hindbrain displays a switch-like behaviour

One property associated with switch systems is a high cell-to-cell variability around the threshold, reflecting the stochastic nature of the control of gene expression. This results in a bimodal distribution of the cell population, with a part of them expressing the gene, whereas the other does not. To determine whether rhombomere cells fall into a bimodal distribution in terms of *krox20* expression following pulsed expression of exogenous *Krox20*, we needed a read-out of *krox20* expression at the cell level. For this purpose, we made use of a zebrafish transgenic line carrying a reporter construct in which a histone h2b-mcherry fusion protein is placed under the control of chick element A (*cA:h2b-mcherry*, generous gift of N. Peyrieras). This reporter line was crossed with the *hsp:mKrox20*$_{HA}$ line (Fig. 3A). As expected, in absence of heat shock, this led to strong, specific and rather homogeneous nuclear mcherry fluorescence in r3 and r5 cells, in about half of the resulting embryos (Fig. 3B,C). Upon heat shock at 5 ss, approximately 25% of the embryos showed mcherry fluorescence in even-numbered rhombomeres 4 h later (Fig. 3D-G). Each rhombomere was analyzed by confocal microscopy, the level of fluorescence in each nucleus was quantified (see Materials & Methods) and the number of cells was plotted according to their level of fluorescence (Fig. 3H,I and data not shown). It should be noted that, since the mcherry is likely to be stable in respect to the time frame of these experiments, the measure of the fluorescence reflects the integration of *krox20* expression level in time rather than the dynamics of expression. No significant modification in the level and distribution of fluorescence was observed in r3 and r5 upon heat shock and the distribution was found to be unimodal (see Fig. 3I for r5). This indicates that exogenous *mKrox20* has no significant effect in rhombomeres where the autoregulatory loop has presumably been fully activated by endogenous *krox20* expression. After heat shock (35°C or 37°C), the level of fluorescence within each even-

numbered rhombomere was found very variable (Fig. 3D-G). However, in both cases, the analysis of the distribution of fluorescence revealed two major peaks, suggesting a bimodal behaviour (see Fig. 3H, depicting the situation in r2). We interpreted the major peak with the highest fluorescence (peak 2) as corresponding to cells that have stably engaged the autoregulatory process, whereas the other major peak (peak 1) would correspond to cells that have failed to do so. After a 37°C heat shock, peak 2 in r2 corresponds to a fluorescence level similar to the unique peak observed in odd-numbered rhombomeres (Fig. 3H,I). This suggests that the pulse of Krox20 provided by the heat shock has been able to activate the autoregulatory loop with kinetics similar to those in odd-numbered rhombomeres, allowing accumulation of mcherry to the same levels. The cells corresponding to the low fluorescence level (peak 1) have also accumulated some mcherry, but this is likely due to direct activation of the reporter construct by the exogenous Krox20 and possibly by some endogenous Krox20 generated by an aborted activation of the autoregulatory loop. Moreover, the 35°C heat shock provides a reduced Krox20 pulse that is likely to lead to a slower kinetics of element A activation at the single cell level (this phenomenon refers to "critical slowing-down effect"). We propose that this explains why the two major peaks of 35°C-heat-shock are displaced compared to the 37°C heat shock (Fig. 3H), since the mcherry reporter has not been able to accumulate to the same levels during a fixed time period.

In conclusion, this analysis establishes that a pulse of *Krox20* expression in the hindbrain results in a bimodal distribution of the cell population. Due to the inertia of our reporter system, the cells become either high or low expressors of the reporter and we propose that these categories correspond to cells that have or have not activated the autoregulatory loop. This interpretation will be confirmed by simulations obtained from the mathematical model (see below).

A mathematical model for *Krox20* transcriptional control at the single-cell level

Since we could not have a direct, *in vivo* experimental access to the activity of the *Krox20* autoregulatory loop in single cells, we decided to develop a mathematical model of the system that could simulate single-cell behaviours, allow predictions and assessment of our hypotheses and interpretations, and eventually reveal additional features of the system. For these purposes, the model should be able to predict the time evolution of the number of Krox20 molecules in single cells. To simplify the model, we defined an initiation phase that involves a pulse of Krox20 production by initiation mechanisms (either endogenous, due to the activity of elements B and C, or exogenous, using the heat shock expression system for instance), beyond which Krox20

production only relies on the autoregulatory loop. As schematised in Fig. 4A, the evolution of the system primarily depends on:

- the number of Krox20 molecules, produced through the initiation mechanism, $Krox20^{I}$. The rate of initiation production is termed $\mathbf{\Phi}_{I}$.
- the activity of element A, that depends on the number of Krox20 binding sites, the binding and the unbinding rates of Krox20 and the transcriptional activity of Krox20 molecules bound to the element A. When activated, the element A produces $Krox20^{A}$ molecules with a rate $\mathbf{\Phi}_{A}$. It should be noted that $Krox20^{I}$ and $Krox20^{A}$ are functionally indistinguishable and simply differ by their mechanism of production. In the case of exogenous production of $Krox20^{I}$, we will be able to experimentally differentiate $Krox20^{I}$ and $Krox20^{A}$.
- the degradation of $Krox20^{I}$ and $Krox20^{A}$, with the same rate $\mathbf{\Psi}$.

In silico analyses and electromobility shift assays (EMSA) performed on a 465-bp DNA fragment corresponding to the element A revealed the presence of three high and one medium affinity Krox20 binding sites (Supplementary Fig. S4 and S5). Element A can therefore lie in 5 states s=0, 1, 2, 3, 4 corresponding to the number of bound Krox20 molecules. At a given time, the system is characterized by two variables: the discrete variable *s* whose value can be 0, 1, 2, 3 or 4, and the total number *n* of Krox20 proteins (the sum of $Krox20^{I}$ and $Krox20^{A}$). We estimate the joint probability $p_s(n,t)$ that the element A is in state *s*, with *n* Krox20 molecules in the environment. At t=0, *n* is null and the pulsed initiation process starts producing Krox20 molecules with a rate $\mathbf{\Phi}_{I}$. These Krox20 molecules bind and activate element A, producing an additional load of Krox20 molecules. Binding and activation events may involve synergy between Krox20 proteins, under the form of binding/unbinding cooperativity and concerted recruitment of the transcriptional apparatus (Georges et al., 2010) (Supplementary Fig. S2). These two processes were implemented in the model as follows:

- the forward binding rate λ and the unbinding rate μ are modelled as Poissonian rates. In biological terms, λ is the inverse of time required for one Krox20 protein to find a binding site; μ represents the inverse of the duration Krox20 sits on one site. If binding is cooperative, the rates of binding and unbinding events depend on the state of A: λ increases with the number of bound proteins, and μ conversely decreases. Under these conditions, λ and μ are actually vectors, termed $\lambda_s = [\lambda_0,\lambda_1,\lambda_2,\lambda_3,0]$ and $\mu_s = [0,\mu_1,\mu_2,\mu_3,\mu_4]$. $\lambda_4=0$ and $\mu_0=0$, since no protein can bind when the 4 sites are occupied and no protein can unbind when none is bound.
- the concerted recruitment of the transcriptional machinery by several Krox20 proteins implies that the production rate $\mathbf{\Phi}_{A}$ is also conditioned by the state of A, hence $\mathbf{\Phi}_{A,s} = \mathbf{\Phi}_{A}.[0,a_1,a_2,a_3,1]$, where a_1-a_3 are multiplicative coefficients of $\mathbf{\Phi}_{A}$.

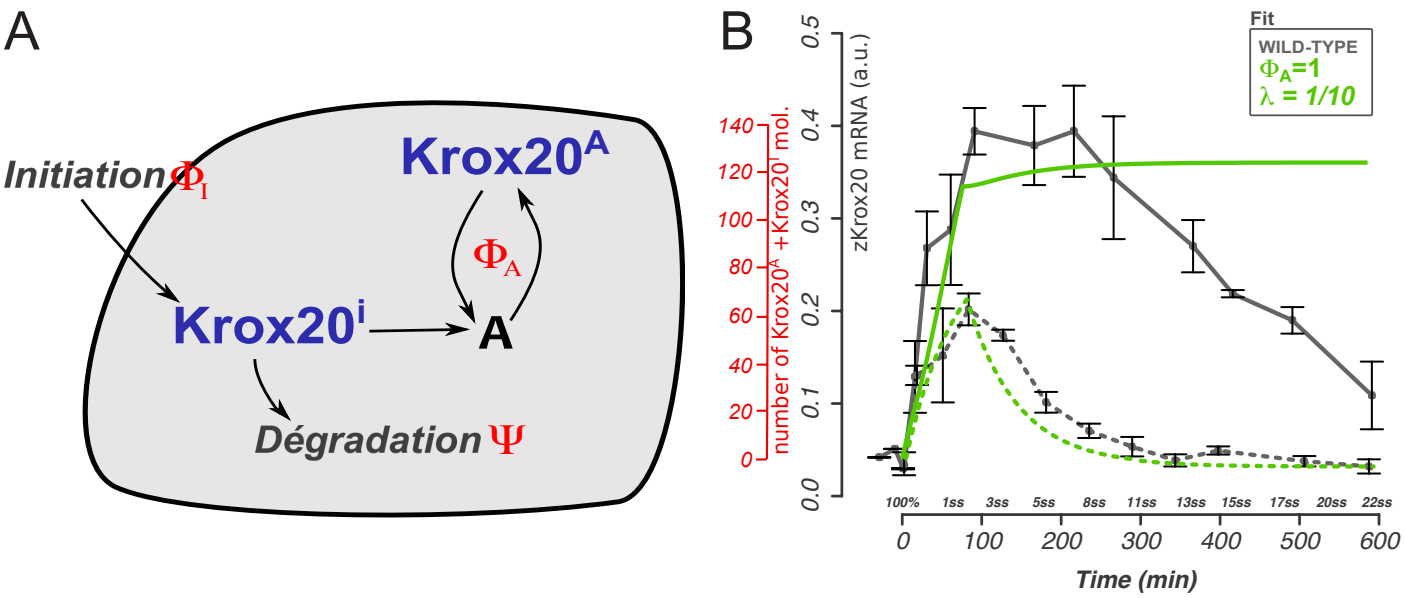

Figure 4: A model of *Krox20* autoregulation.
(A) An initial load of Krox20, termed Krox20^I, is produced upon the rate Φ_I and participates in the activation of A, which in turn produces additional Krox20 molecules, Krox20^A, with a rate Φ_A. Krox20^I and Krox20^A are both subject to degradation, of rate Ψ. According to this model, activation and maintenance of the *Krox20* autoregulatory loop depends on the number of Krox20 molecules present (Krox20^I and Krox20^A) and the rules of element A activation. The latter condition depends on the number of Krox20-binding sites, binding and unbinding rates as well as possible binding cooperativity and concerted recruitment of the transcriptional machinery. All these parameters are implemented in the model. **(B)** Once fully parameterized, the model predicts the endogenous *zkrox20* profile in wild-type embryos, up to t = 250 min. Green curves refer to simulations while grey curves are experimental. The latter were obtained by *zkrox20* RT-qPCR performed on wild-type embryos at different timepoints as shown on the x axis. Dashed curves correspond to the initiation signal resulting from Φ_I; solid curves represent the sum of Krox20^I and Krox20^A, that is experimentally equivalent to *zkrox20* level in wild-type embryos.

The full time-dependent behaviour of the system is analyzed using a Markov chain formulation (Yin & Zhan, 1998, Springer-Verlag Editions), thus capturing the stochastic nature of element A activation. The joint probability is given by the Master equation:

$$\partial_t p_s(n,t) = \Phi_s p_s(n-1,t) + (n+1)\Psi p_s(n+1,t) - (\Phi_s + n\Psi) p_s(n,t)$$
$$+\mu_{s+1} p_{s+1}(n-1,t) + \lambda_{s-1}(n+1) p_{s-1}(n+1,t) - (\mu_s + \lambda_s n) p_s(n,t) \qquad \textbf{(1)}$$

where $\Phi_s = \Phi_{A,s} + \Phi_I (t < T_I)$ and T_I the duration of initiation.

The first line of this equation describes the production and degradation of Krox20, and the second the binding and unbinding dynamics.

The probability distributions of the number of Krox20 molecules and the state of A are:

$$p(n,t) = \sum_{s=0}^{4} p_s(n,t) \qquad \textbf{(2)}$$
$$p_s(t) = \sum_{n=0}^{\infty} p_s(n,t)$$

Equations 1 and 2 describe the time evolution of probabilities, i.e. the average behaviour of a single cell, which is actually equivalent to the behaviour of a cell population. However, we are also interested in the stochastic trajectories of individual cells. To obtain realizations of these trajectories, the dynamics of chemical reactions underlying equation (1) were simulated by applying the Gillepsie algorithm. Model simulations therefore reflect Krox20 dynamics either at the single-cell or population levels and establish the link with tissue-scale patterning.

The model presented above corresponds to a first simplified version, as the production of Krox20 molecules is modelled as an effective production: the initiation and autoregulation phases directly provide proteins that can bind to element A; we omitted the intermediate step of mRNA production. As we will be comparing simulations with mRNA experimental curves, the simulated number of molecules corresponds to mRNA molecules that produce an equal effective number of proteins (i.e. proteins that are involved in binding to element A) (Supp. Fig. S3). This correspondence between the number of mRNA and protein molecules is justified by similar mRNA and protein degradation rates (see Supplementary Information #1). With this simplified model, we therefore underestimate the actual number of proteins, that can be considered as proportional to the mRNA level and depending on a first-order translation rate α. We will justify that the actual number of proteins produced only affects marginally the mRNA dynamics.

A full stochastic description of the model, with the implementation of mRNA, proteins, their respective degradation rates, the mRNA production rate (Φ_I, Φ_A) and the translation rate α (Supplementary Fig. S3A), was found to require excessive computational resources. We circumvented this issue by using a deterministic formulation that is functional excepted in case of

A

Variables	Symbol	Type
States of element A	s	Discrete: s=[0, 1, 2, 3, 4]
Krox20 produced by the initiation	$Krox20^{I}$	Continuous
Krox20 produced by the autorgeulatory loop	$Krox20^{A}$	Continuous

B

Parameters	Symbol	Estimated/Fitted value
Number of Krox20-binding sites		4
Binding rate (state-dependent)	$\lambda_s=[\lambda_0, \lambda_1,\lambda_2,\lambda_3,0]$	[1/1134, 1/12.9, 1/42.3, 1/10, 0]
Unbinding rate (state-dependent)	$\mu_s=[0, \mu_1, \mu_2,\mu_3,\mu_4]$	[0, 1/3, 1/3, 1/3, 1/3]
Production rate during the initiation phase	Φ_I	1.5 (endogenous)
Duration of initiation phase	T_I	80 (endogenous)
Production rate of A (mol./min)	$\Phi_{A,s}=\Phi_A.[0,a_1,a_2,a_3,a_4]$	1.[0 0 0.2 0.5 1]
Degradation rate of Krox20 molecules	Ψ	1/65
Total number of parameters	**16**	

Table 1: Model variables and parameters
(A) The three variables of the model. The sum of $Krox20^{I}$ and $Krox20^{A}$ gives the total number of Krox20 molecules, *n*. **(B)** The 16 free parameters of the model, and the values used in the simulations. The values shown for Φ_I and T_I correspond to the fitted values used in simulations of the endogenous *zkrox20* profile. They were set differently in *hsp:mKrox20*$_{HA}$ experiments, as indicated in the main text.

low mRNA/protein number. In this situation, the model is not able to predict properly the time evolution of the system. All simulations shown below were therefore obtained from the simplified, stochastic version of the model.

Parameterization of the model

The model needs to be fuelled with 16 parameter values that are listed in Table 1. In order to obtain these parameters, we employed two strategies:

- Direct parameterization, i.e. implementation of values found experimentally, was used for the degradation rate, the number of Krox20-binding sites and the binding/unbinding dynamics (see Supplementary information #1 and Fig. S4 and S5). To reduce the parameter space, we considered that all cooperativity is mediated by binding events rather than unbinding, such that $\mu_s=\mu=1/3$ min^{-1}. Electromobility shift assays (EMSA), performed at steady-state, allowed to find a relationship between the five remaining binding parameters, μ, λ_0, λ_1, λ_2 and λ_3, but one degree of freedom remained, i.e. one single value was missing. We chose arbitrarily λ_3. Overall, the parameters λ_3, Φ_I and $\Phi_{A,s}$ are left free after the direct parameterization procedure.

- Indirect parameterization is a method that simply requires consistency between model simulations and experimental results. As a source of experimental data, we used the endogenous *zkrox20* mRNA profiles in wild type and *krox20*$^{-/-}$ mutant embryos shown in Fig. 2N. It should be noted that since the mRNA measurements by RT-qPCR are carried out on entire embryos, they represent the sum of the RNA levels in r3 and r5. This simplification should not affect significantly the parameterization process, as the kinetics of *krox20* expression in r3 and r5 only differ by a small shift in time. λ_3, Φ_I and $\Phi_{A,s}$ were fitted using two conservative criteria derived from the experimental results (see Supplementary Information #2 and Fig. S6 and S7): first the *krox20* mRNA maximal level increases two-fold in presence of autoregulation; second the probability to activate A is decreased to 59% and 51% when the initiation level is reduced to 35% and 27% respectively. These two criteria allowed to fit λ_3 at 1/10 min^{-1} (if only one protein is in the system, it requires 10 minutes to bind the fourth site of element A), Φ_I at 1.5 mol./min (1.5 molecule produced per minute) and Φ_A at 1 mol./min (the element A leads to production of 1 molecule per minute when fully activated). This value of Φ_A is however conditioned by the state of element A, representing the concerted recruitment of the transcriptional machinery. We envisaged four biologically-meaningful scenarios: $\Phi_{A,s}$=1.[0 1 1 1 1] (no synergy among Krox20 proteins in recruiting PolII), 1.[0 0.25 0.5 0.75 1] (additivity), 1.[0 0 0.2 0.5 1] ("light" synergy), 1.[0 0 0 0.3 1] ("strong" synergy) (see Supplementary Information #2). We found that the "light synergy" situation provides the closest fit to the experimental data, hence $\Phi_{A,s}$=1.[0 0 0.2 0.5 1].

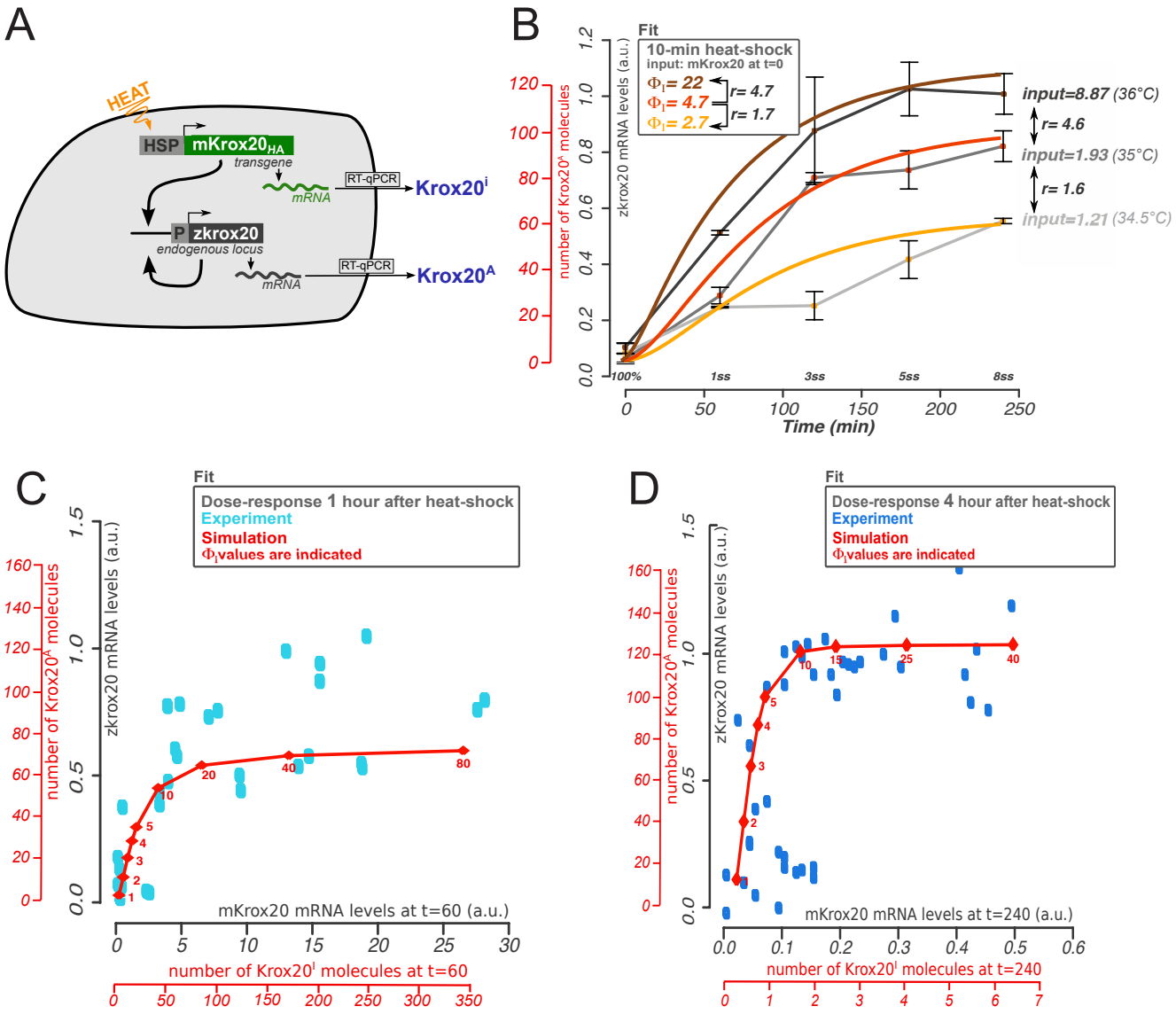

Figure 5: Validation of the model parameterization in *hsp:mKrox20*$_{HA}$

(A) The *hsp:mKrox20*$_{HA}$ experimental system allows to stimulate cells with adjustable levels of input (*mKrox20*, Krox20^{I}) and measure the transcriptional response, i.e. the output (*zkrox20*, Krox20^{A}). Both input and output are measured by RT-qPCR in whole embryos. **(B)** Three stimulations of different temperatures led to three distinct timecourses of transcriptional response (grey curves). The experimental input level was measured as the amount of *mKrox20* at t = 0 min. Fitting the experimental curves with simulated timecourses was performed as follow: a Φ_I value was first chosen to fit the 35°C curve; then the ratio (*r*) between the corresponding input (1.93) and the two other values (1.21 and 8.87) was used to derive two values of Φ_I (2.7 and 22). Simulations performed with these two values provided the yellow and the brown curves. **(D,E)** The input/output relationships of the *hsp:mKrox20*$_{HA}$ system at 1 hour and 4 hours after heat-shock. Each datapoint corresponds to one stimulated embryo where the levels of input (*mKrox20*) and output (*zkrox20*) were measured by RT-qPCR. For each experiment, a series of embryos were subject to heat-shocks of temperatures ranging from 33 to 39°C.

With all parameter values implemented (see Table 1), the model faithfully recapitulates *zkrox20* expression in the *krox20* null mutant situation (Fig. 4B, dashed curves). In the case of wild type embryos, the model reproduces the upregulation and the plateau phases of *krox20* expression timecourse, but not the decrease observed after 8 ss (Fig. 4B, plain curves). This decrease could be due to a modification occurring during development and resulting in a change in one parameter value. We will investigate this hypothesis below.

Validation of the model

To validate the model and its parameters, we used the *hsp:mKrox20*$_{HA}$ transgenic line where the level of input Krox20^{I} (*mKrox20*) can be tuned experimentally by varying the heat-shock temperature and can be discriminated from the level of Krox20^{A} (*zkrox20*) by RT-qPCR (Fig. 5A). The measurements were restricted to the period preceding the phase of decline of endogenous *krox20* expression. We performed 10-min heat-shocks at three temperatures (34.5°, 35° and 36°C), measured the level of *Krox20*^{I} mRNA at time t=0 and the total level of *zkrox20* mRNA from t=0 to 240 min by RT-qPCR. To obtain the level of *zkrox20* mRNA present in even numbered-rhombomeres and therefore due to the activation of the autoregulatory loop by exogenous Krox20, we subtracted the level of *zkrox20* mRNA derived from odd-numbered rhombomeres (Fig. 2N) to the total mRNA level. This gave the three gray curves presented in Fig. 5B). We then varied Φ_I in the model to fit the curve obtained at 35°C. Modelisation profiles at 34.5°C and 36°C were obtained by changing Φ_I in accordance with the ratios of *Krox20*^{I} mRNAs measured at t=0. In these conditions, we observed a good fit between the experimental data and the three simulation curves, providing a first validation of our model.

A second element for the validation of the model was derived from the analysis of the dose-response curves, i.e. the amount of Krox20^{A} produced after activation by increasing levels of Krox20^{I}. Both input and output were measured experimentally 60 min or 240 min after heat-shock. Given the kinetics observed in Fig. 5B, the 240 min condition can be considered as close to steady-state. The comparison between experimental data and simulations are presented in Fig. 5C,D. We observed an excellent fit at 240 min. At 60 min, simulations appear to slightly underestimate the output level, but this might reflect high experimental variability in embryos having not yet reached the steady state level. Nevertheless, globally, the parametric solution chosen above nicely accounts for the dynamics of the system following ectopic activation.

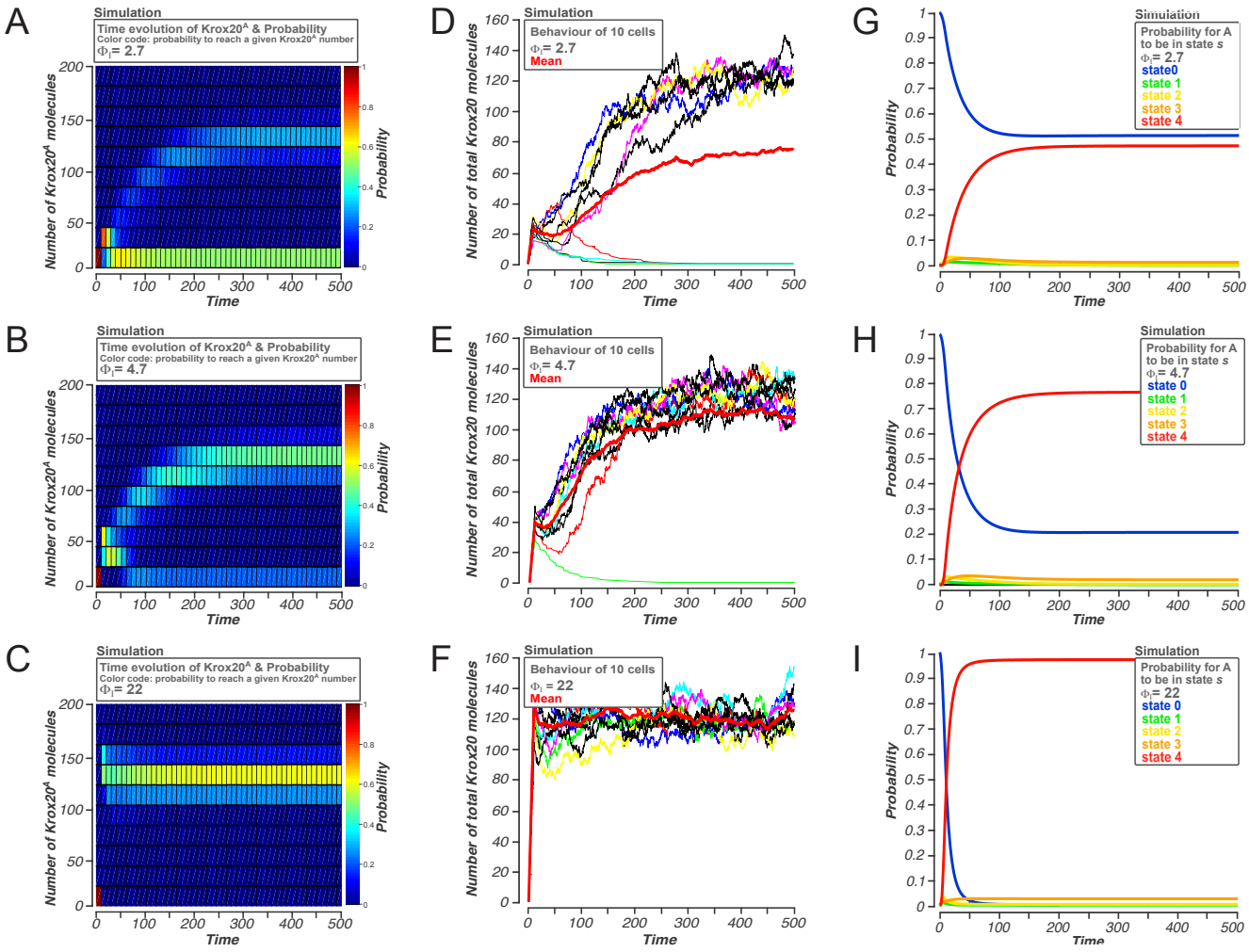

Figure 6: Model predictions: bimodality, cellular bistability and molecular bistability
(A-C) Heat-maps of the time-dependent probability for a cell population to contain a given number of Krox20^A molecules, depending on the level of stimulation. Graded stimulations are shown, with the lowest in A and the highest in C. In A for instance, at steady-state, i.e. after 250 min, 50% of the cells within the population contain between 0 and 20 Krox20^A molecules and the remaining 50% contain between 105 and 165 molecules (15% 105-125; 30% 125-145; 5% 145-165). The population is therefore clived in two subparts, depending on the number of Krox20^A molecules. The proportion of cells in each subpart is modified when the stimulation strength varies, as evidenced when comparing A and B. This input-dependent distribution of cells in two modes is termed bimodal. **(D-E)** Stochastic simulations of single-cell behaviour upon the same stimulations as in A-C. At steady-state, cells can adopt two behaviours, either no Krox20^A (OFF), or 120-130 Krox20^A molecules (ON). **(G-I)** Time-dependent probability of the different states of element A, *s* = 0, 1, 2, 3 or 4, upon the same stimulation levels as in A-C. The probability of intermediate states 1-3 is null. By increasing the input level, the probability of state 0 diminishes while the probability of state 4 increases.

Krox20 autoregulation is a bistable system that underlies a bimodal cell-fate choice

Bimodal distribution of cells that are subject to a Krox20 pulse was presented above as an experimental clue supporting the existence of a bistable mechanism. To determine whether our model predicts this bimodality effect, we plotted the time-dependent probability for a cell to express a given number of $Krox20^A$ molecules depending on the level of the stimulus (Φ_I). The simulations were performed with three Φ_I values in the same order of magnitude as those deduced from the heat shock experiments (Fig. 5B), two non-saturating (2.7 and 4.7 mol./min) and one saturating (22 mol./min) . In non-saturating conditions and at steady-state level (i.e. after 250 minutes), the mean $Krox20^A$ content of a single cell takes two values, either 0 or 120-140 (Fig. 6A-C). This is characteristic of a bimodal distribution. In saturating conditions, the low-level state disappears, as the whole population has activated A (Fig. 6C).

The model can provide single-cell trajectories underlying the collective bimodal effect, as depicted in Fig. 6D-F: cells stochastically switch from the low-level state to the high-level state upon stimulation. In some cases the establishment of the autoregulatory loop can abort (Fig. 6D, red trajectory) or even abort and reinitiate (Fig. 6E, red trajectory). At steady-state, no switch occurs from either one state to the other, indicating that the two possible states are stable in absence of input. Finally, when the level of stimulation is closed to the threshold value (Fig. 6D), cells take more time to reach the ON state. This is reminiscent to the critical slowing-down effect, a hallmark of bistable switches (Wang et al., 2009).

The cell-fate choice is made in accordance with the binding state of element A: upon increasing stimulation levels, the probability for element A to lie in state 0 (no bound Krox20) decreases while the probability to be in state 4 (four Krox20 molecules bound) increases (Fig. 6G-I). Moreover, the intermediate states of element A, s=1, 2 and 3, display a probability close to zero, even at early time-points: the element A mainly lie in two states and the transition between state 0 and state 4 is very fast, hence the bistability of element A, that correlates with the bistability of the cell-fate choice.

In conclusion, the element A binds Krox20 in a bistable manner and this is responsible for the bimodal behaviour of single cells. This molecular and cellular bistability eventually determines the cell-fate choice offered to hindbrain cells between the *krox20*-positive and the *krox20*-negative lineages.

Finally, as our model takes into account Krox20 binding on each site of element A, we sought to understand the molecular basis for the element A bistability. We have shown that the endogenous initiation pulse lasts for 80 min and produces *Krox20* molecules at a rate of 1.5 molecules per min (Supplementary Information #2). Taking into account degradation, this lead to

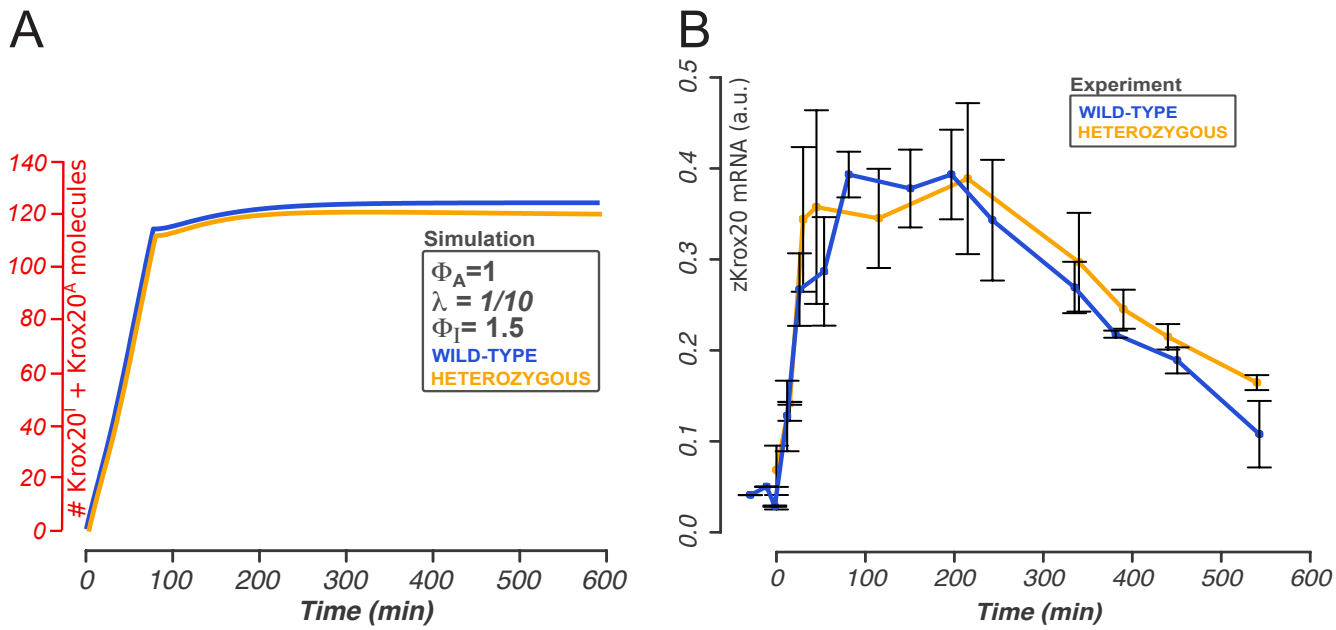

Figure 7: Robustness of the *zkrox20* profile in a heterozygous background. (A) Simulations of the timecourse of zkrox20 levels in wild-type and heterozygous embryos. **(B)** Corresponding experimental profiles. The robustness in the transcriptional response between wild-type and heterozygous is predicted by the model.

a maximal accumulation of about 100 Krox20^{I} molecules. Our fitting procedure estimated moreover the binding rate λ_3 at 1/10 min^{-1} (Supplementary Information #2). Under these conditions, our calculations show that only 6 seconds are required for one protein to bind to the fourth site (Details on the calculation in Supplementary Information #3). Given the deduced values of λ_0, λ_1 and λ_2, we find that the third site is bound in 8 sec, the second one in 25 sec and the first one in 10 minutes (Supplementary information #3). Binding to the first site is therefore the limiting step. Once this site is bound, the system very quickly moves to state s=4. Furthermore, with λ_3= 1/10 min^{-1}, we obtain μ=1/3 min^{-1}: one protein sits for 3 minutes on average on its site. Consequently, once the first site is bound, element A is almost constantly in state 4. Therefore, element A bistable behaviour is essentially based on Krox20 binding dynamics.

The *Krox20* autoregulatory loop provides robustness to the system

An autoregulatory loop can be either detrimental or favourable to the robustness of the system regarding genetic, environmental and stochastic variations (Veitia, 2003a). This depends on the ratio between the level of input and the threshold of the autoregulatory loop. Since two *krox20* alleles have been implemented in the model, we could simulate the effect of a point mutation in the coding sequence abolishing the activity of the protein. As shown in Fig. 7A, the model predicts that a mutation in one allele should not modify the kinetics nor the maximal level of accumulation of total Krox20 (Krox20^{I} + Krox20^{A}), despite that half of the protein is inactive. Indeed, we have found that heterozygous zebrafish *krox20*$^{+/-}$ embryos exhibit a time-course of *krox20* mRNA expression indistinguishable from the wild-type profile (Fig. 7B). This indicates that, in agreement with the model, the establishment of the autoregulatory loop is not significantly affected by a 2-fold decrease in *Krox20* initiation level. The basis of this effect lies in the ratio between the threshold of the loop (number of Krox20^{I} molecules required for activation in 50% of the cells) and the number of Krox20^{I} molecules provided by the initiation mechanism at its maximum. We estimate this ratio around one third: initiation provides three times more proteins than the threshold value (see Supplementary Information #4 and Fig. 10D). This appears as a rather optimal value: a higher threshold would make the activation more sensitive to variations in the initiation signal and a lower threshold might become sensitive to spurious signals. The autoregulatory loop therefore allows to buffer at least two-fold variations in the initiation signal, significantly contributing to the robustness of the system.

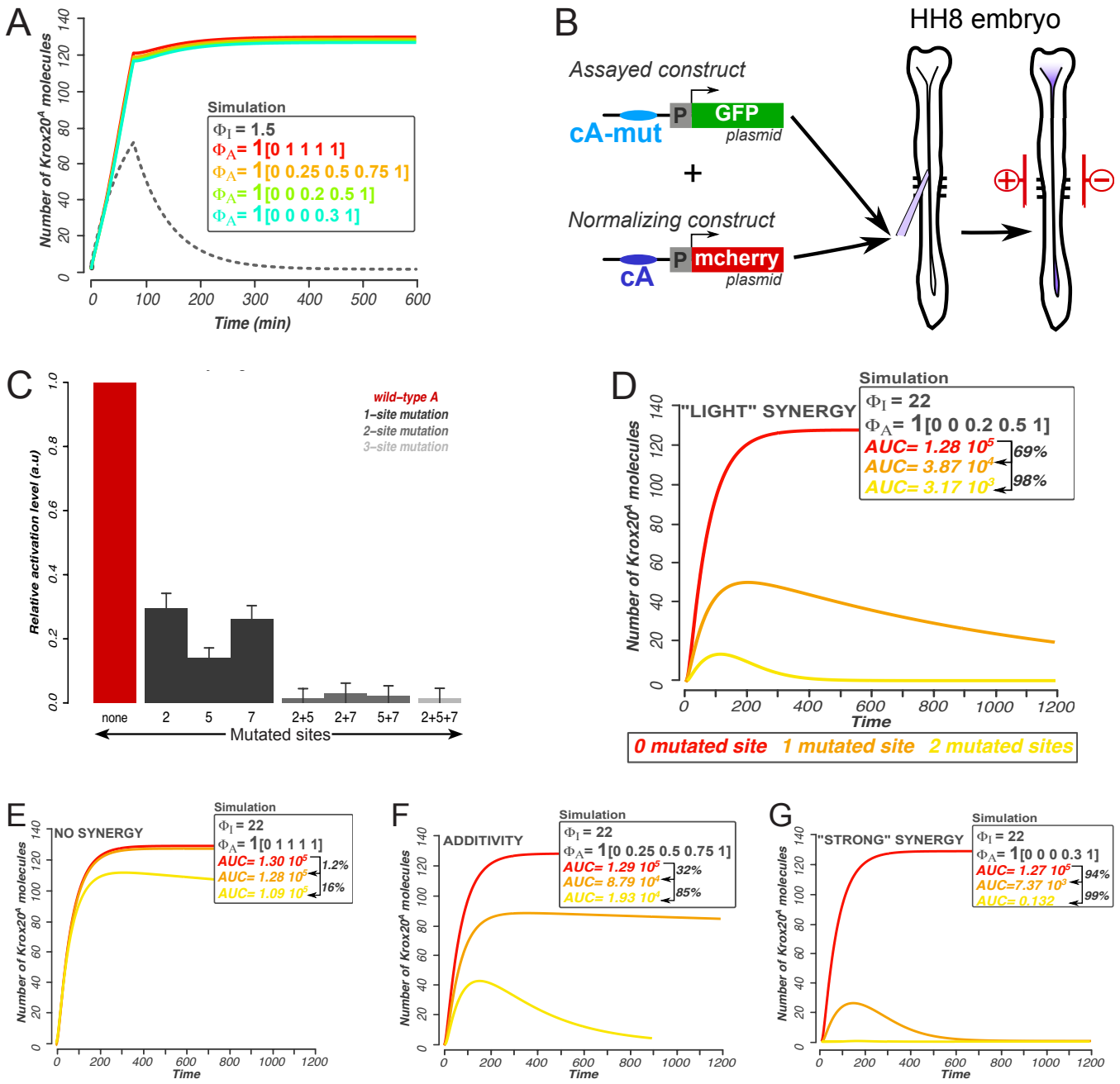

Figure 8: Concerted recruitment of the transcriptional machinery is dispensable for the bistable behaviour of element A.

(A) Simulations of the endogenous *zkrox20* time evolution with four different scenarios for the recruitment of the transcriptional machinery: no synergy (red), additivity (orange), "light" syngergy (green), "strong" synergy (turquoise). No effect can be evidenced. **(B)** Experimental design of the chick electroporation assay.Two constructs were co-electroprated, one in which a mutated element A drives *GFP*, the other in which wild-type element A drives *mcherry* expression. This system allowed to quantify the activity of mutant variants of element A in comparison with wild-type element A. **(C)** Results of the chick electroporation experiments: when one Krox20-binding site is mutated, the resulting activity, 18 hours after electroporation, is reduced by 66 to 80%. When more than one site is mutated, the activity is null. Below each bar, the number refers to the mutated site(s), as shown in figure S4. **(D-G)** Simulations of Krox20^A in situation where 0 (red), 1 (orange) or 2 (yellow) sites are mutated. All four scenarios of PolII recruitment are envisaged. The only situation that recapitulates the experimental results shown in C is the "light" synergy (D): when one site is mutated, the Area Under the Curve (AUC) from 0 to 1080 minutes is decreased by 69%.

Importance of the concerted recruitment of the transcriptional machinery

All simulations presented earlier were carried out with "light synergy" in the recruitment of the transcriptional machinery, that is $\Phi_{A,s}$=1.[0 0 0.2 0.5 1] (see Supplementary Information #2). But in a context where the intermediate states of A, s=1, 2 or 3 display very low probabilities, Φ_A essentially takes only two values: 0 in state 0 and 1 in state 4. The state-dependent recruitment of PolII would therefore have no effect on *krox20* dynamics when the element A lies in a bistable regime. To test this prediction, we simulated the endogenous *zkrox20* profile under the four representative scenarios presented earlier (no synergy, additivity, light synergy and strong synergy). All scenarios led to near-identical simulation curves (Fig. 8A), suggesting that the *krox20* bistable cell-fate choice operates independently of the concerted recruitment of the transcription machinery. However, a "light synergy" was implemented after the parameterization procedure to account for the phenotype observed when the level of *Krox20* initiation is dratiscally reduced (see Supplementary Information #2). This light synergy effect is therefore masked in control situations by the high initiation signal. It may be moreover masked by the rapid, cooperative Krox20 binding dynamics. To confirm this hypothesis, we interfered experimentally with Krox20 binding properties by mutating Krox20 binding sites in element A.

Deleterious mutations were introduced in the three Krox20 high-affinity sites, either alone or in combination. The relative activities of element A mutants were evaluated using electroporation in the chick neural tube. Two reporter plasmids were co-electroporated: a construct in which wild type or mutant element A drives *GFP* expression and a reference construct in which mcherry is driven by wild-type element A (Fig. 8B). Embryos were collected 18 h after electroporation and the levels of GFP and mcherry fluorescence in r3 and r5 were measured by confocal microscopy. The relative fluorescence level of GFP of each mutant as compared to the wild type, after normalization with the level of mcherry fluorescence, was taken as a measure of the relative activity of the mutant A element. Single mutations resulted in 66% to 80% decrease in element A activity and combined mutations of two or three sites essentially abolished element A activity (Fig. 8C). The more-than-additive contribution of the different sites is indicative of a global synergistic action, that may result from cooperative binding and/or concerted recruitment of the transcriptional machinery. To determine whether our model reproduces this global synergy, we simulated the timecourse of $Krox20^A$ profile over 18h (1080 minutes) and evaluated the area under the curve (AUC 0-1080). The AUC reflects the experimental accumulation of the stable GFP we used in the electroporation experiments. The AUC of an element A with one mutation is expected to be reduced to 66%-80% compared with the AUC of a wild-type element A. This is what is observed, with a reduction of 69% with one

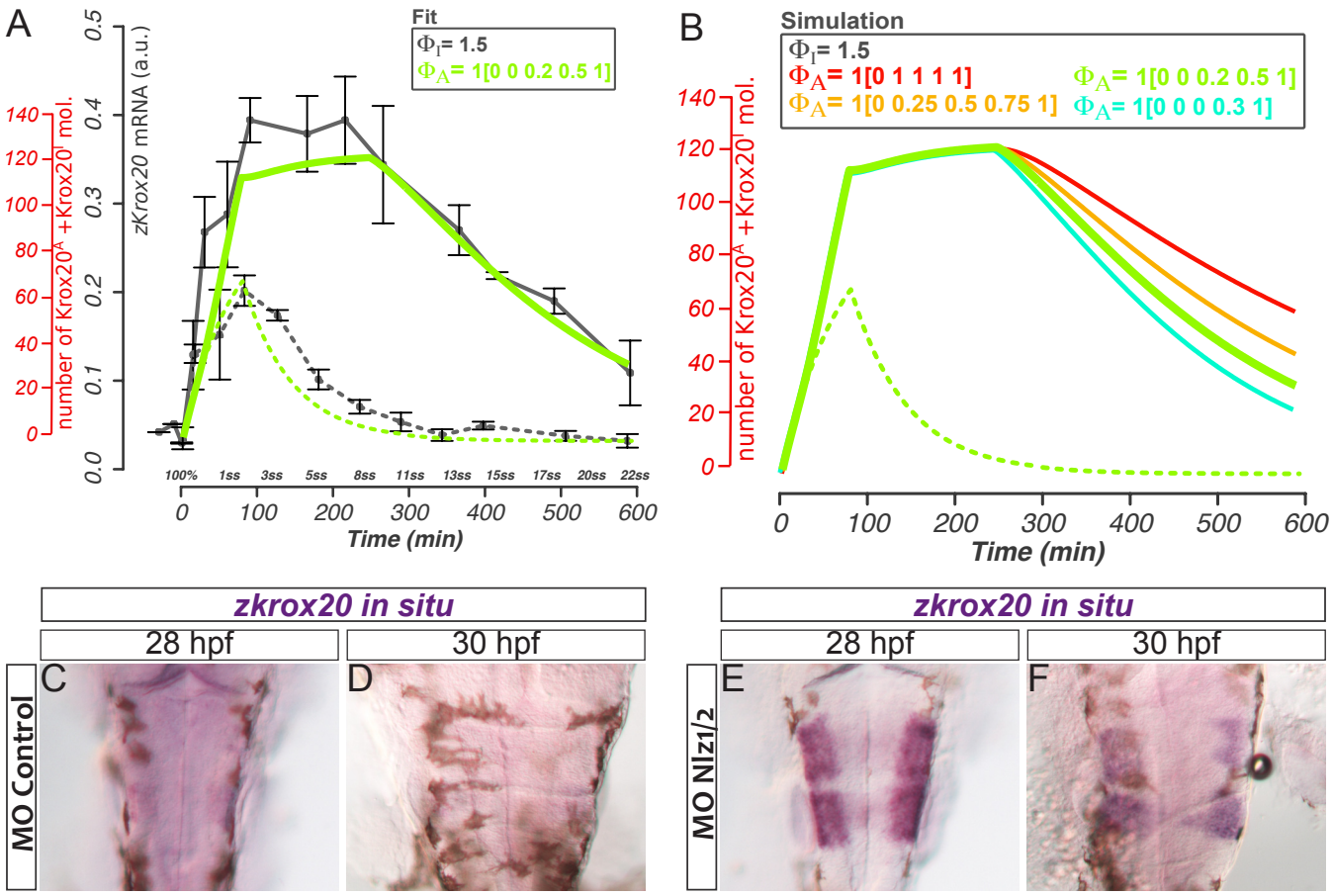

Figure 9: The decline of *Krox20* expression may result from a slowdown in binding dynamics
(A) Experimental and simulated *zkrox20* endogenous profile as shown in figure 4B, with a change of parameter at t=250 minutes. Before this timepoint, single Krox20 proteins bind to the 4 sites in 11 min, 8 sec, 25 sec and 6 sec. After 250 minutes, these durations are increased to 68 min, 46 sec, 152 sec, 37 sec. This change in parameter allows to predict the close-to-linear decrease in *zkrox20* expression. (B) In the decline phase, the output of element A is sensitive to variations in the level of synergy among Krox20 proteins when recruiting the transcriptional apparatus. Hence the variations in the slope of the decline and eventually the duration of total *zkrox20* expression. **(C-F)** *zkrox20 in situ* hybridizations in embryos injected with control morpholinos (MO) (C,D) vs nlz1/2 morpholinos (E,F). The experiment was performed at late stages, 28 and 30 hours post-fertilization (hpf), a time when *zkrox20* expression has almost completely vanished in control embryos. In nlz1/2 MO-treated embryos, the expression is still visible at 28 and 30 hpf, suggesting it has been prolonged.

mutation and of 98% with two mutations (Fig. 8D). Our model therefore reproduces properly the global synergy evidenced experimentally.

To determine the contribution of the concerted recruitment of PolII in the global synergy, we simulated the $Krox20^{A}$ time evolution under the three other scenarios envisaged: no synergy (Fig. 8E), additivity (Fig. 8F) and strong synergy (Fig. 8G). We found that the curves are severely modified by the different scenarios, suggesting that the contribution of the concerted recruitment of PolII is crucial to the global synergy evidenced experimentally. Moreover, the light synergy hypothesis is the only scenario that provides predictions for the relative amount of GFP in accordance with the experimental data. This confirms *a posteriori* the indirect parameterization procedure (Supplementary Information #2).

In conclusion, this analysis confirms that the concerted recruitment of the transcriptional machinery does exist and play a major role in the activity of element A, but that its function is masked in situations where the element A displays a bistable behaviour, i.e. when the initiation level is high and the binding dynamics highly cooperative.

Analysis of the decline in *krox20* expression during hindbrain development reveals the existence of a loop repressor

A striking discrepancy between our model and the experimental system is that *krox20* expression starts to decline with a somehow linear kinetics from 8 ss, whereas the model predicts that the autoregulatory loop should be highly stable once established. We have envisaged that this progressive loss of expression might be due to a modification of one of the parameters of the loop around 8 ss. To model this situation, we performed simulations using the "light synergy" scenario. We attempted to modify various parameters and found that only modifications of the dissociation constant of the Krox20 binding provided satisfactory results (data not shown). In Fig. 9A is presented a simulation in which λ_s conserves its original value (11 min, 8 s, 25 s, 6 s) until 250 min and then changes to 68 min, 46 s, 152 s and 36 s beyond that time (see Supplementary Information #3 for details on how these values were obtained). This simulation appropriately fits with experimental data, including the near-linear decrease beyond the 8 ss (Fig. 9A). In conclusion, we can recapitulate the entire dynamics of the *in vivo* system by the introduction of a modification in the binding characteristics of Krox20.

The modification in Krox20 binding dynamics leads to a change in the regime of autoregulation, from sustained to unsustained. We suspect the synergy in the recruitment of PolII affects the unsustained regime as the element A may not be bistable under such conditions. We simulated *Krox20* timecourse like in figure 9A under the four recruitment scenarios mentioned

above. As expected, the slope of the decline is modified according to the scenario (Fig. 9B), suggesting the actual duration of *Krox20* expression depends on the synergistical recruitment of the transcriptional machinery. This may account for the conservation of this property across evolution: it is dispensable for element A activation and plateau phases but required for the decline.

In biological terms, the change in Krox20 binding dynamics might be the result of a modification of the Krox20 protein or of element A. Recently, we have identified a transcription repressor, Nlz1, that is expressed in r3 and r5 at the right time, can bind to element A *in vivo* and antagonize the activity of the autoregulatory loop (Labalette et al., in preparation). We therefore investigated the possibility that Nlz1 and the closely related factor Nlz2 might be responsible for the decrease in *krox20* expression beyond 8 ss. Zebrafish embryos were co-injected with morpholinos directed against the two mRNAs and *krox20* expression was evaluated by *in situ* hybridization at a stage when the decrease in *krox20* expression has already occurred in control embryos (Fig. 9C,D). *krox20* expression was strongly reinforced in Nlz knock-down embryos (Fig. 9E,F). These data establish that Nlz factors participate in the repression of *krox20* expression at late stages and suggest that they might act through the autoregulatory loop, by perturbing Krox20 binding.

DISCUSSION

Our study aimed at dissecting a simple transcriptional network, the autoregulatory loop of *Krox20*, in order to describe quantitatively its contribution in r3 and r5 development. We show here that *Krox20* expression depends primarily on a pulsatile initiation phase, followed by an autoregulation phase. Autoregulation can be entirely recapitulated in mouse by the function of a 465 bp cis-regulatory sequence, the element A. Deletion of the element A from the mouse genome leads to premature *Krox20* extinction in both r3 and r5. The phenotype can be exclusively attributed to the loss of autoregulation as *Krox20* maintenance was rescued when we restored genetically a heterologous autoregulatory loop.

The output of *Krox20* network (i.e. *Krox20* expression) primarily depends on the ability of the initiation phase to activate the element A and the ability of element A to sustain its own activity. To understand the molecular basis of these two properties as well as their inter-dependence, we employed a computational approach fuelled by (i) measurements of the network responses in developing zebrafish embryos, (ii) captures of its time evolution and (iii) a detailed description of the underlying molecular events. This is, to our knowledge, the first study of this type conducted in vertebrates.

Major teachings of the model

Upon activation, the element A switches quickly and irreversibly from the OFF state (no protein bound) to the ON state (four proteins bound). Both states are stable and the switch is therefore bistable. This property is based on the strong binding cooperativity between Krox20 proteins: the first site is bound within 11 minutes, whereas the three others need less than 25 seconds. As this effect was observed *in vitro*, in a chromatin-free environment, the underlying mechanism must imply direct protein-protein interactions. Krox20 proteins may be assembled in dimers or higher-order complexes, but direct evidence is still missing.

Bistability of the element A underlies the bistable behaviour of single cells that can be either in the low state (no *Krox20* expressed) or the high state (maximal expression of *Krox20*). Cells therefore integrate the initiation signal and commit stochastically into one of the two possible fates: *Krox20*-positive or *Krox20*-negative. At the population level this stochastic choice turns into a bimodal distribution. The element A thus filters out low initiation signals and ensures all cells commit to a well-defined fate. It acts by pulling apart the two steady states and establishes a clear demarcation (bifurcation) between them. In this way, the element A determines the number of cells allocated to the *Krox20* lineage and plays a major role in hindbrain patterning.

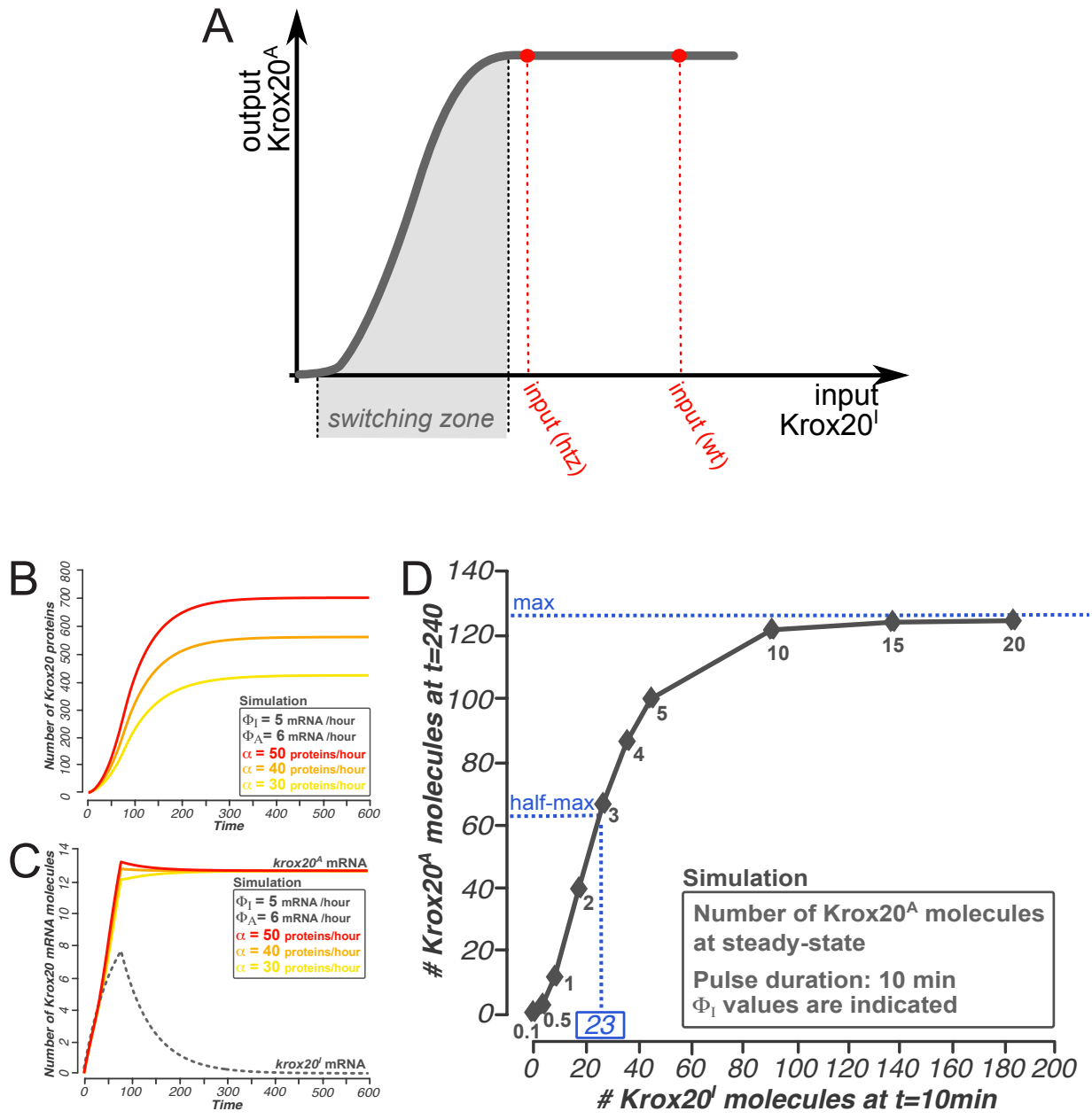

Figure 10: Intrinsic characteristic of the element A-based switch: high input, low threshold.
(A) Theoretical representation of the *Krox20* input/output relationship at equilibrium. We infer the input level of wild-type embryos lies far from the switching zone, hence the robustness of the transcriptional response. In contrast, the response is expected to be more affected by variations in the input level in a heterozygous background. **(B,C)** Simulations of the number of Krox20 proteins (B) and *Krox20* mRNA molecules (C) in a model where both species were implemented. Simulations were performed with different translation rates. The translation rate essentially impacts on the number of proteins at equilibrium but neither on the mRNA number nor its dynamics. **(D)** Simulated *Krox20* input/output relationship at equilibrium. This representation allows to monitor the steady-state maximal number of molecules in *Krox20*-positive cells: 125 under our simplified modelling conditions. Half of this maximum is reached with only 23 Krox20^{I} molecules produced by the initiation phase. This value is the simulated threshold of *Krox20* autoregulatory loop.

As a corollary, *Krox20* autoregulatory loop is a source of robustness. This is best evidenced when simulating the behaviour of heterozygous embryos where *krox20* expression cannot be distinguished from the wild-type curve, as expected from the simulations. This robustness is in contrast with the proposed link between sigmoidal transcriptional responses (i.e. switches) and haploinsufficiency (Veitia, 2003b; 2003a). Haploinsufficiency is defined for a diploid locus as a dominant abnormal phenotype resulting from the loss of the activity of one allele. It may be caused by switches when the level of input is close to the switching zone. The robustness of the *Krox20* network is explained by the fact that the wild-type input level is much further away from the switching zone (Fig. 10A). This also explains why we observe only 10% fluctuations in the rhombomere size of wild-type embryos: the area corresponding to r3 was evaluated at 51.2±5.6 (a.u.) and the r5 area at 59.6±6.0 (a.u.)(mean±sd). Hence, although the state transition at the level of element A and the cellular level are intrinsically stochastic, the final number of *Krox20*-expressing cells is robust: the stochastic regime at the molecular level shifts to a deterministic regime at the population level. This shift is controlled by a high level of initiation. However, more than two-fold reduction of the initiation level leads to smaller rhombomeres (see Supplementary Fig. S7), suggesting that the control of *Krox20*-positive cells is back in a stochastic regime. We showed earlier that *Krox20* initiation level is primarily affected by the level of Fgf signalling (Labalette et al., 2011). In this study, we used the FGFR inhibitor SU5402 to diminish the initiation level. In wild-type embryos, Fgf signalling may therefore act as a pre-patterning factor that ensures maximal switching in cells that initiate *Krox20*, and promotes the robustness of the whole network.

Our model predicts that *Krox20* autoregulatory loop self-sustains. Yet from the 8-somite stage (250 minutes after stimulation), *Krox20* levels decrease in a close-to-linear manner until 25 ss when the expression turns off completely. This slow decline of *Krox20* expression suggests that the promoter is never abruptly shut off. Rather, around 8 ss, the number of new Krox20 proteins produced becomes too low to maintain the loop. This behaviour is not predicted by the model without introducing a change of parameter at 8 ss. We found that a reduction in the binding dynamics is sufficient to reproduce the decline. This reduction may be provoked by the presence of Nlz1 that somehow prevent Krox20 from binding properly to its sites. We are currently investigating the mechanism of this inhibition.

Interestingly, the slope of the decline depends on the level of synergy among Krox20 proteins when recruiting the transcriptional machinery. This mechanism therefore controls the timepoint when *Krox20* expression is completely turned off.

Number of molecules involved in the switch: the minimal hypothesis.

If the element A functions as a bistable switch, what is its threshold, maximal value and steepness? To address these questions, we need to get access to the number of Krox20 proteins produced by the system. This number could neither be determined experimentally with a sufficient accuracy, nor be derived from our simulations because no translation rate was implemented in the simplified version of the model that we present here. By assuming the number of mRNA equals the number of proteins, our simulations underestimate the number of proteins. To verify that the system dynamics is however unaffected, we built a more complex model where stochastic mRNA dynamics determines the mean behaviour of Krox20 proteins, through the translation rate α. (Supplementary Fig. 3A). This model predicts that α modifies the steady-state number of proteins but not the mRNA dynamics (Fig. 10B,C). This suggests that the number of proteins predicted by our model, that is 60 upon initiation and 120 at steady-state (Fig. 9A), corresponds to a minimal hypothesis: *krox20* autoregulatory loop is able to function with 60 proteins and no more than 120 proteins at steady-state. These low-estimate numbers may actually reflect the number of Krox20 proteins available for *krox20* autoregulation, i.e. once all others are buffered by their other DNA targets in the genome.

Under this hypothesis, we can define a threshold value for the element A-based switch. We failed to derive an analytical formula for the steady-state level of $Krox20^{A}$ as a function of $Krox20^{I}$ (see addendum) but an apparent threshold value can be estimated by simulation (Fig. 10D): the threshold is reached with a minimum of 23 proteins of Krox20. This low value confirms that the loop can function in a stochastic regime and justifies *a posteriori* our choice of a Markov formulation. Moreover, it suggests that the loop is very sensitive to the number of Krox20 proteins, hence the non-sigmoidal input/output relationship shown in figure 5D: the low plateau of the sigmoid seems absent because the loop is triggered from very low input values. We believe finally that the high sensitivity of A counteracts a low element A-dependent production rate Φ_A (modelled as 1 molecule per minute) such that the loop is sustainable.

Conclusions

In this study, we unravelled a simple transcriptional network consisting of the element A and a single activating species, Krox20. We studied the network response using a computational model that describes the full stochastic behaviour of the system at both the population and the cell levels. For parameterization and validation, the model was confronted with quantitative data obtained in a vertebrate system, that is zebrafish embryos.

Two major variables determine the network response: the initial load of Krox20 protein and the binding events occurring on the element A. We show that the latter provides a solid basis for a molecular bistable switch that is propagated at the cell level and defines a choice between two distinct fates. Robust commitment to the *Krox20*-positive fate requires in addition that the level of *Krox20* initiation is largely higher than the element A activation threshold. Our predictions suggested on the one hand that the threshold of element A lies around one third of the endogenous initiation level (Supplementary Information #4). This position appears ideal so that the activation of element A is robust to fluctuations of initiation levels but does not respond to parasite signals. On the other hand, *Krox20* initiation level is high thanks to high Fgf signalling. Our model therefore predicts that the element A-based bistable switch and the high Fgf-dependent initiation both control the specification of the *Krox20*-positive fate.

Finally, the modelling approach allowed to make predictions, notably on the decline of *Krox20* expression. This prediction postulated a change of parameter in Krox20 binding dynamics. In parallel, we identified the transcription factor Nlz1 as an inhibitor of the autoregulation. The model prediction therefore suggests that Nlz1 could alter the binding efficiency of Krox20 on element A. Experiments currently in progress in our laboratory are exploring this hypothesis.

ADDENDUM

To reproduce faithfully the behaviour of the *Krox20* transcriptional network, the model had to capture the full time evolution of the system. This was achieved through the use of a Markov chain formulation that allows to model the very early steps of the stochastic activation of element A, when the number of molecules is low. With this type of formulation, the number of possible states for the element A, the complex binding/unbinding cooperative behaviour, and the pulsatile initiation phase make an analyticapproach almost impossible. For instance, in steady-state analyses reported in the literature, the final steady-state usually does not depend on the initial condition, that is the initiation strength and duration. This is the reason why we could not conduct bifurcation, parameter sensitivity or phase-plane analyses. We tried to modify the shape of the model by finding approximations but all attempts of simplifications affected the dynamics. We therefore decided to focus on numerical simulations.

The numerical analysis was also rendered complex by the large parameter space. In this study, we decided to proceed with direct and indirect parameterization strategies. Those strategies have proved successful in finding a solution. Instead of indirect parameterization, we envisaged an unbiased parameterization procedure. This consists of screening systematically the parameter space (Φ_I, Φ_A, λ_3): for every solution, a simulation curve is produced and confronted with experimental data according to pre-determined criteria, similar to the one we used in this study (the two fold-ratio, the robustness upon SU5402 treatments, etc.). A distance between the simulation and the experimental data is calculated using the least-square method, or the absolute value method. The best parameter solution corresponds to the minimum distance value. Several algorithms are available to "smartly" screen the parameter space: Monte-Carlo, grid-search, etc. This so-called inverse problem (i.e. proceeding from the simulations to the parameters) was judged inappropriate in our case given the time required for each simulation.

– Chapter 2 –

Supplementary information

Additional Information #1: Direct Parameterization

Degradation rates

hsp:mKrox20$_{HA}$ embryos were heat-shocked for 10 minutes at 38°C and the amounts of *mKrox20* mRNA and protein were measured every hour by RT-qPCR and semi-quantitative western-blotting respectively. Exponential fitting of the resulting curves revealed mRNA and protein half-lives of 63 min and 65 min respectively (data not shown).

Number of Krox20 binding sites

In silico analysis of the 465-bp chick element A revealed six putative Krox20 binding sites, labelled K2 to K7 (Chomette et al., 2006, Fig. S4A. The K1 site identified in the initial *in silico* studies was considered too distant to possibly bind Krox20 in the present work. This was indeed confirmed experimentally). Electromobility shift assays (EMSA) indicated that three of the putative sites (K2, K5 and K7) were of high affinity and one (K6) was of medium affinity (Fig. S5). The last two sequences (K3, K4) did not bind *Krox20 in vitro* and were neglected in the construction of the model.

Binding/unbinding rates and cooperativity

In vitro binding of Krox20 on element A was assessed by EMSA in saturation experiments where a fixed concentration of DNA is confronted with increasing doses of proteins. The steady-state fraction of bound DNA is shown in Fig. S4B (red curve). The curve was fitted with a Hill function of the form $y = \frac{x^n}{IC50^n + x^n}$, where *IC50* is the amount of protein necessary to reach half-maximal binding (also referred to as *threshold*) and *n* represents the steepness of the curve at the inflexion point (also known as *Hill coefficient*). The fitting procedure provided a Hill coefficient of 4.36, consistent with cooperative binding involving four sites (Fig. S4C). To confirm this cooperativity effect, similar experiments were performed on mutant elements containing point mutations in site 2 or 5. In both cases, the Hill coefficient decreased to 3.2-3.3 (Fig. S4D,E), as expected for a three-site binding configuration. Finally, a two-site mutation led to a saturation curve of steepness n=1.80 (Fig. S4F). These results show that Krox20 binding is cooperative *in vitro*.

To implement these results into our parameters $\lambda_s=[\lambda_0, \lambda_1, \lambda_2, \lambda_3, 0]$ and $\mu_s=[0, \mu_1, \mu_2, \mu_3, \mu_4]$, we started by considering that all cooperativity was derived from binding and not from unbinding, such that $\mu_s=[0, \mu, \mu, \mu, \mu]$. To derive the five remaining parameters, we fitted the

EMSA experimental results to the calculated steady-state fractions of bound DNA. The analytical formula of this steady-state fraction r is :

$$r = \frac{\hat{K}^4 + \hat{K}^3\gamma_4 + \hat{K}^2\gamma_4\gamma_3 + \hat{K}\gamma_4\gamma_3\gamma_2}{\hat{K}^4 + \hat{K}^3\gamma_4 + \hat{K}^2\gamma_4\gamma_3 + \hat{K}^1\gamma_4\gamma_3\gamma_2 + \gamma_1\gamma_2\gamma_3\gamma_4}$$

where $\hat{K}$ is the Krox20 over DNA concentration ratio, and γ_s are the ratios of the unbinding to binding rates ($\gamma_s = \frac{\mu_{s+1}}{\lambda_s}, 0 \le s \le 3$). The fitting of r with the experimental data is shown in Fig. S4G. Because we are at steady state, we could only derive the state-dependent ratio γ_s and not individual values for λ and μ. We found γ_s=[γ_0, γ_1, γ_2, γ_3]=[378, 4.3, 14.1, 3.3]. With these four values, only one degree of freedom remains in Krox20 binding dynamics. We chose λ_3 as the last parameter to fit. The expression of the binding parameters as a function of λ_3 are as follow: $\mu=\gamma_3\lambda_3$, $\lambda_2=\gamma_3\lambda_3/\gamma_2$, $\lambda_1=\gamma_3\lambda_3/\gamma_1$, $\lambda_0=\gamma_3\lambda_3/\gamma_0$.

Additional Information #2: Indirect Parameterization

Indirect parameterization of the model was employed for Φ_I, $\Phi_{A,s}$ and λ_3 by requiring consistency with experimental profiles. To simplify this step, only four representative scenarios will be considered for the concerted recruitment of the transcriptional machinery:

- No synergy: one molecule bound is sufficient to trigger maximal recruitment of the transcriptional machinery; $\Phi_{A,s}=\Phi_A[0\ 1\ 1\ 1\ 1]$
- Additivity: Krox20 proteins cooperate in recruiting the PolII machinery in an additive manner; $\Phi_{A,s}=\Phi_A[0\ 0.25\ 0.5\ 0.75\ 1]$
- "Light" synergy between bound Krox20 proteins: $\Phi_{A,s}=\Phi_A[0\ 0\ 0.2\ 0.5\ 1]$
- "Strong" synergy: $\Phi_{A,s}=\Phi_A[0\ 0\ 0\ 0.3\ 1]$

For each of these scenarios, a range of biologically-significant values for Φ_I, Φ_A and λ_3 was used to perform numerical simulations.

Binding rate λ_3

Simulations were first confronted with the *zkrox20* endogenous mRNA profiles shown in Supplementary Fig. S6A. All four scenarios described above for $\Phi_{A,s}$ provided strictly identical simulations. The reason for this will be clarified below. In this part, we show simulations performed under the "no synergy" condition: $\Phi_{A,s}=\Phi_A[0\ 1\ 1\ 1\ 1]$.

$Krox20^I$ (red dashed curve in Fig. S6A) corresponds to the initiation profile, in absence of autoregulatory loop: the pulse lasts for 80 minutes (T_I), but its height does not allow to determine the input value Φ_I, since the correspondence between the experimental *zkrox20* levels measured by RT-qPCR and the number of $Krox20^I$ molecules provided by the model is unknown. Φ_I value is however constrained by the $Krox20^A$+$Krox20^I$ profile (Supplementary Fig. S6A, grey curve). The ratio between the $Krox20^I$ and the $Krox20^A$+$Krox20^I$ curves maxima approximates 2. We used this ratio as a conservative criterion for the following fitting procedure. For fixed values of Φ_A and Φ_I, 1 and 1.5 respectively for example, as shown in Supplementary Fig. S6B, the system displays two distinct behaviours:

1) when $\lambda \geq 1/10$ (green curves), the maximal steady-state value of *zkrox20* saturates at a level independent of λ_3, but determined by the degradation rate (not shown).

2) when $\lambda < 1/10$ (blue curve), a steady-state is also reached but the level is lower, and determined by the λ value.

Therefore, the 2-fold conservative condition can be met in two ways, either when the steady-state level of *zkrox20* is capped by the degradation rate (Fig. Supplementary S6B) or by the value of λ

(Fig. S6C). The second possibility has two direct implications. First, the steady-state level depends on the input level: increasing Φ_I affects the maximal number of Krox20 proteins (Supplementary Fig. S6D). This situation is in disagreement with the experiments: beyond a certain point, the maximal level of *zkrox20* is merely modified when additional Krox20 is provided by the *hsp:mKrox20*$_{HA}$ system (data not shown). Second implication, the probability to activate A lies below the max value of 1 (blue curve in Supplementary Fig. S6E), suggesting that only part of the cells that initiate *zkrox20* do eventually autoregulate. This is also in contradiction with experimental observations since, in a wild-type embryo, 100% of the cells in r3 and r5 stably express *krox20*, in an autoregulatory loop dependent manner. These two arguments rule out the second behaviour. In conclusion, the conservative criterion of a two-fold difference between Krox20^I and Krox20^A+Krox20^I is satisfied provided the ratio Φ_I/Φ_A=1.5 and $\lambda \geq 1/10$. Three possibilities are depicted in Fig. S6F-H depending on the individual values for Φ_I and Φ_A, and independent of the scenario chosen for the concerted recruitment of the transcriptional apparatus. Higher values of Φ_I and Φ_A may be envisaged but subsequent fitting procedure will show that discrimination among these three possibilities is sufficient.

Production rates Φ_I and Φ_A

To finally set the values of Φ_I, Φ_A and λ, we challenged the element A response to severe reductions of the input level. Experimentally, this can be performed in zebrafish embryos by inhibiting FGF signalling upon treatment with SU5402 (Labalette et al., 2011). We can estimate the reduction in the level of *krox20* initiation by measuring *krox20* mRNA by RT-qPCR in *zkrox20*$^{-/-}$ embryos. The consequences on the activation of the autoregulatory loop can be estimated by measuring the size of r3 + r5 in wild-type embryos, reflecting the number of cells that have successfully activated the loop (Supplementary Fig. S7A-G). In this respect the relative size of the r3 + r5 is equivalent in our model to the probability of element A activation. In addition, the initiation level can be tuned by the duration of SU5402 treatment (Supplementary Fig. S7E,G). A short treatment, from 80% epiboly to 1 ss, reduced the initiation level to 35% and the mean number of *Krox20*-positive cells to 59% (Fig. S7E,F). A longer treatment, from 50% epiboly to 1 ss, led to reductions of the initiation level to 27% and of the mean number of *Krox20*-positive cells to 51% (Fig. S7G,H).

To discriminate among the three possibilities shown in figure S6F-H, we predicted the effect of a decrease in initiation level to 35% and 27% on the probability to activate A. Simulations were performed under the "no synergy" hypothesis ($\Phi_{A,s}=\Phi_A$[0 1 1 1 1]). The simulation closest to the experimental results is provided by Φ_A=1 and Φ_I=1.5 (Fig. S7I). The other two possibilities

display too much robustness as the probability to activate A is merely affected by the change in initiation level (Fig. S7J,K). Hence, values of Φ_A higher than 2 can be ruled out. Excessive robustness is also found when λ>1/10 (Fig. S7L). Φ_A= 1, Φ_I= 1.5 and λ=1/10 therefore provide the closest fit to experimental data. However, the steady-state probabilities depicted in Fig. S7I are higher than expected experimentally. We reasoned that this is due to the "no synergy" hypothesis made concerning the recruitment of PolII. We thus simulated the probability to activate A as in figure S7I under the "additivity", the "light synergy" and the "high synergy" hypotheses, as described above. We found that the "light synergy" condition provides simulations closest to the experimental results (Fig. S7M).

In conclusion, the indirect parameterization procedure based on the robustness of the loop upon fluctuations of initiation levels allowed to fit the following parameters: Φ_A= 1.[0 0 0.2 0.5 1], Φ_I= 1.5 and λ=1/10.

Additional Information #3: Binding Dynamics

λ_s values

By fitting the EMSA experiments presented in Supplementary Fig. S4, we found $\gamma_s = [368, 4.3, 14.1, 3.3]$.

Since $\gamma_s = \frac{\mu_{s+1}}{\lambda_s}$ and $\mu_{s+1} = \mu_s = \mu$, we get $\lambda_s = \frac{\mu}{\gamma_s} = \mu.\left[\frac{1}{378}, \frac{1}{4.3}, \frac{1}{14.1}, \frac{1}{3.3}, 0\right]$.

We fitted $\mu = \frac{1}{3}$, we get $\lambda_s = \left[\frac{1}{1134}, \frac{1}{12.9}, \frac{1}{42.3}, \frac{1}{10}, 0\right]$.

With one molecule in the system, there is one binding event every 1134 minutes (almost 19 hours) on the first site. With 100 molecules in the system, $\frac{100}{1134} = 0.088\,\text{min}^{-1} = 5.29\,hour^{-1}$, 0.106 binding per minute, that is 6.35 per hour. In other words, the first site is bound within $\frac{1}{0.088} = 11.3$ minutes. The same reasoning with sites 2, 3 and 4 gives respectively 7.7 sec, 25.4 sec, 6 sec. These three values are negligible regarding the time required to bind the first site. They can be considered as equal, as the variations between them most probably results from experimental uncertainty.

λ_s values used for the *Krox20* decline phase

We postulated that the Krox20 decline is due to an overall slowdown of the binding dynamics. To simulate this slowdown, we chose $\mu = \frac{1}{18}$ instead of $\mu = \frac{1}{3}$. Following the same reasoning as in the preceding part, we obtain : λ_0= 68 min, λ_1= 46.4 sec, λ_2= 152.3 sec, λ_3= 35.6 sec. The non-proportional change among the λ_s values results from the inverse function that relates λ and μ.

Additional Information #4: Ratio Initiation / Threshold of A

We show in figure 10D that the minimal value of element A threshold is 23 proteins. This value corresponds approximately to one sixth of the maximal, steady-state level. We know moreover that the maximal initiation level corresponds to the half of the steady-state level (Fig. 2N). Based on these two results, we estimate that the maximal initiation level is three times higher than the threshold of element A. In other words, *Krox20* initiation processes provide 3 times more proteins than what is required to have 50% probability to activate A.

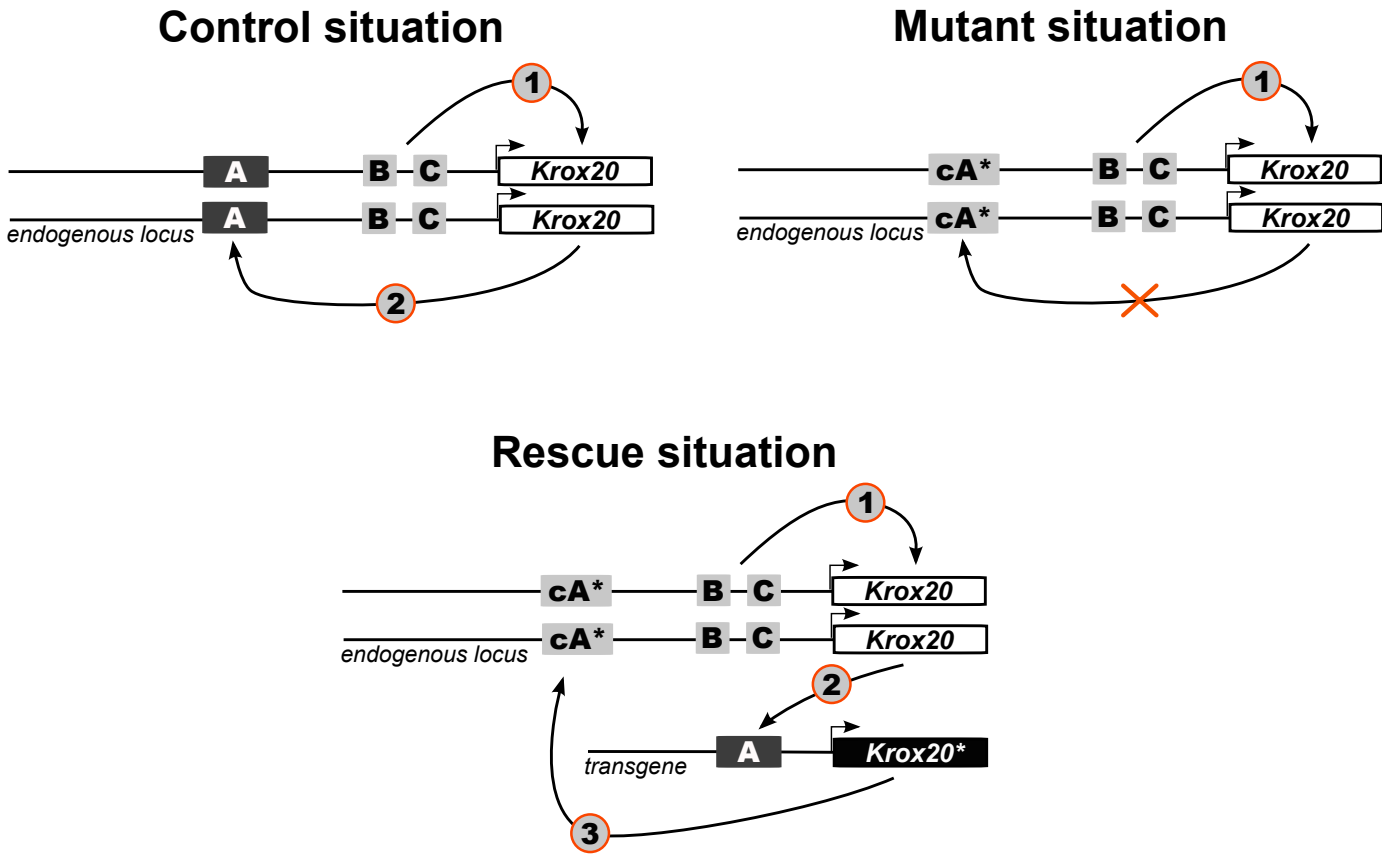

Figure S1: *Krox20* cis-regulation in the control, Krox20{A*}$^{-/-}$ and A:Krox20*;Krox20{A*}$^{-/-}$ situations. In the control situation, *Krox20* expression follows two phases: initiation (1) and autoregulation (2). In the Krox20{A*}$^{-/-}$ mutant, the autoregulation phase is abolished because the element A was replaced by the non-functional A* variant. This mutant situation may be rescued by providing cells with a transgene that express *Krox20** in r3 and r5. In such context, *Krox20* is properly initiated; it activates the exogenous element A driving expression of *Krox20**; Krox20* in turn activates A* on the endogenous locus. In this system, a novel, indirect autoregulatory loop, is set up.

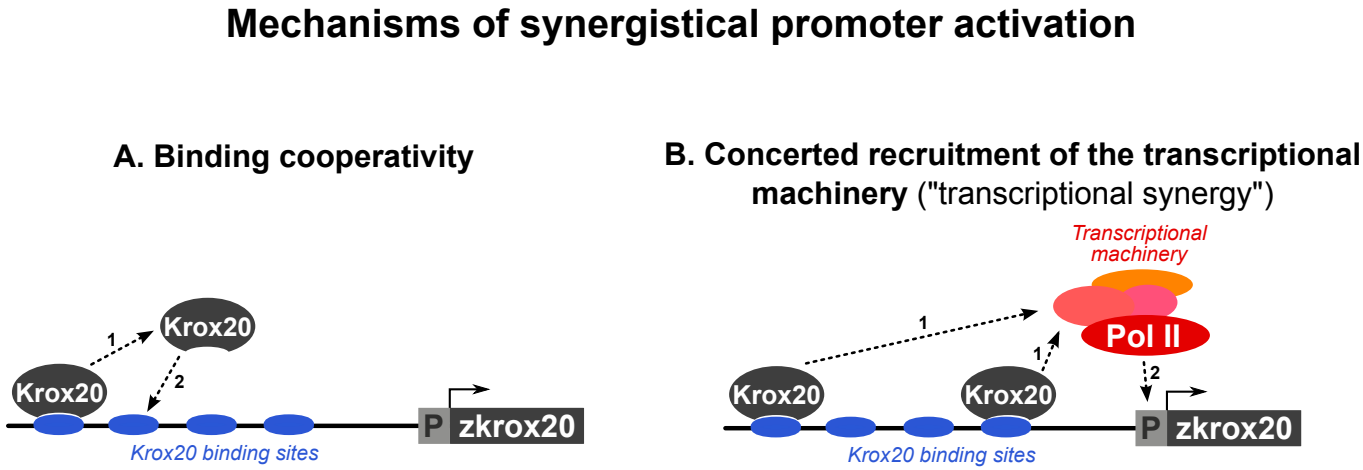

Figure S2: Mechanisms of synergistical promoter activation.
Synergy is defined here between molecular events that are collectively able to increase the rate of promoter activation in a more-than-additive manner. **(A)** One category of events is Krox20 binding on element A. Binding of the first Krox20 molecule may indirectly increase the binding rate of a second molecule. Eventually, this binding cooperativity among Krox20 proteins allows to reach the state of maximal recruitment of PolII faster than without cooperativity. Mechanisms underlying binding cooperativity may be protein-protein interactions, chromatin remodelling, site unmasking (see Vashee *et al.*, 1998). **(B)** Another mechanism that influences the rate of promoter activation is the recruitment of the transcriptional machinery, including PolII. Once bound on element A, two Krox20 proteins may recruit PolII with a rate augmented more than two-fold in comparison with one single protein. Some authors refer to this mechanism as “transcriptional synergy“. We prefer in this study to use the phrase “concerted recruitment of the transcriptional machinery“.

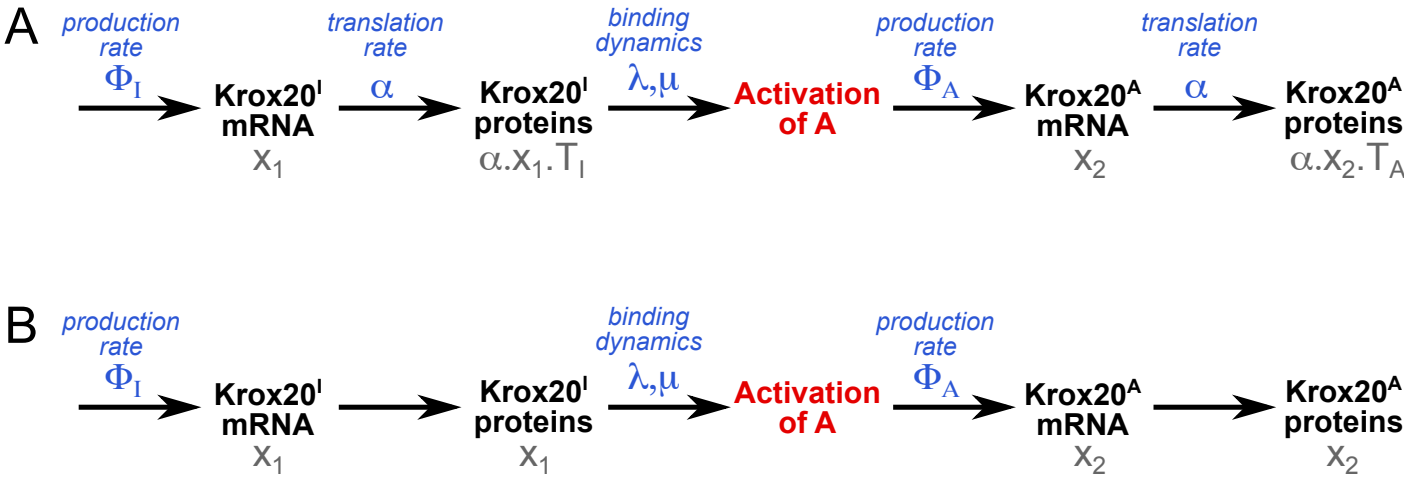

Figure S3: A simplified model of *Krox20* expression.
(A) *Krox20* expression flow, from its production into mRNA to the activation of A and the production of Krox20^A proteins. Theoretical numbers of mRNA and protein molecules are indicated in grey, assuming the translation rate α is linear and T_I, T_A are the durations of the initiation and autoregulation phases respectively. **(B)** The model presented in this study is a simplified version of *Krox20* expression: the number of proteins produced is set as being equivalent to the number of mRNA molecules. We argue that this simplification does not impact on the dynamics of the system.

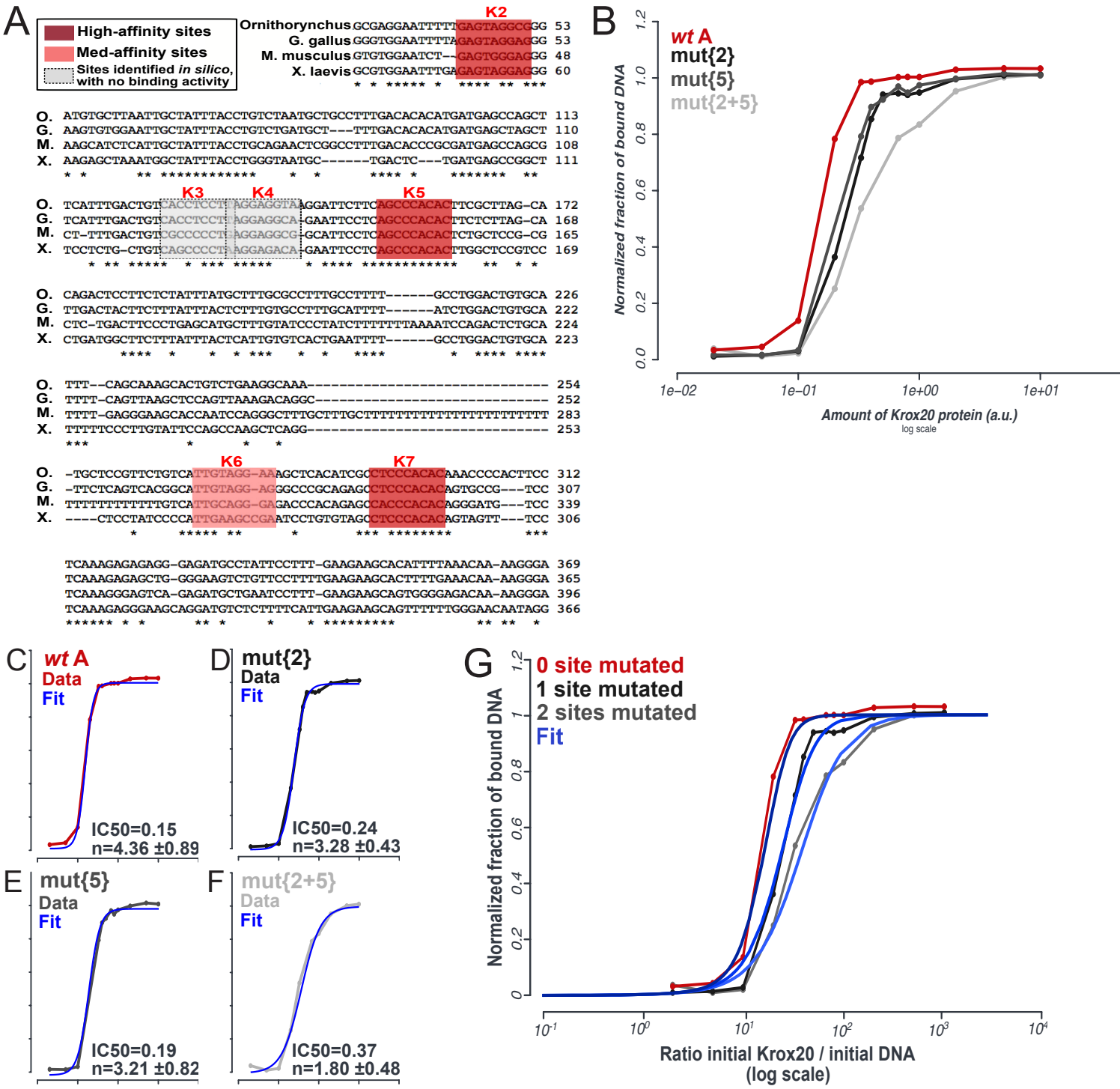

Figure S4: Krox20 activates the element A in a cooperative and synergistic manner
(A) Alignment of the element A sequences taken from diverse vertebrate genomes. Stars indicate conserved nucleotides. The zebrafish sequence is missing because it could not be identified by homology. Krox20-binding sites are highligthed in red. **(B)** Saturation binding curves obtained by EMSA experiments: a fixed quantity of element A was placed in presence of increasing doses of Krox20 protein. The resulting fraction of bound DNA is plotted on the y axis. This experiment was performed on wild-type element A (red) and mutant variants carrying either 1 mutated Krox20 site (dark grey) or 2 mutated sites (light grey). **(C-F)** The single curves shown in B were fitted with a Hill function in order to derive their threshold (IC50) and steepness (Hill coefficient, n): the threshold increases with the number of mutated sites, while the steepnes decreases. This means that Krox20 binding on element A is cooperative. **(G)** By deriving an analytical formula of the saturation curves from our model, we could fit them and therefore determine the binding and unbinding parameters. However, as EMSA experiments are performed at steady-state, one degree of freedom remains, i.e. one parameter value is still to be fitted.

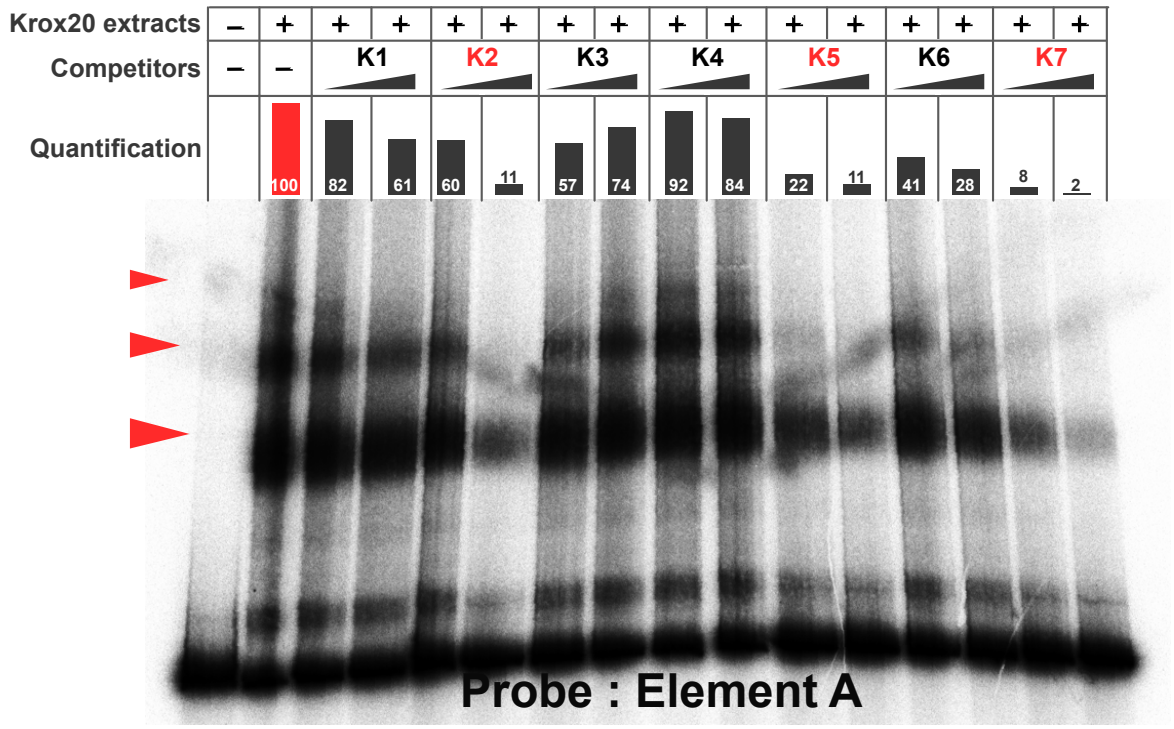

Figure S5: *Krox20* element A carries three high- and one medium-affinity sites
EMSA experiment: full element A was used as radiolabelled DNA probe (25 nM) and confronted to a fixed amount of Krox20 extracts. Three binding complexes are apparent in this configuration (lane 2), suggesting that the element A carries at least three sites. To assess the binding affinity of each site identified in figure S4A, non-radiolabelled double-stranded oligonucleotides containing the sequence of each site were used as competitors. The low concentration was 25 nM and the high concentration 100 nM. Sites 2, 5 and 7 severely affect the binding of Krox20 on element A while site 6 competes to a lesser extent.The three former were therefore considered as high-affinity and site 6 as a medium-affinity site.

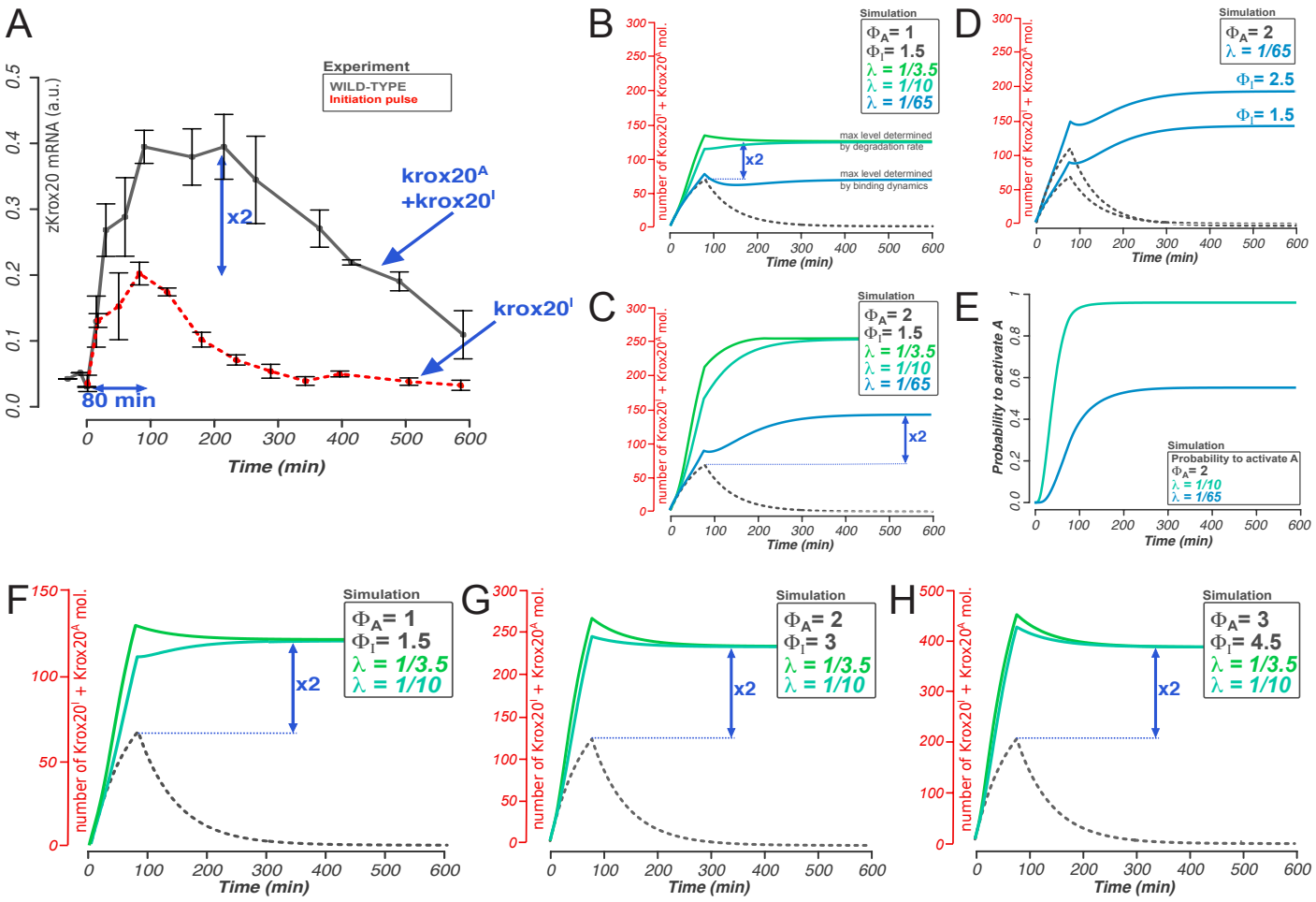

Figure S6: Parameter fitting, approach #1: the endogenous *zkrox20* profile.
(A) The experimental *zkrox20* profile reveals that (i) the initiation pulse lasts for 80 min, (ii) there is a two-fold difference between the initiation and the *zkrox20* mRNA maxima. This two-fold difference was used as a conservative criterion to fit the simulations with the 250 first minutes of the experimental profile. **(B,C)** Simulation of *zkrox20* profile with fixed values of Φ_I, Φ_A and three values of the binding rate λ (actually λ_3). The two-fold criterion is satisfied in B when $\lambda \geq 1/10$ and in C with $\lambda = 1/65$ and a higher Φ_A. In the latter situation, the steady-state number of *zkrox20* molecules varies according to the value of λ (contrary to the situation in B). **(D,E)** The scenario depicted in C implies that: (i) the steady-state number of *zkrox20* molecules increases with the level of input Φ_I (simulated in D), (ii) the probability to activate A lies around 50% (simulated in E, blue curve). **(F-H)** The scenario of figure B may comes in an ifinite number of ways, depending on the values chosen for Φ_I and Φ_A. We found however that the ratio Φ_I/Φ_A must be close to 1.5. Three examples are illustrated. All simulations performed in this figure used the condition $\Phi_{A,s} = \Phi_A[0\ 1\ 1\ 1\ 1]$.

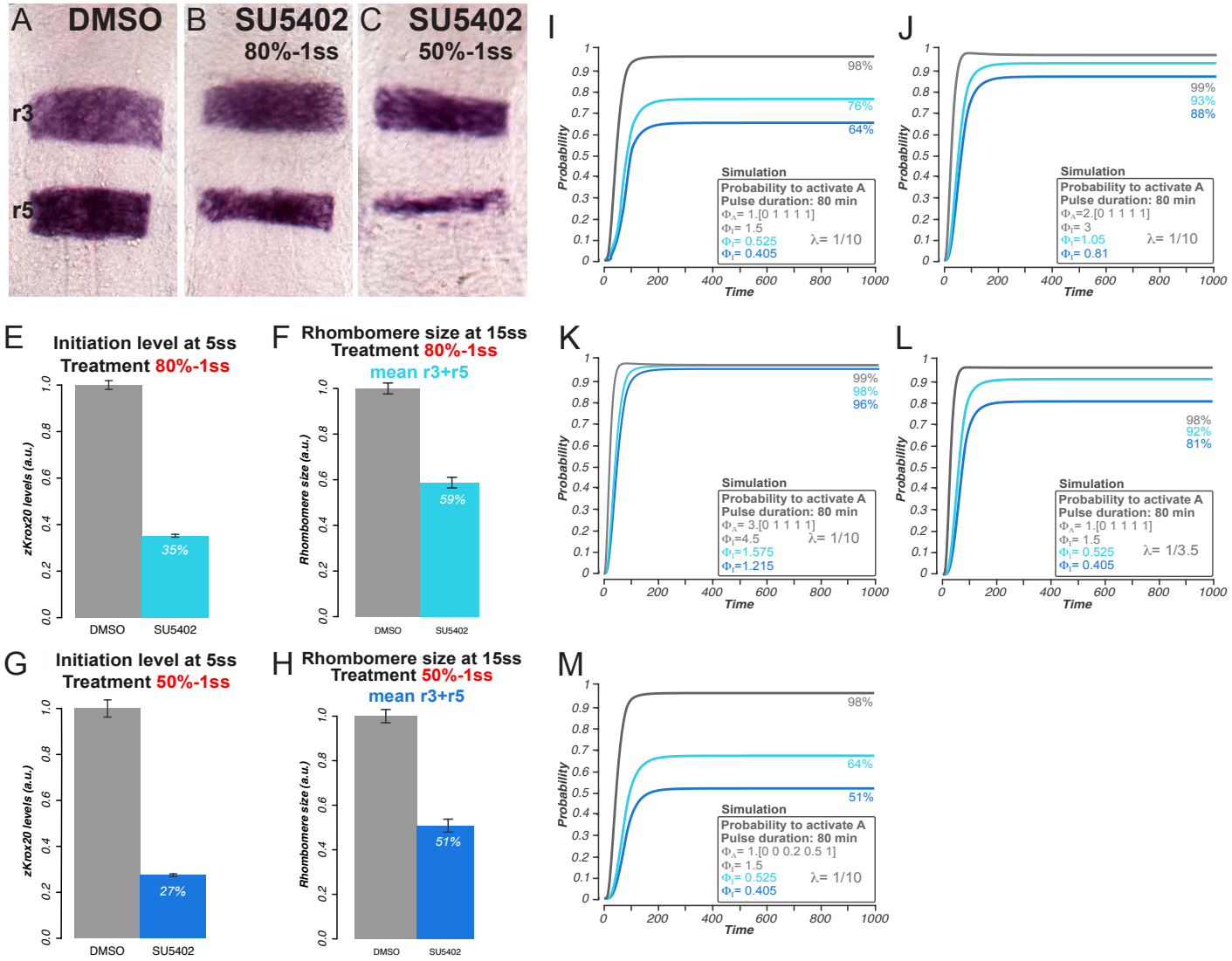

Figure S7: Parameter fitting, approach #2: the robustness of the autoregulatory loop.
(A-C) *zkrox20 in situ* hybridization on wild-type zebrafish embryos treated with the FGFR inhibitor SU5402 (B,C) or mock-treated (A). Two durations of treatments were used: short, from 80% epiboly to 1 ss (B) and long, from 50% epiboly to 1 ss (C). *In situ* hybridzation was performed at 15 ss. **(E,F)** *zkrox20* initiation level was evaluated under short SU5402 treatment by measuring the *zkrox20* mRNA level in *zkrox20*$^{-/-}$ embryos (E). The same treatment applied to wild-type embryos provoked a marked diminution of r3, r5 sizes as quantified by measuring the area of *zkrox20*-positive domain at 15 ss. The mean of r3+r5 area is shown (F). **(G,H)** The same protocol was conducted on embryos treated from 50% to 1ss. **(I-K)** Simulations of the SU5402 treatments using the same parameters as shown in figure S6F-H. To simulate the 35% and 27% initiation levels shown in E, G, the Φ_I level was decreased to 35% and 27% (light blue and dark blue curves respectively). To evaluate the number of *zkrox20*-positive cells, the probability to activate A is shown. The situation depicted in I provides the profile closest to the experimental data, as simulations shown in J and K exhibit too much robustness. **(L)** The loop also appears too robust when λ<1/10, as shown here with λ=1/3.5, hence the chosen value for λ=1/10. (M) In I, the probability is decreased to 76% and 64% while the rhombomere size is respectively decreased to 59% and 51% (F,H) To better conform with the experimental data we performed the same simulation as in I under the "light synergy" scenario. The probabilities to activate A falls to 64% and 51%, closer to the experimental results. With this approach, we fitted Φ_I=1.5, Φ_A=1.[0 0 0.2 0.5 1] and λ=1/10.

Allele	Primer sequences		Exp. Size	Exp. Size (wt)
Krox20{NA*AK}	F	5' ACGAATGTCTATTTGTAGGTCCCAGGC 3'	296 bp	254 bp
	R	5' CAACCACGCTCAATGTTTTC 3'		
Krox20{A*}	F	5' CGCAGTGCCGTCCTCAAAGAGA 3'	374 bp	
	R	5' CAACCACGCTCAATGTTTTC 3'		
Krox20{NA}	F	5' GTAGAAGGTGGCGCGAAGGGGC 3'	390 bp	
	R	5' CCACACTGGAAGCTCGGGTATTG 3'		
Krox20{ΔA}	F	5' GCGAGTTTCCTTGAAAGGAGC 3'	271 bp	
	R	5' CAACCACGCTCAATGTTTTC 3'		
A:Krox20-2ER$_{HA}$	F	5' ATTTGCTCCTCGCACACC 3'	171 bp	
	R	5' CTGAGAAGCCTGTCTTTAACTACTG 3'		

Table S1: Primers sequences used to genotype the mouse knock-in or transgenic embryos used in the study.
The 'Exp. size' and 'Exp. size (wt)' columns refer respectively to the size of the PCR product amplified from the mutant/transgenic allele andor the wild-type allele.
Abbreviations: Exp.: Expected, F: Forward primer, R: Reverse primer.

– Chapter 3 –

Control of positional information in the vertebrate hindbrain by FGF signalling

C. Labalette*, Y.X. Bouchoucha*, J. Le Men, P. Charnay, P. Gilardi-Hebenstreit

IBENS, Ecole Normale Supérieure, Paris, France – INSERM U1024, CNRS UMR 8197

Author contributions:

CL and YXB performed the experiments and analysed the results.

JLM engineered the construct for the *cC::GFP* transgenic line

YXB wrote the manuscript.

CL and PGH reviewed the manuscript.

* equal contributions

Foreword

Early loss-of-function of FGF signalling in the hindbrain provokes a dose-dependent reduction in size of *Krox20*$^{+}$ domain. In chapter 1 and 2, we showed that this phenotype results from diminished level of *Krox20* initiation that in turn weakens the probability to stably activate A. Is this effect patterned in space? As a source of FGF ligands has been identified in r4, FGF signalling could facilitate *Krox20* initiation in a graded manner, with high *Krox20* initial level near r4 and low in more distal regions. In other words, FGF could help determine the position of the borders of segmentation genes domains. This morphogen-like function has been postulated by several authors as it had been demonstrated in other developmental contexts, but conclusive results are still missing. In the following article, we challenge this morphogen hypothesis.

Control of positional information in the vertebrate hindbrain by FGF signalling

INTRODUCTION

Early patterning of the vertebrate brain along its anterior-posterior (A-P) axis has been shown to require the action of several organizing centres, of which the Anterior Neural Ridge (ANR) at the anteriormost tip of the neural tube, the *Zona Limitans Intrathalamica* (ZLI) between the presumptive dorsal and ventral thalamus, and the isthmus located at the midbrain-hindbrain boundary (Wurst and Bally-Cuif, 2001; Wilson and Houart, 2004; Lim and Golden, 2007). Each of these centres secretes signalling molecules that spread over a limited distance, thus shaping concentration gradients. Minute concentration differences along the A-P axis may be interpreted by cells to undergo appropriate specification. Such signalling molecules that act directly on cells to induce distinct responses in a concentration-dependent manner are referred to as 'morphogens'. As a corollary, expression domains of target genes adapt to modifications in the morphogen concentration following the predictions of the French-flag model of Lewis Wolpert (Tabata and Takei, 2004).

The patterning of the hindbrain A-P axis goes through a transient segmentation process, i.e. the definition of six regularly-spaced boundaries delimiting domains of lineage restriction. These are called rhombomeres (r), noted from r1 to r7. Although the molecular events underlying segmentation have been the focus of intense studies over the past two decades, the positioning of boundaries is still poorly understood. At early steps, retinoic acid (RA) is released from the paraxial mesoderm and establishes as a gradient from posterior to anterior hindbrain. It plays a key role in upregulating the expression of Hox genes (Moroni et al., 1993; Sirbu et al., 2005) whose expression patterns are the first proof of coordinates along the hindbrain A-P axis, since their early anterior borders prefigure the position of some future boundaries. However the morphogenetic role of RA in the hindbrain could not be rigorously established (Schilling, 2008). Accordingly no experimental findings support a role of RA in directly setting up the position of hindbrain boundaries. However, in zebrafish gastrula, the expression of other diffusible molecules, the Fibroblast growth factors (Fgf) 3 and 8, is upregulated in a central domain first overlapping pre-r3 and pre-r4 at 90% epiboly, then reinforcing in r4. This *fgf3/8*-positive domain has been proposed to function as an organizing center, i.e. a source of Fgf3 and Fgf8 proteins that diffuse to pattern the neural plate (Maves et al., 2002; Walshe et al., 2002).

The r4 source of Fgf ligands is reminiscent to the two other Fgf-expressing signalling centers, the ANR and the isthmus. The first was shown to provide Fgf8 to pattern the mouse neocortical maps in a morphogenetic manner: the Fgf8 protein distributes in a concentration gradient, activates different target genes according to the distance from the source and therefore controls the size and positions of cortical areas (Toyoda et al., 2010). The second is also a source of the Fgf8 ligand; in mouse, it patterns the posterior midbrain and r1 territory in a time-dependent manner: structures that are close to the isthmus necessitate longer exposure to Fgf8 than structures specified further away. Time of exposure to a morphogen may be interpreted as a dose, considering that cells integrate the signal in time. Therefore, the dose of Fgf determines the type of structure to be specified, suggesting that Fgf may again function as a morphogen in this context. Identification of the target genes and analysis of their behaviour upon alteration of Fgf levels are still missing to confirm this assertion (Sato and Joyner, 2009).

Based on these studies, we formulate the hypothesis that Fgf signalling provides positional information in the zebrafish hindbrain, and we use rhombomere boundaries as markers of A-P coordinates. These boundaries are prefigured by the limits of expression domains of two segmentation genes, namely *krox20* in r3, r5 and *valentino* (*val*) in r5, r6. The expression of these genes is affected in both Fgf loss- and gain-of-function assays in a dose-dependent manner (Walshe et al., 2002; Labalette et al., 2011), hence shifted borders. Of note, Fgf signalling affects *krox20* and *val* expression when it is altered between 50% epiboly and the 1-somite stage (ss), i.e. prior to the onset of *krox20* and *val* expression (Walshe et al., 2002). It is inferred that specification of hindbrain cells takes place between these two timepoints, partly by integrating Fgf signals in time. Beyond 1ss, patterning of the central hindbrain becomes independent of Fgf signalling.

In the present study, we investigate the molecular origin of border positioning in the zebrafish hindbrain. Quantitative analysis of border positions upon Fgf loss-of-function revealed that Fgf signalling does not modify the borders homothetically. We thus reinvestigated the Fgf-dependent downstream pathway in zebrafish, validated two targets and read-outs, ppERK and *erm*, and employed them to test the morphogen hypothesis directly. We found that Fgf morphogenetic effect is not sufficient to account for the changes in border positions. However, Fgfs affect the level of *erm* expression. This effect correlates with the reduced activity of *krox20* cis-regulatory element C in r3. We provide evidence that the level of C activity is crucial to determine the area where *krox20* expression is maintained, i.e. r3. We thus propose a model where the interplay between Fgf signalling and the activity of *krox20* element C is responsible for the positioning of the r3/r4 boundary.

MATERIALS & METHODS

Fish stocks

Zebrafish (*Danio rerio*) were raised and staged as previously described (Kimmel et al., 1995). Embryos were grown in embryo medium (recipe detailed in the Zebrafish Book) at 24°C, 28°C or 33°C to adjust the developmental speed to the experimental constraints. The wild-type lines used were TL and TU. The *hsp:DNFGFR1* line has been described previously (Lee et al., 2005). The *cC::GFP* line was obtained by Tol2-mediated transgenesis of the chick ortholog chick sequence described in (Labalette et al., 2011).

Immunohistochemistry

Embryos of desired stage were fixed overnight at 4°C in 4% paraformaldehyde/phosphate-buffered saline (PBS), rinsed in PBS containing 0.1% v/v Triton X-100 (PBT), dechorionated, dehydrated in a series of methanol/PBT baths and left overnight at -20°C in 100% methanol. Once rehydrated, embryos were blocked in PBT containing 5% v/v Fetal Calf Serum (Sigma) and 1% v/v Bovine Serum Albumin (Sigma). They were then incubated with rabbit anti-phospho-p42/p44 (ERK) primary antibody (Cell Signalling) at 1:200 overnight at 4°C. After three washes of 30 minutes each, embryos were incubated either with an HRP-conjugated anti-rabbit (Invitrogen) diluted at 1:200 or an Alexa488 anti-rabbit secondary antibody (Jackson Immunoresearch) diluted at 1:500. In the former case, we revealed the immunostaining with the TSA amplification kit (Perkin Elmer) including the following steps: 30-minute incubation in TNT buffer (0.1M Tris-HCl pH 7.5, 0.15M NaCl, 0.05% Tween-10), 1 hour in 1:200 Tyramide solution diluted in the provided amplification buffer, extensive overnight washes in TNT. Whole-mount embryos were photographed with a Leica M165FC fluorescent stereomicroscope or a spinning-disk confocal microscope coupled to a CCD camera.

RNA *in situ* hybridization

Antisense RNA probes that detected the following genes were used: *krox20* (Oxtoby and Jowett, 1993), *val* (Moens et al., 1998), *pax2.1* (Krauss et al., 1991), *hoxb1a* (Prince et al., 1998), *erm* and *pea3* (Münchberg et al., 1999). Probe syntheses and whole-mount *in situ* hybridization were performed as previously described (Jowett and Lettice, 1994). Embryos fixed overnight, dechorionated, dehydrated and rehydrated as described for immunohistochemistry. Following the hybridization protocol, embryos were deyolked using 26G syringe needles, flat-mounted in 87% glycerol/H_2O and photographed using a Leica DM5500B microscope.

Injection of morpholino oligonucleotides

Four morpholino oligonucleotides (GeneTools) directed against *pea3* (*etv4*), *erm* (*etv5*), *etv5a* and *sprouty4* were dissolved in Daniau buffer at a concentration of 2 mM and diluted to 0.25 mM. Three nanoliters were injected into 1-cell stage embryos. Morpholinos sequences were previously described for *pea3, erm*, and *etv5a* (Mao et al., 2009) and for *sprouty4* (Labalette et al., 2011).

Treatment of embryos with Fgf pathways inhibitor

Embryos were dechorionated at 30% epiboly after incubation in a 1mg/mL pronase (Sigma) solution during 7 minutes followed by five baths of rinsing medium. Chorions were gently removed with forceps in Petri dishes with a layer of 1% agarose on their base. Embryos were allowed to develop at 28°C until 50% epiboly. Upon reaching this stage, they were incubated with SU5402 (inhibitor of FGF Receptors, Calbiochem), LY294002 (inhibitor of Akt/PI3K pathway, Calbiochem), SB203580 (inhibitor of p38/JNK pathway, Calbiochem), PD184352 (inhibitor of p42/44 ERK pathway, gift from C. Pujades, Barcelona). All compounds were diluted in DMSO at a stock concentration of 3 mM. Working concentration was obtained after dilution in embryo medium. It was typically of 60 μM, unless indicated. Control embryos were incubated in embryo medium containing an equivalent volume of DMSO. Following incubation, embryos were washed in several changes of embryos medium and then grown to the desired developmental stages.

Conditions of heat-shocks

To trigger DNFGFR1 expression in *hsp:DNFGFR1* transgenic embryos, 80% epiboly embryos were placed in large flat-bottom vials containing a minimal amount of embryo medium. Heat-shocks were applied by transferring the vials into a 37°C pre-heated water bath during 10 minutes.

Statistics

Statistical analysis was performed using the open-source R software (www.r-project.org). ANOVA and paired Student t-tests (with Bonferroni correction) were used to assess significant differences in mean boundary positions calculated from control *vs* treated datasets. Data are expressed as mean ± sem. Significance was set as follow: * $p<0.05$, ** $p<0.01$, *** $p<0.001$.

RESULTS

1. FGF signalling affects the position of rhombomere boundaries

To assess quantitatively the position of rhombomere boundaries along the A-P axis, the expression domains of *krox20*, *val* and *pax2.1* were revealed by *in situ* hybridization (Fig. 1A). *krox20* and *val* allowed to mark the identity of rhombomeres: r3 is defined by the expression of *krox20*, r4 by the absence of staining, r5 by the coexpression of *krox20* and *val*, r6 by *val* alone. *pax2.1* marks the midbrain-hindbrain boundary (MHB) as well as the otic vesicles. The expression patterns of the three genes define a region of the hindbrain delimited anteriorly by the MHB and posteriorly by the r6/r7 boundary. In this region, the r2/r3, r3/r4, r4/r5 and r5/r6 boundaries are clearly identified. To inhibit Fgf signalling, we employed transgenic embryos carrying the *hsp:DNFGFR1* construct. Upon heat-shock, all cells of transgenic embryos express a dominant-negative form of the FGF Receptor 1 and therefore become non-responsive to Fgf ligands. Given the high stability of DNFGFR1, the loss-of-function can be considered permanent after the heat-shock. When a 10-minute 37°C heat-shock is performed at 80% epiboly, the expression domains of *krox20* and *val* are reduced in size at 20 ss, and the r1-to-r6 distance is decreased (Fig. 1A-C). The boundary positions were represented using the centre of r4 as an origin since this rhombomere is considered as the source of patterning signal (Fig. 1D). To compare the positions of rhombomere boundaries, we normalized the position values by the total hindbrain length (Fig. 1E). Given the conditions of heat-shock mentioned above we conclude that Fgf loss-of-function entails a diminution in size of odd-numbered rhombomeres accompanied with a relative increase in the size of r4. This confirms that Fgf primarily affects r3 and r5 under these conditions. The result was strengthened by using another approach to knock-down Fgf function, that is the treatment of embryos with 60 μM of the FGFR inhibitor SU5402 from 50% to 95% epiboly (Fig. 1F). These results are consistent with earlier reports showing that the expression of *krox20* and *val* are under the control of Fgfs (Walshe et al., 2002; Maves and Kimmel, 2005; Labalette et al., 2011). By affecting *krox20* and *val* expression domains, Fgf knock-down entails overt changes in border positions, with the exception of r2/r3.

The reduction of total hindbrain length suggests that Fgf loss-of-function leads to decreased proliferation or increased apoptosis rates. In a previous study, we showed that the reverse experiment, Fgf gain-of-function, does not modify the distribution of proliferative cells in the hindbrain (Labalette et al., 2011). Assuming the same conclusion applies to Fgf loss-of-function, we propose that the rhombomere boundaries are shifted in a manner independent of the Fgf general proliferation effect. This assertion is further justified by the early patterning defects

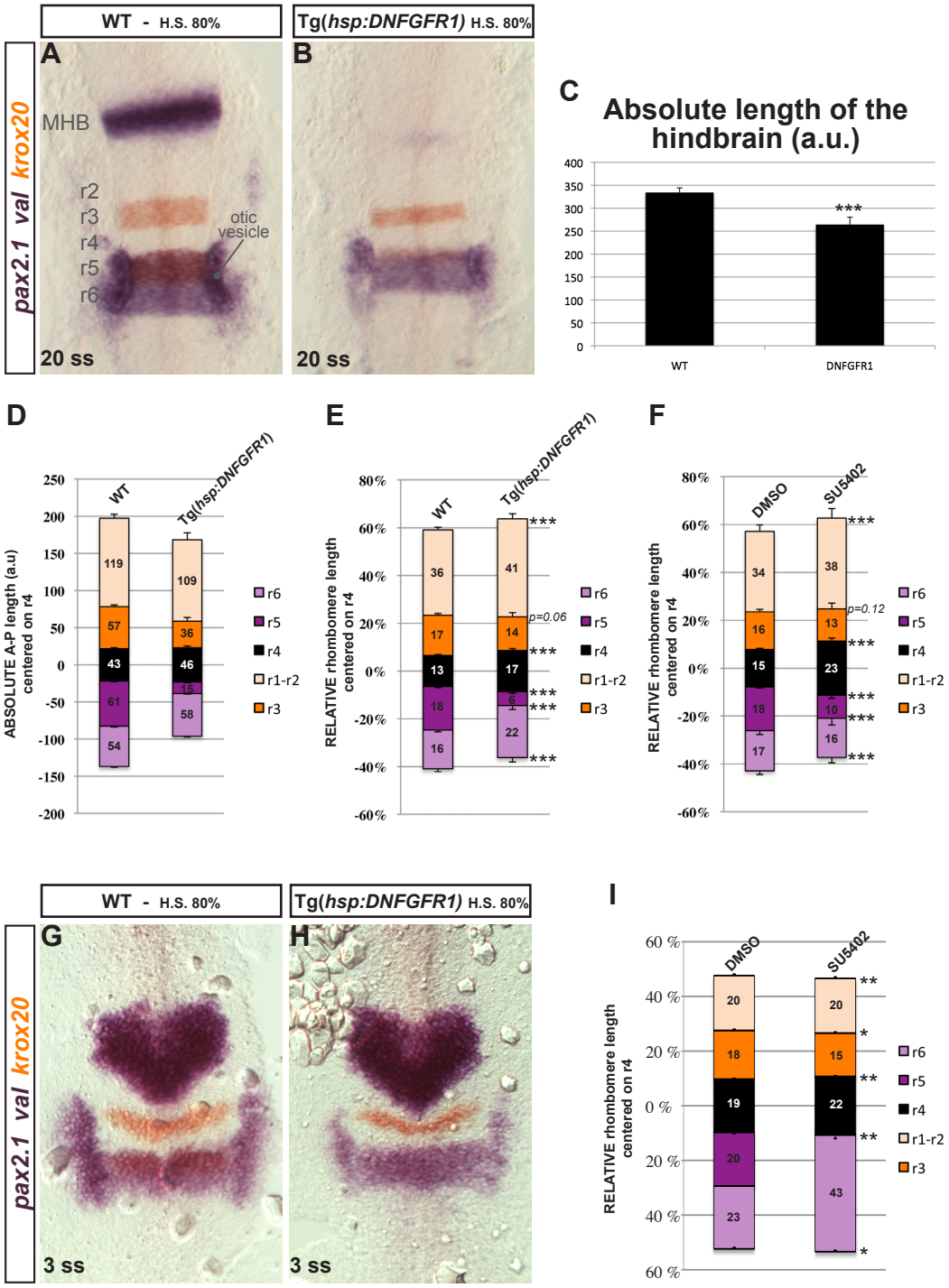

Figure 1: **Fgf signaling affects border positionning in the zebrafish hindbain.**
(A,B) *krox20*, *valentino*, *pax2.1* in situ hybridizations were used to locate future boundaries in the hindbrain (A) and assess their positions in a situation where Fgf signalling is impaired by the expression of a dominant-negative form of FGFR1 (B). **(C)** Expression of DNFGFR1 in the whole embryo entails a reduction in the absolute length of the hindbrain. **(D-E)** Quantification of Fgf knock-down effect on the border positions. Absolute size of each territory is measured and represented by taking the center of r4 as an origin (D). Figures shown are absolute rhombomere size in arbitrary units. When these measurements are normalized with the overall size of the hindbrain, the positions of the borders may be compared between the control and the *hsp:DNFGFR1* conditions (E): all borders, except r2/r3, are shifted due to the marked reduction of r3 and r5. Similar results are obtained when Fgf loss-of-function is achieved by treating embryos with 60 µM SU5402 from 50% to 90% epiboly (F). In E,F, figures shown are the relative rhombomere size; their sum equals 100. **(G-I)** The same results are obtained when border postitions are assessed at an early stage, 3 ss.

evidenced from 3 ss upon Fgf knock-down : r3 and r4 borders are shifted at 3 ss in a manner similar than 20 ss (Fig. 1G-I). This suggests that border positions are set at early stages, and does not result from a late adjustment of expression domains controlled by proliferation and/or apoptosis. The direct demonstration of a non-regionalized effect of proliferation and apoptosis in Fgf knock-down embryos is under way.

To confirm that Fgfs do not affect the r2/r3 border, we assessed its position in embryos treated with doses of SU5402 ranging from 10 μM to 60 μM. This experiment first shows that the effect of Fgf signalling on hindbrain segmentation is dose-dependent (Fig. 2A-H). Although suggested in previous studies (Walshe et al., 2002), it had never been assessed directly. Quantification of the border positions shows in addition that the r2/r3 boundary is not affected in 40 μM and 60 μM treatments compared with the DMSO condition, as opposed to all other borders (Fig. 2I). At the low 10 μM dose, the only modified border is r5/r6, confirming earlier observations that *krox20* expression in r5 is the most sensitive to Fgf knock-down. At 20 μM, the significant shift of r2/r3 was interpreted as an experimental artefact.

Taken together, these results show that Fgf signalling affects hindbrain development in two ways: a general non-regionalized proliferation/apoptosis effect on total hindbrain length, and a patterning effect on rhombomere size resulting in shifted boundaries. All boundaries are not shifted in a concerted manner. r2/r3 for instance was found immobile.

2. FGF signalling is mediated by the MAPKinase pathway and Ets factors in zebrafish

Fgf ligands activate FGF receptors at the cell surface that in turn triggers phosphorylation cascades along three possible paths: PI3K/Akt, p38/JNK or the Ras/ERK (MAP Kinase) (Fig. 3A). The MAPK pathway has been shown to be active in the chick hindbrain and mediates Fgf action on segmentation genes (Aragon and Pujades, 2009; Weisinger et al., 2010). We show here that this finding also applies in zebrafish: embryos treated with the anti-ERK drug PD184352 exhibit the same alterations in *krox20* and *val* expressions as embryos treated under the same conditions with the drug antagonizing all pathways, SU5402. In contrast, drugs directed against the PI3K/Akt and p38/JNK pathways had no effect (Fig. 3B-K). Activation of the Fgf pathway in hindbrain cells thus leads to the double phosphorylation of ERK. ppERK is in turn translocated into the nucleus and phosphorylates target transcription factors, of which the most studied belong to the Ets family (Wasylyk et al., 1993). Two members are described as being expressed in the zebrafish hindbrain, namely, *erm* (*etv5b*) and *pea3* (*etv4*). Their domains of expression uniformly cover the MHB-to-r6/r7 region (Fig. 3L,M) (Raible and Brand, 2001; Roehl and Nüsslein-Volhard, 2001). Morpholinos directed against these two members were injected in

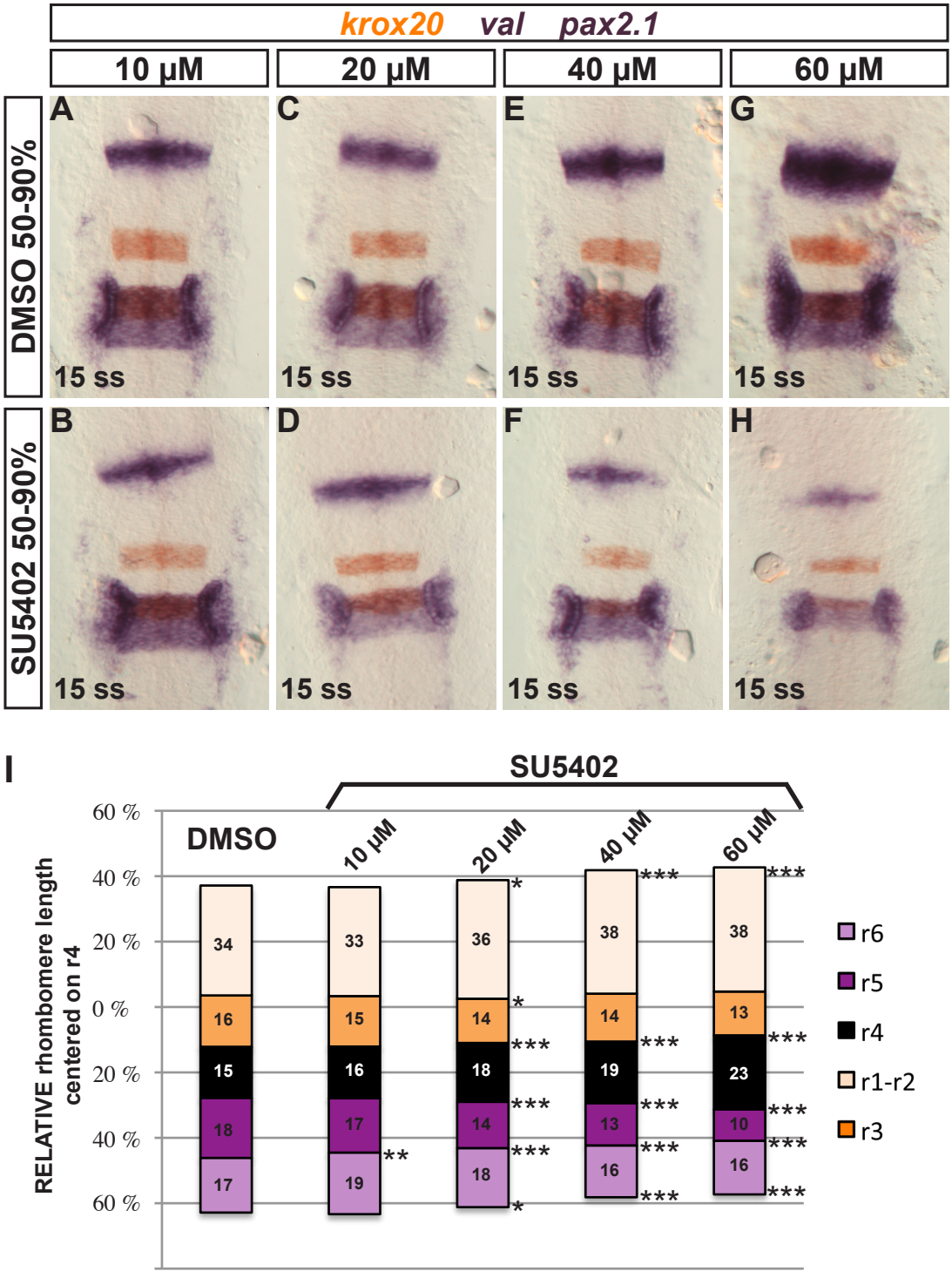

Figure 2: The pattern of segmentation genes is modified in a dose-dependent manner upon alteration of Fgf signalling.
(A-H) *In situ* hybridizations against *pax2.1*, *val* and *krox20* in embryos treated with increasing doses of SU5402, from 50% to 90% epiboly. **(I)** Graphical representation of the boundary positions in each treatment. As the rhombomere sizes are normalized and the hindbrain is represented centered on r4, the positions can be compared. Statistical analysis is represented by asterisks. The position of each boundary in SU5402-treated embryos was compared with the corresponding position in DMSO-treated embryos. Figures shown represent the relative size of each rhombomere, given the total hindbrain length is 100.

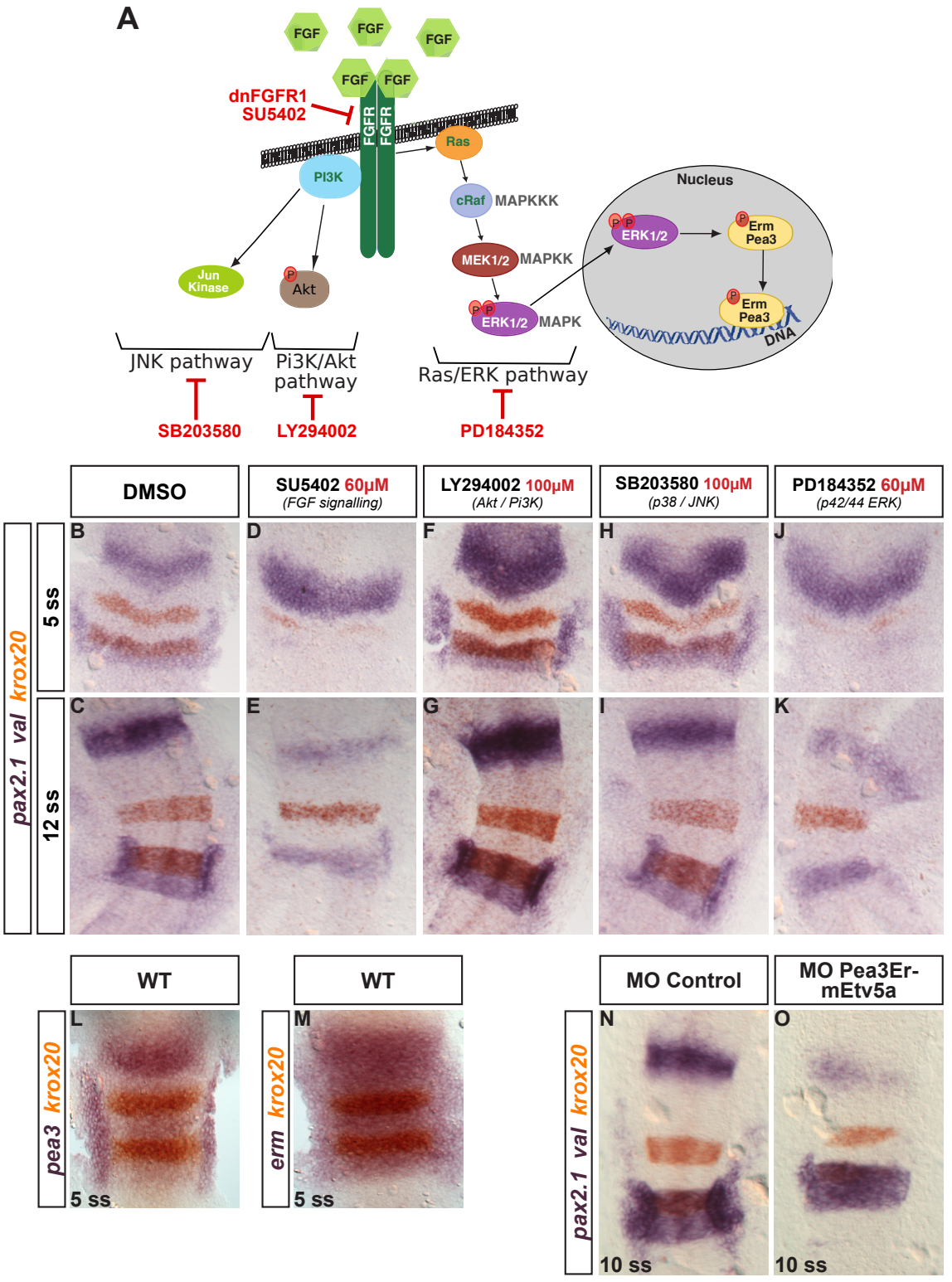

Figure 3: FGF intracellular pathway in the zebrafish hindbrain

(A) Schematic representation of the three reported pathways that may be at stake in cells responsive to Fgf ligands: the Jun Kinase pathway, inhibited by the SB203580 compound; the Pi3K/Akt pataway, inhibited by LY294002 and the Ras/ERK MAP Kinase pathway inhibited by PD184352. Our two other Fgf loss-of-function approaches, i.e. the use of SU5402 and the *hsp:DNFGFR1* line, affect the function of the FGF receptors, thus inhibiting all three intracellular pathways. **(B-K)** Embryos were treated from 50% to 90% epiboly with the compounds and the concentrations indicated. They were subsequently allowed to develop to 5ss or 12ss. *pax2.1*, *krox20* and *val* in situ hybridizations indicate that the SU5402 phenotype is only recapitulated by the anti-ERK drug. **(L,M)** *pea3* and *erm in situ* hybridizations coupled with *krox20*. Both genes are expressed in a region spanning from the MHB to r6. *pea3* looks however downregulated in the r1 territory. **(N,O)** Morpholinos disrupting pea3, erm and etv5a translation were injected in embryos at the 1-cell stage. At 1ss, the patterns of the segmentation genes are severely affected in a manner similar to the *hsp:DNFGFR1*-mediated loss-of-function.

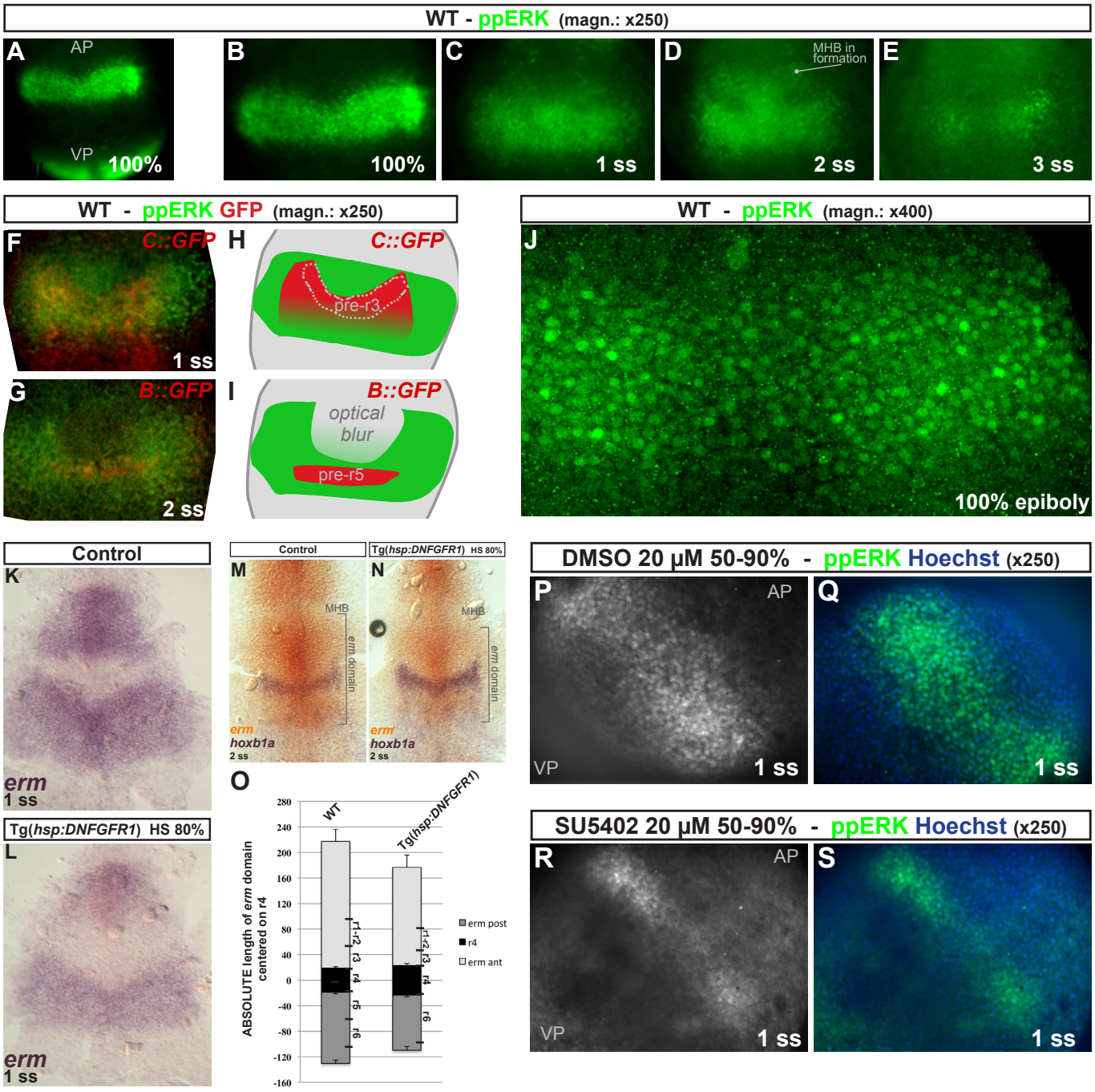

Figure 4: ppERK and *erm* expressions reveal a morphogen-like action of Fgf signalling
(A-E) Immunohistochemistry with tyramide amplification of the double phosphorylated form of ERK, noted ppERK, in whole-mount zebrafish embryos pictures under a stereomicroscope. A wide view reveals that ppERK is also highly present in the tailbud (A). Zoomed-in images show the timecourse of ppERK expression, from 100% epiboly to 3 ss. **(F-I)** Double-immunolabelling of ppERK and GFP in the C::GFP (F) and B::GFP transgenic lines (G). GFP respectively reveals pre-r3 and pre-r5 as more clearly indicated in the schematics (H,I). In G, the ppERK band displays an artefactual central round-shaped zone of low intensity, resulting from a mis-optimized optical sectioning procedure. **(J)** High-magnification picture of the ppERK territory at 100% epiboly. To be able to compare qualitatively the level of signal among cells, the immunohistochemistry has been performed without Tyramide amplification, and embryos were visualized under a spinning-disk microscope. **(K,L)** *In situ* hybridizations directed against *erm* in control (K) and Fgf knocked-down embryos at 1 ss (L). **(M,N)** The same result is shown with a co-labeling of *erm* (orange) and *hoxb1a* (purple) at 2 ss. This allowed to quantify the size of the *erm* domain, as shown in C. **(O)** The size of *erm* and *hoxb1a* domains were quantified; the absolute values are represented centred on r4. Positions of rhombomeres are indicated, based on absolute values of border positions measured at the same stage, 2 ss **(P-S)** Expression of ppERK upon gentle treatment with SU5402 (20 µM) photographed with a spinning-disk microscope: the band appears narrower in treated embryos (R,S) compared with control embryos (P,Q). **Abb.:** AP: Animal Pole, VP: Vegetal Pole.

embryos at the 1-cell stage but led to very minor changes in the segmentation genes pattern (not shown). However, when they were injected in combination with a third morpholino, directed against the *erm* paralog *etv5a*, the extension of *krox20* and *val* domains was found similarly reduced compared with *hsp:DNFGFR1* transgenic embryos heat-shocked from 80% epiboly (Fig. 3N,O). This strongly suggests that FGF pathway is mediated by the redundant function of *erm*, *pea3* and *etv5a* in the hindbrain. Once phosphorylated, *erm* and *pea3* were shown to regulate their own expression, such that their level of expression are widely used as a read-outs of Fgf activity (Raible and Brand, 2001; Roehl and Nüsslein-Volhard, 2001).

In conclusion, the results presented above identify ppERK and *erm* as two effectors of Fgf signalling in the zebrafish hindbrain that can be used as read-outs.

3. Alteration of Fgf signalling reveals a morphogenetic behaviour.

Presence of ppERK in the zebrafish hindbrain was assessed by immunohistochemistry. A band of ppERK appears at 90% epiboly and reinforces until 1 ss, where ERK starts being phosphorylated in the MHB. From 2 ss onwards, the band fades away (Fig. 4A-E). To position this band in the hindbrain, we made use of two transgenic reporter lines where *GFP* expression is driven by two cis-regulatory elements of *krox20*, either B or C. The former is active in r5, the latter in r3 and at low-level in r4 (Chomette et al., 2006; Wassef et al., 2008; Labalette et al., 2011). Double stainings of ppERK and GFP reveals that the ppERK band covers the r2-r6 territory, suggesting it is centred on r4 (Fig. 4F-I).

In the developing neocortex where Fgf acts as a morphogen, ppERK staining distributes in a gradient that recapitulates the spreading of Fgf ligands (Toyoda et al., 2010). We hypothesize here that Fgf3/8 proteins are also distributed in a gradient along the hindbrain A-P axis. However, a close-up on the ppERK band at 100% epiboly does not reveal obvious gradual distribution from the centre of the band towards its periphery (Fig. 4J). ppERK staining looks homogenous in the r2-r6 domain and may not propagate directly the positional information provided by the Fgf3/8 gradient.

erm mRNA expression was also found homogenous, but in a region larger than ppERK, spanning from the MHB to r7 (Fig. 3M and 4K). Consistently, the *erm* band of expression at 1 ss is made of a minimum of 25 cell rows while the ppERK band does not exceed 15 cell rows. As *erm* expression requires ppERK signalling, this result implies that ppERK is actually present in the whole *erm* domain but we detect only the centralmost region of high intensity.

To test whether Fgf signalling provides positional information, we analysed the expression of *erm* and ppERK under Fgf loss-of-function. In 1-somite *hsp:DNFGFR1* embryos, the domain of *erm*

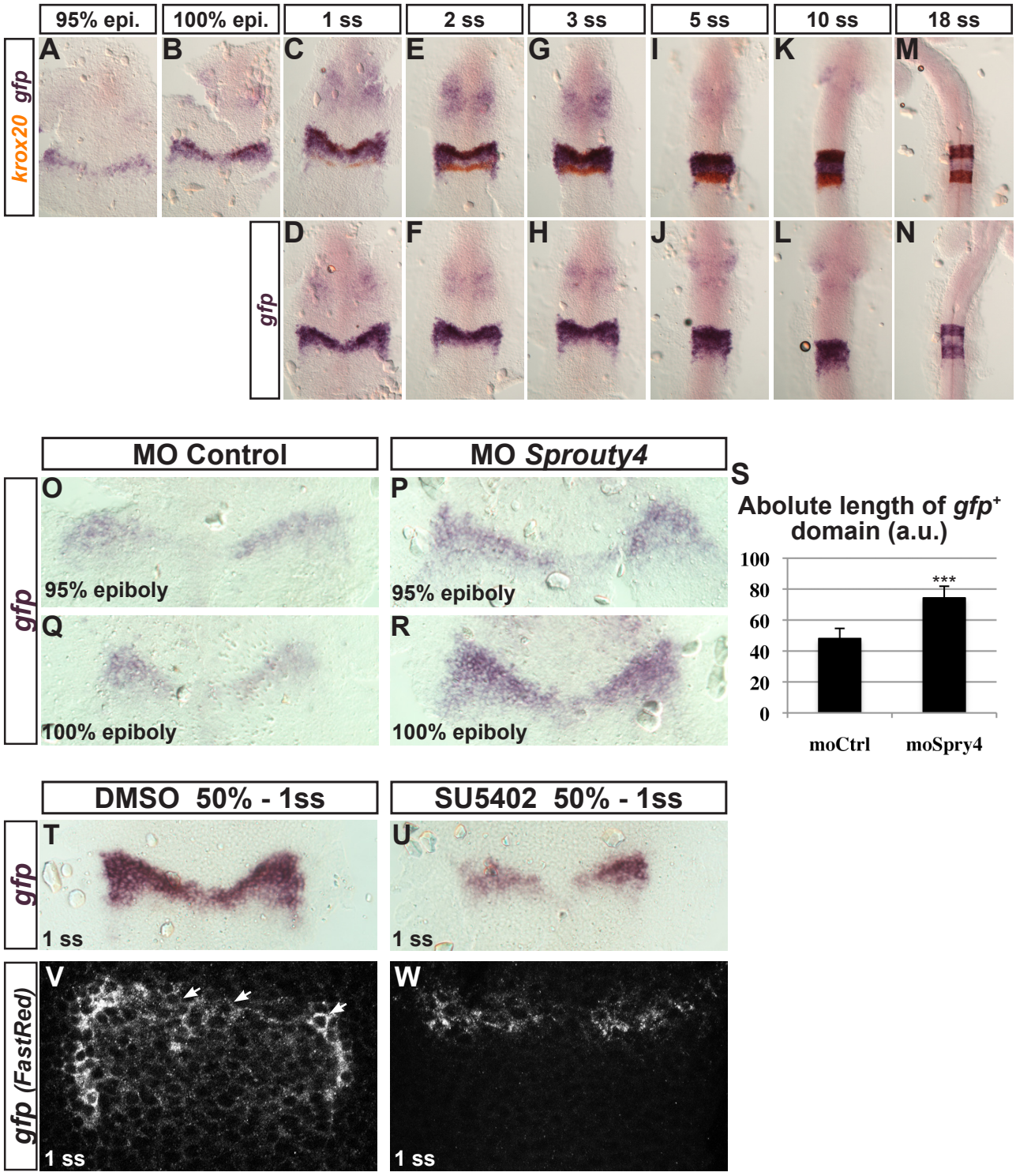

Figure 5: The activity level of *krox20* element C is reduced upon alteration of Fgf signalling
(A-N) *In situ* hybridizations against *krox20* (orange) and *gfp* (purple) in *zC::GFP* transgenic embryos from 95% epiboly to 18 ss. Upper panels show the double *in situ* experiment while lower panels only show the *gfp* profile. **(O-S)** Fgf gain-of-function experiments were performed by morpholino-mediated downregulation of *sprouty4* expression, as described in Labalette *et al.*, 2011. It results in an increase level of C activity, as well as an extension of the C territory, as quantified in S. **(T-W)** The reverse experiment, Fgf knock-down by SU5402 treatment, produces the reverse phenotype: the activity of C looks diminished as well as the extent of its territory. *In situ* hybridizations were revealed with NBT/BCIP (T,U) or FastRed fluorescent compound (V,W). The gradient of C activity in better evidenced in the latter case. Arrowheads in V point to cell in pre-r3 that are reinforcing their level of C.

looked narrower (Fig. 4K,L). Using the r4-specific gene *hoxb1a* as a reference to set the centre of the hindbrain, this reduction was found symmetric around r4 (Fig. 4M-O). Moreover, the *erm* domain was reduced by 18±1.7%, a value significantly higher than the 10±1.5% decrease of the total hindbrain length at the same stage. This shows that *erm* is specifically affected, independently of the Fgf general effect on hindbrain size.

Under similar knock-down conditions, ppERK staining could not be dectected in the hindbrain, presumably because of our detection limit. However, the behaviour of ppERK band could be evidenced in gentle 20 μM SU5402 treatments (Fig. 4P-S): the size of ppERK band was found shortened along its A-P axis, now covering 6 cell rows on average.

In conclusion, Fgf signalling affects *erm* and ppERK domains in a similar manner, by determining the position of their anterior and posterior borders. The effect on *erm* is however much less pronounced. As *erm* is the most downstream effector of Fgf pathway, its expression better reflects the pattern of Fgf activity. In Fgf knock-down conditions where segmentation genes are markedly altered, all borders remain within the homogeneous *erm* domain (Fig. 4O). This result is incompatible with a morphogen-like control of segmentation by Fgf signalling.

Apart from shortening the *erm* domain, Fgf knock-down homogenously affects the level of *erm* expression (Fig. 4K,L), suggesting Fgfs act like a rheostat. We propose that hindbrain cells interpret this rheostat effect by shifting boundaries. To test this hypothesis, we analysed in particular the transcriptional effect of Fgf on *krox20* expression. The regulation of *krox20* expression involves three cis-regulatory elements termed A, B and C. As mentioned above, the two latter are responsible for the initiation respectively in r5 and r3 while the former is autoregulatory (Chomette et al., 2006). We recently showed that Fgfs act exclusively on *krox20* initiation, regulating the activity of both elements B and C (Labalette et al., 2011). In the following sections, we focus on the Fgf-dependent regulation of C and its implication in the positioning of the r3/r4 border.

4. FGF signalling functions as a rheostat on *krox20* initiation

The activity of *krox20* initiator element C was analysed in the reporter transgenic line c*C::GFP* by *in situ* hybridization in order to capture its full dynamics (Fig. 5A-N). The onset of GFP expression occurs at 95% epiboly, shortly before *krox20* upregulates in r3. At the 1-somite stage, the activity of C is clearly reinforced in its anterior domain, i.e. presumptive r3, where *krox20* expression upregulates. Activity of C is also monitored at lower level in r4, although *krox20* is not detected in this rhombomere. This ectopic activity was found in three independent transgenic lines.

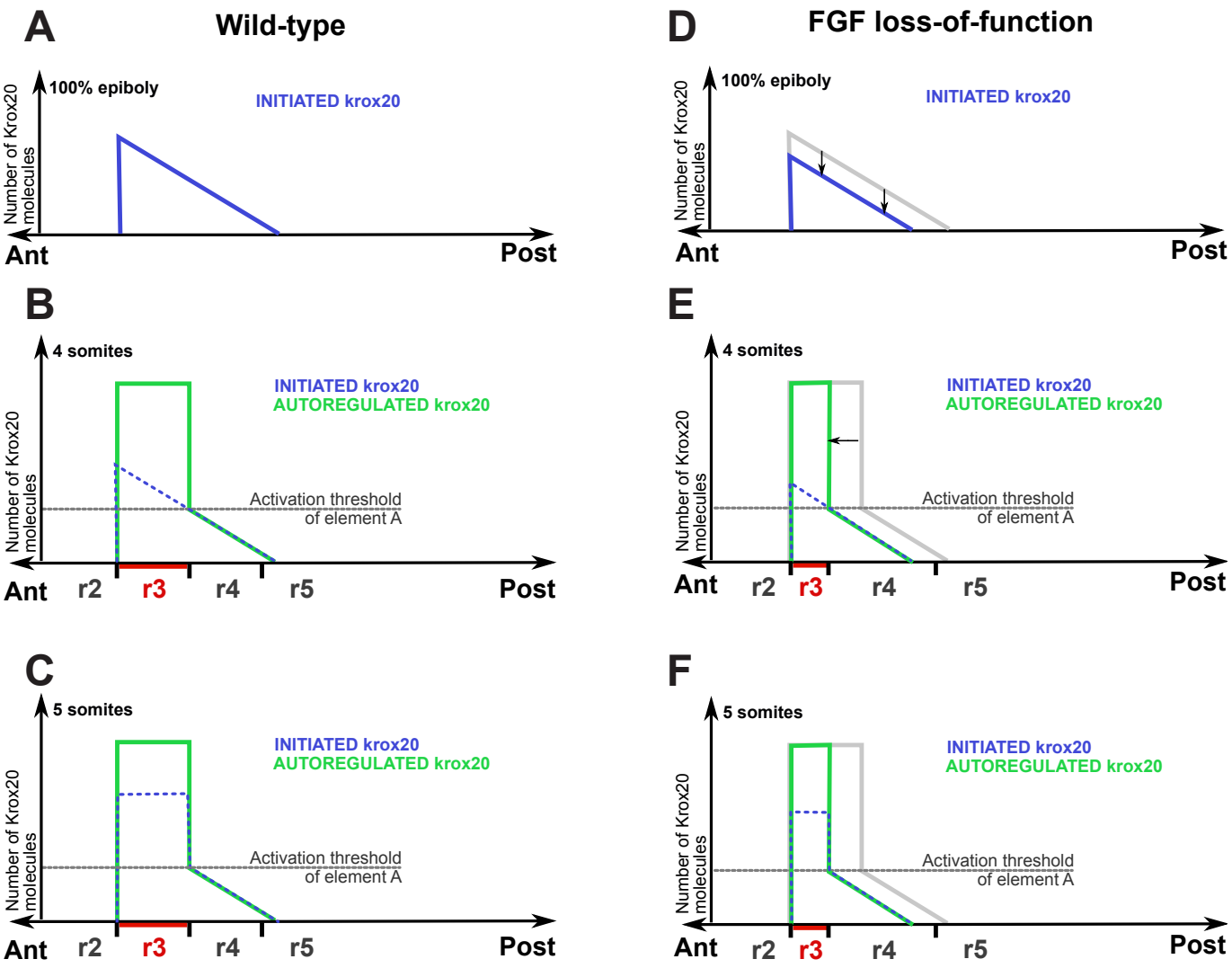

Figure 6: Model for the Fgf-regulated positioning of the r3/r4 boundary
(A-C) C activity profile is asymmetrical: the anterior limit is straight while the posterior end declines gradually (A). Given cells durably express *krox20* only if they activate the autoregulatory loop, the cells that commit to the *krox20*-positive fate lie in the region where the activity of C is above the activity threshold of element A (B). Secondarily, the initiation level is upregulated in cells with high *krox20,* possibly through an indirect loop that involves *hoxa2* and *hoxb2* (C). **(D-F)** Under conditions of Fgf loss-of-function, the activity of C is lowered (D), hence a smaller territory in which cells activate the *krox20* autoregulatory loop. The r3/r4 border is therefore shifted anteriorly (E). Subsequent upregulation of C activity in the resulting r3 occurs accordingly in a smaller domain (F).

A closer look at element C activity in r4 reveals a gradual decrease from the r3/r4 border towards the posterior hindbrain (Fig. 5D,F,H,J,L). This is better evidenced when C activity is revealed by fluorescent *in situ* hybridization (Fig. 5V): the anterior limit of element C activity is sharp while the posterior limit defines a gradient.

Alteration of Fgf levels severely affects the element C activity in the zebrafish hindbrain. The upregulation of Fgf signalling by injection of *Sprouty4* morpholinos increases it (Fig. 5O-R) and extends the posterior limit of its gradual shape (quantified in Fig. 5S). The reverse phenotype is obtained by SU5402-mediated knock-down: the level of C activity is lowered and the posterior limit of its domain is shifted anteriorly (Fig. 5T-W).

Taken together, these results show that Fgf signalling operates as a rheostat on the level of C activity, thus reflecting the effect on *erm*.

5. A model of Fgf-dependent positioning of the r3/r4 boundary.

We showed recently that *krox20* autoregulatory element A functions as a high-pass filter for the initiation signal: in case of low initiation for instance, cells do not contain enough Krox20 proteins to reach the activation threshold of A and commit to the *krox20*-negative fate (see preceding chapter). We propose here that initiation in r3 displays an asymmetric shape with a sharp anterior border and a gradual posterior decline of activity (Fig. 6A). These two properties of *krox20* cis-regulation allow to draw a model for the definition of r3/r4 border position. The position of the border is precisely localized where the initiation level exceeds the activation threshold of element A (Fig. 6B). Anterior to this border, *krox20* level increases due to autoregulation: all cells commit to the *krox20*-positive fate. Concomitantly or shortly after, the activity of C is reinforced (Fig. 6C). This territory defines r3.

In case of Fgf loss-of-function, the overall activity of C is decreased according to a rheostat effect, hence reduced level of initiated *krox20* (Fig. 6D). The r3/r4 border is shifted accordingly, towards the anterior pole, while r2/r3 border remains unaffected because the pattern of element C activity is straight (Fig. 6E). This is consistent with our quantification of border positioning showing that the r2/r3 boundary does not move in case of Fgf knock-down. The same conclusions apply when Fgf signalling is upregulated by use of *Sprouty4* morpholinos: the r2/r3 border is unaffected and the r3/r4 is shifted posteriorly. Consistently, we showed in a previous study that the supernumerary *krox20*-positive cells exclusively expands at the expense of r4 (Labalette et al., 2011).

According to this model, the patterning effect of Fgf signalling in the r3-r4 region is indirect, acting as a rheostat on a regionalized element C domain, hence oriented shifts in border

positions. This mode of action cannot be defined as morphogenetic *per se* because the positional information primarily comes from the asymmetric pattern of C activity and not the gradient of Fgf ligands.

DISCUSSION

Fgf proteins have been shown to control the position and the size of organs or developing areas in a number of contexts. We quoted earlier one study carried out in mouse where Fgf8 is secreted from a discrete source (the ANR) and converted into a gradient of ppERK. Alteration of this gradient affects the patterning of neocortical areas (Toyoda et al., 2010). Similar patterning defects were evidenced in the midbrain-hindbrain boundary region when the dose of Fgf8 secreted by the isthmus is altered (Sato and Joyner, 2009). These results suggest that Fgf8 acts as a morphogen in these contexts, but the rigorous demonstration requires the identification of target genes, to assess the changes in their expression domains upon alteration of Fgf function and confront with the expectations of Wolpert's French-flag model. The zebrafish hindbrain provides an ideal system to interrogate the morphogenetic role of Fgf signalling. Two Fgf ligands, Fgf3/8, were identified as being expressed from late gastrulation in a narrow domain lying at the centre of the hindbrain. Inhibition of their function severely modifies the rhombomere borders, as evidenced by expression of two segmentation genes, *krox20* and *val*. Moreover, Fgf was shown to regulate the expression of *krox20* by acting on its initiator elements, B and C. The work presented above aimed at analysing Fgf-mediated patterning defects in the zebrafish hindbrain in light of the morphogen hypothesis, by using *krox20* as a target.

Fgf morphogenetic effect on its effectors is not sufficient to control the positions of hindbrain boundaries

ppERK and *erm* were identified as two read-outs of Fgf signalling in the hindbrain. Both are homogenously expressed but the ppERK domain looks narrower than *erm*. The former covers the pre-r2-r6 region (15 cell rows at 1 ss) while *erm* expression spans from the presumptive MHB to pre-r7 (25 cell rows). As *erm* is activated by ppERK, we propose that the most peripheral zones of *erm* expression actually contain ppERK but at levels lower than our detection limit. ppERK would therefore be present as a "broken" gradient, with a zone of high intensity at the centre and a zone of low, undetectable level at the periphery (Fig. 7A). We propose in addition a mechanism that restricts the range of Fgf3/8 signalling to the MHB-r7 region at 1 ss. Several mechanisms may affect the length-scale of Fgf gradient. As reported recently, ligand diffusion can be counteracted by the combined effect of ligand endocytosis and intracellular degradation (Scholpp and Brand, 2004; Yu et al., 2009) in cells outside the MHB-r7 zone, or appropriate Fgf receptors could simply be absent. The existence of such a mechanism in zebrafish appears crucial in setting the maximal extent of Fgf signalling as it has been shown in mouse and chick that

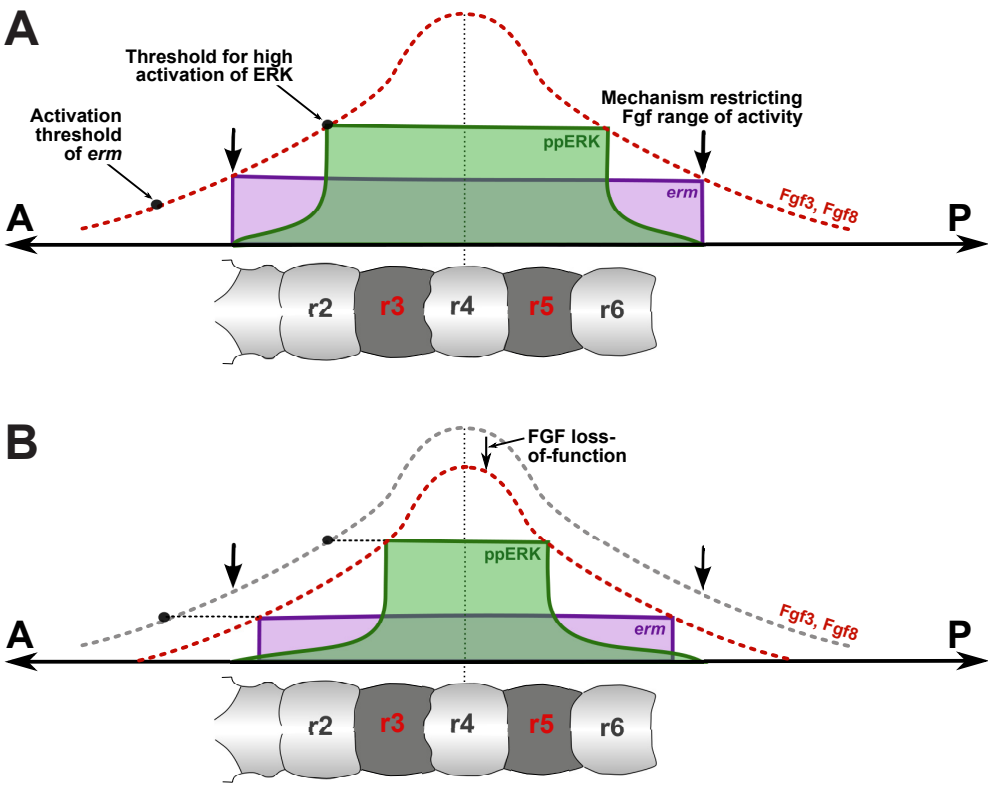

Figure 7: Model for the Fgf-dependent control of ppERK and erm domain borders
(A) In wild-type embryos, a hypothetical gradient of Fgf3/8 proteins defines the borders of the domain where ppERK is highly expressed. In contrast, the *erm* domain is not limited by its activaton threshold but rather truncated by a yet-unknown mechanism that restricts the range of Fgf signalling to the MHB-r7 region **(B)** In situation of low Fgf signalling, the ppERK domain is reduced accordingly, in a morphogenetic manner. The same effect applies to the *erm* domain but it appears less dramatically affected because, in wild-type embryos, its size was underestimated due to the truncation effect.

freely diffusive Fgf8 can travel over long distances, with a minimum of 600 μm in mouse (Chen et al., 2009; Toyoda et al., 2010). In comparison, the length of r2-r6 domain in zebrafish at 1 ss does not exceed 200 μm. The borders of *erm* domain must coincide with these limits of Fgf signalling, as *erm* is one the most sensitive target of Fgf. In Fgf loss-of-function (Fig. 7B), *erm* territory is reduced to a much lesser extent than ppERK: the restriction of Fgf range had masked the effect of Fgf knock-down on *erm* until its activation threshold became predominant, as shown in figure 7B. In contrast, given ppERK domain is smaller than the maximal range of Fgf signalling in wild-type embryos, it is directly impacted by the Fgf knock-down. In conclusion, our results are consistent with a morphogenetic effect of Fgf on its two effectors ppERK and *erm*, but we propose that this effect is attenuated on *erm* because the spreading of Fgf signalling along the A-P axis is tightly controlled.

Under Fgf knock-down conditions, the borders of segmentation genes are shifted within a homogenous *erm* domain. Therefore, the Fgf-mediated morphogenetic effect on *erm* cannot account for the defective boundary positions. We thus propose an alternative model, focused on r3 borders, where the reduced level of *erm* has a profound patterning impact.

Positioning of the r3/r4 boundary depends on the level of Fgf signalling

The Fgf-mediated downregulation of *erm* correlates with the reduced activity of *krox20* element C, although we do not provide the evidence that the effect on C results from the effect on *erm*. We showed moreover that the activity domain of C is patterned such that the anterior border is straight and the posterior border is a gradient. Given *krox20* is durably expressed only in cells that exhibit a high level of initiation (superior to the activation threshold of A), the asymmetry of the C profile is sufficient to explain the shifts of r3/r4 boundary when Fgf signalling is altered. In contrast, the r2/r3 boundary is not affected by Fgf because it is prefigured by the straight anterior border of C activity. According to this model, there are two primary sources of spatial information that determine the positions of r3 borders. First, the pre-patterning process that lead to the triggering of C activation at the right A-P level. This process has been described elsewhere (Wassef et al., 2008). It involves *Hox PG1* genes as well as their *Pbx* and *Meis* cofactors. As these factors are homogenously expressed posteriorly to pre-r2, their expression patterns cannot determine the position of the r3/r4 border. Hence the need of a second source of spatial information: the posterior gradient of element C activity, most evident in r4. This ectopic activity was surprising because it was not monitored when assessing the initiation level of *krox20* in *krox20*$^{-/-}$ mutant embryos. We propose that the strong ectopic activity of C results from a higher and longer activity level of the transgene *cC::GFP* compared with endogenous initiator elements.

The high activity of the transgene therefore unravelled the ectopic activation of endogenous C in r4. The genetic network that shapes this gradient of C activity is still under investigation.

The mechanism we propose for the positioning of r3/r4 boundary has two major implications. First, Fgf signalling only serves as a rheostat of element C activity and does not provide spatial information through the gradient of its ligands. Second, it explains why *krox20*-positive cells expand in the r4 territory in Fgf gain-of-function assays, thus supporting the hypothesis of antagonistic lineages between *hoxb1a*$^{+}$ (r4) and *krox20*$^{+}$ (r3) cells. The *krox20* lineage develops at the expense of *hoxb1a* lineage if the balance provided by Fgf level is not properly tuned. Fgf signalling is thus identified as a primary determinant in the choice between *hoxb1a* and *krox20* lineages.

Addendum

Careful readers may have noticed this study is still at work. The working plan will be organized as follow:

- Evidence that endogenous initiation is patterned in a gradient in r4 will have to be collected. In other words, we need to show that some cells initiate *krox20* expression in r4 but commit to the *hoxb1a* lineage. The only available tool to visualize initiation is the zebrafish *krox20* mutant, where the Krox20 protein produced cannot activate the autoregulatory loop. In the mutants, *in situ* hybridization directed against *krox20* only reveals initiated *krox20*. To test whether some *krox20*-initiating commit to the r4 fate, we could perform *krox20* and *hoxb1a* double hybridization to scrutinize double-positive cells. Although technically simple, this experiment may be unfruitful for two reasons: first, once cells commit to the r4 fate, *krox20* initiation may be immediately turned down and therefore very short-lived; second, *hoxb1a* participates in the activation of *krox20* during the early steps of C activation (Wassef et al., 2008), so we expect few double-positive cells anyway. In the mutant the number of these double-positive cells might be higher. As an alternative to this direct evidence, we will collect indirect proof. For instance, recent results that are not reported here show that *krox20* autoregulation is normally inhibited in r4 (see general discussion). When this inhibition is artificially relaxed, numerous *krox20*-positive cells disperse in anterior r4. This suggests that *krox20* initiation indeed occurs in r4 but is not monitored because the level of *krox20* is too low, except when autoregulation is de-repressed.
- the reinforcement of C activity in r3 is puzzling. *krox20* could itself activate C, possibly through the upregulation of *hoxa2* and *hoxb2*. We will test this hypothesis by assessing the activity of the *cC::GFP* transgene in *krox20* mutants.

- Higher-quality quantitative data will be obtained to evaluate the level of ppERK, *erm* and C activity under conditions of altered Fgf signalling.
- The patterns of proliferation and apotosis under Fgf loss-of-function will be quantitatively assessed in order to verify that it is not regionalized, as suggested by our preliminary results. The aim is to prove that the reduction of total hindbrain length does not result from a lower proliferation or a higher apoptosis rate in the most affected rhombomeres (r3 and r5).
- The relation between the downregulation of *erm* level and the decreased activity of element C will be investigated by (i) assessing the phenotype of morpholinos etv5a/erm/pea3 on C activity, (ii) identifying putative binding sites on element C that mediate the effect. No conserved Ets binding sites could be found; however, we are currently testing the involvement of a candidate transcription factor, sp5-like, as it was shown to bind element C and mediate Fgf actions in other contexts.

DISCUSSION

L'objet premier de cette thèse est de décrypter les liens entre des processus transcriptionnels et le développement d'un organe. Le modèle de développement choisi est la morphogenèse du cerveau postérieur des Vertébrés, le rhombencéphale. Du début des années 90 au milieu des années 2000, le rôle du facteur de transcription Krox20 dans la morphogenèse du rhombencéphale a été décrit en détail, par le biais d'études en perte et en gain de fonction. Une étude fondatrice publiée en 2006 a permis de poser les bases moléculaires du contrôle transcriptionnel de l'expression de *Krox20*, en décrivant les élément cis-régulateurs (*enhancers*) de *Krox20* et leur activité (Chomette et al., 2006). À travers ce travail de thèse, nous avons voulu établir le lien entre l'activité des enhancers de *Krox20* et la morphogenèse du rhombencéphale. Ce projet est d'autant plus prégnant que l'étude de 2006 a identifié trois enhancers dont les activités sont distinctes et se répartissent en deux groupes : une activité de démarrage de l'expression (éléments B et C) et une activité d'autorégulation (élément A). Dès lors, la question de l'interaction fonctionnelle entre ces enhancers et des implications pour la morphogenèse du rhombencéphale se pose. Dans notre étude, nous n'abordons que les interactions génétiques entre les enhancers, passant sous silence les interactions physiques régulées au niveau chromatinien.

Chaque chapitre de l'étude comprend deux temps : la définition d'un phénotype important, à l'origine d'un défaut de morphogenèse du rhombencéphale, puis la recherche des mécanismes transcriptionnels et des acteurs qui le sous-tendent. Ainsi, le chapitre premier aborde le rôle de la signalisation Fgf dans la définition du nombre de cellules *Krox20*$^{+}$, donc de la taille des rhombomères. Dans le chapitre 2, le rôle de l'élément A est étudié au regard de ce même phénotype de taille des rhombomères. Enfin, le chapitre 3 apporte un éclairage sur l'interaction entre les Fgfs et les activités de A et C dans le positionnement des frontières r2/r3 et r3/r4. Les principaux résultats de ces travaux sont discutés ci-dessous, puis intégrés à un modèle général de développement de la région r3-r4.

1. Le réseau transcriptionnel du gène *Krox20* : deux modules en interaction pour le contrôle du destin Krox20^{+}.

La découverte des trois éléments régulateurs contrôlant l'expression de *Krox20* dans le rhombencéphale a permis de postuler l'existence de deux phases temporellement distinctes dans l'expression de *Krox20* : une phase courte de démarrage (initiation) et une phase d'autorégulation permettant d'amplifier et de prolonger l'expression. Dans le chapitre 2 de cette thèse, nous démontrons l'existence de cette expression bi-phasique chez le poisson-zèbre en comparant le niveau d'expression de *krox20* dans des embryons sauvages et des embryons mutants *krox20*$^{-/-}$,

FIGURE 1

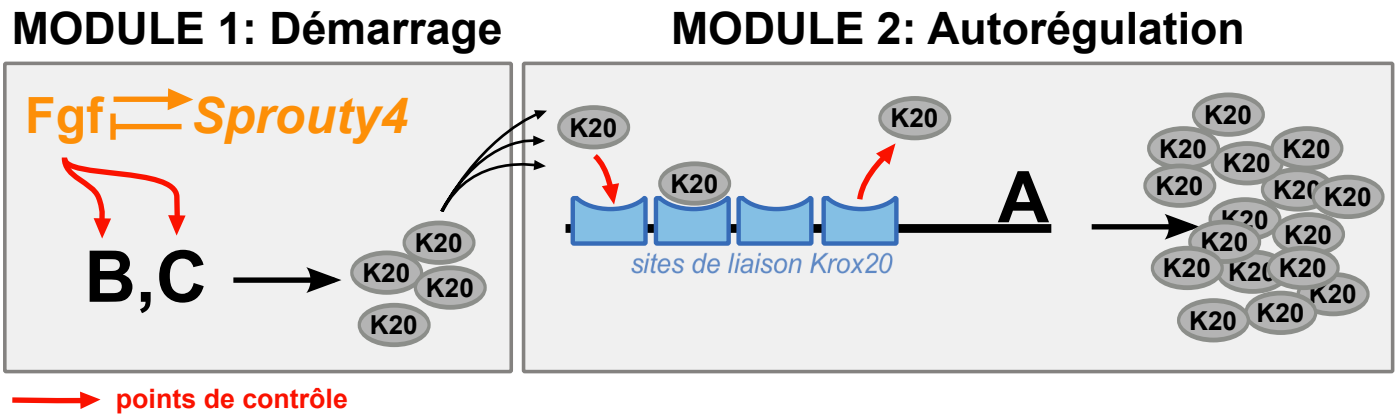

Figure 1 - Le réseau transcriptionnel contrôlant l'expression de *Krox20*

L'expression de *Krox20* est contrôlée par deux modules transcriptionnels connectés : le module de démarrage/initiation qui fournit une quantité réduite de protéines Krox20 et le module d'autorégulation qui s'active uniquement si le nombre de protéines initiales est suffisant. Chaque module possède des points de contrôle génétique : le niveau d'activité des enhancers B et C, dépendant de la signalisation Fgf; la dynamique d'association/dissociation des protéines Krox20 sur l'élément A.

dépourvus d'autorégulation. L'initiation produit des ARNm de 0 à 3 ss ; l'autorégulation amplifie le niveau d'ARNm d'un facteur 2, prolonge l'expression à un haut niveau jusqu'à 8 ss et régule son déclin jusqu'à 25 ss. Vu la conservation de la segmentation du rhombencéphale entre le poisson-zèbre et la souris, vu la conservation de la dynamique d'expression de *Krox20* et du phénotype mutant *Krox20*$^{-/-}$, nous formulons l'hypothèse que les résultats obtenus chez le poisson-zèbre s'appliquent à la souris.

Nous montrons chez la souris que la phase d'autorégulation est entièrement contrôlée par l'élément A, que les cellules *Krox20*$^{+}$ ne sont pas maintenues lorsque A est soustrait au génome de souris, ainsi que la majorité des cellules *EphA4*$^{+}$. Ceci permet de définir le destin cellulaire Krox20^{+} par l'activation de la boucle d'autorégulation. Dès lors, le destin Krox20^{+} est contrôlé par un réseau transcriptionnel impliquant deux modules (Fig. 1): un module d'initiation produisant des protéines Krox20 dont le nombre détermine l'activation du second module : l'autorégulation. Chaque module est représenté physiquement par des éléments régulateurs bien identifiés : B et C pour l'initiation, respectivement dans r5 et r3, et A pour l'autorégulation. Ce réseau présente deux points de contrôle : le niveau d'initiation que nous montrons être dépendant de la signalisation Fgf et la dynamique de liaison des protéines Krox20 sur l'élément A. Cette dynamique doit permettre à la boucle d'autorégulation de se maintenir. D'ailleurs, nous proposons qu'une rupture dans cette dynamique de liaison explique le déclin de l'expression de *Krox20* à partir de 8 ss.

Dans le premier chapitre de cette thèse, nous révélons l'importance d'un contrôle fin du niveau de la signalisation Fgf. Nous proposons que les gènes *Sprouty*, *Sprouty4* en particulier, contribuent à la précision et la robustesse du niveau de Fgf en contrôlant une boucle cellule-autonome de rétrocontrôle négatif : les cellules répondent aux signaux extracellulaires Fgf en activant l'expression de *Sprouty4* qui, en retour, inhibe la voie MAP/Kinase. De la sorte, plus le nombre de récepteurs FGFR activé est grand, plus la sortie (*output*) de la voie MAPK est réduite. Nous prédisons, sans le démontrer ici, que le système atteint un état d'équilibre qui dépend principalement du coefficient d'inhibition de MAPK par *Sprouty4* et non du nombre de FGFR activés. Le système devient donc robuste face aux fluctuations de la quantité de ligands Fgf.

Le rôle de la signalisation Fgf dans le contrôle de l'initiation de *Krox20* est aussi illustré par la différence de comportement entre r3 et r5 face à une inhibition de la voie. r3 est systématiquement moins affecté que r5. Pour expliquer cela, nous avons comparé la dépendance aux Fgfs des éléments initiateurs de r3 (principalement C) et de r5 (B). Des lignées transgéniques *cC::GFP* (chapitre 3) et *cB::GFP* (chapitre 1) ont été obtenues et le niveau d'activité des transgènes a été comparé après traitement au SU5402 (résultats non publiés) : l'élément B est plus sensible

que l'élément C à la baisse de signalisation Fgf. En présence d'une même quantité de SU5402, le nombre initial de protéines Krox20 produites est donc inférieur dans r5 que dans r3, d'où un r5 plus affecté en taille.

2. Rôle de l'élément A : une démonstration hors du commun.

Avant de détailler le fonctionnement du réseau *Krox20* à l'échelle moléculaire, revenons sur l'approche que nous avons utilisée pour définir le rôle de l'élément A dans la morphogenèse du rhombencéphale.

L'activité d'un élément cis-régulateur révélée par lignée transgénique rapportrice n'est pas suffisante pour définir son rôle *in vivo*, notamment parce que la séquence régulatrice se trouve hors de son contexte génomique et le plus souvent en amont d'un promoteur hétérologue. Pour tester directement le rôle d'un élément régulateur, la méthode de choix est la délétion par recombinaison homologue dans le génome murin. Cette approche présente un risque majeur, la redondance avec d'autres séquences régulatrices. Plusieurs études confirment que ce risque se vérifie (Kurokawa, 2004; Montavon et al., 2011), d'où le faible nombre d'articles relatant des délétions d'éléments régulateurs.

Nous montrons dans le chapitre 2 que la délétion de l'élément A (A-KO) aboutit à l'extinction prématurée de l'expression de *Krox20*, confirmant que les 465 paires de bases correspondantes sont nécessaires au maintien de *Krox20*, qu'aucune autre séquence du génome murin est redondante avec l'élément A et qu'aucune autre boucle d'autorégulation indirecte ne permet à *Krox20* de se maintenir. Pour montrer que ce défaut de maintien de *Krox20* est uniquement lié à un défaut de boucle d'autorégulation (et non par exemple à un niveau d'initiation plus faible), nous avons imaginé une expérience de sauvetage où nous rétablissons une boucle d'autorégulation indirecte, impliquant les variants mutants de A et *Krox20*, notés A* et *Krox20**. L'obtention de ces variants est décrite en détail dans le chapitre 4, en annexe. L'établissement de cette boucle de sauvetage permet en effet de sauver le phénotype mutant. Ceci suggère que le niveau d'initiation n'est pas affecté dans le mutant de l'élément A, que seule la boucle d'autorégulation est responsable du phénotype et que par la même, la boucle est suffisante pour le maintien de l'expression de *Krox20*. Cette expérience de sauvetage permet de tirer une autre conclusion, plus générale. Le sauvetage est basé sur un changement du code de reconnaissance entre Krox20 (clé) et A (serrure), puisque les doigts de Krox20 ont été modifiés pour donner Krox20* et les sites de l'élément A ont été mutés pour donner A*, le tout pour établir un nouveau code de reconnaissance, entre Krox20* et A*. Le fait que le sauvetage fonctionne signifie que A* a bien été activé *in vivo*. Or cette activation ne peut être le fait que d'une liaison

directe avec Krox20* puisque A* est fonctionnellement inerte (ceci a été vérifié en transgenèse murine). Puisque la liaison entre Krox20* et A* est directe, celle de Krox20 et A l'est aussi. Certes, nous doutions peu de la véracité de cette conclusion compte tenu des résultats *in vitro*, mais l'avancée mérite d'être notée car il s'agit de la première démonstration formelle de l'activation d'un enhancer par liaison directe d'un facteur de transcription chez les vertébrés. La plupart des études s'attèlent à démontrer la liaison du facteur à l'ADN *in vivo* par ChIP, confirmant que la liaison est directe par des analyses *in vitro*, et testent l'activation de l'enhancer en transgenèse après avoir muté les sites de liaison candidats. Tout ces arguments indirects sont avantageusement remplacés par notre expérience de sauvetage impliquant le système A*/Krox20*. Enfin, une toute autre application de ce système est son utilisation en tant que modèle de biologie synthétique, pour l'étude de l'autorégulation de *Krox20* dans des cellules du rhombencéphale sans altérer leur identité, puisque *Krox20** n'active pas les cibles de *Krox20*. Pour se faire, des lignées de poissons transgéniques *hsp:mKrox20*$^{*}_{HA}$* et *A*::mKrox20*-GFP* sont en cours d'obtention.

Dans ce travail de thèse, nous n'exposons que les résultats les plus immédiats concernant le mutant de l'élément A. Le reste de l'analyse est en cours dans le laboratoire, avec notamment les deux pistes suivantes :

- quel est le devenir des cellules qui ont initié *Krox20*, mais ne l'ont pas maintenu ? Cette question est à double lecture selon que l'on imagine le destin des cellules à court terme, dans le rhombencéphale, ou bien à plus long terme lorsqu'elles deviendront des neurones. Dans le premier cas, deux possibilités non exclusives sont envisagées. Les cellules peuvent entrer dans un processus d'apoptose ou bien être reprogrammées en cellules des rhombomères pairs. Chez le mutant *Krox20*$^{-/-}$, les deux phénomènes ont lieu : les cellules sont d'abord reprogrammées puis éliminées à travers un mécanisme de contrôle de la taille des rhombomères pairs (Voiculescu et al., 2001). Le traçage génétique des cellules A-KO de r3 et r5 permettra de distinguer ces deux possibilités. Un début de réponse est fourni par les deux domaines restreints *EphA4*$^{+}$, maintenus chez le mutant A-KO de part et d'autre de r4. Ces cellules sont donc *EphA4*-positives mais *Krox20*-négatives, suggérant que *Krox20* a pu initier son programme de spécification dans ce nombre restreint de cellules. En utilisant d'autres marqueurs, nous interrogerons l'identité r3 ou r5 de ces cellules, pour savoir si la totalité du programme transcriptionnel *Krox20* a pu être mis en place. Au delà du destin des cellules A-KO dans le rhombencéphale, leur identité neuronale ultérieure sera étudiée. Vu la complexité anatomique des dérivés neuronaux de r3 et r5, nous nous concentrerons dans un premier temps sur les motoneurones. Des résultats préliminaires

indiquent d'ores et déjà que l'organisation des motoneurones est affectée par la mutation de l'élément A, d'une manière sensiblement différente du mutant *Krox20*$^{-/-}$ (Schneider-Maunoury et al., 1997).

- la délétion de l'élément A fournit finalement un système unique chez la souris pour étudier l'importance de la durée d'expression d'un gène de spécification. En effet, chez le mutant, *Krox20* est exprimé moins longtemps. Quelles sont les conséquences de cette courte expression en terme de spécification ? Tous les dérivés neuronaux sont-ils présents, mais en nombre moindre (dans ce cas, la durée d'expression aurait un rôle quantitatif) ? Ou bien seules quelques populations de neurones sont-elles présentes, suggérant que *Krox20* spécifie les types neuronaux les uns après les autres ? Ces questions se heurtent à nouveau à la difficulté de cartographier les dérivés neuronaux du rhombencéphale.

Les études décrites dans les deux alinéas précédents peuvent être compliquées par la variabilité phénotypique des mutants A-KO. Cette variabilité n'est pas nette entre E8.5 à E9.5 à travers les patrons d'expression de *Krox20* et *EphA4*. Mais à P21, nous nous apercevons qu'à peu près 50% des mutants sont morts, soit pendant l'embryogenèse, soit pendant les trois premières semaines de vie. Les mutants survivants n'ont pas de phénotype apparent –si ce n'est une taille légèrement amoindrie à des âges avancés– et sont fertiles. Ceci indique que le phénotype *Krox20* ou *EphA4* à E8.5 représente un cas limite pour la survie des animaux. Chez ceux qui survivent finalement, la neurogenèse a probablement pu avoir lieu dans des proportions plus importantes. La variabilité phénotypique provient vraisemblablement de l'initiation de *Krox20*, plus ou moins longue et soutenue selon les individus. D'où le rôle essentiel de l'élément A dans l'homogénéité de la réponse transcriptionnelle. Les mécanismes moléculaires qui contrôlent ce processus sont discutés ci-dessous.

3. Fonctionnement du réseau transcriptionnel *Krox20* : entre paillasse et ordinateur

Pour décrire expérimentalement le fonctionnement du réseau *Krox20* (Fig. 1) à l'échelle moléculaire, il faut notamment lier sa réponse transcriptionnelle à l'occupation de chaque site Krox20 de l'élément A. L'unique approche *in vivo* dans ce cas est le ChIP mais elle se prête peu à des études dynamiques, sa résolution est insuffisante au regard des courtes distances génomiques qui séparent chaque site (entre 10 et 100 pb), et elle ne saurait renseigner sur le comportement de cellules uniques. D'où notre dévolu sur une approche computationnelle. Nous avons construit un modèle *ab initio* prenant en compte la régulation du niveau d'initiation, l'architecture de l'élément A et l'interaction entre les phases d'initiation et d'autorégulation. Par ailleurs, nous avons choisi un modèle de nature stochastique d'une part parce qu'il a été démontré que la réponse

transcriptionnelle à un signal d'induction est stochastique (Kepler and Elston, 2001), d'autre part parce que nous voulions décrire l'évolution du réseau au cours du temps et non simplement à l'équilibre. Ceci impose de résoudre les interactions dans un environnement contenant très peu de molécules Krox20, une situation qui ne peut être décrite de manière fiable par une représentation déterministe.

La première hypothèse que nous voulions tester avec ce modèle est que le réseau transcriptionnel *Krox20* produit deux états stables à l'échelle cellulaire : soit *Krox20*-positif, soit *Krox20*-négatif. Il s'agit alors d'un système bistable. Cette hypothèse provient d'une expérience chez le poisson-zèbre montrant qu'une population de cellules soumise à une stimulation par l'apport de *Krox20* exogène présente une distribution bimodale, c'est-à-dire qu'une partie des cellules répond en activant A, l'autre partie en ne l'activant pas. Ce résultat laissait supposer que le comportement de cellules uniques est « digital », sur le mode tout-ou-rien, par opposition à un comportement analogique, graduel, proportionnel à l'intensité de stimulation. Autrement dit, les cellules ne peuvent se trouver quand dans deux états. Le comportement digital des cellules est souvent associé à l'existence d'une forme de rétrocontrôle positif, qui n'est cependant pas suffisante pour que les deux états soient stables dans le temps. Cela dépend aussi des paramètres du système, i.e. dans notre cas, des constantes d'affinités de Krox20 pour ses sites, de la vitesse de dégradation, de la quantité de protéines produites pour chacune des phases, etc. L'approche computationnelle donne accès à ces paramètres.

Dans cette étude, nous présentons une solution au modèle qui se conforme à tous nos résultats expérimentaux et à partir de laquelle nous pouvons décrire un phénomène bistable à l'échelle cellulaire et moléculaire : à l'équilibre, les cellules contiennent ou ne contiennent pas de protéines Krox20, selon que leur élément A est activé (c'est-à-dire lorsque quatre protéines Krox20 y sont liées) ou inactif (aucune protéine Krox20 liée). Cette bistabilité provient de la probabilité nulle qu'ont les états intermédiaires de l'élément A d'exister et ce exclusivement en raison de la coopérativité de liaison entre les protéines Krox20. La bistabilité de l'élément A sous-tend le choix binaire offert aux cellules du rhombencéphale, entre le destin r3/r5 (*Krox20*-positif) et le destin *Krox20*-négatif. Est ainsi mis en évidence un effet interrupteur dans l'allocation du destin *Krox20* (*cell-fate switch*). Le modèle permet de retrouver les caractéristiques premières d'un effet interrupteur bistable (Wang et al., 2009) : l'impossibilité pour une cellule de changer de destin une fois qu'elle s'est engagée dans une voie (phénomène d'hystérèse) et l'effet de ralentissement critique (*critical slowing-down effect*).

La bistabilité de l'élément A justifie son rôle dans la définition du nombre de cellules *Krox20*$^{+}$: lorsque le niveau d'initiation est faible, un nombre moins important de cellules peuvent,

statistiquement, passer le seuil d'activation de A et donc « choisir » le destin *Krox20*$^{+}$. Dès lors, l'élément A conditionne la morphogenèse du rhombencéphale dans l'espace, tout autant que dans le temps comme démontré par la perte d'expression de *Krox20* dans le mutant A-KO.

Un autre enseignement de ce modèle est la robustesse de la boucle aux variations du niveau d'initiation. Cette robustesse explique l'absence de phénotype chez les embryons de poisson ou de souris hétérozygotes. Par ailleurs, elle implique que le niveau de *Krox20* se maintient au cours du temps. Pour expliquer le déclin de l'expression de *Krox20*, de 8 ss à 22 ss, il faut donc imaginer un changement de paramètre. Nous proposons qu'un simple ralentissement de la dynamique de liaison de Krox20 à l'élément A suffise à expliquer ce déclin. Durant cette phase, la pente du déclin, donc la durée d'expression de *Krox20* dépend d'un phénomène invisible jusque là : la synergie qui existe entre les protéines Krox20 liées à l'élément A pour recruter la machinerie transcriptionnelle, dont l'ARN polymérase PolII. La durée d'expression de *Krox20* dépend du niveau de synergie.

Notre étude suggère fortement que notre solution au modèle implique un comportement bistable. Cependant, nous ne le démontrons pas de manière définitive car nous n'avons pas encore trouvé le moyen d'analyser notre modèle, c'est-à-dire de résoudre notre système d'équations pour dériver une formule analytique décrivant tout le système à l'équilibre. C'est ce à quoi nous nous emploierons dans un futur proche, en cherchant des simplifications possibles au modèle. Nous pourrons ensuite réaliser une analyse de bifurcation, c'est-à-dire rechercher les transitions spontanées du système, d'un état à un autre, et donc définir les états stables. Nous pourrons tester la « qualité » des états stables à travers une analyse de phases (*phase-plane analysis*), leur robustesse vis-à-vis de fluctuations et définir les valeurs clés de paramètres qui assurent la bistabilité du système (*parameter sensitivity analysis*).

Enfin, avec ce modèle, nous décrivons une réponse digitale principalement basée sur la coopérativité de liaison entre les protéines Krox20. Cette situation rappelle le cas de l'embryon de Drosophile chez qui la protéine Bicoid lie les éléments régulateurs de ses cibles, notamment *hunchback* de façon coopérative (Burz et al., 1998; Crauk and Dostatni, 2005; Lebrecht et al., 2005; Gregor et al., 2007). Il en résulte la définition de frontières bien délimitées. Un mécanisme comparable pourrait définir la position de la frontière r3/r4 dans le rhombencéphale des Vertébrés.

4. Le positionnement de la frontière r3/r4 est indépendant d'un effet morphogène des Fgfs.

Le réseau transcriptionnel décrit ci-dessus prévoit que le niveau d'initiation de *Krox20* et la bistabilité de l'activation de A définissent le nombre de cellules *Krox20*$^{+}$. Le chapitre 3 montre que l'interaction de ces deux propriétés est aussi responsable du positionnement de la frontière r3/r4.

Nos résultats suggèrent que l'élément C, principal initiateur dans r3, présente un profil régionalisé le long de l'axe antéro-postérieur (A-P) : le niveau est nul en amont de la frontière pre-r2/pre-r3, puis l'activité s'établit en gradient depuis la frontière pre-r2/pre-r3 où elle est forte, jusqu'à pre-r5 où elle disparaît. Ces résultats ont été obtenus grâce à trois lignées transgéniques indépendantes. Nous proposons que l'interaction entre le gradient d'activité de C et le seuil d'activation de A définisse la frontière entre un territoire *Krox20*-positif antérieur et un territoire *Krox20*-négatif postérieur. Nous montrons par ailleurs que la signalisation Fgf joue un rôle de rhéostat sur le profil d'activité de C, et que ceci suffit à expliquer la perte de cellules *Krox20*$^{+}$ en cas de perte-fonction Fgf ou le gain de cellules *Krox20*$^{+}$ en cas de gain-fonction Fgf. Ces effets sur le nombre de cellules *Krox20*$^{+}$ ont toujours lieu en faveur ou au détriment de r4 et non r2, puisque la position de la frontière r2/r3 est insensible aux perturbations de la voie Fgf. Ceci s'explique par la limite antérieure très nette du profil d'activité de C.

En marge d'un effet rhéostat, nous décrivons une activité morphogénétique de la signalisation Fgf sur ses effecteurs ppERK et *erm*. Mais cette activité ne permet pas d'expliquer la modification de positions des frontières. Dès lors, les Fgfs ne sont pas une source d'information positionnelle nécessaire au positionnement de la frontière r3/r4. L'information provient en revanche des mécanismes responsables de l'activation C au niveau de pre-r2/pre-r3 et de ceux qui façonnent son gradient d'activité.

Le corollaire à cette étude est l'existence d'un équilibre entre le nombre de cellules de r4, *Hoxb1*-positives, et le nombre de cellules de r3. Selon le niveau de la signalisation Fgf, l'équilibre est perturbé, en gain-de-fonction à la faveur de r3, en perte-de-fonction à la faveur de r4. Ce résultat est confirmé dans des embryons de poissons mutants *krox20*$^{-/-}$, où le territoire *hoxb1a*$^{+}$ est visiblement élargi (Fig. 2). Les règles de la régulation réciproque entre *Krox20* et *Hoxb1* sont détaillées ci-dessous.

FIGURE 2

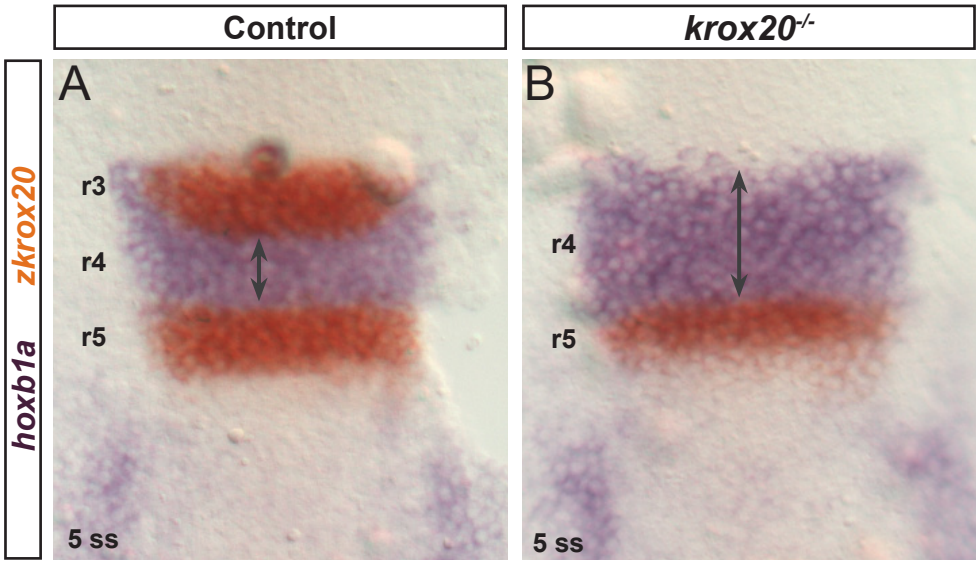

Figure 2 - Le territoire r4 (*hoxb1a*$^{+}$) est élargi dans le mutant *krox20*$^{-/-}$, au détriment de r3 (*krox20*$^{+}$)

Hybridations *in situ krox20* (orange) et *hoxb1a* (violet) sur embryons de poisson-zèbre mutants *krox20*$^{-/-}$ au stade 5ss. A ce stade, r3 est absent chez le mutant *krox20*$^{-/-}$, et le territoire *hoxb1a*$^{+}$ s'étend antérieurement. Expérience réalisée par Charlotte Labalette.

FIGURE 3

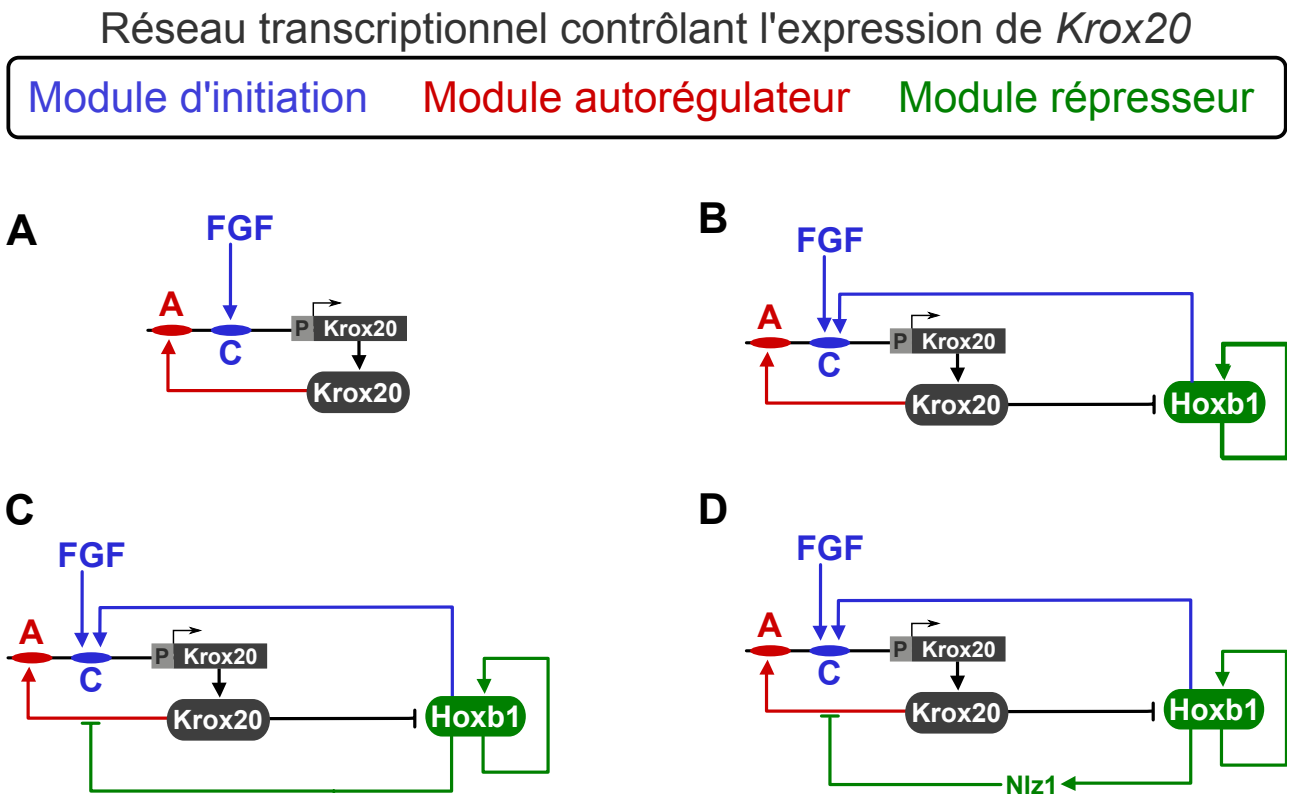

Figure 3 - Enrichissement du réseau transcriptionnel contrôlant l'expression de *Krox20*

(A) Le réseau présenté et défendu dans ce travail de thèse. **(B)** L'activation de *Krox20* par *Hoxb1* a été démontrée en 2008 (Wassef *et al.*, 2008) et l'inhibition de *Hoxb1* par *Krox20* en 2006 (Garcia-Dominguez *et al.*, 2006). Le mécanisme est connu mais on ne sait pas si l'inhibition intervient au niveau de l'initiation de *Hoxb1* ou sur sa boucle d'autorégulation. **(C)** Charlotte Labalette a démontré récemment que *Hoxb1* inhibe en retour l'expression de *Krox20* en réduisant l'efficacité de sa boucle d'autorégulation (non publié). **(D)** Charlotte montre de surcroît que le facteur Nlz1 chez le poisson-zèbre est nécessaire à cette inhibition. Le mécanisme moléculaire précis est à l'étude.

FIGURE 4

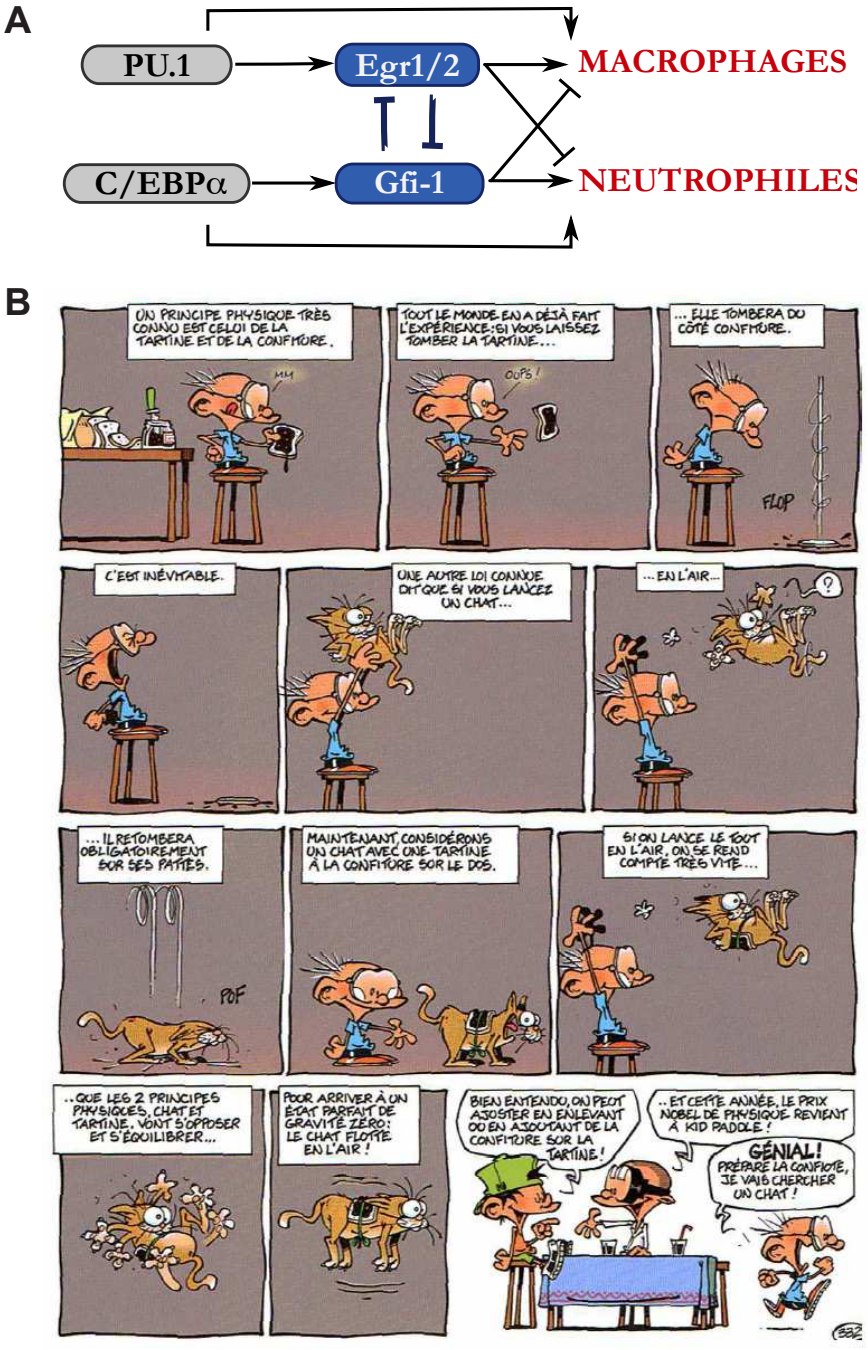

Figure 4 - Le choix de lignage entre les macrophages et les neutrophiles passe par un état «métastable»

(A) Le réseau transcriptionnel contrôlant les lignages antagonistes macrophages et neutrophiles. **(B)** Illustration métaphorique de la notion d'état métastable, à travers le paradoxe bien connu du «Chat et de la Tartine». L'état métastable est ici représenté par l'état de gravité zéro (issue de la bande dessinée Kid Paddle, Album n°9, Editions Dupuis, 2004).

5. Développement de la région r3-r4 : les lignages *Krox20* et *Hoxb1* co-régulés.

Le facteur de transcription à homéodomaine Hoxb1 a été identifié comme activateur de l'élément initiateur C de Krox20 (Wassef et al., 2008). Par ailleurs, *Krox20* inhibe l'expression de *Hoxb1* par un mécanisme indirect : lorsqu'elle est présente en grande quantité, la protéine Krox20 lie et séquestre un activateur de *Hoxb1*, PIASxß (Garcia-Dominguez et al., 2006). Ce mécanisme a été proposé pour expliquer l'absence de co-expression de *Krox20* et *Hoxb1*, la séparation nette des deux lignages et donc l'intégrité des rhombomères 3 et 4. Dès lors, le réseau transcriptionnel contrôlant l'expression de *Krox20* s'étoffe pour intégrer le gène *Hoxb1* (Fig. 3A,B).

Récemment, un processus d'inhibition réciproque, de *Hoxb1* envers *Krox20*, a été découvert par Charlotte Labalette au laboratoire (non publié): par des expériences de perte et de gain-de-fonction, Charlotte démontre en effet que *Hoxb1* inhibe l'activité de l'élément A (Fig. 3C). Le mécanisme d'inhibition de l'élément A par *Hoxb1* est à l'étude. On sait d'ores et déjà qu'il implique chez le poisson-zèbre le facteur à doigts-à-zinc *nlz1*, dont l'expression est renforcée dans r4 (Fig. 3D).

Ces résultats suggèrent que le développement des lignages antagonistes *Hoxb1* et *Krox20* est sous-tendu par une inhibition croisée et deux boucles d'autorégulation directe, celle de *Krox20* et celle de *Hoxb1*. Ce type de régulation est très classique dans le contrôle de lignages cellulaires. Il assure des réponses cellulaires stables, robustes vis-à-vis des variations environnementales (Becskei et al., 2001; Kepler and Elston, 2001).

Le contrôle des lignages *Hoxb1* et *Krox20* n'est pas sans rappeler l'exemple du système hématopoïétique abordé en introduction concernant les lignages antagonistes macrophages et neutrophiles (Cantor and Orkin, 2001; Laslo et al., 2006; Huang et al., 2007). Dans ce cas, deux déterminants primaires, PU.1 (pro-macrophages) et C/EBPα (pro-neutrophiles) activent chacun un déterminant secondaire, *Egr2* (*Krox20*) et *Gfi-1* respectivement, qui se répriment mutuellement (Fig. 4A). Avant spécification, des cellules progénitrices (*Common Myeloid Progenitor*, CMP) co-expriment PU.1 et C/EBPα à faible niveau. Cette situation crée un état dit métastable où *Egr2* et *Gfi-1* sont aussi co-exprimés à faible niveau. L'existence d'un tel état métastable est rappelée à notre intuition à travers l'exemple trivial du « Paradoxe du chat et de la tartine » (Fig. 4B). Puis le CMP s'engage dans une voie de spécification de façon apparemment stochastique pour rejoindre un des deux états stables possibles : macrophage ou neutrophile. Ce système de lignage présente donc trois points fixes, démontrés par une analyse de bifurcation : l'état indéterminé métastable, l'état stable macrophage et l'état stable neutrophile.

Il est possible de construire un modèle de lignage entre les destins r3 et r4 similaire au système hématopoïétique (Fig. 5A). Selon ce modèle, des cellules naïves expriment *Hoxb1* et un facteur

FIGURE 5

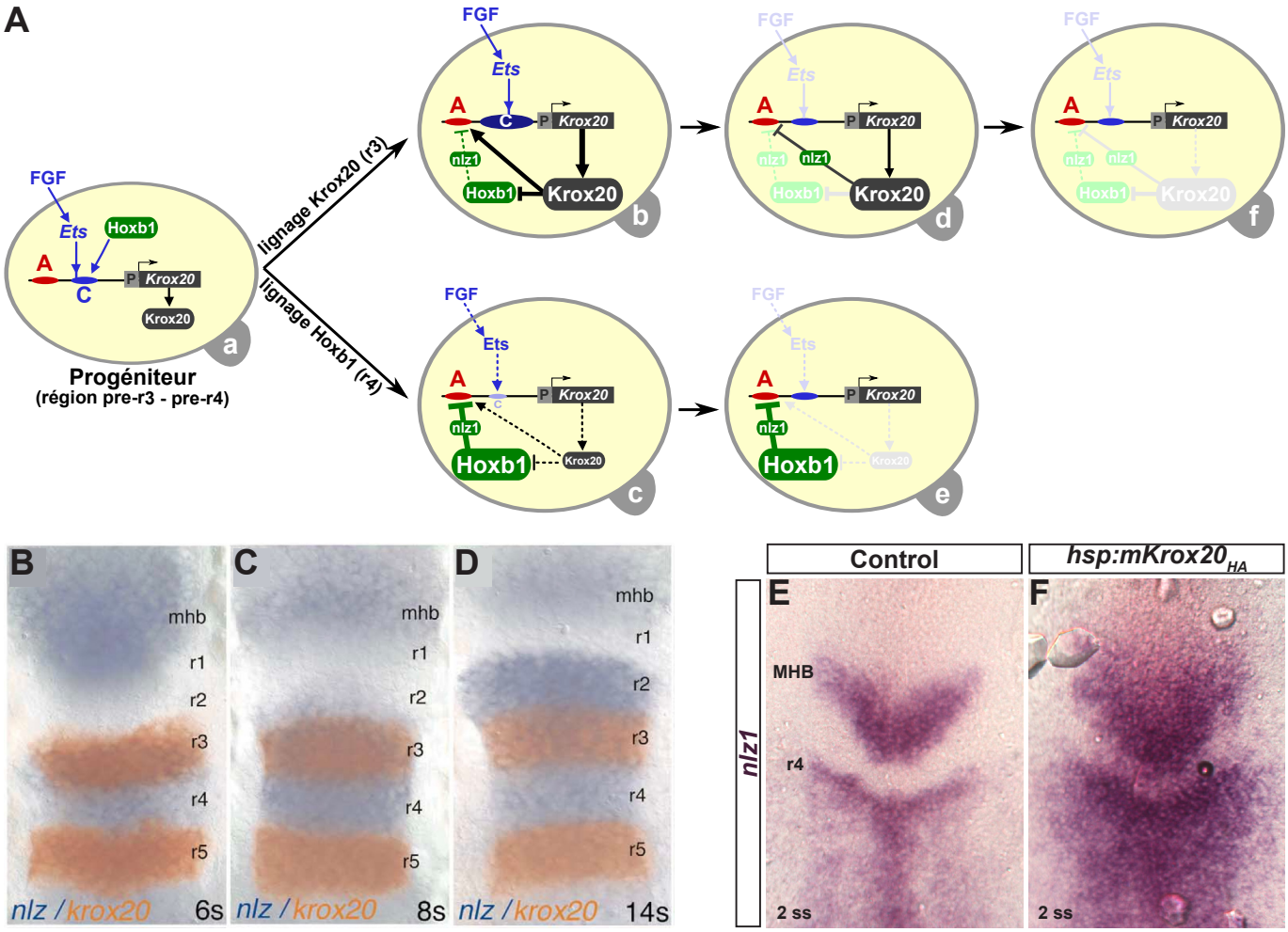

Figure 5 - Modèle hypothétique du contrôle coordonné des lignages *Krox20* et *Hoxb1*.

(A) Evolution au cours du temps d'une cellule naïve du rhombencéphale (cellule a) au moment de l'expression de *Krox20* (100% epibolie chez le poisson-zèbre, E7.75 chez la souris). La séparation entre les lignages *Krox20* et *Hoxb1* est contrôlée par deux biais régionalisés : du côté antérieur, l'activité plus forte de l'élement C (cellule b) ; du côté postérieur, l'inhibition de la boucle *Krox20* par *Hoxb1* via *nlz1* (cellule c,e). Par la suite, *Krox20* inhibe dans r3 sa propre expression en activant le gène *nlz1* (cellules d,e). **(B-D)** Hybridations *in situ nlz1* sur embryons de poisson-zèbre sauvages à 6, 8 et 14 somites. L'expression de *nlz1* colonise progressivement r3 pui r2. Données issues de Runko & Sagerström, 2003. **(E,F)** Hybridations in situ *nlz1* réalisées sur des embryons contrôles (B) et *hsp:mKrox20*$_{HA}$ (C) : la gain-de-fonction *Krox20* provoque la suractivation de *nlz1*, ce qui fournit un mécanisme possible pour expliquer l'expression de *nlz1* dans r3 puis l'exticntion de *Krox20*. Images obtenues par Charlotte Labalette.

Ets, inconnu à ce jour, activé par la signalisation Fgf. *Hoxb1* et le facteur Ets sont nécessaires à l'activation de *Krox20* (Fig. 5A, cellule a). Ces cellules naïves, progénitrices, co-expriment donc *Krox20* et *Hoxb1*. Dès lors, la cellule s'engage dans l'un des deux lignages. Contrairement au cas de l'hématopoïèse, le système r3/r4 est régionalisé donc le choix entre les deux lignages est nécessairement déterministe : des facteurs de *patterning* introduisent un biais et imposent aux cellules antérieures de s'engager vers le lignage *Krox20*$^{+}$, alors que les cellules postérieures deviennent *Hoxb1*$^{+}$. Deux biais sont envisagés. D'abord, le profil d'activité de C en gradient qui impose aux cellules antérieures d'initier *Krox20* plus fortement et, dès lors, prendre le pas sur *Hoxb1* en l'inhibant fortement (Fig. 5A, cellule b). Second biais possible, l'expression de *nlz1* à fort niveau dans les cellules postérieures, d'où une forte inhibition de *Krox20* (Fig. 5A, cellules c,e). Ces deux biais complémentaires participent à la robustesse de la régionalisation, à la séparation nette des deux lignages. Les mécanismes à l'origine du patron régionalisé de l'activité de C et de l'expression de *nlz1* restent à élucider.

Dans un système régionalisé, les réseaux de régulation à inhibition croisée participent à la formation de frontières très nettes entre les domaines d'expression des facteurs de lignages (Veitia and Nijhout, 2006). Nous proposons que ce mécanisme soit à l'œuvre pour la frontière r3/r4. De surcroît, il a été montré chez l'embryon de Drosophile que le niveau d'inhibition entre les gènes gap intervient dans la position des frontières d'expression (Jaeger et al., 2004). Dans le chapitre 3, nous proposons que la position de la frontière r3/r4 soit fixée par le gradient de C et le seuil d'activation de A, mais ceci n'exclut pas l'influence du niveau d'inhibition entre *Hoxb1* et *Krox20*.

Pour aborder ces questions –le rôle précis des biais de régionalisation, l'importance de l'inhibition croisée dans la précision de la frontière, l'impact des coefficients d'inhibitions sur la position de la frontière– nous prévoyons d'établir un nouveau modèle intégrant le rôle de *Hoxb1* dans le développement des segments r3 et r4. De la sorte, nous serons passés d'un modèle centré sur le facteur *Krox20*, présenté dans cette étude, à un modèle défini au niveau d'un réseau de gènes, impliquant *Krox20*, *Hoxb1*, *nlz1*. Cette approche *bottom-up* permet d'enrichir, étape par étape, notre compréhension des mécanismes transcriptionnels responsables du développement de la région r3-r4. À titre d'exemple, le nouveau modèle permettra de tester l'hypothèse d'un second rôle de *nlz1*, dans l'extinction de l'expression de *Krox20*. Cette hypothèse est étayée par deux arguments expérimentaux : (i) au cours du temps, le domaine d'expression de *nlz1* progresse antérieurement, et colonise r3 (Fig. 5B-D) (Runko and Sagerström, 2003); (ii) en utilisant le système gain-de-fonction *hsp:mKrox20*$_{HA}$, Charlotte Labalette a montré récemment que *Krox20* lui-même active *nlz1* (Fig. 5E,F). Ces résultats suggèrent que *Krox20* induit sa propre extinction

en activant l'inhibiteur de sa boucle d'autorégulation, tout en contrôlant la vitesse de décroissance par le recrutement concerté de la machinerie transcriptionnelle (Fig. 5A, cellules d,f). Notre modèle prédit que *nlz1* pourrait ralentir la dynamique de liaison de Krox20 à l'ADN. Cette hypothèse sera testée expérimentalement.

Au delà des relations génétiques, le réseau de gènes décrit ci-dessus peut se trouver régulé par son statut chromatinien. Dans le système hématopoïétique, le déterminant dit primaire PU.1 est un facteur de la famille Ets qui non seulement contrôle l'expression à faible niveau de *Egr2* mais agit au préalable en « pré-activant » les gènes nécessaires au lignage macrophage. Ceci a été démontré pour le locus *c-fms* (Krysinska et al., 2007). La pré-activation consiste en une réorganisation de la chromatine plaçant le gène dans un état « prêt » à être transcrit (*poised*). Dans les progéniteurs (CMP), les gènes spécifiques aux deux lignages sont dans un état chromatinien *poised*. Ainsi, les deux voies de spécification sont initialement prêtes à être démarrées. On parle de *priming* transcriptionnel. La conformation chromatinienne des gènes de lignages caractérise biochimiquement l'état métastable évoqué plus haut, et aboutit à leur co-expression. Ensuite, le déséquilibre dans l'expression des deux facteurs intervient de façon soit stochastique soit régionalisée, et conduit dans l'une ou l'autre des voies. Dans le système r3/r5, la signalisation Fgf et le facteur Ets en aval pourraient fonctionner de manière similaire : pré-activation de *Krox20* via la modification du statut chromatinien de l'élément C, puis activation par *Hoxb1*.

6. Élucubrations (qui n'engagent que leur auteur).

La segmentation du rhombencéphale est un système *a priori* idéal pour l'étude des mécanismes de spécification régionalisée : le système est conservé chez tous les modèles de Vertébrés, les lignages sont physiquement bien délimités, les facteurs de lignage sont identifiés, les réseaux de gènes qui contrôlent leur expression ont été défrichés par de nombreuses études en perte ou en gain de fonction. Pourtant, force est de constater que le nombre de publications concernant le développement du rhombencéphale est de nos jours limité, au point qu'après avoir suscité un fort engouement, le rhombencéphale se transforme en niche de recherche fondamentale. Comment expliquer ce paradoxe ? La première explication est d'ordre technique : la quantité de matériel, le nombre de cellules contenues dans chaque rhombomère est très faible (estimé entre 100 à 200 aux stades d'expression de *Krox20*). Il est donc très difficile d'obtenir une population homogène de cellules issue d'un rhombomère unique. D'où l'impossibilité de comparer les rhombomères au moyen d'études biochimiques (ChIP par exemple) ou de séquençage à haut débit. À titre d'exemple, Johan Le Men, doctorant au laboratoire, est parvenu à établir un répertoire des gènes

exprimés dans le rhombencéphale à E8.5 (par RNA-seq) mais s'est heurté à un mur lorsqu'il a tenté de réaliser la même expérience sur des rhombomères isolés. En outre, une population homogène de cellules issues de rhombomères uniques ne saurait être obtenue en culture, puisqu'aucune méthode n'a permis ni de maintenir des cultures primaires de rhombomères dans un état indifférencié, ni de les immortaliser. Au delà des difficultés techniques, le système rhombencéphale souffre de l'épuisement d'un paradigme en biologie du développement : l'approche perte et gain de fonction de gènes qui conduit à dessiner des flèches activatrices ou inhibitrices entre des facteurs. « Tout à été fait » au cours des vingt dernières années, tout à été muté, surexprimé, chez la souris, chez le poisson, chez le poulet. Certes, tous les facteurs impliqués dans la segmentation du rhombencéphale ne sont pas connus, mais la compréhension des réseaux de gènes est telle que la communauté scientifique ne s'attend plus à faire de grandes découvertes. Et pourtant, les choses commencent enfin à devenir intéressantes !

Fort de notre connaissance des gènes de la segmentation du rhombencéphale et des relations qui les unissent, il est tentant de s'interroger sur la dynamique globale du réseau. C'est ce que nous avons commencé à faire à travers cet embryon de réseau qu'est l'autorégulation de *Krox20*, destiné à s'étendre pour intégrer la régulation par *Hoxb1*. L'accès à la dynamique du réseau requiert une approche computationnelle nourrie de résultats expérimentaux. Les modèles obtenus ne sont bien sûr que des hypothèses, dont on peut défendre la vraisemblance et qui, par définition, sont valables jusqu'à preuve du contraire. Par ailleurs, notre laboratoire a choisi de s'intéresser au développement embryonnaire par le biais des processus transcriptionnels. Ceci permet de construire des modèles à l'échelle moléculaire, pour comprendre les dynamiques d'expression de gènes puis dessiner le comportement du réseau entier. Ce type d'approche, dite de « biologie des systèmes », est à la fois un aveu d'échec puisque l'expérimentaliste ne parvient pas à décrire le système dans ses moindres détails moléculaires, et un formidable outil de synthèse entre l'échelle transcriptionnelle et l'organe en développement. À noter, nous ne relatons dans ce travail que des mécanismes transcriptionnels simples, à savoir la liaison d'un facteur de transcription à l'ADN. Un autre pan de recherche s'attèle à décrire l'influence du statut chromatinien, ou la position des nucléosomes sur la transcription. Certains modèles intègrent déjà ces mécanismes épigénétiques (Kim et al., 2009). Il s'agit là d'une perspective envisageable pour notre travail. Il faudra avant tout retourner à la paillasse et vaincre les lourdeurs techniques liées à l'étude du rhombencéphale pour obtenir les données expérimentales.

ANNEXES

– Chapter 4 –

Putative role of *Krox20* non cell-autonomous activation in controlling the size of r3 and r5

M.A. Wassef*, C. Labalette *, Y.X. Bouchoucha*, C. Desmarquet, P. Gilardi-Hebenstreit, P. Charnay

IBENS, Ecole Normale Supérieure, Paris, France

INSERM U1024 – CNRS UMR 8197

Author contributions:

MW generated the *hsp:mKrox20*$_{HA}$ zebrafish line.

MW and CL performed the experiments on mosaic zebrafish embryos.

YXB worked on chimæric mouse embryos and established the A*/Krox20* system.

CD performed the mouse transgenesis experiments.

All authors collaborated to design and interpret the results.

* equal contributions

Putative role of *Krox20* non cell-autonomous activation in controlling the size of r3 and r5

INTRODUCTION

The vertebrate rhombencephalon is a valuable system to study cellular specification as cell-fate choices are turned into homogeneous morphological units, termed rhombomeres (r), from r1 to r7. The resulting segmented hindbrain later gives rise to the repeated organization of cranial nerves and neural-crest migratory paths, hence the relevance of a robust hindbrain segmentation (Lumsden and Keynes, 1989; Lumsden and Krumlauf, 1996). The size of the rhombomeres for example is found stereotypical among embryos. What are the mechanisms ensuring such robustness in controlling rhombomere size? To address this question, we focus on r3 and r5 as our laboratory is reaching a high level of understanding on their development. Rhombomeres 3 and 5 are defined by the expression of a zinc-finger transcription factor, Krox20 (a.k.a. Egr2). The size of r3/r5 can thus be recapitulated as the number of *Krox20*-positive cells. The number of *Krox20*$^{+}$ cells depends on proper expression of the Krox20 protein itself: in *Krox20*$^{lacZ/lacZ}$ knock-in mice, the expression domain of *lacZ* is smaller than the *Krox20*$^{+}$ domain in a wild-type background at the same stage. The phenotype is most prominent in r3. This suggests that the *Krox20*$^{+}$ domain normally undergoes a step of expansion and that this step is absent in the mutant (Figure 1A)(Schneider-Maunoury et al., 1993). Lineage tracing analysis of *Krox20*$^{+}$ cells further showed that r3 and r5 expand antero-posteriorly and posteriorly respectively (Voiculescu et al., 2001). Moreover, the *lacZ* domain in *Krox20*$^{lacZ/lacZ}$ is not maintained up to the expected end of *Krox20* expression, demonstrating that *Krox20* is somehow autoregulated. This autoregulation was later shown to be direct, through a cis-regulatory element termed A containing several Krox20 binding sites (Chomette et al., 2006). Moreover, gain-of-function experiments, performed by chick electroporation, revealed that *Krox20* not only self-activates in an autonomous manner but also non cell-autonomously. (Figure 1B) (Giudicelli et al., 2001). These results provide a putative mechanism for *Krox20* expansion and therefore the control of rhombomere size (Figure 1C): once initiated by the cooperation between Hoxb1 and a yet-unknown factor X, *Krox20* expression expands through a rapid recruitment of cells by non cell-autonomous activation. To confirm this model, we sought to clarify the mechanism of *Krox20* non cell-autonomous activation. Two hypotheses are envisaged. First *Krox20* activates cell-

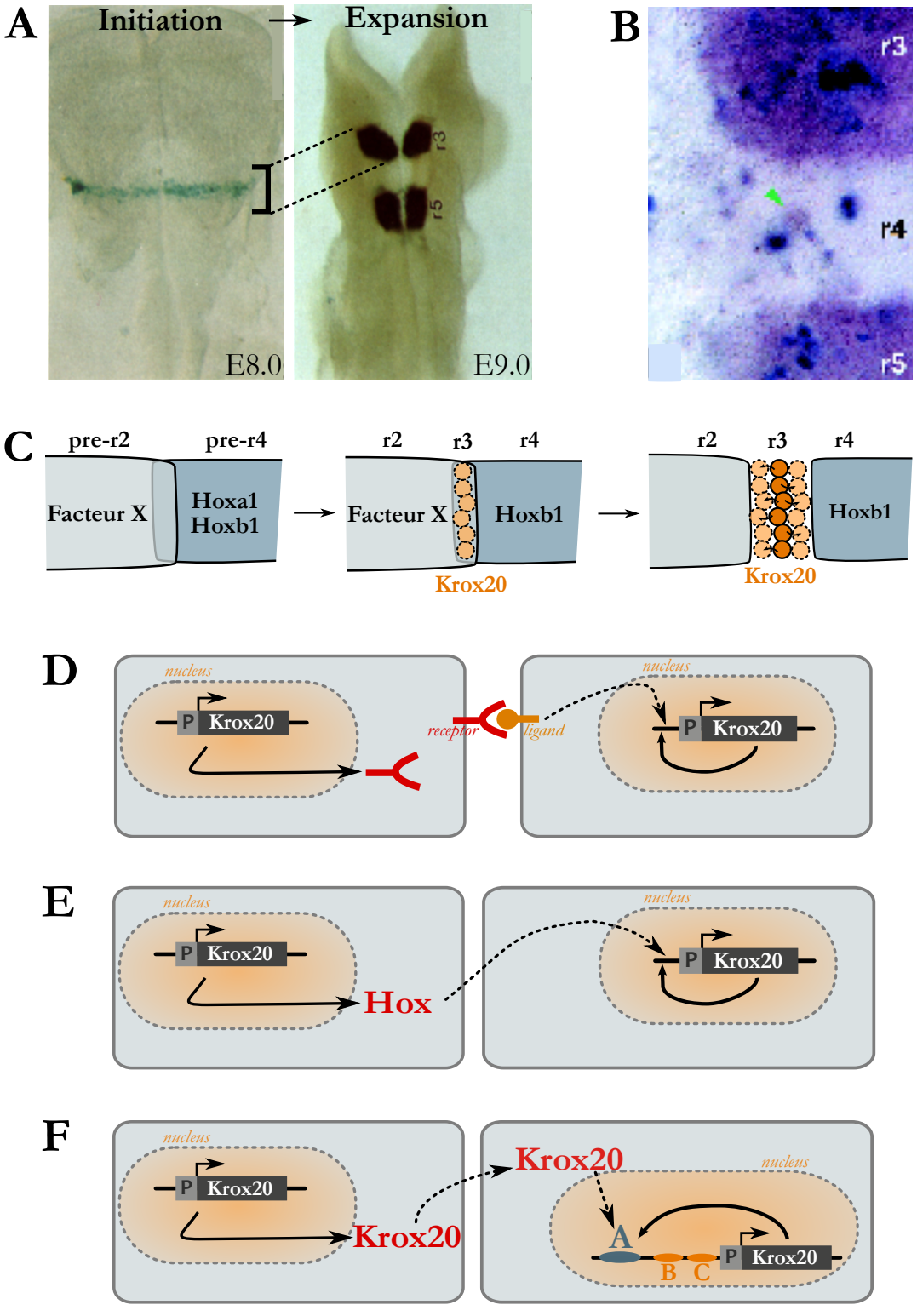

Figure 1 - Putative mechanisms underlying the expansion of Krox20 territories

(A) Mouse heterozygous *Krox20*$^{lacZ/+}$ embryos stained for ß-galactosidase, showing the expansion phase most evident in r3 between the E8.0 and the E9.0 stages. Pictures from Schneider-Maunoury *et al.*, 1993. **(B)** Flat-mount chick hindbrain after electroporation with a bicistronic vector encoding ß-galactosidase and mKrox20$_{HA}$ and subject to X-Gal staining and *in situ* hibridization against *cKrox20*. Green arrow points to a non-electroporated *cKrox20*$^{+}$ cell lying in r4, suggesting non cell-autonomous activation of the *cKrox20* locus controlled by the neighbouring *ß-gal*, *mKrox20*$_{HA}^{+}$ cell. Picture from Giudicelli *et al.*, 2001. **(C)** Model of *Krox20*$^{+}$ domain expansion based on recruitment of cells by non cell-autonomous autoregulation of *Krox20*. **(D-F)** Putative mechanisms underlying the non cell-autonomous activation of Krox20: juxtacrine signalling patway (D), intercellular transfer of a Hox intermediate (E), intercellular transfer of the Krox20 protein (F).

autonomously an intermediate target that in turn induces *Krox20* in the neighbouring cells. The intermediate target could be either a juxtacrine signalling pathway (Figure 1D) or a *Hox* gene (Figure 1E). The most relevant candidate for the former possibility is the FGF pathway as its knock-down leads to smaller rhombomeres while its upregulation leads to the reverse phenotype. Yet, the analysis and understanding of FGF role in hindbrain patterning, presented in chapters 1 and 2, are incompatible with a function in *Krox20* expansion. Concerning *Hox* genes, the hypothesis is supported by numerous studies showing that homeobox proteins are able to cross cell membranes in some contexts, including during early brain patterning (Chatelin et al., 1996; Brunet et al., 2007; Holcman et al., 2007). Moreover, *Krox20* activates *Hoxa2/b2* in r3/r5, Hoxb3 in r5 (Sham et al., 1993; Nonchev et al., 1996; Seitanidou et al., 1997) and can be activated by Hox factors in r3 (Wassef et al., 2008). Although attractive, this possibility is contradictory to the double *Hoxa1/b1* or *Hoxa2/b2* mutant phenotypes where the size of r3 and r5 is unaffected (Capecchi, 1999; Davenne et al., 1999). The second hypothesis is the intercellular transfer of Krox20 protein itself, followed by the activation of A (Figure 1F). Preliminary electroporation experiments in chick using a bicistronic vector encoding the *ß-galactosidase* and $Krox20_{HA}$ suggest that some cells devoid of ß-galactosidase (i.e. non-electroporated) contain $Krox20_{HA}$ of exogenous origin. Based on this observation, we decided to concentrate on the Krox20 transfer hypothesis to explain its non cell-autonomous activation.

In the present study, we re-investigate the non cell-autonomous activation of *Krox20* in mouse embryos using the morula aggregation technique to produce mosaic embryos in a more robust way than chick electroporation. We then address the "transfer hypothesis" in a crude manner in zebrafish before presenting a state-of-the-art strategy that has not been employed yet. The reasons for this are discussed in detail.

MATERIALS & METHODS

DNA constructs and mutagenesis

pAdRSV expression vectors containing *Krox20* and *Krox20-2ER* genomic DNA were used for ubiquitous expression under the control of the strong RSV promoter. The p1230 reporter plasmids used for chick electroporation contained the chick version of element A upstream of a the minimal ßglobin promoter/*lacZ* reporter. A:Krox20-2ER$_{HA}$ and A669:Krox20-2ERGFP vectors were generated by replacing the lacZ coding sequence in p1230 A:lacZ and A669:lacZ by Krox20-2ER$_{HA}$ and Krox20-2ERGFP cDNA respectively. Mutations within Krox20 binding sites in element A were introduced by PCR using the Phusion^{TM} Site-Directed Mutagenesis kit (Finnzyme). Finally, the hsp:mKrox20$_{HA}$ construct, dedicated to fish transgenesis, was built in a modified pTol2 vector.

Mouse lines

The Krox20^{GFP} (Vermeren et al., 2003) and 42kb:Krox20$_{HA}$ (unpublished) lines were maintained in a B6D2F1 background, while the GFPU line was kept in the OF1/Swiss background. For the generation of the A:Krox20-2ER$_{HA}$ transgenic line, inserts were extracted from the corresponding p1230 vector, purified by agarose gel electrophoresis and Elutip-d (Schleicher & Schuell) and suspended in TE (10 mM Tris pH 7.5, 0.1 mM EDTA) for microinjection. Transgenesis was performed as described previously (Sham et al., 1993). Briefly, fertilised eggs from superovulated B6D2F1 females were injected with DNA at a final concentration of 1.5 ng/µL. Injected embryos were reimplanted at the one-cell stage into pseudopregnant B6/CBA mice and allowed to develop to term. For testing the activity of A669 fragment, founder embryos were analyzed at E8.5.

Fish breeding and transgenesis

Breeding fish were maintained at 28°C on a 14-hour light, 10-hour dark cycle. The hsp:mKrox20$_{HA}$ transgenic line was obtained from embryos injected at the one-cell stage with the hsp:mKrox20$_{HA}$ pTol2 construct together with *tol2 transposase* mRNA.

Chick electroporation

Commercial fertilized eggs were incubated typically for 30h, up to stages HH8-HH10. Expression and reporter plasmids were injected into the neural tube lumen at a final concentration of 0.5 µg/µL by use of a pulled glass capillary. A drop of L15 medium (Life

Technologies) was poured onto the egg membrane and electroporation was performed with a BTX830 electroporator (Quantum) and CUY611 platinum-coated electrodes (Tr Tech) using the following parameters: four pulses of 21 V and 50 ms at a frequency of 1 Hz. Embryos were harvested in PBS 24h after electroporation, fixed in 4% PFA for 10 minutes and stained with X-Gal (Sigma).

Gel-shift experiments

The mouse Krox20 protein was expressed in BL21 bacteria using the pET3a system (Novagen). Crude extracts were prepared as previously described (Nardelli et al., 1992). DNA probes A, A728 and A669 were prepared by *HindIII-XhoI* digestion of the corresponding p1230 reporter plasmids. The fragments were dephosphorylated and radiolabeled using T4 polynucleotide kinase and [γ-^{32}P]-ATP. Labelled fragments were purified using Microspin S-200 HR Columns (GE Healthcare) and used in band-shift experiments: 2µL of Krox20 bacterial extracts were first pre-incubated on ice for 10 minutes in binding buffer (20 mM Tris-HCl pH 7.5, 50 mM KCl, 10 mM $MgCl_2$, 1 mM EDTA, 1 mM DTT) supplemented with 3 µg of polydIdC (Sigma) and 8% Ficoll. 0.5 ng of radiolabelled probe was subsequently added and the incubation was pursued for 20 additional minutes on ice. The mixture was then loaded on a 5% polyacrylamide gel and electrophoresis was performed for four hours at 14.5 V/cm in 1X TBE buffer. The gels were dried and exposed to a photographic film at -80°C.

Aggregation of mouse morula

Morula from GFPU, wild-type, 42kb:Krox20$_{HA}$ and Krox20$^{GFP/+}$ mice were collected at E2.5 by flushing the oviducts in M2 medium (Sigma). Subsequently they underwent zona pellucida removal after short treatment with Tyrode's acid (Sigma), extensive rinsing in M2 and equilibration in M16 medium (Sigma) for two hours in a 37°C/5% CO_2 incubator. The remaining healthy-looking morula were then agglutinated two by two after a short treatment of phytoagglutinin PHA-P 0.5 mg/mL (Sigma) and pursue their development by incubating overnight in a drop of M16 hanging on the cover of a 35-mm plate. Properly aggregated embryos developed up to the blastocyst stage and were reimplanted in the uterus of E2.5 B6/CBA pseudopregnant females.

Mosaic analysis in fish

Wild-type host embryos were injected at the one-cell stage with 25 pg of *histone2b:mcherry* mRNA. Donor embryos were derived from the hsp:mKrox20$_{HA}$ transgenic line and developed up to the

shield-stage stage. At this time, cells were transplanted into shield-stage host embryos, in the region that gives rise to the hindbrain. Grafted embryos were left to develop until 100% epiboly or 13 somites, subject to a 38°C heat-shock during 30-60 minutes, fixed 75 minutes later for 12 hours and processed for immunohistochemistry.

Immunohistochemistry and ß-galactosidase staining

ß-galactosidase staining on chick embryos was performed by 2-hour incubation at 30°C in a PBS solution containing 1 mg/mL X-Gal, 5 mM $K_3Fe(CN)_6$, 5 mM $K_4Fe(CN)_6$, 2 mM $MgCl_2$. Immunohistochemistry on fish and mouse embryos was performed on whole-mount and dissected neural tubes respectively. The primary antibodies used were a rabbit polyclonal anti-GFP (1:500, Molecular Probes), rat monoclonal anti-HA (1:200, Roche), rabbit polyclonal anti-DsRed (1:500, Clontech). Goat Alexa488 anti-rabbit and Donkey Cy3 anti-rat secondary antibodies (Jackson ImmunoResearch) were used at a 1:500 dilution. Embryos were flat-mounted and pictured with a Leica sp5 confocal microscope.

RESULTS

Re-investigation of the non cell-autonomous activation of *Krox20* in mouse embryos.

The traditional way to address non cell-autonomous activity during development consists in producing mosaic embryos. "Emitting" cells that provide the putative secreted factor are juxtaposed with "receiving" cells where the presence of the factor can be read-out. In mouse, mosaic embryos are generally artificial chimaeras produced either by morula aggregation or injection of ES cells into the inner cell mass of blastocysts. We chose the former technique as it avoids delicate manipulation of ES cells. To set the technique, we derived morula from wild-type and GFP^+ females (Figure 2A). Their *zona pellucida* was removed and the morula were aggregated overnight in M16 medium until the blastocyst stage. Blastocysts were reimplanted into pseudo-pregnant females and developed up to E8.5 where GFP could be immunostained to assess the level of chimærism (estimated at ~50% in figure 2A). To interrogate the non cell-autonomous activity of *Krox20*, the procedure was applied to the following genotypes: (i) the emitting cells carried the *42kb:Krox20$_{HA}$* transgene, leading to the expression of $Krox20_{HA}$ in r3/r5 as well as in few cells in r2/r4/r6 (unpublished, Figure 3A); the origin of this ectopic expression has not been identified. (ii) the receiving cells were derived from the knock-in line $Krox20^{GFP/+}$ (Vermeren et al., 2003), used as a reporter of the *Krox20* endogenous locus activation. If *Krox20* can self-activate in a non cell-autonomous manner in mouse, we expect to see GFP signal in r2/r4/r6 in cells juxtaposed to $Krox20_{HA}^+$ cells (Figure 2B, bottom part). Morula aggregation was successfully carried out using the two aforementioned genotypes (Figure 3B,B' and E,E'). Few GFP^+ cells were detected in r2/r4/r6 in contact with $Krox20_{HA}^+$ cells (Figure 3C-D, F-G), suggesting that $Krox20_{HA}$ could activate the *Krox20* locus in the neighbouring cells. However, the number of ectopic GFP^+ cells was always found low, irrespective of the embryo stage. This reveals that the efficiency of this non cell-autonomous activation is low, somehow inconsistent with the rapid, effective expansion of $Krox20^+$ domain in r3.

The same chimæric embryos were used to address the Krox20 transfer hypothesis in a direct manner (Figure 2B, upper part): we closely looked at HA signal in GFP^+ cells in r3 and r5 in order to identify directly the transfer of $Krox20_{HA}$ protein from one cell to another. We failed to see convincing overlap between HA and GFP signals in all embryos analysed (Figure 3H-H"). However, this negative finding may result from the very limited amount of $Krox20_{HA}$ being transferred.

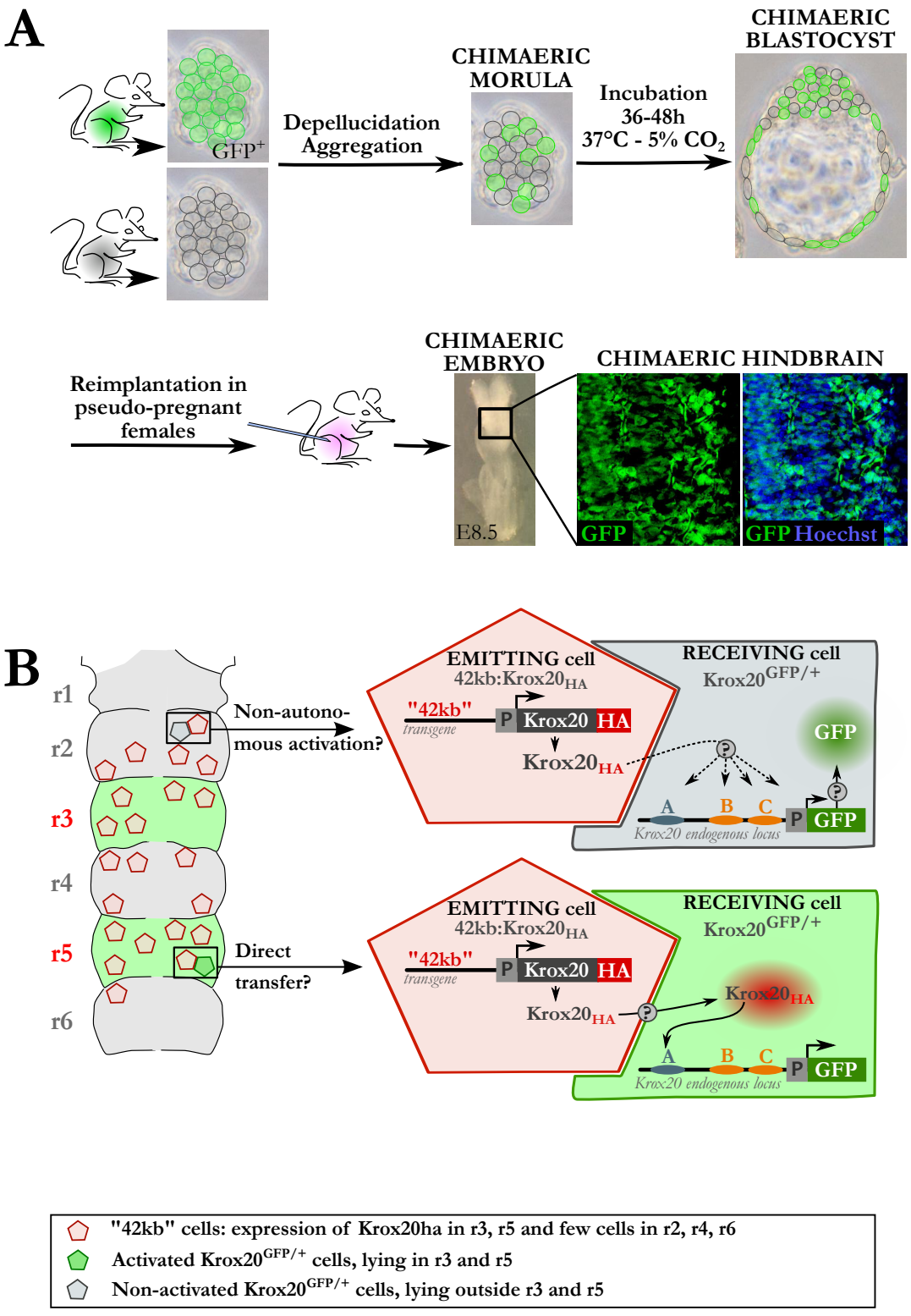

Figure 2 - Strategy to test *Krox20* non cell-autonomous activation in mouse

(A) Experimental design of mouse morula aggregation, as exemplified here with the GFP^+ (derived from the GFPU line) and wild-type cells. **(B)** Chimæric mice made of 42kb:$Krox20_{HA}$ and $Krox20^{GFP/+}$ cells allow to address two questions: in odd-numbered rhombomeres, where *Krox20* is not expressed, presence of GFP signal in non-$Krox20_{HA}$ cells reveals non cell-autonomous activation of *Krox20* locus (bottom part); in r3/r5, presence of HA signal in GFP^+ cells reveals transfer of the $Krox20_{HA}$ protein (upper part).

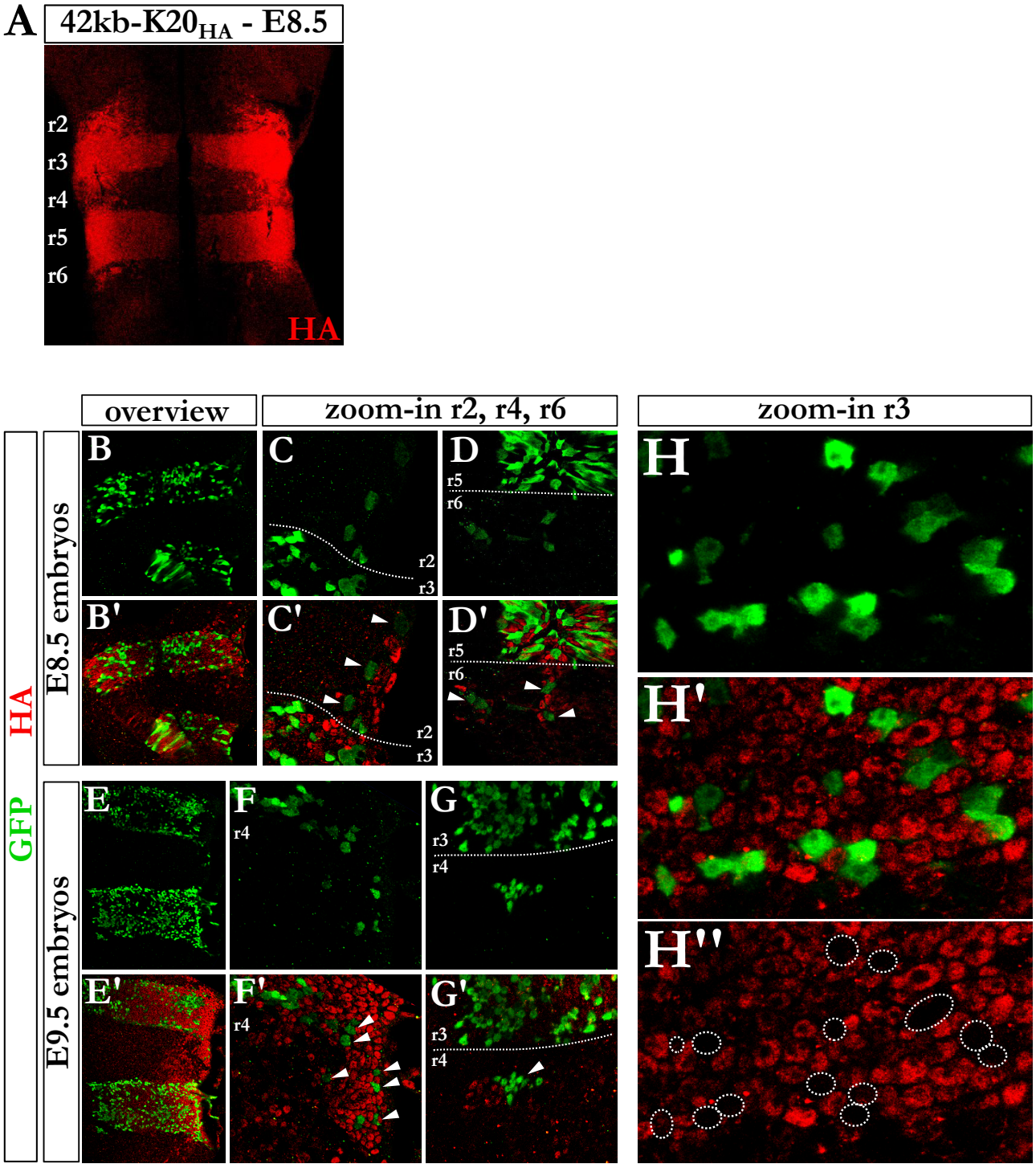

Figure 3 - Non cell-autonomous activation of *Krox20* in mouse

(A) HA staining in a 42kb:Krox20$_{HA}$ mouse embryo at late E8.5. **(B-G)** Representative confocal images of mosaic embryos made of 42kb:Krox20$_{HA}$ and Krox20$^{GFP/+}$ cells at E8.5 (B-D) and E9.5 (E-G). Arrowheads indicate *GFP*$^{+}$ cells present ectopically in even-numbered rhombomeres. (B,E) Large overviews. (C,D-F,G) Higher magnification. **(H-H")** High-magnification confocal picture of a mosaic rhombomere 3, where no HA signal could be detected in *GFP* $^{+}$cells.

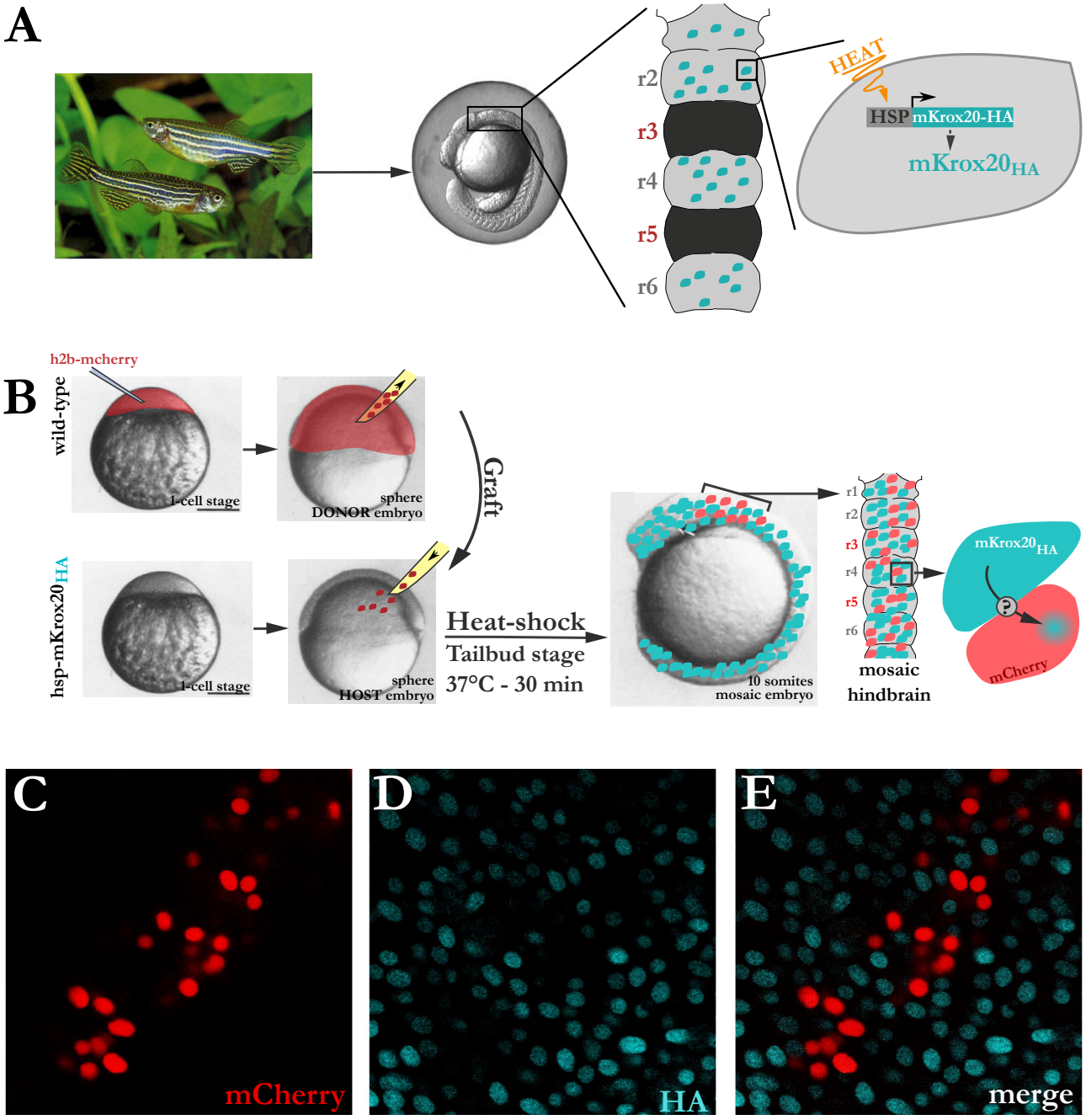

Figure 4 - Testing the intercellular transfer hypothesis in zebrafish mosaic embryos

(A) Design of the hsp:mKrox20$_{HA}$ zebrafish line: the HA-tagged mouse version of *Krox20* is expressed under the control of a heat-shock promoter and activates in turn the endogenous element A, hence the expression of *zkrox20* in the whole hindbrain. **(B)** Procedure to make mosaic embryos at the shield-stage by grafting cells from a donor (hsp:mKrox20$_{HA}$) to a host (wild-type, injected with h2b:mcherry mRNA at the one-cell stage). Such mosaics are used to challenge the transfer hypothesis by testing the presence of HA signal in *mCherry*$^{+}$ cells. **(C-E)** Results of one representative experiments showing cells in the hindbrain co-stained fro HA and mCherry. No overlap could be detected.

Exploring the "intercellular transfer hypothesis" in zebrafish embryos.

To overcome the limitation of emitting factor quantity encountered in mouse, we set and conducted a strategy in zebrafish embryos. It was based on mosaic embryos obtained by grafting the emitting cells from a donor to a host made of receiving cells. The donor embryos were derived from a newly engineered transgenic line called hsp:mKrox20$_{HA}$, where expression of an HA-tagged version of the murine Krox20 was placed under the control of the *hsp70* heat-shock promoter (Figure 4A). Efficiency of Krox20$_{HA}$ expression upon heat-shock was assessed by hybridization *in situ* and immunohistochemistry (not shown). The host was a wild-type embryo whose nuclei were stained with mCherry thanks to prior injection of *histone2b-mcherry* mRNA (Figure 4B). By grafting at the shield-stage, donor cells could be precisely targeted to the presumptive posterior brain, leading to a high-level of mosaicism in the resulting rhombencephalon. Two hours after grafting, at the tailbud stage, embryos were subject to a 38°C heat-shock during 30-60 minutes in order to trigger mKrox20$_{HA}$ expression. 75 minutes later, i.e. at a time when the level of Krox20$_{HA}$ protein peaks, embryos were processed for immunohistochemistry against HA and mCherry and pictured on a confocal microscope. No HA signal could be detected in mCherry^{+} cells in all embryos analysed (Figure 4 C-E). Similar results were obtained from embryos heat-shocked at the 13-somite stage. Enhancing the HA signal using the tyramide amplification strategy did not provide us with positive results. Altogether, this argues against the Krox20 transfer hypothesis.

Innovative, improved strategy to address the "transfer hypothesis".

The previous strategies used to tackle Krox20 intercellular transfer aimed at detecting directly the secreted species, Krox20$_{HA}$, in ectopic cells, assuming its level lies above the detection limit. We propose here a more advanced strategy where the secreted factor is detected indirectly after activating an autoregulatory loop, in r3 and r5 (Figure 5). This strategy can be conducted in either mouse or zebrafish embryos. It requires cells of two distinct genotypes derived from two transgenic lines: the emitting cells contain the *A:Krox20*$^{*}_{HA}$ transgene, where a mutant version of Krox20, noted Krox20*, is placed under the control of element A activity. Importantly, Krox20* is not able to activate A. The receiving cell type contains the transgene *A*:Krox20*GFP*, where A* is a mutated element A engineered such that Krox20* activates A* but Krox20 does not. Krox20*GFP is a fusion protein made of Krox20* and GFP. We established that the transactivation activity of Krox20*GFP is as potent as Krox20* (not shown). Thus, in the configuration depicted in figure 5, emitting cells located in r3/r5 produce Krox20*$_{HA}$ under the

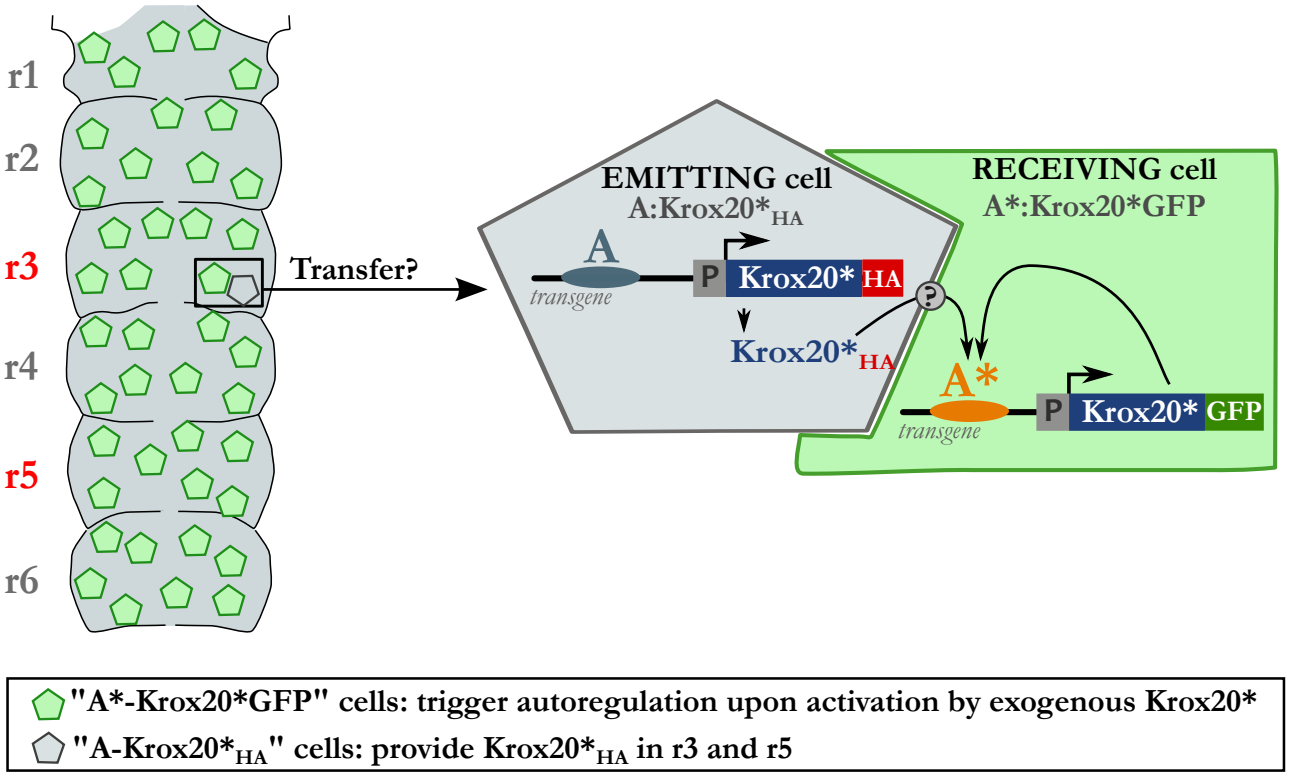

Figure 5 - Strategy to test the Krox20 transfer hypothesis in r3 and r5, in an autoregulated system

Scheme of a mosaic hindbrain made of A:Krox20*$_{HA}$ and A*:Krox20*GFP cells. If transfer occurs, Krox20*$_{HA}$ activates non cell-autonomously the element A* which in turn triggers an autoregulatory loop through expression of the fusion protein Krox20*GFP. This system allows to detect very limited amount of transferred protein, in the native territories of Krox20 activity, r3 and r5. The key requirement for this strategy to provide faithful results is the robust, non-leaky activity of A*.

control of A. In case of transfer, Krox20*$_{HA}$ is in turn transferred to the neighbouring receiving cell where it activates A* and therefore an artificial autoregulatory loop involving Krox20*GFP and A*. As wild-type Krox20, present in both emitting and receiving cells, cannot activate A*, detection of HA signal in receiving cells would be a solid demonstration of intercellular transfer.

To design Krox20*, we took advantage of a previous study from our laboratory showing that two point mutations in Krox20 second zinc-finger, H381E and T384R, modify the recognition of Krox20 consensus 9-bp binding site, from $^{5'}$GCGG**G**GGCG$^{3'}$ to $^{5'}$GCGG**C**GGGG$^{3'}$ (Figure 6A,B) (Nardelli et al., 1991; 1992). Krox20{H381E;T384R} was termed Krox20-2ER and used as Krox20*. We then sought to engineer the seven identified Krox20 binding sites on element A so that they no longer bind Krox20 but strongly recognize Krox20* (Figure 6C). To meet these conditions, we simply used the mutant element A, termed A728, designed by Diane Chomette (Chomette et al., 2006), where central guanines of all seven sites were mutated into cytosines. By electromobility-shift assays (EMSA), we could show that element A728 exhibits no binding of Krox20 protein (Figure 6D, compare lanes 2 and 5) but, surprisingly, no binding of Krox20-2ER either (see lane 6). This was in contrast with our prediction based on Jeannette Nardelli's pioneer work. Therefore we identified the sites of strongest Krox20 binding in wild-type element A by EMSA, namely sites 2, 5 and 7 (not shown) and decided to alter their sequences to the consensus GCGG**C**GGCG to maximize Krox20-2ER binding. The other sites, 1, 3, 4 and 6 were left with guanine-to-cytosine central mutation. The resulting element, noted A669, indeed binds Krox20-2ER but not Krox20 (Figure 6D, compare lanes 8 and 9). A669 was used as A*.

Finally, to investigate the proper activation of A* by Krox20* *in vivo*, we performed electroporation experiments in the chick neural tube by co-transfecting an expression vector containing Krox20* and a reporter plasmid where A* controls the activation of the *lacZ* gene. Results are shown in figure 6E: Krox20* activates A* to a level comparable with the activation of A by Krox20 (compare figures 6Eb and 6Ef). Moreover, Krox20* does not activate efficiently A (Figure 6Ec) and Krox20 does not activate A* (Figure 6Ee). To confirm this latter point, as it is crucial in the strategy described above, we assessed the activity of element A* in mouse transgenics carrying the A*:lacZ construct. Not a single cell was found *lacZ*$^{+}$(not shown).

In order to perform the strategy depicted in figure 5 in mouse, we successfully generated the A-Krox20* transgenic line, but failed to obtain A*:Krox20*$_{HA}$ pups despite repeated attempts. A similar system will thus be employed in zebrafish embryos with GFP replacing HA in receiving cells, such that the non cell-autonomous activation of the A*/Krox20* loop can be followed by time-lapse microscopy.

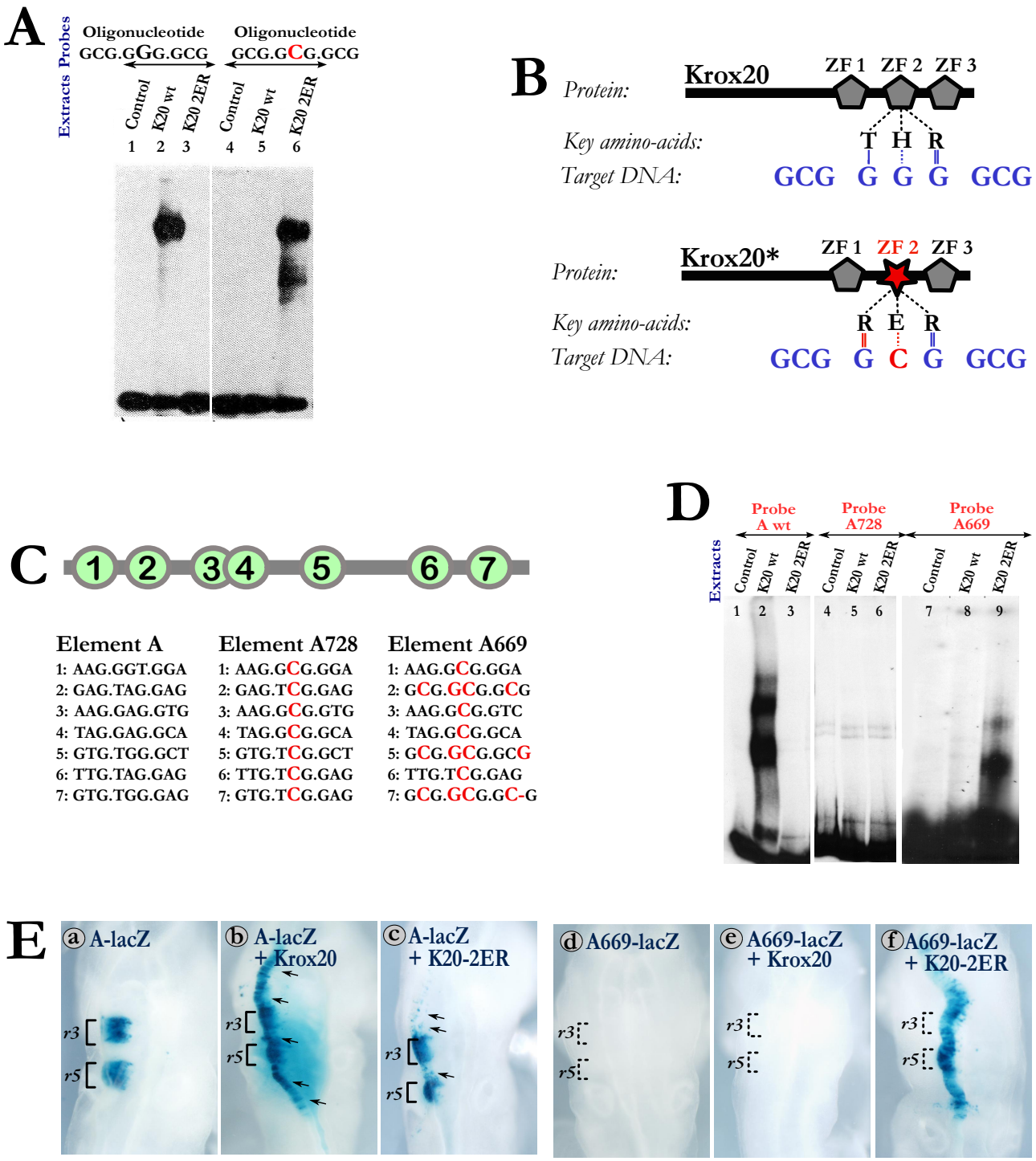

Figure 6 - Engineering the synthetic autoregulation system A* (A669) / Krox20* (Krox20-2ER)

(A) Gel-shift experiments showing high stringency in the recognition of GCGG**G**GGCG and GCGG**C**GGCG consensus oligonucleotides by Krox20 and Krox20-2ER respectively. Results from Nardelli *et al.*, 1991. **(B)** Scheme of Krox20 and Krox20-2ER proteins, and the recognition code between key amino acids of the second zinc-finger and the aforementionned consensus oligonucleotides. Two point mutations (T>R, H>E) in the second zinc-finger allow to shift from recognition of one oligonucleotide to the other. **(C)** Sequences of the seven Krox20 binding sites found in the chick element A sequence. Mutations introduced in elements A728 and A669 are also shown. **(D)** Gel-shift experiments showing Krox20 and Krox20-2ER binding efficiency to A, A728 and A669. **(E)** Chick embryos stained for ß-galactosidase after electropration with reporter vectors containing A or A669 and expression vectors containing either *Krox20* or *Krox20-2ER* coding sequences.

DISCUSSION

The mechanisms underlying the expansion of *Krox20*$^{+}$ domains in the vertebrate hindbrain have not been identified. Experiments performed in chick suggested that non cell-autonomous autoregulation of *Krox20*, presumably through direct intercellular transfer of Krox20 protein, could play a key role. Chick neural tubes were electroporated with a bicistronic vector encoding ß-galactosidase and the HA-tagged murine version of Krox20. In this system, it is expected that ß-gal^{+} cells are electroporated while all others are not, thus forming a mosaic hindbrain. Some non-ßgal cells were shown to express the endogenous chick Krox20, revealing non cell-autonomous autoregulation. Moreover, some non-ßgal cells displayed HA staining, suggesting a direct transfer of mKrox20$_{HA}$. But we realised with time and additional control experiments that chick electroporation suffers, in this context, from two major drawbacks. First, electroporation leads to transient transfection of cells. The bicistronic vector may be present in a cell at time *t*, leading to low levels of ß-gal and mKrox20$_{HA}$, but absent in its progeny where inherited ß-gal levels are below the detection limit but Krox20$_{HA}$ levels are high enough to activate endogenous element A. Consistently, we showed in chapter 3 that the activation threshold of element A is very low. The second non-exclusive drawback is the cistron translation efficiency that may vary dramatically from one cell to another. cKrox20^{+}, non-ßgal cells may be electroporated cells where the first cistron is less efficiently translated than the second one, hence activation of endogenous A but no detection of ß-gal. In most bicistronic system, efficiency of translation is supposed to be higher on the first cistron, but the reverse situation might occur occasionally. In the present study, we challenged the non cell-autonomous and transfer hypotheses using mouse and zebrafish embryos as they are more suited for mosaic analyses.

Few cells activate *Krox20* in a non cell-autonomous manner in mouse embryos

Juxtaposition of Krox20$^{GFP/+}$ cells and Krox20$_{HA}$-expressing cells in odd-numbered rhombomeres allowed to detect few cases of non cell-autonomous *Krox20* locus activation. But these cases were low in number, and we could not detect colonies of GFP^{+} cells that would have supported a cell-by-cell recruitment mechanism, even when mosaic embryos were left to develop up to E9.5. We were thus puzzled by this low efficiency as it is not consistent with the rapid expansion of r3 between the 1- and the 5-somite stage in mouse. It may result from our experimental design, as we are studying the non cell-autonomous activity of Krox20 ectopically, in r2/r4/r6. Some factors, restricted to pre-r3 and pre-r5 may be necessary to facilitate the process. If so, these factors would not act on the capacity of element A to respond as we have shown that

autoregulation can be readily activated in the region r2-r6 (unpublished). Alternatively, we may be misinterpreting the presence of GFP^+ cells in r2/r4/r6. These cells could actually result from early ectopic activation of the *Krox20* locus as it happens in non-mosaic embryos where they are subsequently sorted towards r3 and r5, or reprogrammed, or subject to programmed cell death. In the mosaic situation, those cells could avoid cell-sorting, death and reprogramming simply because they are now surrounded by friendly *Krox20*$^+$ cells. In any case, we failed to demonstrate the existence of an effective non cell-autonomous activation of *Krox20* expression in mouse embryos.

An autoregulated system is required to test conclusively the "transfer hypothesis"

Another way to test the non cell-autonomous autoregulation of *Krox20* is to directly address one putative mechanism, the direct transfer of Kox20 protein from one cell to another. We could not detect exogenous $Krox20_{HA}$ protein in the neighbouring non-$Krox20_{HA}$ cells either in zebrafish or mouse mosaics. As we showed in chapter 3 that the activation threshold is very low, the amount of transferred protein required to activate non cell-autonomously the element A might reside below our detection limit. We thus designed a genetic strategy to unequivocally test the transfer hypothesis in r3 and r5 by shifting from the A/Krox20 loop to an artificial A*/Krox20*. The strategy requires the establishment of two transgenic lines, A:$Krox20*_{HA}$ and A*:Krox20*GFP. Unfortunaltely, the latter could not be obtained in mouse. In zebrafish, the strategy has not been attempted yet, as it has been judged risky and came up against fierce competition from other projects running in the lab.

Conclusions

The results presented above shed some doubts over the expansion model outlined in figure 1C. If non cell-autonomous autoregulation is not a major contributor of r3 expansion, the simplest alternative model involves pre-patterning factors that shape in time and space the area co-expressing Hoxa1/b1 and factor X. This would results in shaping the activity profile of the initiator element C, as suggested by our results presented in chapter 2. The expansion of r3 would thus reflect the expansion of element C profile; the size of the rhombomere would subsequently be determined both by the activation threshold of A and the shape of element C profile. Somehow, as we gathered data supporting this model with no requirement for Krox20 non cell-autonomous activity, we now believe that this fancy property, if confirmed, has a marginal-to-null effect on hindbrain patterning.

Acknowledgements

We are very grateful to Sylvie Schneider-Maunoury for teaching us the technique of mouse morula aggregation.

– Chapter 5 –

Ablation of *egr2*-positive cells in the anterior pituitary leads to an atypical Isolated Growth-Hormone Deficiency model

Y.X. Bouchoucha, P. Charnay, P. Gilardi-Hebenstreit
IBENS, Ecole Normale Supérieure, Paris, France
INSERM U1024 – CNRS UMR 8197

Author contributions:

YXB performed the experiments.

YXB, PC, PGH designed the experiments and wrote the manuscript.

Foreword

The study presented in this chapter was conceived as a side-project, as it is marginal to the main interest of my co-workers. Yet a first study had been published by the lab in 1997 on the role of *Krox24/Egr1* in the pituitary gland. This work revealed incidentally that the brother-gene *Krox20* is also expressed in the anterior gland. Highly attracted again by the pituitary gland as an elegant model of cell specification, we decided to use all murine genetic tools available in the lab to address a simple question: what is the function of *Krox20* in the pituitary gland, if any?

Ablation of *Egr2*-positive cells in the anterior pituitary leads to atypical Isolated Growth-Hormone Deficiency

INTRODUCTION

The pituitary gland is a key component of the vertebrate endocrine system, regulating a number of major body functions, such as growth, lactation, metabolic homeostasis and stress response. The pituitary gland comprises three lobes. The anterior lobe (adenohypophysis) contains five distinct hormonal cell types: somatotrophs produce growth hormone (GH), lactotrophs prolactin (PRL), thyrotrophs thyroid-stimulating hormone (TSH), corticotrophs adrenocorticotrophic hormone (ACTH) and gonadotrophs luteinizing hormone (LH) and follicule-stimulating hormone (FSH). The intermediate lobe contains melanotrophs that express melanocyte-stimulating hormone (MSH). Finally, the posterior lobe essentially consists of hypothalamic neuron axon terminals. The anterior and intermediate lobes share the same embryological origin as they derive from a small region of the oral ectoderm, which subsequently develops into the Rathke's Pouch (RP). In contrast, the posterior lobe derives from the ventral diencephalon. In the mouse, by embryonic day (E) 11.5, proliferative progenitors located close to the RP lumen exit the cell-cycle and differentiate while migrating ventrally (Bilodeau et al., 2009). Differentiation of the different hormonal cell types occurs between this stage and E14.5 (Davis et al., 2011) and the hormones are produced in a temporally-ordered manner, starting with ACTH at E12.5 and ending with LH and FSH at E16.5 (Rizzoti and Lovell-Badge, 2005; Kelberman et al., 2009). During early postnatal life, the anterior lobe expands rapidly, reflecting cell proliferation stimulation by the Hypothalamic Releasing Hormone (HRH). Subsequently, although the total cell number does not grossly change, the anterior lobe demonstrates high plasticity, as extrinsic cues can modulate the relative expansion of the different hormonal populations.

Deciphering the genetic basis of pituitary development constitutes an important step in the understanding of the etiology of pituitary disorders and ultimately in the development of efficient treatments. Pituitary Hormone Deficiencies (PHD) form a family of syndromic disorders affecting pituitary hormone secretion. Among them, Isolated Growth-Hormone Deficiency (IGHD) is the most common endocrinopathy, with an incidence ranging from 1:3,500 to 1:10,000 (Zhu et al., 2007; Kelberman et al., 2009). IGHD results in reduced levels of

plasmatic GH, whereas production of the other hormones is unaffected. In congenital IGHD, the fall in GH levels occurs during early childhood, resulting in short stature and metabolic disorders. Adult-onset IGHD may also occur, usually after brain injury or, more often, surgical segmentectomy of pituitary tumours (Mathioudakis and Salvatori, 2008). In this situation, patients only display abnormal metabolic functions. GH has a number of well-established metabolic effects: (i) it increases hydrolysis of triglycerides and free fatty acids (FFA) in the visceral and subcutaneous adipose tissue; (ii) it counteracts insulin signalling, leading to inhibition of glucose oxydation; (iii) it stimulates protein synthesis. IGHD patients thus display many features of the "metabolic syndrome", including central obesity, raised triglycerides and insulin resistance. This is accompanied with cardiovascular complications, osteopenia, osteoporosis and overall diminution of Quality of Life (Groop et al., 2005; Doga et al., 2006). The links between GH metabolic functions and IGHD syndromic disorders are however not fully understood (Vijayakumar et al., 2010). To this end, rodent models of GHD have been widely used, in particular naturally-occurring mutants in mouse (Camper et al., 1990; Li et al., 1990; Sornson et al., 1996) and rat (Charlton et al., 1988) where the whole Pit1 lineage is affected, i.e. the GH, PRL and TSH populations. Early-onset IGHD in particular is better recapitulated by immuno-neutralization of GH (Chandrashekar and Bartke, 1998), targeted disruption of the GH-IGF1 axis (Baker et al., 1996; Zhou et al., 1997; Bartke, 1999) or ablation of GH-positive cells (Behringer et al., 1988). For adult-onset IGHD, a mouse model has been recently engineered using a specific, time-dependent ablation of somatotrophs in the anterior pituitary (Luque et al., 2011). However, so far, these models have not been able to recapitulate the complexity and wide range of GHD-associated troubles in humans, indicating that additional animal models are required to fully unravel their genetic or metabolic origin.

To develop a novel mouse model of IGHD, we have taken advantage of our knowledge of the Early-growth response factor 2 (Egr2, also known as Krox20 or Zif268). Egr2 belongs to the four-member Egr-family of zinc-finger transcription factors, which were first identified as components of the cell response to growth factors or mitogens (Chavrier et al., 1988a; 1988b; Gashler and Sukhatme, 1995). Numerous studies have later revealed that Egr factors play important roles in a variety of cellular and developmental processes, including pattern formation (Giudicelli et al., 2001; Voiculescu et al., 2001), synaptic plasticity (Worley et al., 1993), T cell differentiation (Safford et al., 2005), macrophage maturation (Gibbs et al., 2008), myelination (Topilko et al., 1994), ossification(Levi et al., 1996), muscle spindle formation (Tourtellotte and Milbrandt, 1998), etc. *Egr1* (also known as *Zif268* and *Krox24*) and *Egr2* are expressed in the pituitary and this expression has been shown to be modulated by gonadotropin-releasing

hormone (GnRH) pulses that trigger periodic induction of LHβ expression (Lawson et al., 2007). Egr1 is actually required for GnRH-dependent transcriptional activation of the LHβ gene and *Egr1*$^{-/-}$ mice display complete absence of LH in the anterior lobe, as well as reduction in the number of somatotrophs, absence of LH receptors in the ovary and disrupted development of Leydig cells (Topilko et al., 1998). Egr1 is therefore a direct regulator of hypothalamic-induced pituitary plasticity. In contrast, the function of Egr2 in the pituitary gland has not been investigated.

In the present study, we have performed a detailed analysis of *Egr2* expression in the pituitary gland and investigated the phenotypes associated with its disruption. We show that *Egr2* is initially expressed in all differentiating hormonal cell types, but that its expression is subsequently restricted to a subset of hormonal cells, mostly somatotrophs. *Egr2* knock-out leads to hypoplasia of the anterior pituitary. However this effect is not organ-autonomous, as demonstrated by the analysis of a conditional mutation affecting only the anterior pituitary. Taking advantage of the late preferential expression of *Egr2* in somatotrophs, we performed a specific ablation of *Egr2*-positive cells in the pituitary to investigate the consequences on animal development and metabolism. The ablation leads to progressive depletion of the somatotroph population and elimination of circulating GH after birth. This is accompanied by progressive body growth deficit, starting from postnatal day 10, and altered metabolic functions. Consistent with the GH deficit, increased insulin sensitivity is observed. However, in contrast to previous studies, this is not correlated with a modification in the balance between fat and lean tissues in the body. Nevertheless, this analysis revealed a reduced metabolic adaptability between glucose and lipid oxidation conditions. In conclusion, this work shows that the genetically ablated animals constitute a novel and atypical model of early-onset isolated GH deficiency.

MATERIALS & METHODS

Mouse lines, dissections and ethical considerations

All procedures involving mice were approved by the Charles Darwin National Committee on Ethics in Animal Experimentation (CNREEA, Pitié-Salpétrière Hospital, Paris, France) under the protocol number Ce5/2011/025. The four mice lines used in this study were described previously and carry the *Pit1-Cre* transgene (Olson et al., 2006) and the three knock-in alleles $Egr2^{GFP(DT)}$ (Vermeren et al., 2003), $Egr2^{flox}$ (Taillebourg et al., 2002), $Egr2^{lacZ}$ (Schneider-Maunoury et al., 1993), respectively. They were maintained in a B6D2F1 background. Dissections of pituitary glands were conducted on animals previously euthanized in chambers saturated of carbon dioxide. Intraperitoneal injections of BrdU (70 mg/kg) were performed 2 h before euthanasia.

Immunohistochemistry

Dissected pituitary glands were fixed for 3 h at 4°C in 4% paraformaldehyde, rinsed, soaked in 20% sucrose overnight and embedded in OCT compound (Tissue-Tek) for cryostat sectioning. For hormone staining, 12-µm sections were blocked in 5% goat serum, incubated overnight with rabbit primary antibodies (Dr A.F. Parlow, NHPP, NIDDK) at a 1:200 dilution. BrdU staining required beforehand a DNA denaturation step in a 37°C bath of 6% HCl during 20 min, followed by primary antibody incubation with a rat anti-BrdU (1:20, gift from Sonia Garel, IBENS, Paris, France). Sections were subsequently stained with 1:500 solutions of Alexa 594- or Alexa 488-conjugated antirabbit/rat antibodies (Molecular Probes, Life Invitrogen). Slides were mounted with Fluoromount-G (Southern Biotech), and photographed with a 40x oil objective using an SP5 Leica confocal microscope.

mRNA analysis

Total RNA was extracted and purified from dissected anterior lobes using the RNAqueous kit (Ambion, Life Applied). 500 ng of RNA were reverse transcribed (SuperscriptIII RT, Life Invitrogen) in the presence of random hexamer and oligodT primers (Life Invitrogen). Quantitative real-time PCR was performed in duplicate using the SYBR Green technique on a Roche LC480 device. Gene copy numbers were calculated using the standard curve method. Target genes expression levels were normalized against the mean of ß-actin, protoporphyrinogen oxidase and ß-tubulin levels.

Metabolic functions and circulating GH and IGF-1 levels

All the analyses were performed in the Mouse Clinical Institute (Illkirch, France) on 9 male control and 9 male *Pit1Cre;egr2*$^{GFP(DT)/+}$ mice, aged between 26 and 31 weeks. Whole body composition was analyzed on conscious fed animals by quantitative Nuclear Magnetic Resonance (Minispec+, Bruker). Glucose tolerance tests (GTT) and insulin sensitivity tests (IST) were performed during the light period on animals after a 16-hour overnight fast and a 2-hour fast respectively. For GTT, hyperglycaemia was induced by oral administration of a standardized glucose bolus (2 g/kg). For IST, a standardized insulin load (0.5 UI/kg) was administrated by intraperitoneal injection. Blood glucose was measured at different timepoints using blood glucose monitor and glucose test strips (Roche Diagnostics, Accu-Chek). Assessment of respiratory metabolism was performed with an open flow respirometric system (TSE, Labmaster, Germany), over 24 h under a 12-hour light/12-hour dark photo-period (7 am/7 pm), at ambient temperature (21°C ± 2). An activity and food/water intake monitoring system was integrated in the set up. For GH and IGF-1 measurements, blood was collected by retro-orbital puncture under isoflurane anesthesia after 4-hour fasting. GH and IGF-1 plasmatic levels were measured by immunoenzymatic methods using the rat GH immunoassay kit (SPI bio, #A05104) and the Quantikine Mouse IGF-I Immunoassey kit (R&D Systems).

Statistical analyses

Statistical analyses were performed using the open-source R software (www.r-project.org). Student t-tests were used to assess significant difference in means calculated from control *vs* mutant datasets. The effect of genotype on mRNA levels, oral glucose tolerance test (OGTT), intra-peritoneal insulin sensitivity tests (IPIST) and indirect calorimetry measurements was assessed by one-way, two-way ANOVA or ANOVA repeated measure tests, followed by Fischer's least significance difference tests. All data are expressed as mean ± sem. Significance was set as follow: * $p<0.05$, ** $p<0.01$, *** $p<0.001$.

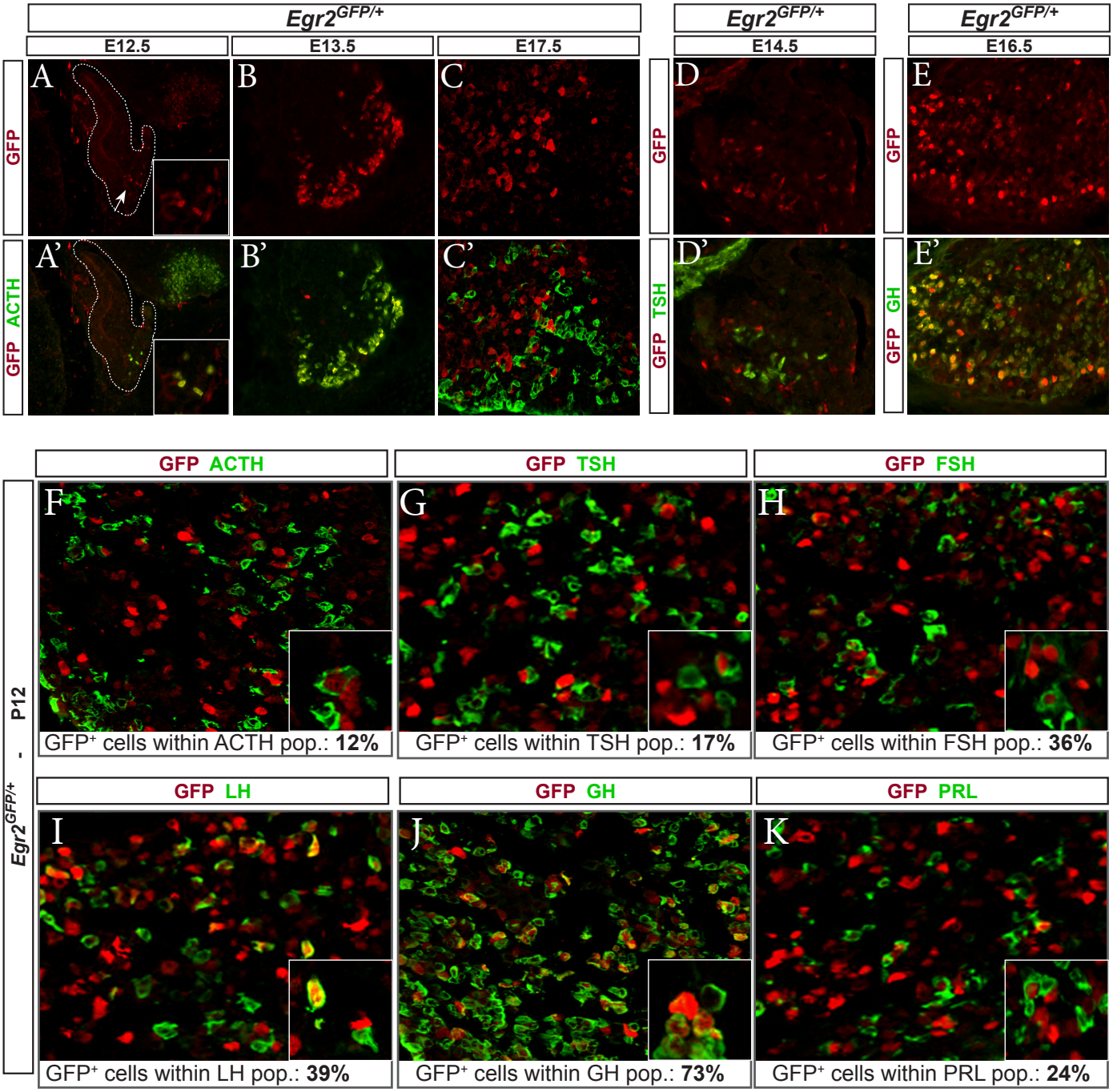

Figure 1. *Egr2* is expressed in all hormonal cells during embryogenesis and preferentially in somatotropes in the adult. GFP and the indicated hormones were co-labelled by immunohistochemistry in *Egr2*$^{GFP/+}$ pituitary glands at the indicated stages. **(A,B,A',B')** GFP is first detected in the Rathke's pouch at E12.5 and colocalizes with ACTH until E13.5. **(C-E,C'-E')** From E14.5, most ACTH-positive cells have ceased expressing GFP, while differentiating TSH and GH cells are successively GFP-positive. **(F-K)** At P12 most GH cells are positive for GFP, whereas in the other lineages this is the case for only a minority of the cells.

RESULTS

Egr2 expression in the anterior pituitary during embryonic and postnatal development

To investigate the function of *Egr2* in the pituitary, it was first necessary to perform a detailed analysis of its expression. To follow the expression of the gene, we took advantage of a *knock-in* allele in which the *EGFP* coding sequence has been inserted in frame into the *Egr2* gene (*Egr2*$^{GFP(DT)}$). In this situation, GFP expression has been shown previously to precisely recapitulate *Egr2* expression in several tissues and at various developmental stages (Vermeren et al., 2003). GFP expression was first detected in *Egr2*$^{GFP(DT)/+}$ embryos in the ventral anterior lobe, opposite to the lumen, at E12.5 (Fig. 1A, arrow). This is the site and time of the first differentiation of hormone-expressing cells in the pituitary. The number of GFP-positive cells rapidly increased during development and at E17.5 they were distributed over the entire anterior lobe, with however a sparse pattern (Fig. 1A-D). This pattern was maintained until adulthood (data not shown).

To determine which cell types express *Egr2*, we performed double-immunohistochemistry against GFP and all six hormones present in the anterior lobe. At early stages, *Egr2* expression appears to follow precisely the onset of hormone expression. For instance, GFP appears at E12.5 in the first hormone-expressing cells, the corticotrophs (Fig. 1A,A'). At E14.5, all newborn TSH-positive cells are GFP-positive, whereas some GFP-positive cells are not TSH-positive, presumably because GFP is still expressed in corticotrophs (Fig. 1D,D'). The same phenomenon is observed with the other hormonal cell types (GH-, PRL- and LH-, FSH-positive cells): as they sequentially appear, they co-express *GFP* (Fig. 1E,E' and data not shown). However, although all hormone-expressing cells express *GFP* at early stages, most of them loose GFP staining within 2-3 days (data no shown), such that at P12 GFP expression is restricted a small subset of each hormonal population, with the exception of somatotrophs for which a large proportion still expresses *GFP* (Fig. 1F-K).

In conclusion, *Egr2* expression in the anterior pituitary appears initially associated with the differentiation of hormone-expressing cells. This expression is transient in most cell-types and is not maintained at later stages, with the exception of somatotrophs. In the postnatal period, there is a large overlap between somatotrophs and *Egr2*-positive cells.

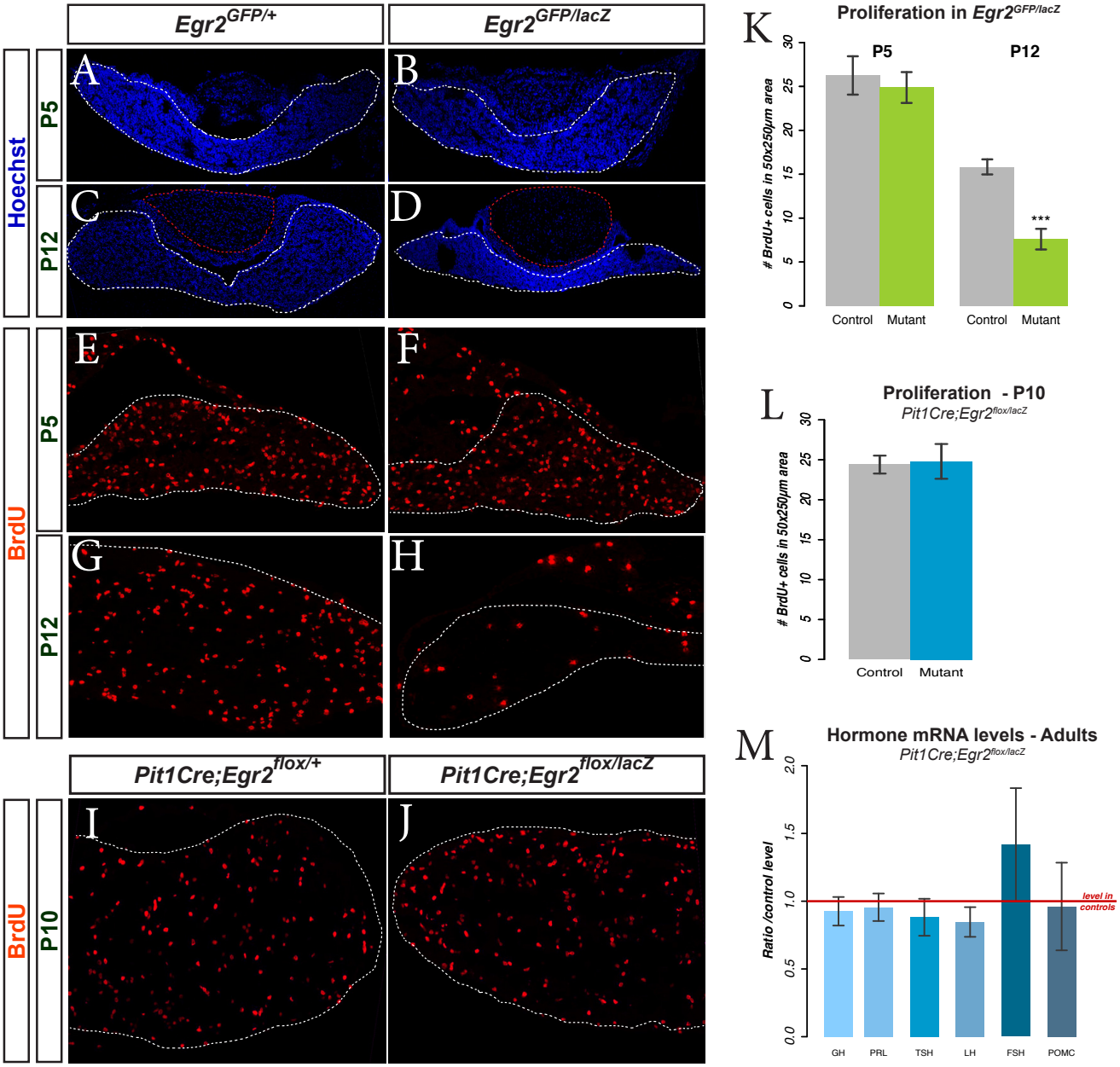

Figure 2. Inactivation of *Egr2* leads to non-autonomous decrease of the rate of cell proliferation in the anterior lobe. **(A-D)** Nuclear staining (Hoechst) of whole pituitary glands at P5 (A,B) and P14 (C,D). The size of the mutant anterior pituitary lobe (white outline) is severely reduced at P14, whereas the size of the posterior lobe (red outline in C,D) is not affected. **(E-J)** BrdU labelling was performed at the indicated stages on pituitary glands from null (*Egr2*$^{GFP/lacZ}$) and conditional (*Pit1Cre;Egr2*$^{flox/lacZ}$) mutants as well as from littermate controls. **(K,L)** Quantification of the BrdU labelling experiments. **(M)** Hormone mRNA levels were measured by RT-qPCR in the conditional mutant and normalized by the levels in control animals at the adult stage**.**

Egr2 loss-of-function results in reduced cell proliferation and hypoplasia in the anterior pituitary

As reported previously, *Egr2* knock-out is lethal after birth (Schneider-Maunoury et al., 1993). Half of the homozygous null mutants die within the first 48 postnatal hours, presumably due to defects in the respiratory rhythm (Chatonnet et al., 2007). The other half dies between the first and second postnatal weeks and exhibit a dramatic reduction in body size and weight as compared to wild-type and heterozygous littermates. Since *Egr2* is expressed in the pituitary and in particular in the somatotroph lineage, we wondered whether this phenotype might be related to defects in the pituitary. We examined the gland in $Egr2^{-/-}$ mice (carrying either $Egr2^{GFP(DT)}$ or $Egr2^{lacZ}$ knock-in alleles, each of them being null for Egr2 activity) at embryonic and postnatal stages. Whereas null mutant anterior lobes had a normal size until P5 (Fig. 2A,B, white outline), at P10 they were found smaller than in littermates controls (Fig. 2C,D). In contrast, the posterior lobe was not affected by the *Egr2* loss-of-function (Fig. 2C,D, red outline). To investigate the origin of this phenotype, we analyzed proliferation and apoptosis rates in the anterior pituitary. To evaluate the proliferation rate, we measured BrdU labelling at P5 and P12 after a single pulse of BrdU incorporation. At P12, the density of BrdU-positive cells was significantly reduced in $Egr2^{-/-}$ as compared to heterozygotes anterior lobes, whereas no significant difference was observed at P5 (Fig. 2E-H,K). In contrast, no difference in the density of apoptotic cells was detected at these two stages (data not shown). The reduction in cell proliferation in the homozygous mutants is consistent with the relative reduction in size of the anterior lobe, suggesting a possible causative link. This could in turn participate in the development of the general size deficit of $Egr2^{-/-}$ animals.

Although *Egr2* is expressed in the pituitary, the analysis of knock-out animals does not establish whether the phenotype is organ-autonomous, since *Egr2* is also expressed in a number of other tissues. To investigate this issue, we generated a pituitary-specific conditional mutant. For this purpose, we used an *Egr2* floxed allele ($Egr2^{flox}$, (Taillebourg et al., 2002)) together with a Cre driver line, in which Cre is under the control of the *Pit1* promoter (Olson et al., 2006). *Pit1* is transcribed in all cell lineages of the anterior lobe, but the protein is only found in GH-, PRL- and TSH-producing cells (Pellegrini et al., 2006). Using a lineage tracing approach with a Cre-inducible reporter, we observed that, from E13.5, the *Pit1-Cre* transgene is indeed expressed in approximately 80% of the anterior lobe cells, irrespective of the cell types (Supplemental Fig. 1A-F and data not shown). The introduction of the *Pit1-Cre* transgene into a compound heterozygous $Egr2^{flox/lacZ}$ background led to excision of the floxed allele in a large majority of the anterior lobe cells (Supplemental Fig. 1G,H) and to a dramatic reduction in the level of *Egr2*

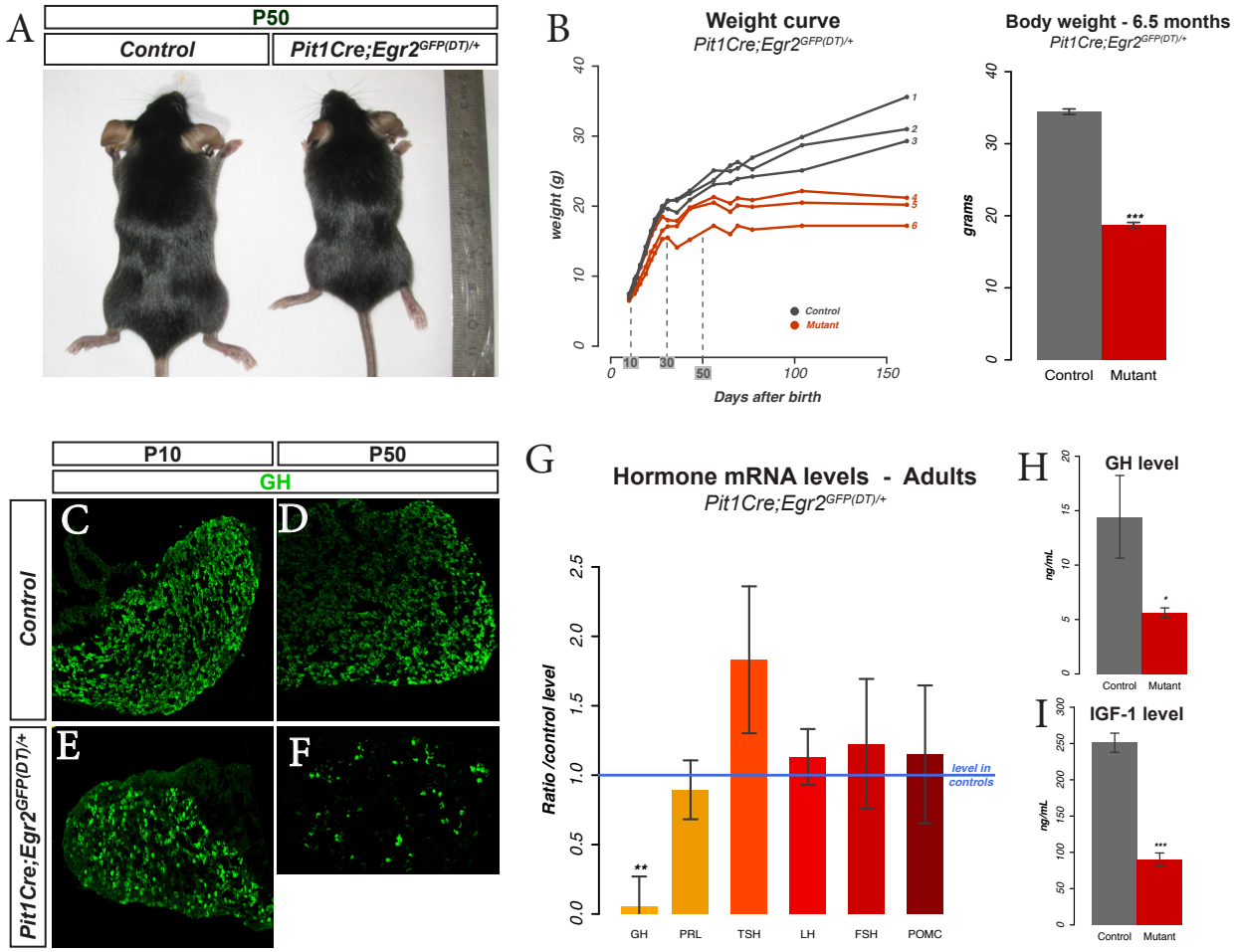

Figure 3. Conditional ablation of *Egr2*-positive cells leads to a drastic reduction in the number of somatotropes. **(A)** Control and *Pit1Cre;Egr2*$^{GFP(DT)/+}$ animals photographed 50 days after birth. **(B)** Weight curves of six representative female mice from P10 to P160 and mean body weight at 6.5 months. Animals 1-3 were wild-type while animals 4-6 were *Pit1Cre;Egr2*$^{GFP(DT)/+}$. **(C-F)** Reduction of somatotropes in ablated animals becomes evident at P10 (C,E) and worsens subsequently to reach a bottom level shown at P50 (D,F). **(G)** Quantification of mRNA levels in control and ablated 6 month-old females. GH production is dramatically decreased while other Pit1-dependent hormones are unaffected (PRL) or mildly upregulated (TSH). **(H,I)** Levels of circulating GH (H) and IGF-1 (I) in 6.5-month old control and *Pit1Cre;Egr2*$^{GFP(DT)/+}$ mice.

mRNA (Supplemental Fig. 1I). Therefore this genetic combination is appropriate for the conditional *Egr2* loss-of-function in the pituitary gland from E13.5 onwards.

Pit1-Cre;Egr2$^{flox/lacZ}$ animals are viable, fertile and do not exhibit obvious morphological or behavioural defect throughout life. When analyzed in 10-day-, 3- and 9-month-old animals, the size of the pituitary gland was not found different from littermate controls (data not shown). Consistently, BrdU labelling did not reveal any significant difference in the rate of cell proliferation at P10 (Fig. 2I,J,L). In addition, at P80, the density of hormone expressing cells (Supplemental Fig. 2) or the levels of hormone mRNAs (Fig. 2M) were not modified in the conditional mutant as compared to controls.

In conclusion, this analysis indicates that the hypoplasia of the pituitary gland in *Egr2* null mice results from a non-autonomous effect. The hypothalamus constituted an obvious candidate for being at the origin of the phenotype. However, lineage tracing analyses, performed with the *Egr2^{Cre}* driver (see below), failed to detect any *Egr2*-positive cells in this organ (data not shown).

Ablation of *Egr2*-positive cells specifically depletes the somatotroph lineage

As indicated above, although *Egr2* is initially expressed in all hormone-expressing cells, postnatal expression is mainly restricted to the somatotroph lineage. We therefore investigated whether this would provide us with a tool to specifically eliminate this lineage. For this purpose, we made use of the *Egr2$^{GFP(DT)}$* allele: when transcribed, this allele gives rise to GFP; however, upon Cre recombination, the GFP coding sequence is excised, allowing transcription of the diphteria toxin A chain gene (Supplemental Fig. 1E and (Vermeren et al., 2003)). We combined the *Egr2$^{GFP(DT)}$* allele with the *Pit1-Cre* transgene, to restrict recombination to the anterior pituitary. Analysis of the presence of the GFP cassette in anterior pituitary DNA indicated that, at P5, recombination had already occurred in a majority of the cells (Supplemental Fig. 1F). The mutants were viable and of normal size at birth (data not shown). However, from P10 their weight curve started to diverge from their control littermates and at P50 they had stopped growing, in contrast to the controls (Fig. 3A,B). At 6.5 months they weighted almost twice less than their littermates (Fig. 3A-B).

We analysed the pituitary in mutant animals and observed a dramatic decrease in the number of somatotrophs, which were already partially depleted at P10, and had almost disappeared at P50 (Fig. 3C-F). Therefore the decrease in the relative number of somatotrophs preceded the evolution of the weight. In contrast the numbers of cells expressing the other hormones were not severely affected (Supplemental Fig. 3). Consistent with the cell numbers,, the levels of GH mRNA and circulating GH were markedly decreased in adult mutant animals,

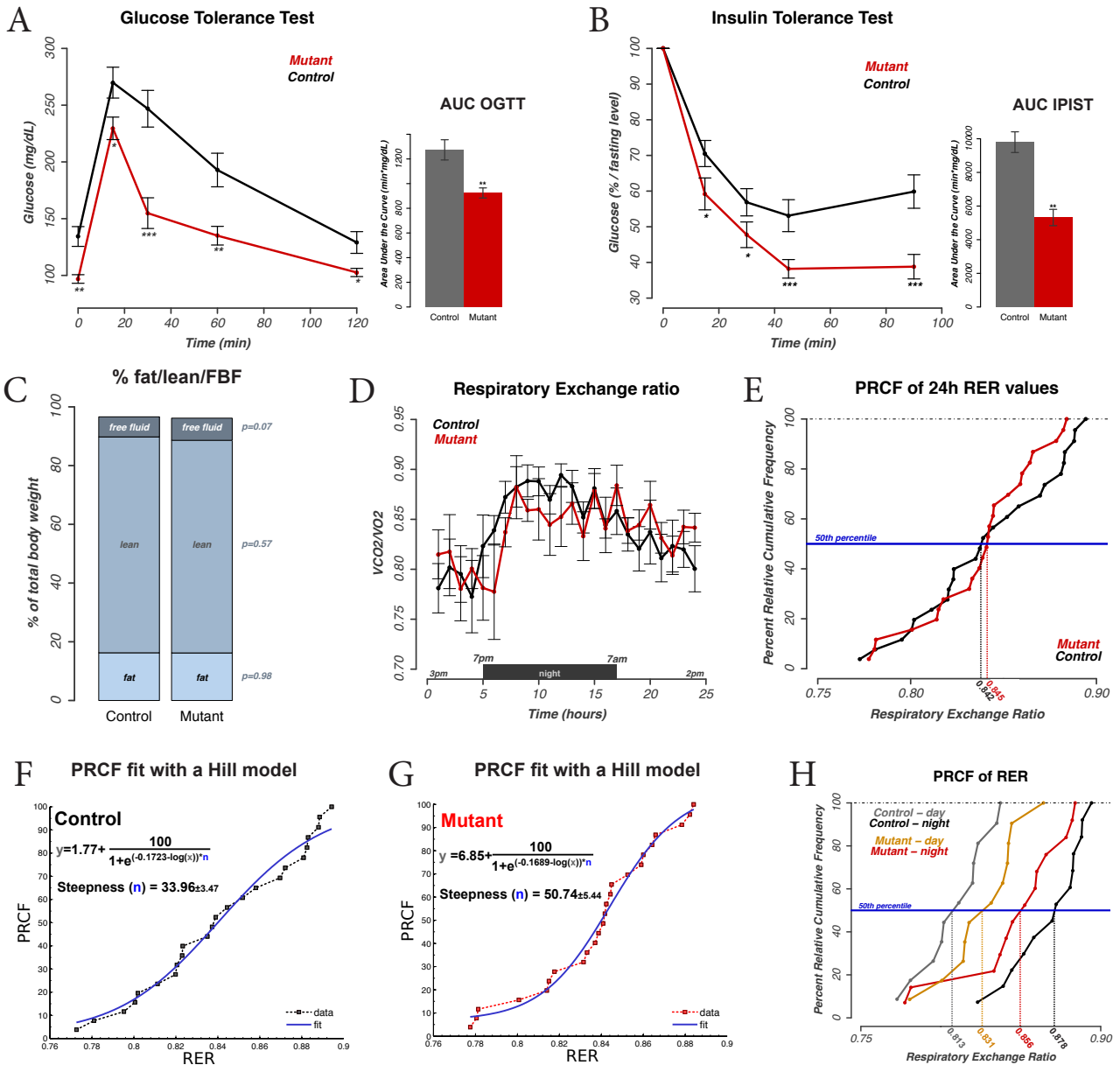

Figure 4. Ablation of *Egr2*-positive cells affect metabolic function in an atypical manner. **(A)** Oral glucose tolerance test (OGTT) performed on overnight fasted animals by oral administration of a standardized glucose bolus (2g/kg). **(B)** Intra-peritoneal insulin sensitivity test (IPIST) by i.p. injection of a standardized insulin load (0.5UI/kg) in animals fatsed for two hours. **(C)** Body composition measured by Nuclear Magnetic Resonance (NMR). **(D)** Respiratory exchange ratio RER (a.k.a. respiratory quotient, VCO_2/VO_2) was calculated after VO_2 and VCO_2 24-hour measurements by indirect calorimetry. RER defines metabolic substrate preference between carbohydrates and lipids. **(E-G)** Analysis of RER curves by the Percent Relative Cumulatice Frequency (PRCF) method (Riachi *et al.*, 2004). When measurements are averaged throughout the day (E), the mean RER values are very similar between control and *Pit1Cre;Egr2*$^{GFP(DT)/+}$ mice. But their steepness is slightly different as evidenced after fitting the curves with a Hill equation (F,G). Comparison of day RER and night RER between controls and mutants reveals a much lower adaptability of *Pit1Cre;Egr2*$^{GFP(DT)/+}$ animals to the day/night switch, i.e. the shift from the fasted to the fed condition (H).

whereas the expression of the other hormones was not significantly affected (Fig. 3G-H). Further indications that gonadotroph and lactotroph functions were not seriously altered in the mutants came from the analysis of females, which were fertile, produced litters of expected sizes and weaned their pups properly.

Genetic ablation of *Egr2*-positive cells leads to atypical GH-related metabolic defects

As indicated above, *Pit1Cre;Egr2*$^{GFP(DT)/+}$ mice exhibit a marked decline in linear growth, starting at around P10, and they reach a plateau by P50 (Fig. 3B). This is likely to result from the specific and progressive decrease in GH levels (Fig. 3C-G). *Pit1Cre;Egr2*$^{GFP(DT)/+}$ animals might therefore constitute a novel animal model for early-onset IGHD. To further characterize the model, we investigated whether GH-related metabolic functions were altered. A series of tests were performed on 6-7 month-old male mice fed with a standard chow diet (17% kcal from fat, 56% from carbohydrate, 27% from protein) throughout the study. Insulin output was evaluated by oral glucose tolerance test (OGTT) and intra-peritoneal insulin sensitivity test (IPIST). OGTT revealed faster glucose clearance and lower basal glucose levels than controls (Fig. 4A), and the IPIST curve revealed a hypoglycaemic behaviour (Fig. 4B). Both features are hallmarks of increased insulin sensitivity.

In previously published GHD models, where GH fails to exert its lipolytic effect, the higher insulin sensitivity was considered as a consequence of increased fat mass, mainly visceral and subcutaneous, at the expense of lean mass (del Rincon et al., 2007). Surprisingly, qNMR analysis of *Pit1Cre;Egr2*$^{GFP(DT)/+}$ animal body composition did not reveal any significant difference in the proportions of fat and lean masses as compared to controls (Fig. 4C). This is consistent with the results of other studies suggesting the existence of a fat-independent pathway controlling insulin output and, more generally, glucose homeostasis (Boyle et al., 1992; Yakar et al., 2004; Sasaki-Suzuki et al., 2009). Enhanced insulin sensitivity usually correlates with preferential oxidation of carbohydrates (CHO) rather than lipids. To investigate this point in our model, we performed indirect calorimetry measurements. The basis of such an analysis is that respiratory gases reflect the balance between substrate oxidation, mainly CHO and lipids, and to a lesser extent proteins. The respiratory exchange ratio (RER) is defined as the ratio between volumes of expired CO_2 and O_2 (VCO_2 and VO_2). At rest, the RER lies between 0.7 and 1. A value close to 0.7 reveals a metabolism dominated by catabolism of lipids, whereas predominance of CHO catabolism brings it close to 1 (Jensen et al., 2001). As the RER varies fluctuates throughout the day, with a strong variation at evening hours when the animals start actively feeding (Fig. 4D), comparisons were performed between the percent relative cumulative frequencies (PRCF, (Riachi

et al., 2004)) of RER values collected for 24 h (Fig. 4E). The control and mutant PRCF curves intersect the 50th percentile line at similar RER values, indicating that glucose metabolism is not taking over lipid metabolism in mutant mice, in contrast to other GHD models. However, the slope of the mutant PRCF appears slightly steeper. This can be quantified by modelling the PRCF curves with a Hill function. The Hill coefficient, n, indicates the steepness of the curves at the inflexion point (compare Fig. 4F and G). The higher steepness of the curve corresponding to the mutant indicates reduced variations in RER dynamics throughout the day. To further investigate this point, we drew distinct PRCF curves for night and daytime. At evening hours, control mice modify their RER towards preferential glucose metabolism (compare grey and black curves in Fig. 4H). The same phenomenon occurs in mutant animals (compare orange and red curves in Fig. 4H), but to a lesser extent, suggesting that the metabolism of *Pit1Cre;egr2*$^{GFP(DT)/+}$ mice is less adaptive to the diurnal rhythm, i.e. fasting versus feeding conditions. Altered metabolism is also revealed by the daytime increases in VO_2, VCO_2 and corresponding energy expenditure, whereas general activity (ambulatory and grooming) is reduced (Supplementary Fig. 4A-E). Considering that mutant mice consume more food and water relative to their body weight (Supplemental Fig. 4F), these results indicate that the overall metabolic rate of mutants is increased as compared to their wild type littermates. Taken together, these indirect calorimetry measurements suggest that the increased insulin sensitivity is accompanied by a higher metabolic rate, with no change in the mean ratio of lipid versus CHO oxidation but reduced flexibility.

DISCUSSION

In this study we have investigated the expression and the function of the zinc finger transcription factor Egr2 during the development of the adenohypophysis. We found that the gene is transiently activated in all differentiated cell types at the onset of hormone expression and is subsequently turned off in most of each population, except in somatotrophs. Despite this general, early expression, Egr2 function is not required in the pituitary for proper development of this organ. Indeed, the severe pituitary hypoplasia that we observed in *Egr2* knock-out animals is not pituitary-autonomous, as demonstrated by subsequent analysis of conditional mutants. Genetic ablation of *Egr2*-positive cells led to specific loss of somatotrophs, generating a novel and atypical model for isolated GH-deficiency.

Specific loss of somatotrophs in mice ablated of *Egr2*-positive cells

Our *Pit1Cre;Egr2b*$^{GFP(DT)/+}$ mice display two striking characteristics. First, as *Egr2* is expressed during embryogenesis when cells start differentiating, why don't they all die before birth? Part of the answer may rely on the Pit1Cre transgene that drives the genetic ablation. *Pit1* starts being expressed in the vast majority of adenohypophysis cells at E13.5. As the recombination events may take several days, depending on the level of *Pit1* expression, a significant number of cells differentiate, activate the *Egr2* locus while the recombination has not occurred yet. These cells would thus escape the ablation. This scenario is very likely for the ACTH, TSH, GH and PRL lineages that differentiate between E12.5 and E15.5, and may still apply for gonadotrophs that differentiate from E16.5. Delayed recombination event therefore explains why the *Pit1Cre;Egr2b*$^{GFP(DT)/+}$ mice do not display hormonal phenotypes during embryogenesis. Second striking feature of the *Egr2*-ablated mice: the postnatal phenotype is restricted to the somatotroph lineage. At postnatal stages, the anterior pituitary starts responding to hypothalamic cues by triggering waves of cell proliferation. Cells of the Pit1 lineage and somatotrophs in particular were shown to participate massively in this postnatal expansion. At postnatal stages, an increasing number of cells expressing *Egr2* (either because the expression was maintained from embryogenesis or because it was re-activated) recombine the locus so that they start expressing the Diphteria Toxin and die. As *Egr2* is expressed in approximately 73% of the somatotrophs, the DT causes much more death in the somatotrophs than in lineages with a lower proportion of *Egr2*-positive cells. The rapid decrease of somatotroph number would therefore result from the recombination events whose frequency increases with developmental time. This suggests that other cells types are also affected by the DT, but in a lower proportion of cells, and the remaining

cells are sufficient to compensate for the loss by proliferating for example. In contrast, in the somatotrope lineage, the 73% proportion is too high for the surviving cells to compensate.
In summary, we propose that the somatotropes are preferentially affected in *Pit1Cre;Egr2b*$^{GFP(DT)/+}$ mice because their population contains the highest proportion of *Egr2*-expressing cells.

A novel model for isolated GH-deficiency

Specific ablation of *Egr2*-positive cells severely affected the somatotroph postnatal expansion and led to dwarf mice. Apart from linear growth, GH has diverse metabolic functions, best evidenced in adult-onset GHD, where growth is unaffected. We explored the metabolic functions of *Egr2*-expressing cells ablated mice and found that they were hypoglycaemic and displayed highly improved insulin sensitivity and glucose clearance. This is in accordance with a recently published AOiGHD model (Luque et al., 2011), although the responses to insulin and glucose are further increased in our mutant, presumably because GHD appears at an earlier stage. Increased insulin sensitivity appears in contrast with the fact that human GHD syndromes are usually associated with insulin resistance. However, it has been proposed that most GHD clinical studies were performed on cohorts of patients with different aetiologies, severities, age, lifestyles and diets. By reproducing the work on more homogeneous groups of patients, they concluded that a direct causative link between GHD and insulin resistance could not be established (Riedl et al., 2000; Oliveira et al., 2012).
Besides insulin signalling, the metabolic features of our early-onset IGHD model are atypical. (i) Two other early-onset IGHD mouse models, namely Ames (*Prophet-ot-Pit1* loss-of-function) and a GH Receptor knock-out, were reported as glucose intolerant, while insulin was hypersensitive (Dominici et al., 2000; 2002). The authors found that the glucose intolerance was probably due to impaired insulin production by the pancreas and, in the case of Ames, they could indeed show that the number of Langerhans islets was reduced. In contrast, our early-onset IGHD mice display improved glucose tolerance, suggesting that the pancreatic function is unaffected. (ii) Global fat mass is not significantly different between our mutant and control mice, reflecting comparable lipidemic states upon standard diet. Consistently, analysis of the respiratory exchange ratio did not reveal any preferential oxidation of CHO. This is surprising because the reduced rate of lipolysis in IGHD is expected to result in a shift from lipid to CHO catabolism and therefore increased abdominal and subcutaneous fat (Mauras et al., 2000). Our study confirms the existence of a fat-independent effect of GH on insulin action (Yakar et al., 2004; Luque et al., 2011). (iii) During daytime, our mutant mice exhibit high-energy expenditure. This is consistent with the mild increase in relative food and water intakes, but in contrast with the drastic

diminution of general activity. We interpret these results as indicative of a higher metabolic rate and speculate that this might constitute the origin of the lean phenotype and the stagnation of lipidaemia.

In conclusion, the *Pit1Cre;Egr2*$^{GFP(DT)/+}$ mice constitute a valuable genetic model to study the effect of a strong insulin hypersensitivity in a context where the pancreatic function seems normal and the balance between fat and glucose metabolisms is largely unaffected. This context may unravel emergent properties like the one detailed in the following section.

A novel role of GH in the control of metabolic flexibility

High insulin sensitivity has been reported as associated with metabolic flexibility and protection against Diet-induced Obesity (DiO) and type-2 diabetes. Our *Pit1Cre;Egr2b*$^{GFP(DT)/+}$ display in contrast a high insulin sensitivity associated with a reduced flexibility.

Metabolic flexibility is defined as the ability to switch from lipid to glucose metabolism while feeding and vice-versa during fasting periods. Skeletal muscles consume most of the lipids and CHO and the chemistry controlling this metabolic switch has been defined in skeletal muscles as the Randle glucose-fatty acid cycle. This cycle is impaired in obese patients who generally display increased lipolysis, higher free fatty acids and triglycerides plasmatic levels, diminished RER, insulin resistance and metabolic inflexibility. In adults, considerable evidence establishes a causative link between alteration of metabolic flexibility and the development of insulin resistance in obesity (Kelley and Mandarino, 2000). The role of GH in this context is suggested by recent findings revealing that obese patients display impaired GH pulsatility during fasting periods and upon stimulation by ghrelin (the ligand of the GH secretagogue receptor) (Huda et al., 2011). *Egr2*-expressing cells ablated mice exhibit a non-diabetic profile, with high insulin sensitivity and hypoglycaemia, but reduction of metabolic flexibility. Does this discrepancy reveal a Randle-independent function of GH in metabolic flexibility? In other words, may GH affect the metabolic flexibility without affecting the insulin output? This would suggest GH regulates the susceptibility to DiO and type-2 diabetes in a glucose-independent way. Further work is required to solve this discrepancy between the protective insulin hypersensitivity (Zigman, 2005; Longo et al., 2008) and the deleterious metabolic inflexibility (Storlien et al., 2007) that *Pit1Cre;Egr2*$^{GFP(DT)/+}$ mice exhibit.

Acknowledgements

We are grateful to Mathias Treier (MDC, Berlin, Germany) and Robin Lovell-Badge (NIMR, London, UK) for providing us the Pit1-Cre mouse line. We also thank Dr A.F. Parlow (NHPP, NIDDK, Torrance, USA) for providing us with all the hormone antisera.

– Chapter 5 –

SUPPLEMENTARY INFORMATION

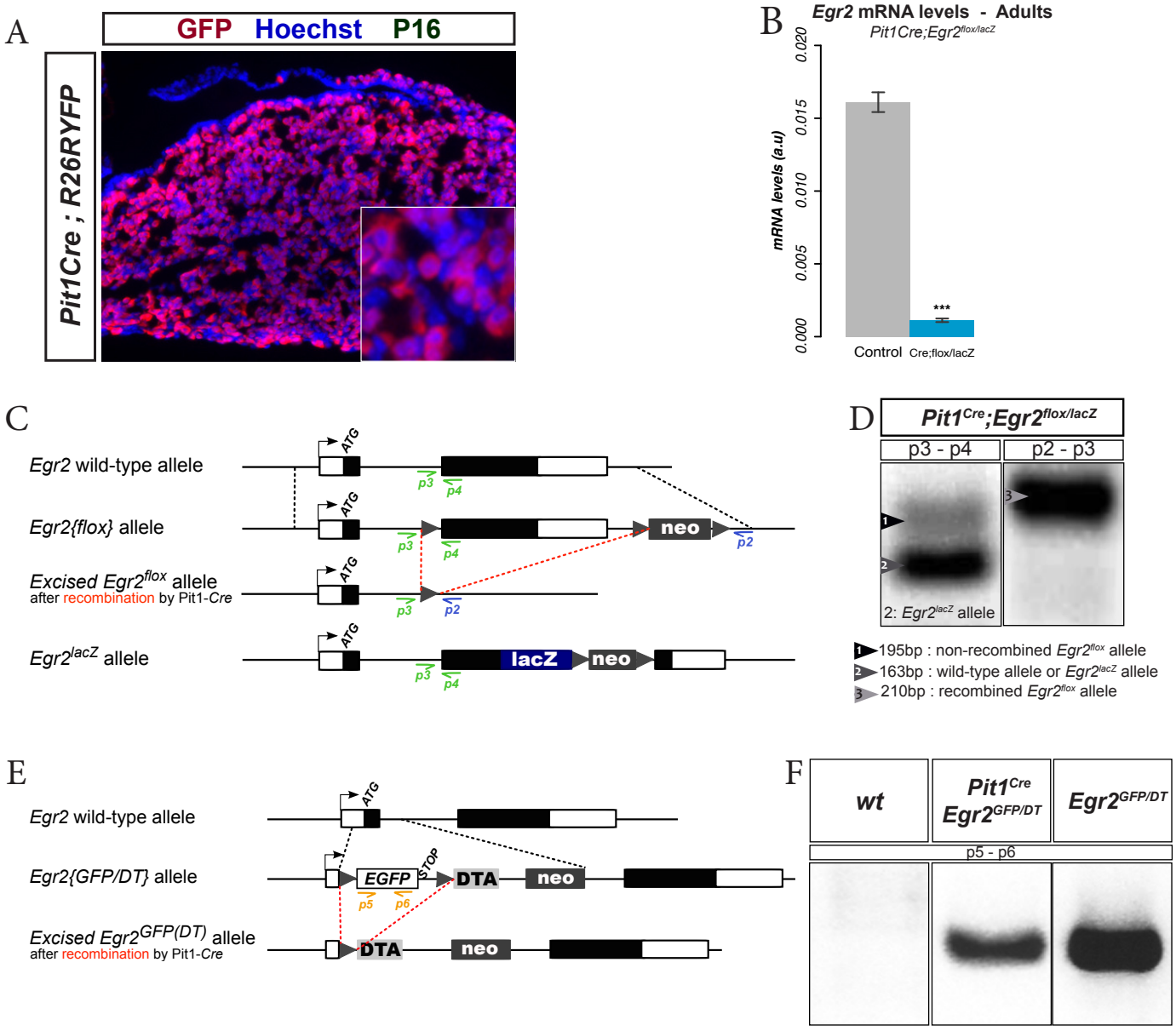

Supplemental Figure 1. Validity of the *Pit1Cre;Egr2*$^{flox/lacZ}$ and *Pit1Cre;Egr2*$^{GFP(DT)/+}$ systems. **(A)** Tracing of the Pit1-Cre^{+} cells using the ROSA26YFP reporter allele shows that about 80% of anterior lobe cells express *Pit1* at P16. **(B)** RT-qPCR analysis of *Egr2* mRNA levels in control and *Pit1Cre;Egr2*$^{flox/lacz}$ animals. **(C)** The *Egr2* locus in its wild-type, *Egr2*^{flox} and *Egr2*^{lacZ} configurations, as well as the primer design to identify the recombination events. The *Egr2*^{flox} allele carries two flox sequences flanking *Egr2* exon 2. The *Egr2*^{lacZ} allele corresponds to an in-frame insertion of the lacZ coding sequence within *Egr2* exon 2, leaving the complementary region of primer 4 unaffected. **(D)** PCR performed on genomic DNA extracted from a single anterior lobe of *Pit1Cre,Egr2*$^{flox/lacZ}$ mice. The non-recombined allele (band 1) is present in much less abundance compared with recombined allele (band 3), suggesting that the recombination occured in the majority of the cells. We speculate that the non-recombined cells correspond to the *Pit1*-negative cells. **(E)** Schematic of the *Egr2*$^{GFP(DT)}$ allele: a floxed GFP cassette followed by the Diphteria Toxin (DT) coding sequence were inserted in frame in the *Egr2* locus, such that GFP is expressed under the control of *Egr2* regulatory sequences in absence of Cre recombinase, and DT is expressed upon recombination. **(F)** Recombination efficiency was estimated by PCR using primers p5 and p6 to detect the presence of the GFP cassette.

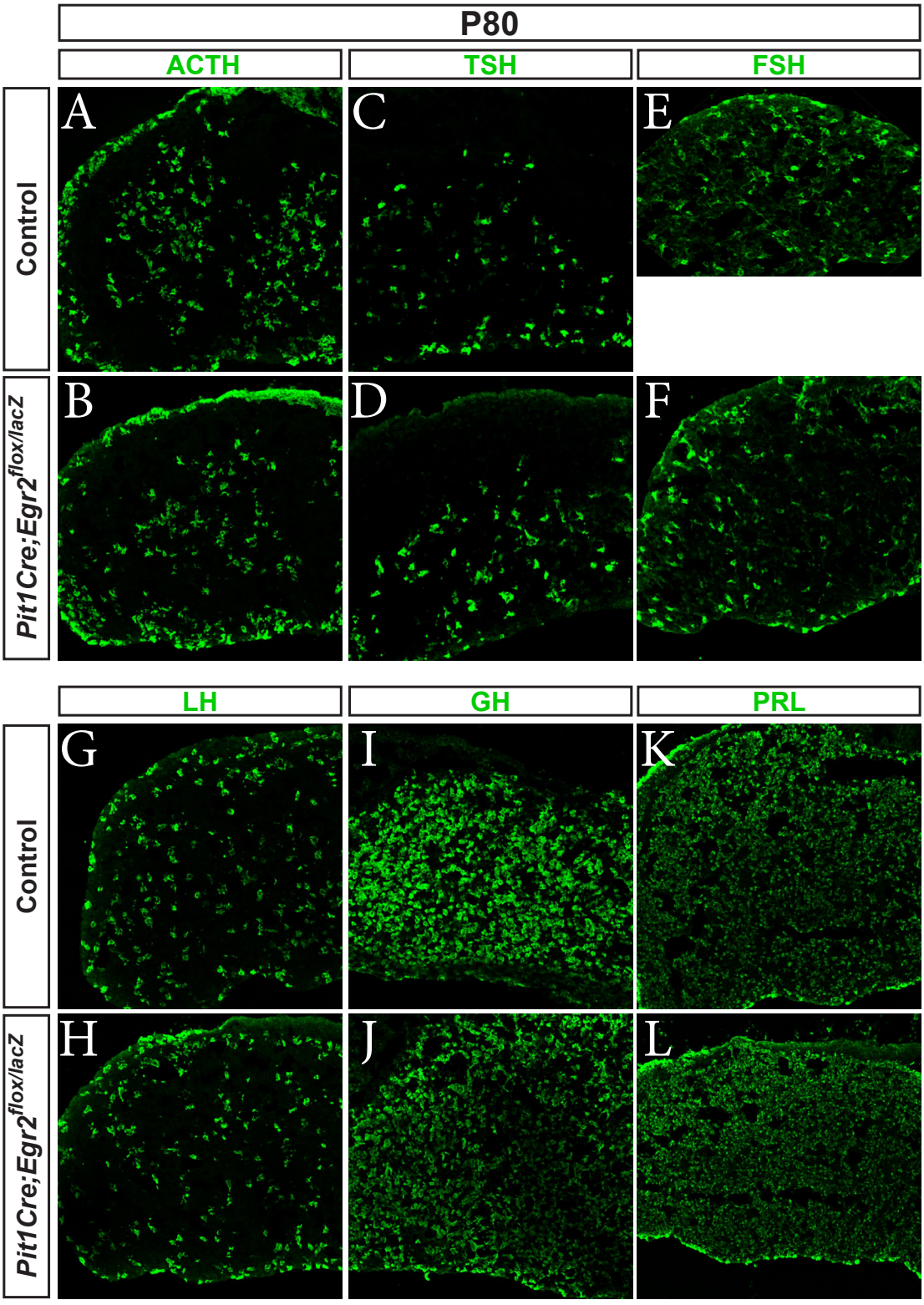

Supplemental Figure 2. *Egr2* conditional knock-out displays no hormonal defect. Immunostaining against all six hormonal cell types in control **(A,C,E,G,I,K)** and *Pit1Cre;Egr2*$^{flox/lacZ}$ **(B,D,F,H,J,L)** pituitary anterior lobes. The *Pit1Cre;Egr2*$^{flox/lacZ}$ mutation does not affect the number of cells of each type.

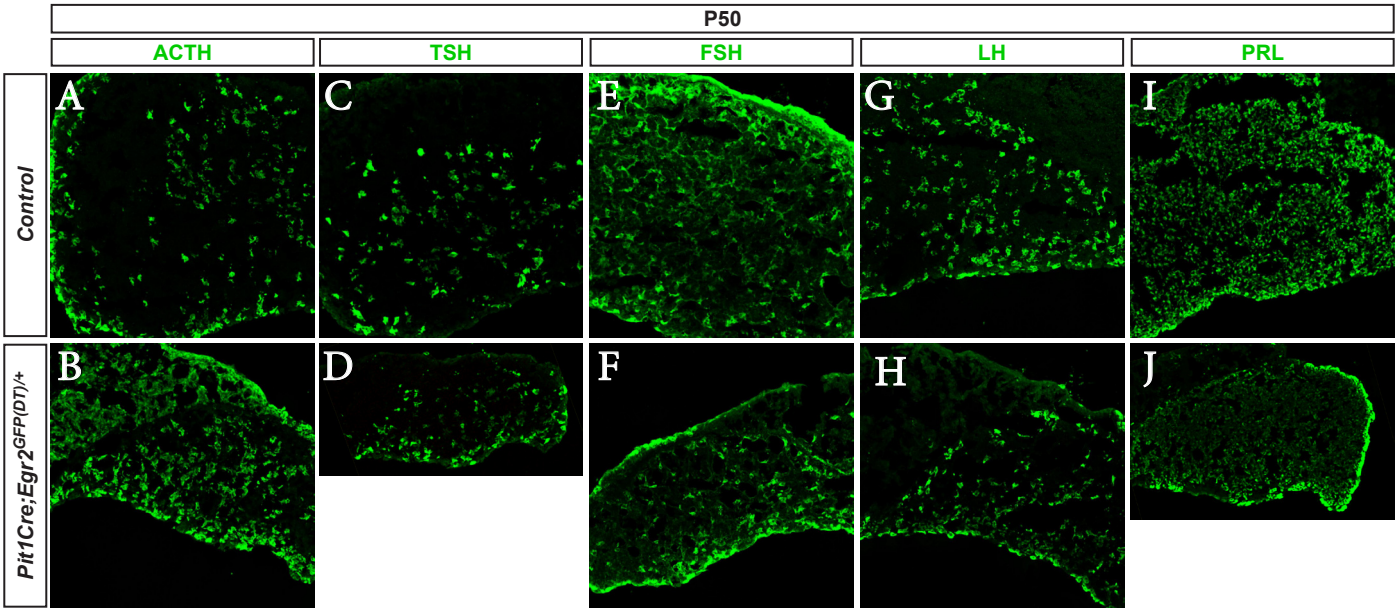

Supplemental Figure 3. Ablation of *Egr2*-positive cells in the *Pit1Cre;Egr2*$^{GFP(DT)/+}$ does not lead to overt modification of hormone expression other than GH. **(A,C,E,G,I)** Control pituitary glands. **(B,D,F,H,J)** *Pit1Cre;Egr2*$^{GFP(DT)/+}$ pituitary glands.

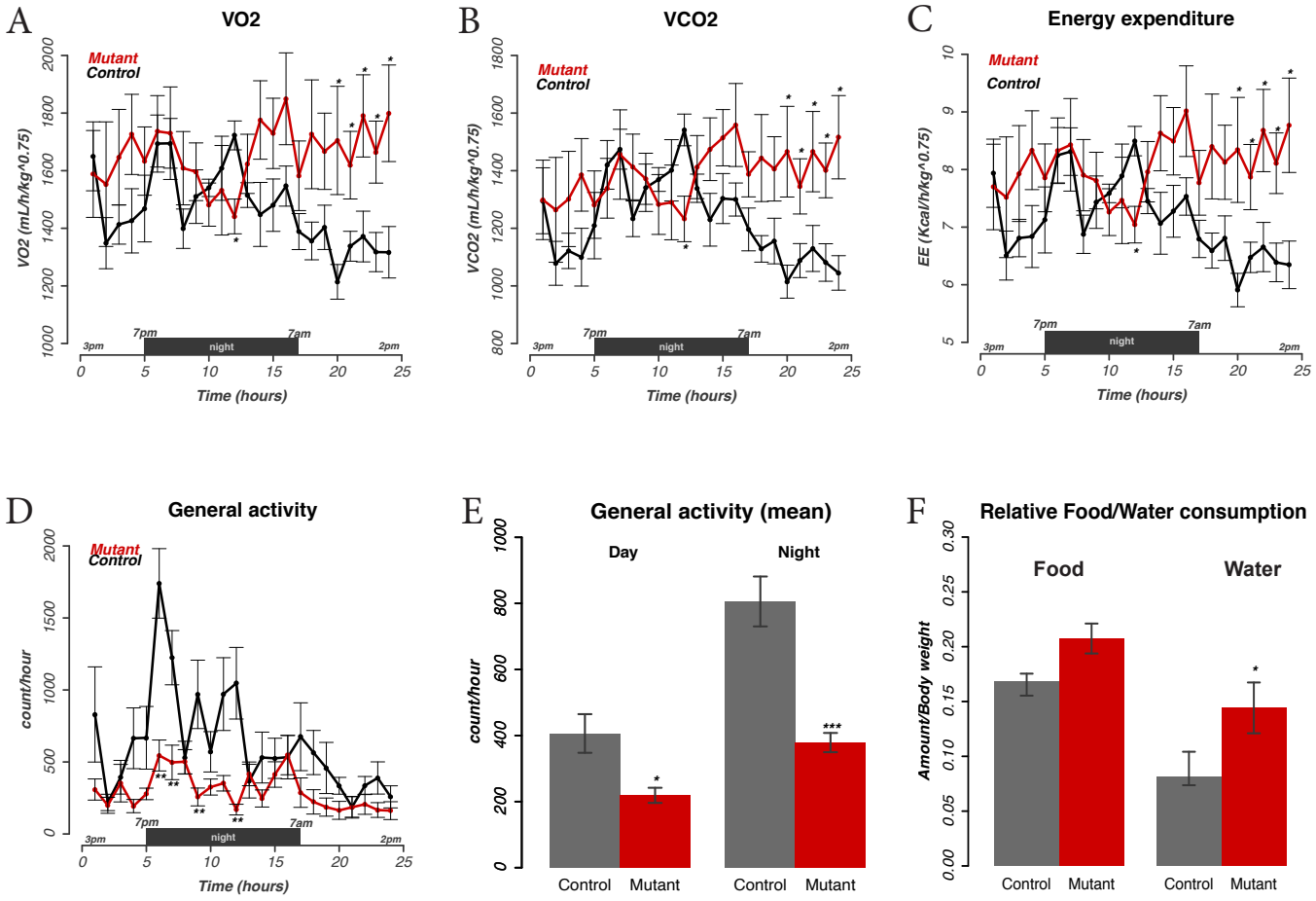

Supplemental Figure 4. Modified diurnal rhythm in *Pit1Cre;Egr2*$^{GFP(DT)/+}$ animals. **(A,B,C)** Indirect calorimetry measurments of VO_2 (A), VCO_2 (B) and calculated energy expenditure (C) over a period of 24 hours. The mutant curves exhibit an out-of-phase behaviour during daytime. **(D,E)** General activity (ambulatory and grooming) was evaluated for 24h. While control mice increase their level of activity during at night, mutants remain as apathetic as during daytime. **(F)** Normalized amount of food and water consumed by control and mutant mice. Respective body weight was taken as normalizing factor.

RÉFÉRENCES BIBLIOGRAPHIQUES

Alexander, T., Nolte, C., and Krumlauf, R. (2009). Hox genes and segmentation of the hindbrain and axial skeleton. Annu. Rev. Cell Dev. Biol. *25*, 431–456.

Amaya, E., Musci, T.J., and Kirschner, M.W. (1991). Expression of a dominant negative mutant of the FGF receptor disrupts mesoderm formation in Xenopus embryos. Cell *66*, 257–270.

Amoyel, M., Cheng, Y.-C., Jiang, Y.-J., and Wilkinson, D.G. (2005). Wnt1 regulates neurogenesis and mediates lateral inhibition of boundary cell specification in the zebrafish hindbrain. Development *132*, 775–785.

Aragon, F., and Pujades, C. (2009). FGF signaling controls caudal hindbrain specification through Ras-ERK1/2 pathway. BMC Dev Biol *9*, 61.

Atkinson, M.R., Savageau, M.A., Myers, J.T., and Ninfa, A.J. (2003). Development of genetic circuitry exhibiting toggle switch or oscillatory behavior in Escherichia coli. Cell *113*, 597–607.

Baker, J., Hardy, M.P., Zhou, J., Bondy, C., Lupu, F., Bellvé, A.R., and Efstratiadis, A. (1996). Effects of an Igf1 gene null mutation on mouse reproduction. Mol Endocrinol *10*, 903–918.

Bartke, A. (1999). Role of growth hormone and prolactin in the control of reproduction: what are we learning from transgenic and knock-out animals? Steroids *64*, 598–604.

Becskei, A., and Serrano, L. (2000). Engineering stability in gene networks by autoregulation. Nature *405*, 590–593.

Becskei, A., Séraphin, B., and Serrano, L. (2001). Positive feedback in eukaryotic gene networks: cell differentiation by graded to binary response conversion. Embo J *20*, 2528–2535.

Bedford, D.C., Kasper, L.H., Fukuyama, T., and Brindle, P.K. (2010). Target gene context influences the transcriptional requirement for the KAT3 family of CBP and p300 histone acetyltransferases. Epigenetics *5*, 9–15.

Behringer, R.R., Mathews, L.S., Palmiter, R.D., and Brinster, R.L. (1988). Dwarf mice produced by genetic ablation of growth hormone-expressing cells. Genes & Development *2*, 453–461.

Bel-Vialar, S., Itasaki, N., and Krumlauf, R. (2002). Initiating Hox gene expression: in the early chick neural tube differential sensitivity to FGF and RA signaling subdivides the HoxB genes in two distinct groups. Development *129*, 5103–5115.

Bénazéraf, B., François, P., Baker, R.E., Denans, N., Little, C.D., and Pourquié, O. (2010). A random cell motility gradient downstream of FGF controls elongation of an amniote embryo. Nature *466*, 248–252.

Bilodeau, S., Roussel-Gervais, A., and Drouin, J. (2009). Distinct developmental roles of cell cycle inhibitors p57Kip2 and p27Kip1 distinguish pituitary progenitor cell cycle exit from cell cycle reentry of differentiated cells. Mol Cell Biol *29*, 1895–1908.

Blak, A.A., Naserke, T., Weisenhorn, D.M.V., Prakash, N., Partanen, J., and Wurst, W. (2005). Expression of Fgf receptors 1, 2, and 3 in the developing mid- and hindbrain of the mouse. Dev Dyn *233*, 1023–1030.

Bouhassira, E.E., Westerman, K., and Leboulch, P. (1997). Transcriptional behavior of LCR enhancer elements integrated at the same chromosomal locus by recombinase-mediated cassette

exchange. Blood *90*, 3332–3344.

Boyle, P.J., Avogaro, A., Smith, L., Shah, S.D., Cryer, P.E., and Santiago, J.V. (1992). Absence of the dawn phenomenon and abnormal lipolysis in type 1 (insulin-dependent) diabetic patients with chronic growth hormone deficiency. Diabetologia *35*, 372–379.

Brown, C.D., Johnson, D.S., and Sidow, A. (2007). Functional architecture and evolution of transcriptional elements that drive gene coexpression. Science *317*, 1557–1560.

Brunet, I., Di Nardo, A.A., Sonnier, L., Beurdeley, M., and Prochiantz, A. (2007). The topological role of homeoproteins in the developing central nervous system. Trends Neurosci *30*, 260–267.

Burz, D.S., Rivera-Pomar, R., Jäckle, H., and Hanes, S.D. (1998). Cooperative DNA-binding by Bicoid provides a mechanism for threshold-dependent gene activation in the Drosophila embryo. Embo J *17*, 5998–6009.

Butler, J.E., and Kadonaga, J.T. (2001). Enhancer-promoter specificity mediated by DPE or TATA core promoter motifs. Genes & Development *15*, 2515–2519.

Camper, S.A., Saunders, T.L., Katz, R.W., and Reeves, R.H. (1990). The Pit-1 transcription factor gene is a candidate for the murine Snell dwarf mutation. Genomics *8*, 586–590.

Cantor, A.B., and Orkin, S.H. (2001). Hematopoietic development: a balancing act. Curr Opin Genet Dev *11*, 513–519.

Capdevila, M.P., and Garcia-Bellido, A. (1974). Development and genetic analysis of bithorax phenocopies in Drosophila. Nature *250*, 500–502.

Capecchi, M.R.A.M.R. (1999). Hoxa1 and Hoxb1 mutants and craniofacial development. 1–14.

Carbajo-Pérez, E., and Watanabe, Y.G. (1990). Cellular proliferation in the anterior pituitary of the rat during the postnatal period. Cell Tissue Res. *261*, 333–338.

Carroll, S.B. (2005). Evolution at two levels: on genes and form. PLoS Biol *3*, e245.

Chandrashekar, V., and Bartke, A. (1998). The role of growth hormone in the control of gonadotropin secretion in adult male rats. Endocrinology *139*, 1067–1074.

Charlton, H.M., Clark, R.G., Robinson, I.C., Goff, A.E., Cox, B.S., Bugnon, C., and Bloch, B.A. (1988). Growth hormone-deficient dwarfism in the rat: a new mutation. J Endocrinol *119*, 51–58.

Chatelin, L., Volovitch, M., Joliot, A.H., Perez, F., and Prochiantz, A. (1996). Transcription factor hoxa-5 is taken up by cells in culture and conveyed to their nuclei. Mech Dev *55*, 111–117.

Chatonnet, F., Wrobel, L.J., Mézières, V., Pasqualetti, M., Ducret, S., Taillebourg, E., Charnay, P., Rijli, F.M., and Champagnat, J. (2007). Distinct roles of Hoxa2 and Krox20 in the development of rhythmic neural networks controlling inspiratory depth, respiratory frequency, and jaw opening. Neural Development *2*, 19.

Chavrier, P., Janssen-Timmen, U., Mattéi, M.G., Zerial, M., Bravo, R., and Charnay, P. (1989). Structure, chromosome location, and expression of the mouse zinc finger gene Krox-20: multiple gene products and coregulation with the proto-oncogene c-fos. Mol Cell Biol *9*, 787–797.

Chavrier, P., Lemaire, P., Revelant, O., Bravo, R., and Charnay, P. (1988a). Characterization of a mouse multigene family that encodes zinc finger structures. Mol Cell Biol *8*, 1319–1326.

Chavrier, P., Vesque, C., Galliot, B., Vigneron, M., Dollé, P., Duboule, D., and Charnay, P. (1990). The segment-specific gene Krox-20 encodes a transcription factor with binding sites in the promoter region of the Hox-1.4 gene. Embo J *9*, 1209–1218.

Chavrier, P., Zerial, M., Lemaire, P., Almendral, J., Bravo, R., and Charnay, P. (1988b). A gene encoding a protein with zinc fingers is activated during G0/G1 transition in cultured cells. Embo J *7*, 29–35.

Chen, Y., Mohammadi, M., and Flanagan, J.G. (2009). Graded levels of FGF protein span the midbrain and can instruct graded induction and repression of neural mapping labels. Neuron *62*, 773–780.

Chomette, D., Frain, M., Cereghini, S., Charnay, P., and Ghislain, J. (2006). Krox20 hindbrain cis-regulatory landscape: interplay between multiple long-range initiation and autoregulatory elements. Development *133*, 1253–1262.

Cinquin, O., and Demongeot, J. (2002). Roles of positive and negative feedback in biological systems. C R Biol *325*, 1085–1095.

Cooke, J., Moens, C., Roth, L., Durbin, L., Shiomi, K., Brennan, C., Kimmel, C., Wilson, S., and Holder, N. (2001). Eph signalling functions downstream of Val to regulate cell sorting and boundary formation in the caudal hindbrain. Development *128*, 571–580.

Cooke, J.E., and Moens, C.B. (2002). Boundary formation in the hindbrain: Eph only it were simple. Trends Neurosci *25*, 260–267.

Cooke, J.E., Kemp, H.A., and Moens, C.B. (2005). EphA4 is required for cell adhesion and rhombomere-boundary formation in the zebrafish. Curr Biol *15*, 536–542.

Crauk, O., and Dostatni, N. (2005). Bicoid determines sharp and precise target gene expression in the Drosophila embryo. Curr Biol *15*, 1888–1898.

Creyghton, M.P., Cheng, A.W., Welstead, G.G., Kooistra, T., Carey, B.W., Steine, E.J., Hanna, J., Lodato, M.A., Frampton, G.M., Sharp, P.A., et al. (2010). Histone H3K27ac separates active from poised enhancers and predicts developmental state. Proc Natl Acad Sci USA *107*, 21931–21936.

Dasen, J.S., and Jessell, T.M. (2009). Hox networks and the origins of motor neuron diversity. Curr. Top. Dev. Biol. *88*, 169–200.

Davenne, M., Maconochie, M.K., Neun, R., Pattyn, A., Chambon, P., Krumlauf, R., and Rijli, F.M. (1999). Hoxa2 and Hoxb2 control dorsoventral patterns of neuronal development in the rostral hindbrain. Neuron *22*, 677–691.

del Rincon, J.-P., Iida, K., Gaylinn, B.D., McCurdy, C.E., Leitner, J.W., Barbour, L.A., Kopchick, J.J., Friedman, J.E., Draznin, B., and Thorner, M.O. (2007). Growth hormone regulation of p85alpha expression and phosphoinositide 3-kinase activity in adipose tissue: mechanism for growth hormone-mediated insulin resistance. Diabetes *56*, 1638–1646.

Doga, M., Bonadonna, S., Gola, M., Mazziotti, G., and Giustina, A. (2006). Growth hormone

deficiency in the adult. Pituitary *9*, 305–311.

Dominici, F.P., Arostegui Diaz, G., Bartke, A., Kopchick, J.J., and Turyn, D. (2000). Compensatory alterations of insulin signal transduction in liver of growth hormone receptor knockout mice. J Endocrinol *166*, 579–590.

Dominici, F.P., Hauck, S., Argentino, D.P., Bartke, A., and Turyn, D. (2002). Increased insulin sensitivity and upregulation of insulin receptor, insulin receptor substrate (IRS)-1 and IRS-2 in liver of Ames dwarf mice. J Endocrinol *173*, 81–94.

Draper, B.W., Stock, D.W., and Kimmel, C.B. (2003). Zebrafish fgf24 functions with fgf8 to promote posterior mesodermal development. Development *130*, 4639–4654.

Duboule, D. (1998). Vertebrate hox gene regulation: clustering and/or colinearity? Curr Opin Genet Dev *8*, 514–518.

Dubreuil, V., Thoby-Brisson, M., Rallu, M., Persson, K., Pattyn, A., Birchmeier, C., Brunet, J.-F., Fortin, G., and Goridis, C. (2009). Defective respiratory rhythmogenesis and loss of central chemosensitivity in Phox2b mutants targeting retrotrapezoid nucleus neurons. J Neurosci *29*, 14836–14846.

Dubrulle, J., and Pourquié, O. (2004). fgf8 mRNA decay establishes a gradient that couples axial elongation to patterning in the vertebrate embryo. Nature *427*, 419–422.

Dubrulle, J., McGrew, M.J., and Pourquié, O. (2001). FGF signaling controls somite boundary position and regulates segmentation clock control of spatiotemporal Hox gene activation. Cell *106*, 219–232.

Dymecki, S.M., Ray, R.S., and Kim, J.C. (2010). Mapping cell fate and function using recombinase-based intersectional strategies. Meth Enzymol *477*, 183–213.

Elkouby, Y.M., Elias, S., Casey, E.S., Blythe, S.A., Tsabar, N., Klein, P.S., Root, H., Liu, K.J., and Frank, D. (2010). Mesodermal Wnt signaling organizes the neural plate via Meis3. Development *137*, 1531–1541.

Ellis, T., Wang, X., and Collins, J.J. (2009). Diversity-based, model-guided construction of synthetic gene networks with predicted functions. Nat Biotechnol *27*, 465–471.

Elowitz, M.B., and Leibler, S. (2000). A synthetic oscillatory network of transcriptional regulators. Nature *403*, 335–338.

Elowitz, M.B., Levine, A.J., Siggia, E.D., and Swain, P.S. (2002). Stochastic gene expression in a single cell. Science *297*, 1183–1186.

Ferrell, J.E. (2002). Self-perpetuating states in signal transduction: positive feedback, double-negative feedback and bistability. Curr Opin Cell Biol *14*, 140–148.

Ferrell, J.E., Pomerening, J.R., Kim, S.Y., Trunnell, N.B., Xiong, W., Huang, C.-Y.F., and Machleder, E.M. (2009). Simple, realistic models of complex biological processes: Positive feedback and bistability in a cell fate switch and a cell cycle oscillator. FEBS Lett *583*, 3999–4005.

Ferretti, E., Cambronero, F., Tümpel, S., Longobardi, E., Wiedemann, L.M., Blasi, F., and Krumlauf, R. (2005). Hoxb1 enhancer and control of rhombomere 4 expression: complex

interplay between PREP1-PBX1-HOXB1 binding sites. Mol Cell Biol *25*, 8541–8552.

Forsberg, E.C., Zaboikina, T.N., Versaw, W.K., Ahn, N.G., and Bresnick, E.H. (1999). Enhancement of beta-globin locus control region-mediated transactivation by mitogen-activated protein kinases through stochastic and graded mechanisms. Mol Cell Biol *19*, 5565–5575.

Fraser, S., Keynes, R., and Lumsden, A. (1990). Segmentation in the chick embryo hindbrain is defined by cell lineage restrictions. Nature *344*, 431–435.

Garcia-Bellido, A., and Lewis, E.B. (1976). Autonomous cellular differentiation of homoeotic bithorax mutants of Drosophila melanogaster. Developmental Biology *48*, 400–410.

Garcia-Dominguez, M., Gilardi-Hebenstreit, P., and Charnay, P. (2006). PIASxbeta acts as an activator of Hoxb1 and is antagonized by Krox20 during hindbrain segmentation. Embo J *25*, 2432–2442.

Gashler, A., and Sukhatme, V.P. (1995). Early growth response protein 1 (Egr-1): prototype of a zinc-finger family of transcription factors. Prog. Nucleic Acid Res. Mol. Biol. *50*, 191–224.

Gaszner, M., and Felsenfeld, G. (2006). Insulators: exploiting transcriptional and epigenetic mechanisms. Nat Rev Genet *7*, 703–713.

Gehring, W.J. (1987). Homeo boxes in the study of development. Science *236*, 1245–1252.

Georges, A.B., Benayoun, B.A., Caburet, S., and Veitia, R.A. (2010). Generic binding sites, generic DNA-binding domains: where does specific promoter recognition come from? The FASEB Journal *24*, 346–356.

Gertz, J., Siggia, E.D., and Cohen, B.A. (2009). Analysis of combinatorial cis-regulation in synthetic and genomic promoters. Nature *457*, 215–218.

Gibbs, J.D., Liebermann, D.A., and Hoffman, B. (2008). Egr-1 abrogates the E2F-1 block in terminal myeloid differentiation and suppresses leukemia. Oncogene *27*, 98–106.

Gilardi-Hebenstreit, P., Nieto, M.A., Frain, M., Mattéi, M.G., Chestier, A., Wilkinson, D.G., and Charnay, P. (1992). An Eph-related receptor protein tyrosine kinase gene segmentally expressed in the developing mouse hindbrain. Oncogene *7*, 2499–2506.

Giudicelli, F., Gilardi-Hebenstreit, P., Mechta-Grigoriou, F., Poquet, C., and Charnay, P. (2003). Novel activities of Mafb underlie its dual role in hindbrain segmentation and regional specification. Developmental Biology *253*, 150–162.

Giudicelli, F., Taillebourg, E., Charnay, P., and Gilardi-Hebenstreit, P. (2001). Krox-20 patterns the hindbrain through both cell-autonomous and non cell-autonomous mechanisms. Genes & Development *15*, 567–580.

Gospodarowicz, D., and Moran, J.S. (1974). Stimulation of division of sparse and confluent 3T3 cell populations by a fibroblast growth factor, dexamethasone, and insulin. Proc Natl Acad Sci USA *71*, 4584–4588.

Graham, T.G.W., Tabei, S.M.A., Dinner, A.R., and Rebay, I. (2010). Modeling bistable cell-fate choices in the Drosophila eye: qualitative and quantitative perspectives. Development *137*, 2265–2278.

Gregor, T., Tank, D.W., Wieschaus, E.F., and Bialek, W. (2007a). Probing the limits to positional information. Cell *130*, 153–164.

Gregor, T., Wieschaus, E.F., McGregor, A.P., Bialek, W., and Tank, D.W. (2007b). Stability and nuclear dynamics of the bicoid morphogen gradient. Cell *130*, 141–152.

Gremeaux, L., Fu, Q., Chen, J., and Vankelecom, H. (2011). Activated Phenotype of the Pituitary Stem/Progenitor Cell Compartment During the Early-Postnatal Maturation Phase of the Gland. Stem Cells and Development 111116074556008.

Groop, L., Segerlantz, M., and Bramnert, M. (2005). Insulin Sensitivity in Adults with Growth Hormone Deficiency and Effect of Growth Hormone Treatment. Horm Res *64*, 45–50.

Guet, C.C., Elowitz, M.B., Hsing, W., and Leibler, S. (2002). Combinatorial synthesis of genetic networks. Science *296*, 1466–1470.

Guthrie, S., and Lumsden, A. (1991). Formation and regeneration of rhombomere boundaries in the developing chick hindbrain. Development *112*, 221–229.

Hadjur, S., Williams, L.M., Ryan, N.K., Cobb, B.S., Sexton, T., Fraser, P., Fisher, A.G., and Merkenschlager, M. (2009). Cohesins form chromosomal cis-interactions at the developmentally regulated IFNG locus. Nature *460*, 410–413.

Hauptmann, G., and Gerster, T. (1994). Two-color whole-mount in situ hybridization to vertebrate and Drosophila embryos. Trends Genet *10*, 266–266.

Heintzman, N.D., Hon, G.C., Hawkins, R.D., Kheradpour, P., Stark, A., Harp, L.F., Ye, Z., Lee, L.K., Stuart, R.K., Ching, C.W., et al. (2009). Histone modifications at human enhancers reflect global cell-type-specific gene expression. Nature *459*, 108–112.

Heintzman, N.D., Stuart, R.K., Hon, G., Fu, Y., Ching, C.W., Hawkins, R.D., Barrera, L.O., Van Calcar, S., Qu, C., Ching, K.A., et al. (2007). Distinct and predictive chromatin signatures of transcriptional promoters and enhancers in the human genome. Nat Genet *39*, 311–318.

Hernandez, R.E., Rikhof, H.A., Bachmann, R., and Moens, C.B. (2004). vhnf1 integrates global RA patterning and local FGF signals to direct posterior hindbrain development in zebrafish. Development *131*, 4511–4520.

Holcman, D., Kasatkin, V., and Prochiantz, A. (2007). Modeling homeoprotein intercellular transfer unveils a parsimonious mechanism for gradient and boundary formation in early brain development. J Theor Biol *249*, 503–517.

Hongo, I., Kengaku, M., and Okamoto, H. (1999). FGF signaling and the anterior neural induction in Xenopus. Developmental Biology *216*, 561–581.

Hou, C., Dale, R., and Dean, A. (2010). Cell type specificity of chromatin organization mediated by CTCF and cohesin. Proc Natl Acad Sci USA *107*, 3651–3656.

Huang, S., Guo, Y.-P., May, G., and Enver, T. (2007). Bifurcation dynamics in lineage-commitment in bipotent progenitor cells. Developmental Biology *305*, 695–713.

Huda, M.S.B., Dovey, T.M., Wong, S.P., English, P.J., Halford, J.C.G., McCulloch, P., Cleator, J., Martin, B., Cashen, J., Hayden, K., et al. (2011). Ghrelin does not orchestrate the metabolic

changes seen in fasting but has significant effects on lipid mobilisation and substrate utilisation. European Journal of Endocrinology *165*, 45–55.

Jackman, W. (2000). islet Reveals Segmentation in the Amphioxus Hindbrain Homolog. Developmental Biology *220*, 16–26.

JACOB, F., SUSSMAN, R., and MONOD, J. (1962). [On the nature of the repressor ensuring the immunity of lysogenic bacteria]. C. R. Hebd. Seances Acad. Sci. *254*, 4214–4216.

Jaeger, J., Blagov, M., Kosman, D., Kozlov, K.N., Manu, Myasnikova, E., Surkova, S., Vanario-Alonso, C.E., Samsonova, M., Sharp, D.H., et al. (2004). Dynamical analysis of regulatory interactions in the gap gene system of Drosophila melanogaster. Genetics *167*, 1721–1737.

Jensen, D., Gayles, E., Ammon, S., Phillips, R., and Eckel, R. (2001). A self-correcting indirect calorimeter system for the measurement of energy balance in small animals. J Appl Physiol *90*, 912–918.

Johnston, R.J., Jr., and Desplan, C. (2010). Stochastic Mechanisms of Cell Fate Specification that Yield Random or Robust Outcomes. Annu. Rev. Cell Dev. Biol. *26*, 689–719.

Jowett, T., and Lettice, L. (1994). Whole-mount in situ hybridizations on zebrafish embryos using a mixture of digoxigenin- and fluorescein-labelled probes. Trends Genet *10*, 73–74.

Kagey, M.H., Newman, J.J., Bilodeau, S., Zhan, Y., Orlando, D.A., van Berkum, N.L., Ebmeier, C.C., Goossens, J., Rahl, P.B., Levine, S.S., et al. (2010). Mediator and cohesin connect gene expression and chromatin architecture. Nature *467*, 430–435.

Kelberman, D., Rizzoti, K., Lovell-Badge, R., Robinson, I.C.A.F., and Dattani, M.T. (2009). Genetic regulation of pituitary gland development in human and mouse. Endocrine Reviews *30*, 790–829.

Kelley, D.E., and Mandarino, L.J. (2000). Fuel selection in human skeletal muscle in insulin resistance: a reexamination. Diabetes *49*, 677–683.

Kepler, T.B., and Elston, T.C. (2001). Stochasticity in transcriptional regulation: origins, consequences, and mathematical representations. Biophys J *81*, 3116–3136.

Kim, F.A., Sing l, A., Kaneko, T., Bieman, M., Stallwood, N., Sadl, V.S., and Cordes, S.P. (2005). The vHNF1 homeodomain protein establishes early rhombomere identity by direct regulation of Kreisler expression. Mech Dev *122*, 1300–1309.

Kim, H.D., Shay, T., O'Shea, E.K., and Regev, A. (2009). Transcriptional regulatory circuits: predicting numbers from alphabets. Science *325*, 429–432.

Kimmel, C.B., Ballard, W.W., Kimmel, S.R., Ullmann, B., and Schilling, T.F. (1995). Stages of embryonic development of the zebrafish. Dev Dyn *203*, 253–310.

Klug, A. (2010). The discovery of zinc fingers and their applications in gene regulation and genome manipulation. Annu. Rev. Biochem. *79*, 213–231.

Klug, A., and Rhodes, D. (1987). Zinc fingers: a novel protein fold for nucleic acid recognition. Cold Spring Harb Symp Quant Biol *52*, 473–482.

Knight, R.D., Panopoulou, G.D., Holland, P.W., and Shimeld, S.M. (2000). An amphioxus Krox gene: insights into vertebrate hindbrain evolution. Dev Genes Evol *210*, 518–521.

Kramer, B.P., and Fussenegger, M. (2005). Hysteresis in a synthetic mammalian gene network. Proc Natl Acad Sci USA *102*, 9517–9522.

Kramer, B.P., Viretta, A.U., Daoud-El-Baba, M., Aubel, D., Weber, W., and Fussenegger, M. (2004). An engineered epigenetic transgene switch in mammalian cells. Nat Biotechnol *22*, 867–870.

Krauss, S., Johansen, T., Korzh, V., Moens, U., Ericson, J.U., and Fjose, A. (1991). Zebrafish pax[zf-a]: a paired box-containing gene expressed in the neural tube. Embo J *10*, 3609–3619.

Krysinska, H., Hoogenkamp, M., Ingram, R., Wilson, N., Tagoh, H., Laslo, P., Singh, H., and Bonifer, C. (2007). A Two-Step, PU.1-Dependent Mechanism for Developmentally Regulated Chromatin Remodeling and Transcription of the c-fms Gene. Mol Cell Biol *27*, 878–887.

Kumano, G., and Smith, W.C. (2002). Revisions to the Xenopus gastrula fate map: implications for mesoderm induction and patterning. Dev Dyn *225*, 409–421.

Kurokawa, D. (2004). Regulation of Otx2 expression and its functions in mouse forebrain and midbrain. Development *131*, 3319–3331.

Labalette, C., Bouchoucha, Y.X., Wassef, M.A., Gongal, P.A., Le Men, J., Becker, T., Gilardi-Hebenstreit, P., and Charnay, P. (2011). Hindbrain patterning requires fine-tuning of early krox20 transcription by Sprouty 4. Development *138*, 317–326.

Laslo, P., Spooner, C.J., Warmflash, A., Lancki, D.W., Lee, H.-J., Sciammas, R., Gantner, B.N., Dinner, A.R., and Singh, H. (2006). Multilineage transcriptional priming and determination of alternate hematopoietic cell fates. Cell *126*, 755–766.

Lawson, M.A., Tsutsumi, R., Zhang, H., Talukdar, I., Butler, B.K., Santos, S.J., Mellon, P.L., and Webster, N.J.G. (2007). Pulse sensitivity of the luteinizing hormone beta promoter is determined by a negative feedback loop Involving early growth response-1 and Ngfi-A binding protein 1 and 2. Mol Endocrinol *21*, 1175–1191.

Lebrecht, D., Foehr, M., Smith, E., Lopes, F.J.P., Vanario-Alonso, C.E., Reinitz, J., Burz, D.S., and Hanes, S.D. (2005). Bicoid cooperative DNA binding is critical for embryonic patterning in Drosophila. Proc Natl Acad Sci USA *102*, 13176–13181.

Lecaudey, V., Anselme, I., Rosa, F., and Schneider-Maunoury, S. (2004). The zebrafish Iroquois gene iro7 positions the r4/r5 boundary and controls neurogenesis in the rostral hindbrain. Development *131*, 3121–3131.

Lee, Y., Grill, S., Sanchez, A., Murphy-Ryan, M., and Poss, K.D. (2005). Fgf signaling instructs position-dependent growth rate during zebrafish fin regeneration. Development *132*, 5173–5183.

Lei, E.P., and Corces, V.G. (2006). RNA interference machinery influences the nuclear organization of a chromatin insulator. Nat Genet *38*, 936–941.

Levi, G., Topilko, P., Schneider-Maunoury, S., Lasagna, M., Mantero, S., Cancedda, R., and Charnay, P. (1996). Defective bone formation in Krox-20 mutant mice. Development *122*, 113–120.

Li, B., Kuriyama, S., Moreno, M., and Mayor, R. (2009). The posteriorizing gene Gbx2 is a direct target of Wnt signalling and the earliest factor in neural crest induction. Development *136*, 3267–3278.

Li, S., Crenshaw, E.B., Rawson, E.J., Simmons, D.M., Swanson, L.W., and Rosenfeld, M.G. (1990). Dwarf locus mutants lacking three pituitary cell types result from mutations in the POU-domain gene pit-1. Nature *347*, 528–533.

Lim, Y., and Golden, J.A. (2007). Patterning the developing diencephalon. Brain Res Rev *53*, 17–26.

Liu, A., Losos, K., and Joyner, A.L. (1999). FGF8 can activate Gbx2 and transform regions of the rostral mouse brain into a hindbrain fate. Development *126*, 4827–4838.

Longo, K.A., Charoenthongtrakul, S., Giuliana, D.J., Govek, E.K., McDonagh, T., Qi, Y., DiStefano, P.S., and Geddes, B.J. (2008). Improved insulin sensitivity and metabolic flexibility in ghrelin receptor knockout mice. Regulatory Peptides *150*, 55–61.

Lopes, F.J.P., Vanario-Alonso, C.E., Bisch, P.M., and Vieira, F.M.C. (2005). A kinetic mechanism for Drosophila bicoid cooperative binding. J Theor Biol *235*, 185–198.

Losick, R., and Desplan, C. (2008). Stochasticity and cell fate. Science *320*, 65–68.

Lumsden, A., and Keynes, R. (1989). Segmental patterns of neuronal development in the chick hindbrain. Nature *337*, 424–428.

Lumsden, A., and Krumlauf, R. (1996). Patterning the vertebrate neuraxis. Science *274*, 1109–1115.

Lupien, M., Eeckhoute, J., Meyer, C.A., Wang, Q., Zhang, Y., Li, W., Carroll, J.S., Liu, X.S., and Brown, M. (2008). FoxA1 translates epigenetic signatures into enhancer-driven lineage-specific transcription. Cell *132*, 958–970.

Luque, R.M., Lin, Q., Córdoba-Chacón, J., Subbaiah, P.V., Buch, T., Waisman, A., Vankelecom, H., and Kineman, R.D. (2011). Metabolic impact of adult-onset, isolated, growth hormone deficiency (AOiGHD) due to destruction of pituitary somatotropes. PLoS ONE *6*, e15767.

Maconochie, M.K., Nonchev, S., Studer, M., Chan, S.K., Pöpperl, H., Sham, M.H., Mann, R.S., and Krumlauf, R. (1997). Cross-regulation in the mouse HoxB complex: the expression of Hoxb2 in rhombomere 4 is regulated by Hoxb1. Genes & Development *11*, 1885–1895.

Manzanares, M., Bel-Vialar, S., Ariza-McNaughton, L., Ferretti, E., Marshall, H., Maconochie, M.M., Blasi, F., and Krumlauf, R. (2001). Independent regulation of initiation and maintenance phases of Hoxa3 expression in the vertebrate hindbrain involve auto- and cross-regulatory mechanisms. Development *128*, 3595–3607.

Manzanares, M., Cordes, S., Ariza-McNaughton, L., Sadl, V., Maruthainar, K., Barsh, G., and Krumlauf, R. (1999). Conserved and distinct roles of kreisler in regulation of the paralogous Hoxa3 and Hoxb3 genes. Development *126*, 759–769.

Manzanares, M., Cordes, S., Kwan, C.T., Sham, M.H., Barsh, G.S., and Krumlauf, R. (1997). Segmental regulation of Hoxb-3 by kreisler. Nature *387*, 191–195.

Mao, J., McGlinn, E., Huang, P., Tabin, C.J., and McMahon, A.P. (2009). Fgf-dependent Etv4/5 activity is required for posterior restriction of Sonic Hedgehog and promoting outgrowth of the vertebrate limb. Dev Cell *16*, 600–606.

Marchal, L., Luxardi, G., Thomé, V., and Kodjabachian, L. (2009). BMP inhibition initiates neural induction via FGF signaling and Zic genes. Proc Natl Acad Sci USA *106*, 17437–17442.

Marín, F., and Charnay, P. (2000). Hindbrain patterning: FGFs regulate Krox20 and mafB/kr expression in the otic/preotic region. Development *127*, 4925–4935.

Marín, F., and Puelles, L. (1995). Morphological fate of rhombomeres in quail/chick chimeras: a segmental analysis of hindbrain nuclei. Eur. J. Neurosci. *7*, 1714–1738.

Marshall, H., Nonchev, S., Sham, M.H., Muchamore, I., Lumsden, A., and Krumlauf, R. (1992). Retinoic acid alters hindbrain Hox code and induces transformation of rhombomeres 2/3 into a 4/5 identity. Nature *360*, 737–741.

Mathioudakis, N., and Salvatori, R. (2008). Adult-onset growth hormone deficiency: causes, complications and treatment options. Curr Opin Endocrinol Diabetes Obes *15*, 352–358.

Mauras, N., O'Brien, K.O., Welch, S., Rini, A., Helgeson, K., Vieira, N.E., and Yergey, A.L. (2000). Insulin-like growth factor I and growth hormone (GH) treatment in GH-deficient humans: differential effects on protein, glucose, lipid, and calcium metabolism. J Clin Endocrinol Metab *85*, 1686–1694.

Maves, L., and Kimmel, C.B. (2005). Dynamic and sequential patterning of the zebrafish posterior hindbrain by retinoic acid. Developmental Biology *285*, 593–605.

Maves, L., Jackman, W., and Kimmel, C.B. (2002). FGF3 and FGF8 mediate a rhombomere 4 signaling activity in the zebrafish hindbrain. Development *129*, 3825–3837.

McGinnis, W., and Krumlauf, R. (1992). Homeobox genes and axial patterning. Cell *68*, 283–302.

McGinnis, W., Hart, C.P., Gehring, W.J., and Ruddle, F.H. (1984). Molecular cloning and chromosome mapping of a mouse DNA sequence homologous to homeotic genes of Drosophila. Cell *38*, 675–680.

McKay, I.J., Muchamore, I., Krumlauf, R., Maden, M., Lumsden, A., and Lewis, J. (1994). The kreisler mouse: a hindbrain segmentation mutant that lacks two rhombomeres. Development *120*, 2199–2211.

Mello, C.V., and Clayton, D.F. (1995). Differential induction of the ZENK gene in the avian forebrain and song control circuit after metrazole-induced depolarization. J. Neurobiol. *26*, 145–161.

Meyers, E.N., and Martin, G.R. (1999). Differences in left-right axis pathways in mouse and chick: functions of FGF8 and SHH. Science *285*, 403–406.

Meyers, E.N., Lewandoski, M., and Martin, G.R. (1998). An Fgf8 mutant allelic series generated by Cre- and Flp-mediated recombination. Nat Genet *18*, 136–141.

Mito, Y., Henikoff, J.G., and Henikoff, S. (2005). Genome-scale profiling of histone H3.3 replacement patterns. Nat Genet *37*, 1090–1097.

Mito, Y., Henikoff, J.G., and Henikoff, S. (2007). Histone replacement marks the boundaries of cis-regulatory domains. Science *315*, 1408–1411.

Moens, C.B., and Prince, V.E. (2002). Constructing the hindbrain: insights from the zebrafish. Dev Dyn *224*, 1–17.

Moens, C.B., Cordes, S.P., Giorgianni, M.W., Barsh, G.S., and Kimmel, C.B. (1998). Equivalence in the genetic control of hindbrain segmentation in fish and mouse. Development *125*, 381–391.

Moens, C.B., Yan, Y.L., Appel, B., Force, A.G., and Kimmel, C.B. (1996). valentino: a zebrafish gene required for normal hindbrain segmentation. Development *122*, 3981–3990.

Monk, K.R., and Talbot, W.S. (2009). Genetic dissection of myelinated axons in zebrafish. Curr Opin Neurobiol *19*, 486–490.

Monk, K.R., Naylor, S.G., Glenn, T.D., Mercurio, S., Perlin, J.R., Dominguez, C., Moens, C.B., and Talbot, W.S. (2009). A G protein-coupled receptor is essential for Schwann cells to initiate myelination. Science *325*, 1402–1405.

Montavon, T., Soshnikova, N., Mascrez, B., Joye, E., Thevenet, L., Splinter, E., de Laat, W., Spitz, F., and Duboule, D. (2011). A Regulatory Archipelago Controls Hox Genes Transcription in Digits. Cell *147*, 1132–1145.

Moroni, M.C., Viganó, M.A., and Mavilio, F. (1993). Regulation of the human HOXD4 gene by retinoids. Mech Dev *44*, 139–154.

Münchberg, S.R., Ober, E.A., and Steinbeisser, H. (1999). Expression of the Ets transcription factors erm and pea3 in early zebrafish development. Mech Dev *88*, 233–236.

Nardelli, J., Gibson, T., and Charnay, P. (1992). Zinc finger-DNA recognition: analysis of base specificity by site-directed mutagenesis. Nucleic Acids Res *20*, 4137–4144.

Nardelli, J., Gibson, T.J., Vesque, C., and Charnay, P. (1991). Base sequence discrimination by zinc-finger DNA-binding domains. Nature *349*, 175–178.

Nativio, R., Wendt, K.S., Ito, Y., Huddleston, J.E., Uribe-Lewis, S., Woodfine, K., Krueger, C., Reik, W., Peters, J.-M., and Murrell, A. (2009). Cohesin is required for higher-order chromatin conformation at the imprinted IGF2-H19 locus. PLoS Genet *5*, e1000739.

Nieto, M.A., Gilardi-Hebenstreit, P., Charnay, P., and Wilkinson, D.G. (1992). A receptor protein tyrosine kinase implicated in the segmental patterning of the hindbrain and mesoderm. Development *116*, 1137–1150.

Nittenberg, R., Patel, K., Joshi, Y., Krumlauf, R., Wilkinson, D.G., Brickell, P.M., Tickle, C., and Clarke, J.D. (1997). Cell movements, neuronal organisation and gene expression in hindbrains lacking morphological boundaries. Development *124*, 2297–2306.

Nonchev, S., Vesque, C., Maconochie, M., Seitanidou, T., Ariza-McNaughton, L., Frain, M., Marshall, H., Sham, M.H., Krumlauf, R., and Charnay, P. (1996). Segmental expression of Hoxa-2 in the hindbrain is directly regulated by Krox-20. Development *122*, 543–554.

Nordström, U., Jessell, T.M., and Edlund, T. (2002). Progressive induction of caudal neural character by graded Wnt signaling. Nat. Neurosci. *5*, 525–532.

Nordström, U., Maier, E., Jessell, T.M., and Edlund, T. (2006). An early role for WNT signaling in specifying neural patterns of Cdx and Hox gene expression and motor neuron subtype identity. PLoS Biol *4*, e252.

Novick, A., and Weiner, M. (1957). ENZYME INDUCTION AS AN ALL-OR-NONE PHENOMENON. Proc Natl Acad Sci USA *43*, 553–566.

Oliveira, C.R.P., Salvatori, R., Barreto-Filho, J.A.S., Rocha, I.E.S., Mari, A., Pereira, R.M.C., Campos, V.C., Menezes, M., Gomes, E., Meneguz-Moreno, R.A., et al. (2012). Insulin Sensitivity and -Cell Function in Adults with Lifetime, Untreated Isolated Growth Hormone Deficiency. J Clin Endocrinol Metab *97*, 1013–1019.

Olson, L.E., Tollkuhn, J., Scafoglio, C., Krones, A., Zhang, J., Ohgi, K.A., Wu, W., Taketo, M.M., Kemler, R., Grosschedl, R., et al. (2006). Homeodomain-mediated beta-catenin-dependent switching events dictate cell-lineage determination. Cell *125*, 593–605.

Oury, F. (2006). Hoxa2- and Rhombomere-Dependent Development of the Mouse Facial Somatosensory Map. Science *313*, 1408–1413.

Oxtoby, E., and Jowett, T. (1993). Cloning of the zebrafish krox-20 gene (krx-20) and its expression during hindbrain development. Nucleic Acids Res *21*, 1087–1095.

Packer, A.I., Crotty, D.A., Elwell, V.A., and Wolgemuth, D.J. (1998). Expression of the murine Hoxa4 gene requires both autoregulation and a conserved retinoic acid response element. Development *125*, 1991–1998.

Panne, D. (2008). The enhanceosome. Curr. Opin. Struct. Biol. *18*, 236–242.

Pellegrini, I., Roche, C., Quentien, M.-H., Ferrand, M., Gunz, G., Thirion, S., Bagnis, C., Enjalbert, A., and Franc, J.-L. (2006). Involvement of the pituitary-specific transcription factor pit-1 in somatolactotrope cell growth and death: an approach using dominant-negative pit-1 mutants. Mol Endocrinol *20*, 3212–3227.

Pouilhe, M., Gilardi-Hebenstreit, P., Desmarquet-Trin Dinh, C., and Charnay, P. (2007). Direct regulation of vHnf1 by retinoic acid signaling and MAF-related factors in the neural tube. Developmental Biology *309*, 344–357.

Pöpperl, H., Bienz, M., Studer, M., Chan, S.K., Aparicio, S., Brenner, S., Mann, R.S., and Krumlauf, R. (1995). Segmental expression of Hoxb-1 is controlled by a highly conserved autoregulatory loop dependent upon exd/pbx. Cell *81*, 1031–1042.

Preiss, A., Rosenberg, U.B., Kienlin, A., Seifert, E., and Jäckle, H. (1985). Molecular genetics of Krüppel, a gene required for segmentation of the Drosophila embryo. Nature *313*, 27–32.

Price, S.R., De Marco Garcia, N.V., Ranscht, B., and Jessell, T.M. (2002). Regulation of motor neuron pool sorting by differential expression of type II cadherins. Cell *109*, 205–216.

Prince, V.E., Moens, C.B., Kimmel, C.B., and Ho, R.K. (1998). Zebrafish hox genes: expression in the hindbrain region of wild-type and mutants of the segmentation gene, valentino. Development *125*, 393–406.

Prud'homme, B., Gompel, N., and Carroll, S.B. (2007). Emerging principles of regulatory evolution. Proc Natl Acad Sci USA *104 Suppl 1*, 8605–8612.

Ptashne, M. (1986). Gene regulation by proteins acting nearby and at a distance. Nature *322*, 697–701.

Raab, J.R., and Kamakaka, R.T. (2010). Insulators and promoters: closer than we think. Nat Rev Genet *11*, 439–446.

Rada-Iglesias, A., Bajpai, R., Swigut, T., Brugmann, S.A., Flynn, R.A., and Wysocka, J. (2011). A unique chromatin signature uncovers early developmental enhancers in humans. Nature *470*, 279–283.

Raible, F., and Brand, M. (2001). Tight transcriptional control of the ETS domain factors Erm and Pea3 by Fgf signaling during early zebrafish development. Mech Dev *107*, 105–117.

Redemann, N., Gaul, U., and Jäckle, H. (1988). Disruption of a putative Cys-zinc interaction eliminates the biological activity of the Krüppel finger protein. Nature *332*, 90–92.

Reifers, F., Böhli, H., Walsh, E.C., Crossley, P.H., Stainier, D.Y., and Brand, M. (1998). Fgf8 is mutated in zebrafish acerebellar (ace) mutants and is required for maintenance of midbrain-hindbrain boundary development and somitogenesis. Development *125*, 2381–2395.

Riachi, M., Himms-Hagen, J., and Harper, M.-E. (2004). Percent relative cumulative frequency analysis in indirect calorimetry: application to studies of transgenic mice. Can. J. Physiol. Pharmacol. *82*, 1075–1083.

Riedl, M., Ludvik, B., Pacini, G., Clodi, M., Kotzmann, H., Wagner, O., Kautzky-Willer, A., Prager, R., and Luger, A. (2000). The increased insulin sensitivity in growth hormone-deficient adults is reduced by growth hormone replacement therapy. European Journal of Clinical Investigation *30*, 771–778.

Rizzoti, K., and Lovell-Badge, R. (2005). Early development of the pituitary gland: induction and shaping of Rathke's pouch. Rev Endocr Metab Disord *6*, 161–172.

Robert, L., Paul, G., Chen, Y., Taddei, F.C.O., Baigl, D., and Lindner, A.B. (2011). Pre-dispositions and epigenetic inheritance in the Escherichia coli lactose operon bistable switch. Mol Syst Biol *6*, 1–12.

Roehl, H., and Nüsslein-Volhard, C. (2001). Zebrafish pea3 and erm are general targets of FGF8 signaling. Curr Biol *11*, 503–507.

Rosenfeld, N., Young, J.W., Alon, U., Swain, P.S., and Elowitz, M.B. (2005). Gene regulation at the single-cell level. Science *307*, 1962–1965.

Rowan, S., Siggers, T., Lachke, S.A., Yue, Y., Bulyk, M.L., and Maas, R.L. (2010). Precise temporal control of the eye regulatory gene Pax6 via enhancer-binding site affinity. Genes & Development *24*, 980–985.

Roy, N.M., and Sagerström, C.G. (2004). An early Fgf signal required for gene expression in the zebrafish hindbrain primordium. Brain Res Dev Brain Res *148*, 27–42.

Ruf, F., Park, M.-J., Hayot, F., Lin, G., Roysam, B., Ge, Y., and Sealfon, S.C. (2006). Mixed analog/digital gonadotrope biosynthetic response to gonadotropin-releasing hormone. J Biol Chem *281*, 30967–30978.

Runko, A.P., and Sagerström, C.G. (2003). Nlz belongs to a family of zinc-finger-containing repressors and controls segmental gene expression in the zebrafish hindbrain. Developmental Biology *262*, 254–267.

Russo, M.W., Sevetson, B.R., and Milbrandt, J. (1995). Identification of NAB1, a repressor of NGFI-A- and Krox20-mediated transcription. Proc Natl Acad Sci USA *92*, 6873–6877.

Safford, M., Collins, S., Lutz, M.A., Allen, A., Huang, C.-T., Kowalski, J., Blackford, A., Horton, M.R., Drake, C., Schwartz, R.H., et al. (2005). Egr-2 and Egr-3 are negative regulators of T cell activation. Nat. Immunol. *6*, 472–480.

Sagai, T., Hosoya, M., Mizushina, Y., Tamura, M., and Shiroishi, T. (2005). Elimination of a long-range cis-regulatory module causes complete loss of limb-specific Shh expression and truncation of the mouse limb. Development *132*, 797–803.

Sasaki-Suzuki, N., Arai, K., Ogata, T., Kasahara, K., Sakoda, H., Chida, K., Asano, T., Pessin, J.E., Hakuno, F., and Takahashi, S.-I. (2009). Growth hormone inhibition of glucose uptake in adipocytes occurs without affecting GLUT4 translocation through an insulin receptor substrate-2-phosphatidylinositol 3-kinase-dependent pathway. J Biol Chem *284*, 6061–6070.

Sato, T., and Joyner, A.L. (2009). The duration of Fgf8 isthmic organizer expression is key to patterning different tectal-isthmo-cerebellum structures. Development *136*, 3617–3626.

Schilling, T.F. (2008). Anterior-posterior patterning and segmentation of the vertebrate head. Integr. Comp. Biol. *48*, 658–667.

Schneider-Maunoury, S., Gilardi-Hebenstreit, P., and Charnay, P. (1998). How to build a vertebrate hindbrain. Lessons from genetics. C. R. Acad. Sci. III, Sci. Vie *321*, 819–834.

Schneider-Maunoury, S., Seitanidou, T., Charnay, P., and Lumsden, A. (1997). Segmental and neuronal architecture of the hindbrain of Krox-20 mouse mutants. Development *124*, 1215–1226.

Schneider-Maunoury, S., Topilko, P., Seitandou, T., Levi, G., Cohen-Tannoudji, M., Pournin, S., Babinet, C., and Charnay, P. (1993). Disruption of Krox-20 results in alteration of rhombomeres 3 and 5 in the developing hindbrain. Cell *75*, 1199–1214.

Scholpp, S., and Brand, M. (2004). Endocytosis controls spreading and effective signaling range of Fgf8 protein. Curr Biol *14*, 1834–1841.

Seitanidou, T., Schneider-Maunoury, S., Desmarquet, C., Wilkinson, D.G., and Charnay, P. (1997). Krox-20 is a key regulator of rhombomere-specific gene expression in the developing hindbrain. Mech Dev *65*, 31–42.

Serls, A.E., Doherty, S., Parvatiyar, P., Wells, J.M., and Deutsch, G.H. (2005). Different thresholds of fibroblast growth factors pattern the ventral foregut into liver and lung. Development *132*, 35–47.

Serpente, P., Tümpel, S., Ghyselinck, N.B., Niederreither, K., Wiedemann, L.M., Dollé, P., Chambon, P., Krumlauf, R., and Gould, A.P. (2005). Direct crossregulation between retinoic acid receptor {beta} and Hox genes during hindbrain segmentation. Development *132*, 503–513.

Sha, W., Moore, J., Chen, K., Lassaletta, A.D., Yi, C.-S., Tyson, J.J., and Sible, J.C. (2003).

Hysteresis drives cell-cycle transitions in Xenopus laevis egg extracts. Proc Natl Acad Sci USA *100*, 975–980.

Sham, M.H., Vesque, C., Nonchev, S., Marshall, H., Frain, M., Gupta, R.D., Whiting, J., Wilkinson, D., Charnay, P., and Krumlauf, R. (1993). The zinc finger gene Krox20 regulates HoxB2 (Hox2.8) during hindbrain segmentation. Cell *72*, 183–196.

Sirbu, I.O., Gresh, L., Barra, J., and Duester, G. (2005). Shifting boundaries of retinoic acid activity control hindbrain segmental gene expression. Development *132*, 2611–2622.

Sornson, M.W., Wu, W., Dasen, J.S., Flynn, S.E., Norman, D.J., O'Connell, S.M., Gukovsky, I., Carrière, C., Ryan, A.K., Miller, A.P., et al. (1996). Pituitary lineage determination by the Prophet of Pit-1 homeodomain factor defective in Ames dwarfism. Nature *384*, 327–333.

Spemann, H., and Mangold, H. (2001). Induction of embryonic primordia by implantation of organizers from a different species. 1923.

Stedman, A., Lecaudey, V., Havis, E., Anselme, I., Wassef, M., Gilardi-Hebenstreit, P., and Schneider-Maunoury, S. (2009). A functional interaction between Irx and Meis patterns the anterior hindbrain and activates krox20 expression in rhombomere 3. Developmental Biology *327*, 566–577.

Stern, C.D. (2001). Initial patterning of the central nervous system: how many organizers? Nat Rev Neurosci *2*, 92–98.

Stern, C.D. (2005). Neural induction: old problem, new findings, yet more questions. Development *132*, 2007–2021.

Storlien, L., Oakes, N.D., and Kelley, D.E. (2007). Metabolic flexibility. Proc. Nutr. Soc. *63*, 363–368.

Sturgeon, K., Kaneko, T., Biemann, M., Gauthier, A., Chawengsaksophak, K., and Cordes, S.P. (2011). Cdx1 refines positional identity of the vertebrate hindbrain by directly repressing Mafb expression. Development *138*, 65–74.

Taatjes, D.J., Marr, M.T., and Tjian, R. (2004). Regulatory diversity among metazoan co-activator complexes. Nat Rev Mol Cell Biol *5*, 403–410.

Tabariès, S., Lapointe, J., Besch, T., Carter, M., Woollard, J., Tuggle, C.K., and Jeannotte, L. (2005). Cdx protein interaction with Hoxa5 regulatory sequences contributes to Hoxa5 regional expression along the axial skeleton. Mol Cell Biol *25*, 1389–1401.

Tabata, T., and Takei, Y. (2004). Morphogens, their identification and regulation. Development *131*, 703–712.

Taillebourg, E., Buart, S., and Charnay, P. (2002). Conditional, floxed allele of the Krox20 gene. Genesis *32*, 112–113.

Taniguchi, Y., Yasutaka, S., Kominami, R., and Shinohara, H. (2002). Proliferation and differentiation of rat anterior pituitary cells. Anat Embryol *206*, 1–11.

Theil, T., Frain, M., Gilardi-Hebenstreit, P., Flenniken, A., Charnay, P., and Wilkinson, D.G. (1998). Segmental expression of the EphA4 (Sek-1) receptor tyrosine kinase in the hindbrain is

under direct transcriptional control of Krox-20. Development *125*, 443–452.

Topilko, P., Schneider-Maunoury, S., Levi, G., Baron-Van Evercooren, A., Chennoufi, A.B., Seitanidou, T., Babinet, C., and Charnay, P. (1994). Krox-20 controls myelination in the peripheral nervous system. Nature *371*, 796–799.

Topilko, P., Schneider-Maunoury, S., Levi, G., Trembleau, A., Gourdji, D., Driancourt, M.A., Rao, C.V., and Charnay, P. (1998). Multiple pituitary and ovarian defects in Krox-24 (NGFI-A, Egr-1)-targeted mice. Mol Endocrinol *12*, 107–122.

Tourtellotte, W.G., and Milbrandt, J. (1998). Sensory ataxia and muscle spindle agenesis in mice lacking the transcription factor Egr3. Nat Genet *20*, 87–91.

Toyoda, R., Assimacopoulos, S., Wilcoxon, J., Taylor, A., Feldman, P., Suzuki-Hirano, A., Shimogori, T., and Grove, E.A. (2010). FGF8 acts as a classic diffusible morphogen to pattern the neocortex. Development *137*, 3439–3448.

Tsai, M.-C., Manor, O., Wan, Y., Mosammaparast, N., Wang, J.K., Lan, F., Shi, Y., Segal, E., and Chang, H.Y. (2010). Long noncoding RNA as modular scaffold of histone modification complexes. Science *329*, 689–693.

Tümpel, S., Cambronero, F., Ferretti, E., Blasi, F., Wiedemann, L.M., and Krumlauf, R. (2007). Expression of Hoxa2 in rhombomere 4 is regulated by a conserved cross-regulatory mechanism dependent upon Hoxb1. Developmental Biology *302*, 646–660.

Tümpel, S., Cambronero, F., Sims, C., Krumlauf, R., and Wiedemann, L.M. (2008). A regulatory module embedded in the coding region of Hoxa2 controls expression in rhombomere 2. Proc Natl Acad Sci USA *105*, 20077–20082.

Umulis, D.M., Serpe, M., O'Connor, M.B., and Othmer, H.G. (2006). Robust, bistable patterning of the dorsal surface of the Drosophila embryo. Proc Natl Acad Sci USA *103*, 11613–11618.

Vankelecom, H. (2007). Stem cells in the postnatal pituitary? Neuroendocrinology *85*, 110–130.

Vashee, S., Melcher, K., Ding, W.V., Johnston, S.A., and Kodadek, T. (1998a). Evidence for two modes of cooperative DNA binding in vivo that do not involve direct protein-protein interactions. Curr Biol *8*, 452–458.

Vashee, S., Willie, J., and Kodadek, T. (1998b). Synergistic activation of transcription by physiologically unrelated transcription factors through cooperative DNA-binding. Biochem Biophys Res Commun *247*, 530–535.

Veitia, R.A. (2003a). A sigmoidal transcriptional response: cooperativity, synergy and dosage effects. Biol Rev Camb Philos Soc *78*, 149–170.

Veitia, R.A. (2003b). Nonlinear effects in macromolecular assembly and dosage sensitivity. J Theor Biol *220*, 19–25.

Veitia, R.A., and Nijhout, H.F. (2006). The robustness of the transcriptional response to alterations in morphogenetic gradients. Bioessays *28*, 282–289.

Vermeren, M., Maro, G.S., Bron, R., McGonnell, I.M., Charnay, P., Topilko, P., and Cohen, J. (2003). Integrity of developing spinal motor columns is regulated by neural crest derivatives at

motor exit points. Neuron *37*, 403–415.

Vesque, C., and Charnay, P. (1992). Mapping functional regions of the segment-specific transcription factor Krox-20. Nucleic Acids Res *20*, 2485–2492.

Vesque, C., Maconochie, M., Nonchev, S., Ariza-McNaughton, L., Kuroiwa, A., Charnay, P., and Krumlauf, R. (1996). Hoxb-2 transcriptional activation in rhombomeres 3 and 5 requires an evolutionarily conserved cis-acting element in addition to the Krox-20 binding site. Embo J *15*, 5383–5396.

Vijayakumar, A., Novosyadlyy, R., Wu, Y., Yakar, S., and LeRoith, D. (2010). Biological effects of growth hormone on carbohydrate and lipid metabolism. Growth Hormone & IGF Research *20*, 1–7.

Voiculescu, O., Taillebourg, E., Pujades, C., Kress, C., Buart, S., Charnay, P., and Schneider-Maunoury, S. (2001). Hindbrain patterning: Krox20 couples segmentation and specification of regional identity. Development *128*, 4967–4978.

Walshe, J., Maroon, H., McGonnell, I.M., Dickson, C., and Mason, I. (2002). Establishment of hindbrain segmental identity requires signaling by FGF3 and FGF8. Curr Biol *12*, 1117–1123.

Wang, J., Ellwood, K., Lehman, A., Carey, M.F., and She, Z.S. (1999). A mathematical model for synergistic eukaryotic gene activation. J Mol Biol *286*, 315–325.

Wang, L., Walker, B.L., Iannaccone, S., Bhatt, D., Kennedy, P.J., and Tse, W.T. (2009). Bistable switches control memory and plasticity in cellular differentiation. Proc Natl Acad Sci USA *106*, 6638–6643.

Waskiewicz, A.J., Rikhof, H.A., and Moens, C.B. (2002). Eliminating zebrafish pbx proteins reveals a hindbrain ground state. Dev Cell *3*, 723–733.

Wassef, M.A., Chomette, D., Pouilhe, M., Stedman, A., Havis, E., Desmarquet-Trin Dinh, C., Schneider-Maunoury, S., Gilardi-Hebenstreit, P., Charnay, P., and Ghislain, J. (2008). Rostral hindbrain patterning involves the direct activation of a Krox20 transcriptional enhancer by Hox/Pbx and Meis factors. Development *135*, 3369–3378.

Wasylyk, B., Hahn, S.L., and Giovane, A. (1993). The Ets family of transcription factors. Eur J Biochem *211*, 7–18.

Weisinger, K., Kayam, G., Missulawin-Drillman, T., and Sela-Donenfeld, D. (2010). Analysis of expression and function of FGF-MAPK signaling components in the hindbrain reveals a central role for FGF3 in the regulation of Krox20, mediated by Pea3. Developmental Biology.

Weisinger, K., Wilkinson, D.G., and Sela-Donenfeld, D. (2008). Inhibition of BMPs by follistatin is required for FGF3 expression and segmental patterning of the hindbrain. Developmental Biology *324*, 213–225.

Wiellette, E.L., and Sive, H. (2003). vhnf1 and Fgf signals synergize to specify rhombomere identity in the zebrafish hindbrain. Development *130*, 3821–3829.

Wiellette, E.L., and Sive, H. (2004). Early requirement for fgf8 function during hindbrain pattern formation in zebrafish. Dev Dyn *229*, 393–399.

Wilkinson, D.G., Bhatt, S., Chavrier, P., Bravo, R., and Charnay, P. (1989). Segment-specific expression of a zinc-finger gene in the developing nervous system of the mouse. Nature *337*, 461–464.

Wilson, S.W., and Houart, C. (2004). Early steps in the development of the forebrain. Dev Cell *6*, 167–181.

Wizenmann, A., and Lumsden, A. (1997). Segregation of rhombomeres by differential chemoaffinity. Mol Cell Neurosci *9*, 448–459.

Wolpert, L. (1969). Positional information and the spatial pattern of cellular differentiation. J Theor Biol *25*, 1–47.

Worley, P.F., Bhat, R.V., Baraban, J.M., Erickson, C.A., McNaughton, B.L., and Barnes, C.A. (1993). Thresholds for synaptic activation of transcription factors in hippocampus: correlation with long-term enhancement. J Neurosci *13*, 4776–4786.

Wurst, W., and Bally-Cuif, L. (2001). Neural plate patterning: upstream and downstream of the isthmic organizer. Nat Rev Neurosci *2*, 99–108.

Xu, Q., Mellitzer, G., and Wilkinson, D.G. (2000). Roles of Eph receptors and ephrins in segmental patterning. Philosophical Transactions of the Royal Society B: Biological Sciences *355*, 993–1002.

Xu, Q., Mellitzer, G., Robinson, V., and Wilkinson, D.G. (1999). In vivo cell sorting in complementary segmental domains mediated by Eph receptors and ephrins. Nature *399*, 267–271.

Yakar, S., Setser, J., Zhao, H., Stannard, B., Haluzik, M., Glatt, V., Bouxsein, M.L., Kopchick, J.J., and LeRoith, D. (2004). Inhibition of growth hormone action improves insulin sensitivity in liver IGF-1-deficient mice. J Clin Invest *113*, 96–105.

Yamagata, K., Kaufmann, W.E., Lanahan, A., Papapavlou, M., Barnes, C.A., Andreasson, K.I., and Worley, P.F. (1994). Egr3/Pilot, a zinc finger transcription factor, is rapidly regulated by activity in brain neurons and colocalizes with Egr1/zif268. Learn. Mem. *1*, 140–152.

Yamaguchi, T.P., Harpal, K., Henkemeyer, M., and Rossant, J. (1994). fgfr-1 is required for embryonic growth and mesodermal patterning during mouse gastrulation. Genes & Development *8*, 3032–3044.

Yan, S.-J., Zartman, J.J., Zhang, M., Scott, A., Shvartsman, S.Y., and Li, W.X. (2009). Bistability coordinates activation of the EGFR and DPP pathways in Drosophila vein differentiation. Mol Syst Biol *5*, 278.

Yao, H., Brick, K., Evrard, Y., Xiao, T., Camerini-Otero, R.D., and Felsenfeld, G. (2010). Mediation of CTCF transcriptional insulation by DEAD-box RNA-binding protein p68 and steroid receptor RNA activator SRA. Genes & Development *24*, 2543–2555.

Yu, S.R., Burkhardt, M., Nowak, M., Ries, J., Petrášek, Z., Scholpp, S., Schwille, P., and Brand, M. (2009). Fgf8 morphogen gradient forms by a source-sink mechanism with freely diffusing molecules. Nature *461*, 533–536.

Yuh, C.H., Bolouri, H., and Davidson, E.H. (1998). Genomic cis-regulatory logic: experimental